



**Rational design of small molecule probes for
investigating the mechanism of action of the
chemotherapeutic agents CDDO and artemisinin**

Thesis submitted in accordance with the requirements of the University of Liverpool for the degree of

Doctor in Philosophy

Michael Wong

January 2015

Declaration

This thesis is the result of my own work. The material contained in the thesis has not been presented, nor is currently being presented, either wholly or in part for any other degree or other qualification.

Michael Wong

This research was carried out in the Department of Chemistry and the Department of Molecular and Clinical Pharmacology at the University of Liverpool

Table of Contents

	Acknowledgements	1
	Definitions and abbreviations	2
	Publications	9
	Abstract	10
Chapter 1	General introduction	12
Chapter 2	The synthesis and biological profiling of CDDO derivatives	44
Chapter 3	Design and synthesis of irreversible analogues of CDDO	100
Chapter 4	Examination of the role of ferrous iron and phosphatidylcholine in the bioactivation of novel tetraoxane antimalarials	166
Chapter 5	Design and synthesis of click functionalised derivatives of artemisinin and CDDO as probes for investigating chemical mechanism of action	221
Chapter 6	Final conclusion and future work	282

Acknowledgements

I wish to thank my primary supervisors Professor Kevin Park and Professor Paul O'Neill for giving me the opportunity to study this PhD. Their guidance, support and patience throughout the past five years are highly appreciated. I would also like to especially thank Dr Ian Cople for his continued guidance, support and patience. The opportunity to watch and learn from his knowledge and experience is greatly appreciated. I would like to thank the MRC for their financial support.

Special thanks to Holly Bryan for her help and assistance during my time at pharmacology, Roz for the LCMS, Ally for the antimalarial data and Dr Neil Berry for the molecular modelling. Thanks to all of the technical staff at the Department of Chemistry, in particular to Dr Jon Iggo, Tony and Konstantin for their NMR expertise and Moya and Jean at MS and Microanalysis.

I would like to thank all those who have helped and assisted me past and present; Ian, Holly, Pika, Dammy, Jo, Roz, Ana Hi, Chris, Neil, Adam, Jon in Pharmacology, Dave, James, Richard, Paul S, Chandra, Shirley, Peter, Emma Y, Nham, Vicky and Louise in Chemistry (sorry if I missed anyone out there are so many people across both departments).

I would like to thank everyone past and present for making this PhD journey so enjoyable and fun; everyone mentioned above including Bhav, Beth and Christina - thank you for the lunch time meetings and being a support when I needed it, Matt, Emma S, Natalie, Francesc, Olivier, Rudi, Sunil, Robin, Neil K, Kathryne, Paul M, Raman and Zeyn thank you for making this so fun and enjoyable. Special thanks to Nham, Matt, Shirley and Dave for the drinks after work when stress levels were high.

I would like to thank my loving family (especially my parents, Wing Lok and Xin Lian and my in-laws Zerong and Liandi) for their support and patience throughout my PhD. They have given me time and space to complete my studies and have always been there during the stressful times. Finally, a special thank you goes to my wife Katie, who has looked after our little 6 month old baby girl, Phoebe during the most stressful time of the PhD.

Definitions and abbreviations

(TrxS) ₂	Oxidised thioredoxin
+ve CTRL	Positive control
°C	Degrees Celsius
μL	Microliter
μM	Micromolar concentration
μmol	Micromole concentration
¹³ C NMR	Carbon-13 nuclear magnetic resonance
¹ H NMR	Proton nuclear magnetic resonance
3D7	Chloroquine sensitive strain (whole cell parasite) of <i>Plasmodium falciparum</i>
Å	Angstrom
Å ³	Cubic Angstrom
ABPP	Activity based protein profiling
ACN	Acetonitrile
ACT	Artemisinin based combination therapy
ADRs	Adverse drug reactions
AMP	Adenosine monophosphate
Amu	Atomic mass units
Aq	Aqueous
ARE	Antioxidant response element
ARP3	Actin-related protein 3
ATP	Adenosine triphosphate
BCA	Bicinchoninic acid
BF ₃ .OEt ₂	Boron trifluoride diethyl etherate
BL21	<i>Escherichia coli</i>
BPs	Biotinylated probes
BSA	Bovine serum albumin
BzCl	Benzoyl chloride
C ₁₈	Octadecyl carbon chain
CD36	Cluster of Differentiation 36
CDDO	2-Cyano-3,12-dioxooleana-1,9(11)-dien-28-oic acid
CDDO-Epoxyde	2β-Cyano-3,12-dioxo-1,2-epoxyolean-9(11)-en-28-oate

Definitions and abbreviations

CDDO-Im	2-Cyano-3,12-dioxooleana-1,9-dien-28-imidazolide
CDDO-Me	Methyl 2-cyano-3,12-dioxooleana-1,9(11)-dien-28-oate
CI	Chemical ionisation
CKD	Chronic kidney disease
Conc.	Concentrated
C-radical	Carbon radical
c-Rel	Proto-oncogene c-Rel
CRM1	Exportin-1
Cys	Cysteine
d	Doublet
DCM	Dichloromethane
dd	Doublet of doublets
ddd	Doublet of doublet of doublets
DDO-Epoxyde	Methyl 3,12-dioxo-1,2-epoxyolean-9(11)-en-28-oate
DDO-Me	Methyl 3,12-dioxooleana-1,9(11)-dien-28-oate
DDQ	2,3-Dichloro-5,6-dicyano- <i>p</i> -benzoquinone
ddq	Doublet of doublet of quartets
ddt	Doublet of doublet of triplets
DEPT135	Distortionless enhancement by polarization transfer 135°
Dex-mes	Radiolabelled dexamethasone 21-mesylate
DHA	Dihydroartemisinin
DMAP	4-Dimethylaminopyridine
DMEM	Dulbecco's modified eagle medium
DMF	Dimethylformamide
DMPK	Drug metabolism and pharmacokinetics
DMSO	Dimethyl sulfoxide
DMSO-d ⁶	Deuterated dimethyl sulfoxide
DNA	Deoxyribonucleic acid
dt	Doublet of triplets
EC ₂₀₀	Effective concentration to double response
ECL	Enhanced chemiluminescence
EDCI	1-Ethyl-3-(3-dimethylaminopropyl)carbodiimide
EDTA	Ethylenediaminetetraacetic acid
EI	Electron ionisation

emPAI	Exponentially modified protein abundance index
EPI	Enhanced product ion
equiv	Equivalent
ErbB2	Receptor tyrosine-protein kinase erbB-2
ESI / ES	Electron spray ionisation
FA	Formic acid
FAD	Flavin adenine dinucleotide
FADH ₂	Reduced flavin adenine dinucleotide
FBS	Fetal bovine serum
Fe ²⁺	Ferrous iron / iron(II)
FeO ³⁺	Iron (II) oxide
G6PD	Glucose-6-phosphate dehydrogenase
GR	Glutathione reductase
GSH	Glutathione
GSSH	Oxidised glutathione
GSTP1	Glutathione-S-transferase <i>pi</i>
H4IIE	Rat hepatoma cell line
HEPES	4-(2-Hydroxyethyl)piperazine-1-ethanesulfonic acid
His	Histidine
HMQC	Heteronuclear multiple-quantum correlation
HPLC	High-performance liquid chromatography
HPLC-UV	Ultraviolet detection by high-performance liquid chromatography
hr	Hour(s)
HRMS	High resolution mass spectrometry
HRP	Horseradish peroxidase
Hz	Hertz
IC ₅₀	The half maximal inhibitory concentration
IFN-γ	Interferon gamma
IKK	IκB kinase
IKKβ	Inhibitor of nuclear factor kappa-B kinase subunit beta
IL-1	Interleukin 1
iNOS	Inducible nitric oxide synthase
IPTG	Isopropyl β-D-1-thiogalactopyranoside
IR	Infrared spectroscopy

Definitions and abbreviations

I κ B	Inhibitor of nuclear factor kappa B
<i>J</i>	Coupling constant (hertz)
JAK	Janus kinase
kD	Kilodaltons
Keap1	Kelch-like ECH-associated protein 1
LB	Lysogeny broth
LCMS	Liquid chromatography mass spectrometry
LDA	Lithium diisopropylamide
lit	Literature
LMB	Leucomethylene blue
M	Molar concentration
m	Multiplet
m/z	Mass to charge ratio
mA	Milliamps
Mafs	Transcription factor Maf
MB	Methylene blue
<i>m</i> CPBA	<i>meta</i> -Chloro-peroxybenzoic acid
MG132	Proteasome inhibitor
MHz	Megahertz
mins	Minutes
mL	Millilitre
mM	Millimolar concentration
mm	Millimetre
mm ³	Cubic millimetre
mmol	Millimole
MMP	Matrix metalloproteinase
MOPS	3-(<i>N</i> -Morpholino)propanesulfonic acid
mp	Melting point
mRNA	Messenger ribonucleic acid
MS	Mass spectrometry
MS/MS	Tandem mass spectrometry
MudPIT	Multidimensional protein identification technology
n=	Number of repeats
NAC	<i>N</i> -acetyl cysteine

Definitions and abbreviations

NADPH	Nicotinamide adenine dinucleotide phosphate
NF-κB	Nuclear factor kappa B
nL	Nanolitre
nM	Nanomolar concentration
nm	Nanometre
NMR	Nuclear magnetic resonance
nOe	Nuclear Overhauser effect
NQO1	NAD(P)H:quinone oxidoreductase 1
Nrf2	Nuclear factor erythroid 2-related factor 2
OAT	Ornithine δ-aminotransferase
OD ₆₀₀	Optical density reading measured at 600 nm
<i>P. falciparum</i>	<i>Plasmodium falciparum</i>
p50/p105 (NF-κB1)	Nuclear factor NF-kappa-B p105 subunit
p52/p100 (NF-κB2)	Nuclear factor NF-kappa-B p100 subunit
PAH	Pulmonary arterial hypertension
PAL	Photoaffinity labelling
PBS	Phosphate buffered saline
PC	Phosphatidylcholine
PfATP6	Sarco/endoplasmic reticulum calcium ATPase of <i>P. falciparum</i>
pH	log ₁₀ hydrogen ion concentration
Ph ₃ P=CHCO ₂ Et	Ethyl (triphenylphosphoranylidene) acetate
pK _a	Acid dissociation constant
PPARγ	Peroxisome proliferator-activated receptor gamma
ppm	Parts per million
PTFE	Polytetrafluoroethylene
<i>p</i> -TsCN	<i>p</i> -Toluenesulfonyl cyanide
Pyr	Pyridine
r.t.	Room temperature
RelA (p65)	Nuclear factor NF-kappa-B p65 subunit / transcription factor p65
RelB	Transcription factor RelB
R _f	Retention factor
RIPA	Radioimmunoprecipitation assay
ROS	Reactive oxygen species
rpm	Revolutions per minute

s	Singlet
S.D.	Standard deviation
SAR	Structure activity relationship
sec	Second(s)
STAT	Signal transducer and activator of transcription
t	Triplet
TBS	Tris buffered saline
td	Triplet of doublets
TEA	Triethylamine
TFA	Trifluoroacetic acid
THF	Tetrahydrofuran
TLC	Thin layer chromatography
TMS	Trimethylsilyl
TNF- α	Tumour necrosis factor alpha
TrxSH	Reduced thioredoxin
UV / U.V.	Ultra violet
V	Volt(s)
v/v	Volume to volume
-ve CTRL	Negative control
vs.	Versus
VT-NMR	Variable temperature Nuclear magnetic resonance
w/v	Weight to volume
w/w	Weight to weight
XIC	Extracted ion count
X-ray	X radiation
β -ME	β -Mercaptoethanol
δ	Chemical shift (parts per million)

Publications

1. Ian M. Copple, Holly K. Bryan, **Michael H. L. Wong**, Rosalind E. Jenkins, Alvin J. L. Chia, Jaclyn Bibby, Neil G. Berry, Neil R. Kitteringham, Christopher E. Goldring, Paul M. O'Neill, B. Kevin Park. Chemical tuning of the potent Nrf2 inducer Bardoxolone Methyl reveals sites of interaction with Keap1. **2015** (Submitted)
2. Joanne Walsh, Rosalind E. Jenkins, **Michael Wong**, Adedamola Olayanju, Helen Pwell, Ian Copple, Paul M. O'Neill, Christopher E. P. Goldering, Neil R. Kitteringham and B. Kevin Park. Identification and quantification of the basal and inducible Nrf2-dependent proteomes in mouse liver: Biochemical, pharmacological and toxicological implications, *Journal of Proteomics*, **2014**, 108, 171-187.
3. Ian M. Copple, Amy E. Mercer, James Firman, Gail Donegan, Bram Herpers, **Michael H.L. Wong**, James Chadwick, Andreia D. Bringela, Maria L.S. Cristiano, Bob van de Water, Stephen A. Ward, Paul M. O'Neill and B. Kevin Park. Examination of the cytotoxic and Embryotoxic Potential and Underlying Mechanisms of Next-Generation Synthetic Trioxolane and Tetraoxane Antimalarials. *Molecular Medicine*, **2012**, 18 (1), 1045-1055.
4. Fatima Bousejra-El Garah, **Michael He-Long Wong**, Richard K. Amewu, Sant Muangnoicharoen, James L. Maggs, Jean-Luc Stigliani, B. Kevin Park, James Chadwick, Stephen A. Ward and Paul M. O'Neill. Comparison of the reactivity of Antimalarial 1,2,4,5-Tetraoxanes with 1,2,4-Trioxolanes in the presence of Ferrous Iron Salts, Heme, and Ferrous Iron Salts/Phosphatidylcholine. *Journal of Medicinal Chemistry*, **2011**, 54 (19), 6443-6455.

Abstract

Adverse drug reactions (ADR) are a major concern for the pharmaceutical industry and health practitioners as they can cause morbidity and in severe cases mortality. ADRs are one of the major reasons why drugs fail during clinical trials so research directed at predicting ADRs to minimise failure is essential. The CDDO (2-cyano-3,12-dioxo-oleana-1,9(11)-dien-28-oate) and the synthetic endoperoxide series are two promising classes that have potential for the treatment of cancers and malaria and may revolutionise treatment, within their fields, if approved for clinical use. The two main aims that are presented in this thesis are to; (i) design and synthesise novel analogues and chemical probes to identify potential molecular targets for both the CDDO and endoperoxide series (ii) develop appropriate in vitro test systems to help define the molecular mechanism of each class of drug.

CDDO-Me (methyl 2-cyano-3,12-dioxo-oleana-1,9(11)-dien-28-oate) is one of the most potent inducers of Nrf2, a transcription factor that regulates the expression of numerous cell defence genes in mammalian cells. Nrf2 is sequestered in the cytosol by Keap1, which 'senses' chemical and oxidative stress *via* its 27 cysteine residues. Although CDDO-Me is one of the most potent inducers of Nrf2, the molecular target and chemical mechanism is still not defined. Current literature suggests that a reversible 1,4 conjugate addition to specific cysteine residue(s) located on the Keap1 protein results in an increase in Nrf2 levels. In order for SAR work to be performed a synthetic route to CDDO and analogues was developed which involved nine steps using oleanolic acid as starting material. Highlights of the chemistry included addition of the ketone using mCPBA and incorporation of the cyano group in steps 3 and 7 of the synthesis. In addition to preparing the target molecule CDDO a number of additional molecules were prepared to define the importance of functional groups in the A and C rings of CDDO.

Genetically modified H4IIE rat hepatoma cells transiently transfected with the an Nrf2-sensitive luciferase reporter gene were used to screen the CDDO-Me analogues, including DDO-Me which lacks a cyano group on the A ring, for their ability to induce Nrf2. NMR studies with model thiols were performed to determine the ability of these compounds to form reversible or non-reversible adducts. Mass spectrometry (MS) was used to confirm the NMR data and interpretations. In total, four probes were identified that reacted in a non-reversible fashion: DDO-Me, DDO-Al and DDO-Az (click probe versions of the parent DDO-Me that can be used to facilitate proteomic studies) and CDDO-Epoxy (a probe with similar overall structure to CDDO-Me but can react at the β -carbon in a non-reversible fashion; this feature should aid proteomic approaches to reactive cysteine residue identification). To further investigate if these compounds were reactive to cysteine residues within a model protein, recombinant human GSTP1 was used as a model protein for chemically reactive molecules. Cys-47 located on GSTP1 has been shown to react with other electrophiles and during our studies LCMS has confirmed that all four of the synthesised active probes were capable of attaching covalently to Cys-47 of GSTP1.

The emergence of malaria parasite resistance to most available drugs, including the semi-synthetic artemisinin derivatives artemether and artesunate, has led to efforts to create

new synthetic peroxides as potential antimalarial agents. Leading examples of synthetic endoperoxides include OZ277 (arterolane), a molecule in phase III clinical trials in combination with piperaquine, and OZ439, a second generation derivative with improved pharmacokinetics and enhanced *in vivo* antimalarial activity. 1,2,4,5-Tetraoxanes are another class of endoperoxide with proven excellent antimalarial profiles against both chloroquine-resistant and chloroquine-sensitive strains of *Plasmodium falciparum* and oral activity in murine models of the disease. It is currently widely accepted that endoperoxides have a similar antimalarial mechanism to artemisinin, whereby Fe²⁺ mediated generation of cytotoxic carbon-centred radicals, results in death of the parasite. It is presumed that C-radicals can react with important key proteins; however, the specific molecular target(s) that leads to eventual parasite death are still unknown.

A chemical synthesis of tetraoxane probes that contain a UV chromophore was performed and analogues were subsequently screened for antimalarial activity. The most active tetraoxane identified was exposed to a range of Fe²⁺ salts and conditions developed to mimic the biological environment. Primary, secondary and novel carbon-centred radical derived products (surrogate markers of bioactivation) were purified using UV-HPLC, characterised and submitted as chemical probes and standards for biological studies.

In order for proteomic studies to be initiated, an allyl or azide group was incorporated into a semi-synthetic artemisinin skeleton. The azide (and alkyne) functional group within these probes provides a handle for protein pull down *via* click chemistry. Azide and acetylenes were chosen over direct linkage to the biotin group to reduce steric hindrance in the semi-synthetic probe. The synthesised click probes were tested for antimalarial activity and were submitted for protein pull down and identification of potential molecular targets. Similarly DDO allyl and azide were synthesised and were tested for Nrf2 induction and further confirmed as viable probes *via* NMR experiments with simple thiols and GSTP1.

In summary, novel CDDO non reversible probes were synthesised and have shown potential as chemical tools to identify the molecular targets/mechanisms by which these compounds activate Nrf2. Tetraoxanes also have been prepared along with artemisinin click probes and the latter have been submitted for click chemistry pull down experiments, within *Plasmodium falciparum* parasites, to identify potential molecular targets.

CHAPTER 1

General introduction

Chapter 1

1.1. Basic principles of pharmacology	14
1.2. Drug interactions	15
1.2.1. Reversible drug interactions (non-covalent)	16
1.2.2. Non-reversible drug interactions (Covalent)	16
1.2.3. Drug target identification and validation	20
1.3. Malaria - Antimalarials	23
1.3.1. Artemisinin	23
1.3.1.1. Model studies	25
1.3.2. Next-generation synthetic antimalarial drugs	26
1.3.2.1. Trioxolanes and tetraoxanes	27
1.4. CDDO and derivatives	29
1.4.1. Pharmacology of CDDO	29
1.5. Cellular protection against stress	31
1.5.1. Nuclear factor kappa B (NF- κ B)	31
1.5.2. Nuclear factor erythroid 2-related factor 2 (Nrf2)	33
1.5.3. CDDO derivatives - potent inducers of Nrf2	33
1.6. Toxicity issues	36
1.7. Aims of this thesis	36
1.8. References	38

1.1. Basic principles of pharmacology

Pharmacology is the study of a chemical substance (drug) that exhibits a biological effect upon exposure/administration to a living organism.¹ Pharmacology has two major sub-disciplines; pharmacokinetics (the study of the fate of a chemical substance once administered to a living organism), and pharmacodynamics (the study of the biological effects provoked by a chemical compound).¹ For a biological effect to occur, the administered drug must reach its site of action. However, there are many factors that will influence the bioavailability of a drug. These include phase I metabolism, drug absorption and influx and efflux proteins.¹ Many pharmacologically active compounds that are administered as therapeutic drugs overcome these factors and initiate a biological effect by binding to a specific protein target, such as a receptor, enzyme or ion channel. This binding can be covalent (generally non-reversible) or non-covalent (reversible) in nature, and often induces a change in protein structure and/or function, thus triggering a biological response.² Table 1.1 lists a selection of drugs that are known to have a reversible or irreversible mechanism of action.

Drug	Target and activity	Treatment	Reversibility
Salbutamol	β_2 -receptor agonist	Asthma	reversible
Propranolol	β_1 -receptor antagonist	Hypertension, anxiety and panic	reversible
Warfarin	Vitamin K reductase	Anti-coagulant	reversible
Floxuridine	Thymidylate synthase	Anti-cancer (anti-metabolite)	Irreversible
Penicillins	DD-transpeptidase	Bacterial infections	Irreversible
Omeprazole	Hydrogen-potassium adenosinetriphosphatase	Peptic ulcer disease	Irreversible

Table 1.1: List of reversible and non-reversible drugs.²⁻⁴

The mechanism of action for these drugs can be defined due to their known target. However, this is not true for all therapeutic compounds that are currently available.

A perfect example of this is paracetamol (acetaminophen). Paracetamol was first discovered in 1877 and introduced as a mild analgesic in 1893, which is still use today.⁵ However, toxicity still remains a problem and has a clinical burden on hospitals and the health care system.⁶ The exact mechanism of paracetamol's pharmacological and toxicological action remains unclear. The ability to dissociate beneficial pharmacological activity from its harmful toxicological effect is vital for the design and development of safe new medicines. In order to achieve this, the mechanism of action including the molecular target must be understood. However, this is not always straight forward and will be discussed in more detail below.

1.2. Drug interactions

In modern day drug discovery, drugs must be designed to achieve a number of goals. This includes maintaining or improving potency, reducing or potentially eliminating adverse drug reactions (ADRs) and improving bioavailability.⁷ these are generally achieved through chemical structure alterations and structure activity relationship (SAR) studies. These modifications are primarily driven by medicinal chemists but guided by pharmacology and clinical studies.⁸

For the majority of drugs, non-covalent target interaction is the main binding involved in a drug target interaction. Studies dating back to the 1970s and 80s have identified that reactive metabolites resulting from covalent interactions can potentially form off-target interactions. Therefore, avoiding incorporation of such

groups during the drug discovery stage was understood to reduce ADRs.⁹⁻¹¹ ADRs are one of the major contributors to drug failure or withdrawal from the market and clinical use.^{12,13}

1.2.1. Reversible drug interactions (non-covalent)

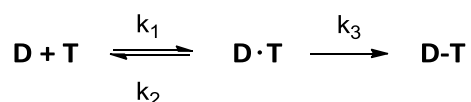
Reversible binding interactions between drug and target generally involves weaker interactions such as hydrogen bonding, van der Waals interactions, π - π stacking, ionic bonding and others.^{7,14,15} These interactions can be disrupted and broken, and are thus considered reversible. This is a major advantage over covalent interactions as this provides a reversible function that can associate, allowing a drug compound to enforce its pharmacological effect, but also the ability to dissociate. This enables vital functional proteins such as enzymes to be reused as the *de novo* synthesis of certain vital proteins may be difficult. Therefore non-covalent interactions are favoured over covalent interactions during the drug discovery stage.¹⁶

The most common interaction between a drug and target is hydrogen bonding. This interaction occurs between a hydrogen atom bound to an electronegative atom such as oxygen, nitrogen and sulphur forming a weak non-covalent interaction.¹⁵ Although hydrogen bonding is a non-covalent interaction and can normally be disrupted, a collection of hydrogen bonds can form stable aggregates. An example of this is the complementary strands within DNA.^{7,17}

1.2.2. Non-reversible drug interactions (Covalent)

As described above, many drugs are designed to be non-covalent, however, nearly 30% of drugs on the market act *via* a covalent interaction.¹⁰

During covalent interaction between a drug and its molecular target, initial non-covalent interactions occur between drug and target. This is similar to reversible binding. Once this interaction has been established, subsequent covalent bond formation occurs between the drug compound and its molecular target.¹⁰ This is shown in the equation below which is rendered irreversible in nature.



Equation 1.1: The rate equation for covalent binding where k is the rate coefficient of the reaction, D is the drug and T is the molecular target.

Modern medical chemistry has evolved to identify specific groups of atoms also known as functional groups that will potentially form direct covalent interactions or through activation of specific groups.^{1,7,12} This is shown in Table 1.2 and includes functional groups that are metabolised during phase I metabolism.

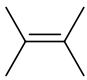
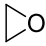
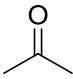
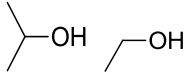
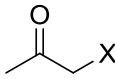
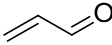
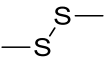
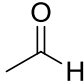
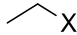
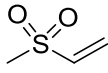
 Alkenes	 Epoxides	 Ketones	 Alcohols	 α -halo carbonyls	 Michael acceptors
—SH Thiols	 Disulphides	 Aldehydes	 Halo alkanes	 Vinyl sulfones	

Table 1.2: Some functional groups that are capable of forming covalent interactions.^{1,7,12}

Covalent interactions can occur between a drug and cellular proteins or lipids. This can occur between cysteine residues, glutathione (GSH) incorporation or radical alkylation with proteins or lipids.¹⁰ This can result in a number of responses, such as, cell death or immune stimulated response hence ADRs occur. However, not all such covalent interactions form detectable thiol adducts.¹⁰ It is understood that the micro-environment within protein structures appears to be crucial in determining specific binding.¹³ The micro-environment is influenced by factors such as acid dissociation constant (pK_a), hydrophobicity, pH and others.¹³

Although there are risks with covalent interactions such as the ones mentioned above, there are also many advantages, that include:-

- Sustained duration where the pharmacological effect for covalent interactions depends on the *de novo* re-synthesis rate of the functional protein. The longer the re-synthesis the longer the pharmacological effect.^{11,18}

- Less frequent dosing which is due to the sustained duration. Less drug is required to maintain a pharmacological effect and the therapeutic window, therefore, resulting in a lower systemic drug exposure.^{11,18}
- Preventing emergence of drug resistance due to consistent target suppression.^{11,18}

In addition, unlike non-covalent interactions, covalent interactions allow potential identification of their molecular target by employing a wide range of techniques including mass spectroscopy, peptide mapping and protein immunoblotting.¹⁰ This will be discussed further.

1.2.3. Drug target identification and validation

Identifying and validating molecular targets can be achieved by analysing the drug compound bound to its molecular target(s). The drug's ability to bind is also known as affinity.⁷ Specific chemical interactions between the drug and the molecular target will determine its affinity.¹⁹ The affinity of a covalent compound allows for the identification and verification of molecular targets to be a simple process. However, for non-covalent drugs the specific chemical interactions are reversible and therefore detection of the molecular target can prove difficult.

In the laboratory, protein validation can comprise of a number of techniques. Competition experiments between compounds with similar chemical structure, chemical functionality, or activity towards a known target can be utilised as a tool to validate a specific target protein.²⁰ Genetics can be used during *in vivo* and *in vitro* studies to produce transgenic or knockout models. These can then be utilised as pharmacological validation techniques, where knockout or point mutations can be introduced and tested for the viability of a target.²¹ However, this only provides further evidence of the pharmacological effects and does not give direct evidence of the molecular targets and the exact chemical mechanism. A direct approach in identifying protein targets involves the isolation of the drug directly bound to its target. This generally involves labelling of potential proteins with the drug of interest. Labelling or pull-down methods can be optimised to allow incubation with the protein or cell lysate followed by purification and analysis of potential targets by techniques such as liquid chromatography coupled with mass spectroscopy (LCMS) and protein immunoblotting.^{22,23} Examples of such techniques include

affinity tagged proteins such as biotin tagged drugs.²² Although this is the most direct approach in identifying protein targets, there are still disadvantages especially when dealing with non-covalent drugs. Direct techniques rely upon non-covalent drugs to have a high affinity towards the protein target.^{22,23} Large amounts of extracts are generally required followed by stringent washing when using direct approach methods.²³ Pharmacological and toxicological effects can be missed through stringent washing. Therefore, stringent washing introduces bias towards higher affinity binding drugs.²⁴

Covalent non-reversible drugs provide a potential solution to the disadvantages that non-covalent reversible drugs currently possess. Typically, this involves the use of medicinal chemists and the strategic manipulation of functional groups to create a bespoke irreversible drug probe.¹⁸ The irreversible probe must still be pharmacologically or toxicologically relevant compared with the original compound. An example of an irreversible probe has been achieved with sulforaphane. Sulforaphane is a naturally occurring compound found in vegetables and is well known for its anti-inflammatory and antioxidant properties.²⁵ The chemical mechanism of sulforaphane is reversible (shown in Figure 1.1A) and therefore poses as an obstacle during the purification process as this disrupts the binding of sulforaphane, yielding very little data about its targets. The use of chemical manipulation has resulted in an irreversible version of sulforaphane allowing validation of its target molecule (Figure 1.1B).²⁵ The bias views towards non-covalent interactions within drug discovery are now beginning to change due to the potential advantages that covalent interactions offer.

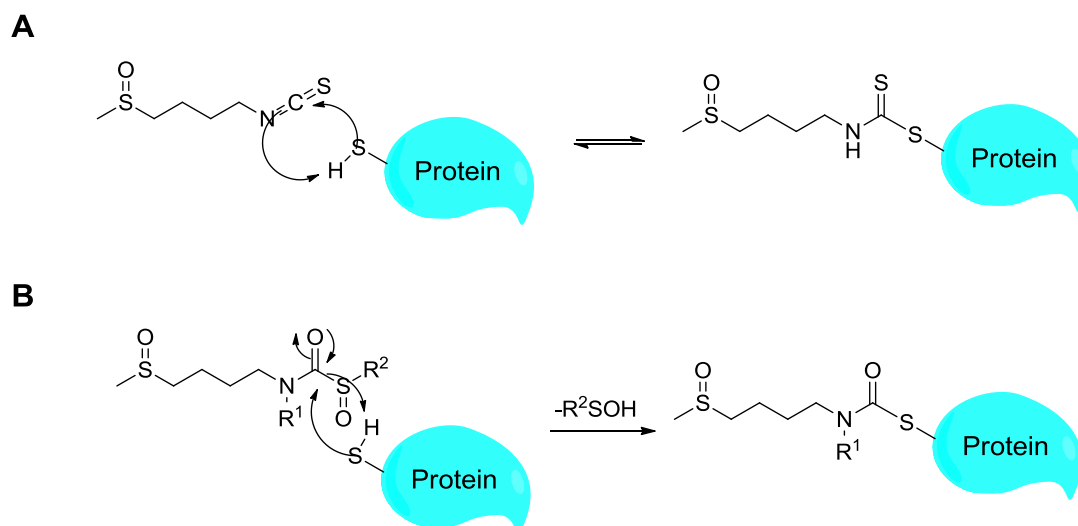


Figure 1.1: (A) Reversible chemical mechanism of sulforaphane and a thiol on a protein. (B) Template analogue of irreversible sulforaphane where R^1 and R^2 are chemically modifiable points. Irreversible chemical mechanism of the template analogue towards a thiol on a protein. Figure adapted from Ahn *et al* 2010.²⁵

ADRs and toxic events can be lessened through optimisation, careful design of strategically placed electrophiles (that lead to the selective covalent modifications of the target protein) and reducing off target interactions.¹⁰ Two classes of promising drug compounds are the antimalarial endoperoxides and anticancer compounds from the CDDO series and endoperoxide series. These two classes of compounds have demonstrated extraordinary pharmacological activity within their potential fields of treatment. However, there are also concerns over their safety and use in practise as potential ADRs could occur during clinical use. The endoperoxides such as the artemisinins are the front line drug for the treatment of malaria. The CDDO series are a promising class of drugs that can be used for the treatment of inflammation and cancers. These two classes of drugs are therefore

important but their mechanisms of action and biological targets are still poorly understood. These classes of compounds will be discussed further below.

1.3. Malaria - Antimalarials

Malaria is a preventable and curable disease caused by various species of parasite from the genus *Plasmodium*. It is transmitted to humans through the bite of an infected female *Anopheles* mosquito.^{26,27} Although there are many different types of *Plasmodia*, only four types are known to cause malaria in humans; *Plasmodium falciparum*, *Plasmodium vivax*, *Plasmodium malariae* and *Plasmodium ovale*. Of these, *Plasmodium falciparum* results in the highest number of deaths.²⁶ An estimated 207 million cases of malaria and 0.6 million associated deaths were reported in 2012, with the majority being among African children.²⁸ Drug resistance to traditional antimalarial treatments have now become prevalent in disease endemic areas, fuelling the search for new antimalarial drugs that are active against drug-insensitive parasites.²⁹ Endoperoxides such as artemisinin are currently the first line treatment for drug resistant malaria and therefore an important class of drugs.

1.3.1. Artemisinin

Artemisinin is a naturally occurring compound that is also known as qinghaosu.³⁰ The chemical structure was elucidated in 1972 and was used by the Chinese as a herbal infusion.³¹ Artemisinin-based combination therapy (ACT) is currently the first line treatment for drug resistant malaria. The mechanism of action of artemisinin has yet to be fully defined, although one widely accepted concept involves the

formation of toxic carbon-centred radicals within the parasite (Figure 1.2).³² This requires a ferrous iron source that can cleave the endoperoxide bridge of the parent compound.^{32,33} The food vacuole within the parasite contains a high concentration of heme due to hemoglobin degradation. It is proposed that free heme in oxidation state two (Fe^{2+}) can catalyse the formation of oxy radicals *via* reductive activation of the endoperoxide bridge.³⁴ The oxy radical products undergo rearrangement to form a primary carbon-centred radical or secondary carbon-centred radical species.³⁴ The carbon-centred radicals are thought to react with proteins, lipids and amino acids by alkylation reactions or peroxidation forming non-reversible covalent adducts which ultimately leads to parasite death.^{35,36}

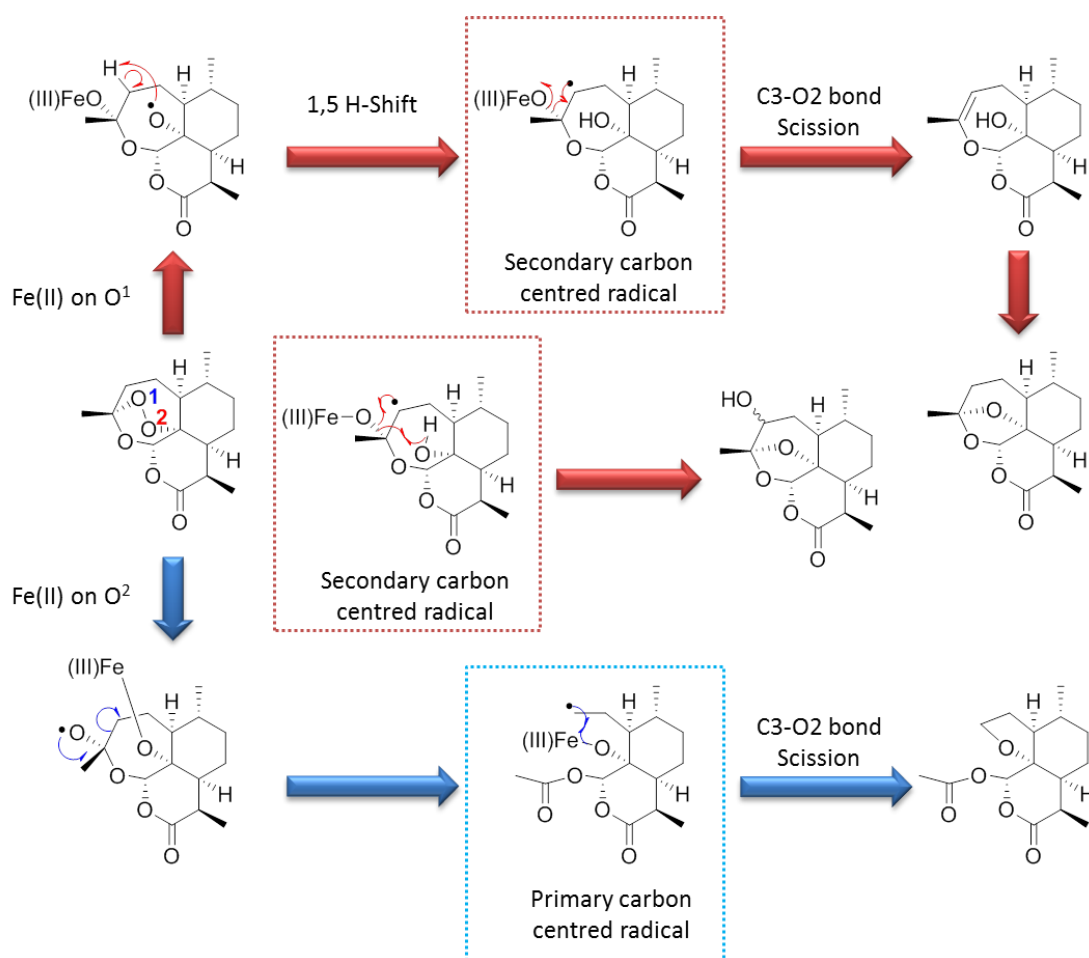


Figure 1.2: Suggested chemical mechanism underlying the antimalarial action of artemisinin, based on the formation of the primary and secondary carbon-centred radicals.³³

1.3.1.1. Model studies

As described above, the formation of primary and secondary carbon centred radicals is thought to be involved in artemisinin's mode of action. Although it is postulated that radical alkylation or peroxidation of essential molecular target(s) is key to parasitic cell death, the exact molecular target is yet to be defined. A couple of decades ago, biomedical scientists were unfamiliar with the chemical processes that artemisinins undergo.³⁷ Hence, collaboration with chemists resulted in the generation of different theories about artemisinins mechanism of action.³⁸

Potential mechanisms of action include:

- Heme which is a suggested molecular target since the malaria life cycle involves the degradation of hemoglobin and the formation of free heme. The heme is located in the food vacuole and it has been shown that alkylated heme cannot crystallise therefore resulting in toxic levels of heme and inhibition of hemozoin formation.³⁹
- Alkylation of cysteine residues in proteins. Functional proteins/ enzymes containing ferric iron can also catalyse the cleavage of the endoperoxide bridge resulting in bioactivation and formation of C-radical intermediates. These radicals can be quenched by GSH or alkylated within or in close proximity to important cysteine residues resulting in inhibition of important functional proteins/ enzymes.⁴⁰

In recent years, artemisinin resistant parasites have emerged in Southeast Asia, further inhibiting efforts to halt the spread of malaria in this region.^{26,30,41} The validity of the present theories are yet to be proved and therefore understanding and identifying the main targets will help develop more effective and safer antimalarial drugs.

1.3.2. Next-generation synthetic antimalarial drugs

Due to the emergence of drug-resistant malaria parasite, great efforts are being made to design and develop novel antimalarial drugs with improved efficacy, bioavailability and potency. The active pharmacophore within artemisinin is understood to be the endoperoxide bridge.⁴² Using this knowledge, new synthetic derivatives have been produced that are cheaper, less reliant on the availability of

natural precursors, and pharmacologically more active than current antimalarial drugs. Examples include the trioxolane OZ277 (arterolane), OZ439 and the tetraoxane RKA182 (Figure 1.3).^{30,32}

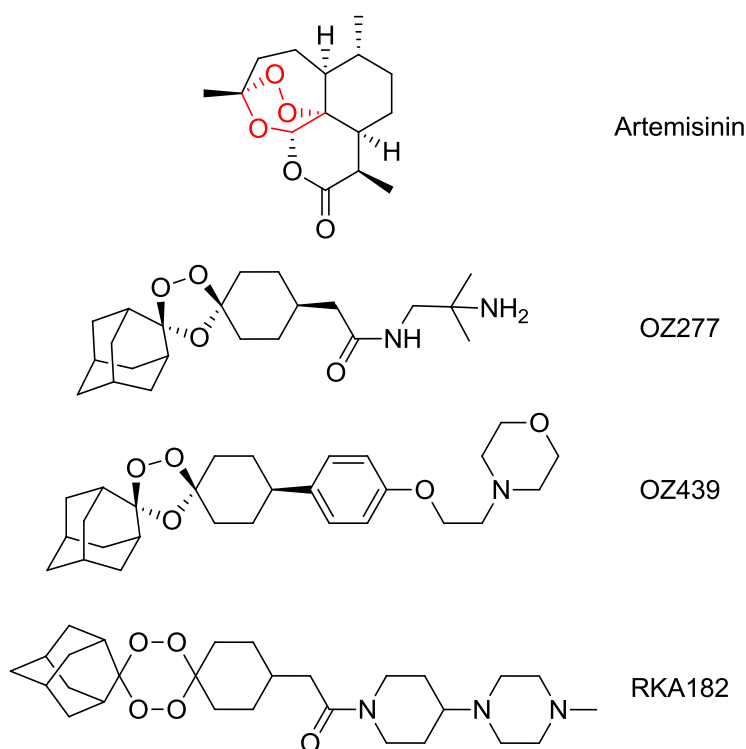


Figure 1.3: Artemisinin with the active pharmacophore endoperoxide bridge highlighted, trioxolane OZ277, OZ439 and tetraoxane RKA182.³²

1.3.2.1. Trioxolanes and tetraoxanes

OZ277 was approved in 2012 for use on the Indian market as a combination drug with piperazine phosphate for the treatment of malaria. OZ277 is a 1,2,4-trioxolane that was first discovered by the Vennerstrom group.⁴³ Since then, hundreds of peroxide derivatives have been synthesised including 1,2-dioxolane, 1,2,4-trioxane and 1,2,4,5-tetraoxanes (Figure 1.4).³⁵

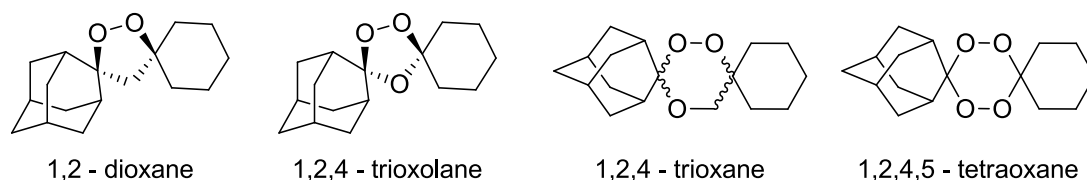


Figure 1.4: General template structure for 1,2-dioxane, 1,2,4-trioxolane, 1,2,4-trioxane and 1,2,4,5-tetraoxanes.³⁵

In a phase II clinical trial, OZ277 was found to be unstable in the plasma of malaria patients, causing the compound to have an unacceptably short half-life.³⁰ OZ439, is a second generation derivative with improved pharmacokinetics and enhanced *in vivo* antimalarial activity.⁴⁴ Tetraoxanes, such as the 1,2,4,5-tetraoxane RKA182 discovered by the O'Neill group,³⁰ have shown greater stability in plasma compared to the trioxolanes. They are cheap to produce as the tetraoxanes are achiral and are easily synthesised using inexpensive materials.⁴⁵ RKA182 is the first water soluble tetraoxane that has antimalarial activity and is currently undergoing preclinical trials.³⁰ Although both trioxolanes and tetraoxanes have impressive antimalarial activities, the mechanism of action of these compound classes is still under debate. However, it is suggested that they have a similar mechanism to that of artemisinin, with ferrous iron catalysing the formation of toxic carbon-centered radicals and alkylation of important parasitic proteins.³³ Understanding the chemical and molecular mechanisms of action of these natural and synthetic series of antimalarial drugs will ultimately aid their on-going chemical optimisation, minimise toxic liabilities, and thus enhance their clinical utility.

1.4. CDDO and derivatives

2-Cyano-3,12-dioxooleana-1,9(11)-dien-28-oic acid (CDDO), 2-cyano-3,12-dioxooleana-1,9-dien-28-imidazolide (CDDO-Im) and methyl 2-cyano-3,12-dioxooleana-1,9(11)-dien-28-oate (CDDO-Me, bardoxolone methyl) are all semi-synthetic derivatives of oleanolic acid synthesised by the Sporn group (Figure 1.5).^{46,47} These compounds exhibit a wide range of properties including anti-inflammatory and anticancer activity. These compounds have generated great interest due to their multi-functionality and therapeutic potential.

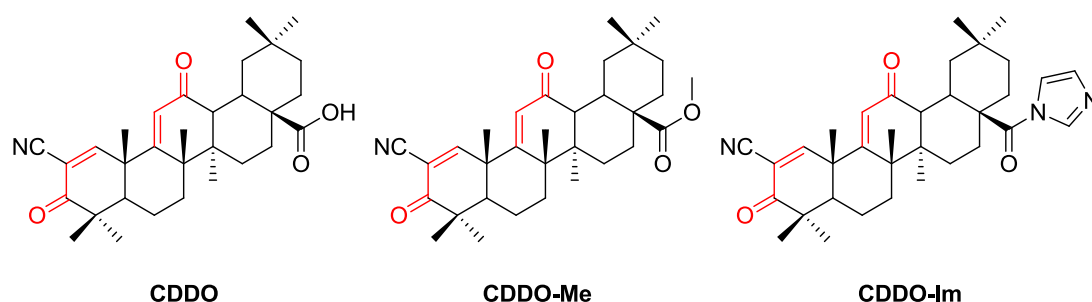


Figure 1.5: Chemical structure of CDDO, CDDO-Me and CDDO-Im with the α,β unsaturated carbonyl motifs highlighted.

1.4.1. Pharmacology of CDDO

It has often been documented that there is a strong correlation between inflammation and cancer.⁴⁸ Inflammation, oxidative stress and cell proliferation are said to promote the onset of cancers.⁴⁸ Oxidative stress is due to an imbalance between production of free radicals also known as reactive oxygen species (ROS) and antioxidant responses. This imbalance results in DNA damage and vital functional proteins.⁴⁹ Oxidative stress can result in the activation of a variety of transcription factors as a means of cell defence. This includes nuclear factor kappa

B (NF- κ B), nuclear factor erythroid 2-related factor 2 (Nrf2) and many more.⁴⁹

Molecules that activate this cell defence mechanism without the cause of oxidative stress are known as antioxidants.⁴⁹

CDDO and its analogues have substantial biological responses at nanomolar and micromolar concentrations in cell-based *in vitro* experiments (Figure 1.6). At low nanomolar concentrations, these compounds are antioxidants where they can suppress NF- κ B, *via* the direct inhibition of the inhibitor of nuclear factor kappa-B kinase subunit beta (IKK β),^{14,50} and activate cytoprotective Nrf2 signalling.^{15,51} In the micromolar range, the targets shift more towards actin-related protein 3 (ARP3) and other parts of the cytoskeleton, resulting in an inhibition of cell proliferation, and ultimately the induction of apoptotic cell death.⁵²

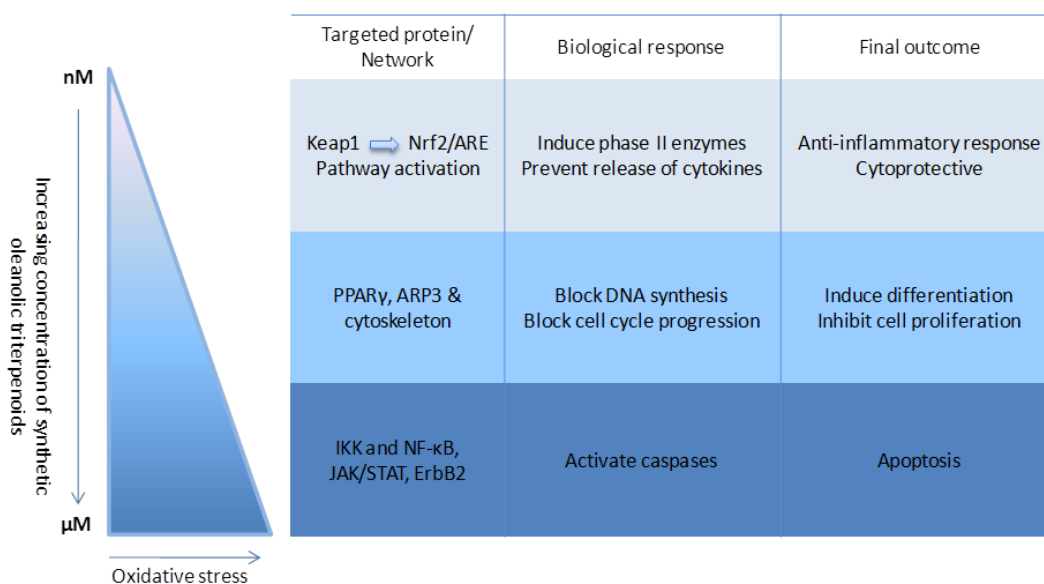


Figure 1.6: Dose-dependent biological responses of synthetic oleanolic triterpenoids. Adapted from Liby *et al* 2012.⁵²

Given that the CDDO series demonstrate impressive anti-inflammatory and anticancer properties, understanding how these novel naturally derived compounds exhibit their pharmacological and chemical activity are therefore important for future drug development.

1.5. Cellular protection against stress

Cells are constantly stressed by xenobiotics such as drugs, ROS, viral and other biological infections and environmental factors such as ultraviolet light.⁵³ Inflammation serves as a key mechanism of defence against such stresses, although prolonged/aberrant inflammation can be deleterious to health. In addition, mammalian cells have evolved means of detecting such cell stresses that result in the upregulation and increased expression of antioxidant and other cytoprotective genes in the presence of hazardous chemical and biological entities. Knowledge of the molecular mechanisms that regulate these processes has offered medicinal chemists opportunities to design compounds capable of manipulating their activities for therapeutic benefit.

1.5.1. Nuclear factor kappa B (NF- κ B)

NF- κ B is a transcription factor that can induce or repress the expression of inflammatory genes. There are five NF- κ B family members, transcription factor p65 (RelA or p65), transcription factor RelB (RelB), proto-oncogene c-Rel (c-Rel), nuclear factor NF-kappa-B p105 subunit (p50/p105 or NF- κ B1) and the nuclear factor NF-kappa-B p100 subunit (p52/p100 or NF- κ B2).³¹ NF- κ B exists as homo- or heterodimer of these subunits and is sequestered in the cytoplasm by isoforms of

inhibitors of nuclear factor kappa B (I κ B).⁴⁰ Activation of NF- κ B involves phosphorylation of I κ B by I κ B kinase (IKK), resulting in the dissociation of I κ B from NF- κ B, and enabling NF- κ B to translocate to the nucleus and manipulate the expression of inflammatory and other genes.^{10,40} The IKK complex is typically activated by pro-inflammatory cytokines such as tumour necrosis factor- α (TNF- α) and interleukin-1 (IL-1), or by ROS (Figure 1.7).

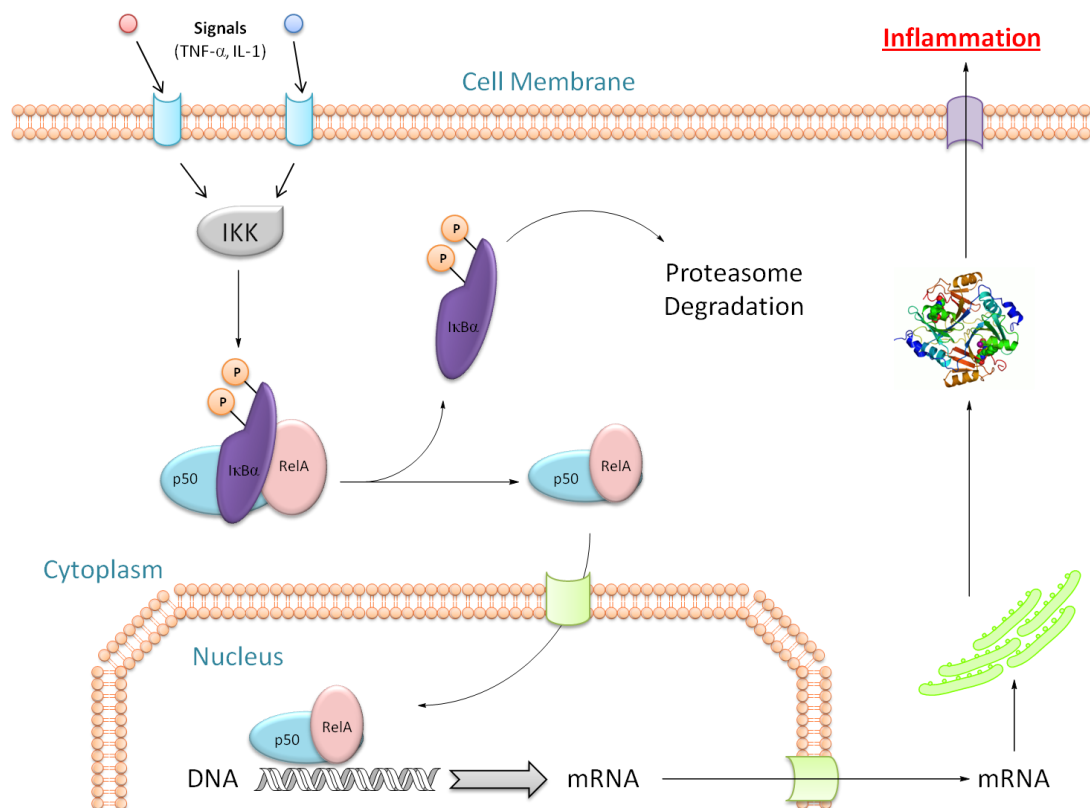


Figure 1.7: TNF- α or IL-1 activates IKK, which phosphorylates I κ B (I κ B α used in this example), resulting in the dissociation and nuclear translocation of NF- κ B (p50-RelA). Within the nucleus, NF- κ B induces the expression of pro-inflammatory genes.

1.5.2. Nuclear factor erythroid 2-related factor 2 (Nrf2)

Nrf2 is a transcription factor that regulates the basal and inducible expression of a large number of genes encoding detoxification enzymes, antioxidant protein and other stress response mediators.⁵⁴ Kelch-like ECH-associated protein 1 (Keap1) serves as the cytosolic repressor of Nrf2 by facilitating its ubiquitination and proteasomal degradation.^{55,56} Keap1 contains many cysteine residues that act as sensors of chemical and oxidative stress.⁵⁷ Modification of specific cysteine(s) by Nrf2 inducers is thought to cause a conformational change in Keap1, rendering it incapable of efficiently targeting Nrf2 for ubiquitination and proteasomal degradation.⁵⁸ This results in the saturation of Keap1 with Nrf2 and an accumulation of the transcription factor in the nucleus of stressed cells.^{57,59} Here, Nrf2 heterodimerises with cofactors such as small Mafs and binds to the antioxidant response element (ARE) in the promoter region of target genes, resulting in their transcriptional up-regulation.^{59,60} The net effect of this adaptive response is an increased capacity to detoxify chemical and oxidative stresses and limit their harmful cellular effects (Figure 1.8).

1.5.3. CDDO derivatives - potent inducers of Nrf2

CDDO and derivatives are well known inducers of Nrf2 at nanomolar concentrations.⁶¹ However, the chemical and molecular features that underlie the extraordinary potencies of CDDO derivatives as inducers of Nrf2 are unclear. The active pharmacophores of the CDDO derivative are the α,β unsaturated ketones located on the A and C ring (Figure 1.5). Ultraviolet (UV) and nuclear magnetic resonance (NMR) studies by Sporn *et al* have demonstrated that these compounds

have the potential to form covalent adducts to simple thiols *via* 1,4 conjugate addition.⁶² It has been proposed that CDDO derivatives interact with cysteine residues, particularly Cys-151, on Keap1.⁵⁵ However, confirmation is problematic due to the reversible nature of the conjugate addition reaction of CDDO. CDDO and their derivatives are less able to induce Nrf2 in cells expressing a Keap1 protein in which Cys-151 has been mutated.^{63,64} However, the ability of CDDO and derivatives to induce Nrf2 is unaltered in embryonic fibroblast derived from transgenic mice expressing a Keap1-Cys-151 mutant.⁵⁶ Therefore, the precise nature of the interaction between CDDO and derivatives and the Keap1-Nrf2 pathway requires clarification in order to support the ongoing optimisation of these compounds as therapeutic agents.

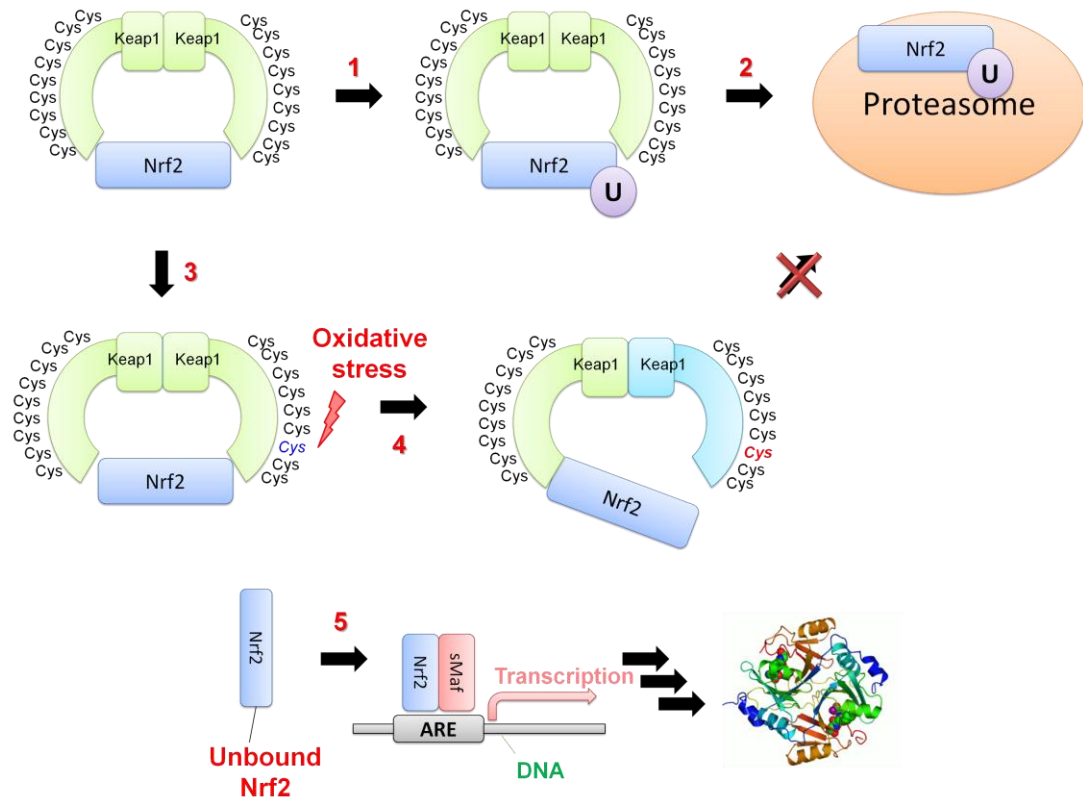


Figure 1.8: (1) Normal – Nrf2 is bound to Keap1 ready to be ubiquitinated within the cytosol; (2) Nrf2 relocates to the proteasome for degradation; (3) Under oxidative stress, cysteine residues act as sensors on Keap1. Changes to specific cysteine residues alters the structure of Keap1 such that it can no longer efficiently target Nrf2 for ubiquitination; (4) Nrf2 is no longer degraded and so Keap1 becomes saturated and newly-synthesised Nrf2 accumulates within the cell; (5) Nrf2 accumulates within the nucleus and heterodimerizes with other cofactors which binds to the ARE located in the promoter regions of target genes. This promotes transcription of cytoprotective genes, thereby reducing oxidative stress and inflammation.

1.6. Toxicity issues

In 2012, CDDO-Me, also known as bardoxolone methyl, was in phase III clinical trials for the treatment of advanced chronic kidney disease.⁶⁵ However, Reata Pharmaceuticals terminated this trial upon recommendation of the independent data monitoring committee, due to serious adverse reactions and mortality in patients.⁶⁶ The precise nature of these adverse events suggests cardiovascular causes were responsible for the ADRs and mortality of the patients.⁶⁷ However, the underlying chemical and molecular mechanism is unclear, yet such knowledge is vital if this class of compound is to have clinical utility.

1.7. Aims of this thesis

Given the uncertain chemical and molecular mechanisms of antimalarial endoperoxides and anti-inflammatory CDDO derivatives, this thesis aims to provide chemical tools to enable characterisation and in depth understanding of such mechanisms. As mentioned earlier direct techniques are the most advantageous. Such analysis to identify proteins utilising LCMS or protein immunoblotting analysis allows confidence and accuracy. Bespoke probes can be designed to explore the chemical mechanism and potential use of pull down experiments, resulting in the identification and verification of target proteins.

The identification of the molecular targets for these compounds will allow for the design of safer and more efficacious derivatives, along with the potential to influence current clinical practice. In order to achieve these aims, both CDDO and endoperoxide antimalarials will be synthesised to:

- I. Enabling identification of important pharmacophores and potential functionalization of certain groups will involve the development of a SAR profile. This will allow the development of strategies for medicinal chemistry optimisation of potency and drug metabolism and pharmacokinetics (DMPK) properties
- II. Create novel chemical probes which can be used to define the molecular targets of these compounds in biologically-relevant contexts. In the case of CDDO specifically, chemical probes are urgently required to test the hypothesis that Keap1 is indeed the molecular target responsible for the induction of Nrf2 by this compound.

1.8. References

- 1 Rang, H. P., Dale, M. M., Ritter, J. M., Flower, R. J. & Henderson, G. *Pharmacology*. Seventh edn, (Elsevier Churchill Livingstone, 2012).
- 2 Imming, P., Sinning, C. & Meyer, A. Drugs, their targets and the nature and number of drug targets. *Nature Reviews Drug Discovery* **5**, 821-834, doi:10.1038/nrd2132 (2006).
- 3 Swaminath, G., Deupi, X., Lee, T. W., Zhu, W., Thian, F. S., Kobilka, T. S. & Kobilka, B. Probing the β_2 Adrenoceptor Binding Site with Catechol Reveals Differences in Binding and Activation by Agonists and Partial Agonists. *Journal of Biological Chemistry* **280**, 22165-22171, doi:10.1074/jbc.M502352200 (2005).
- 4 Hirsh, J., Dalen, J. E., Anderson, D. R., Poller, L., Bussey, H., Ansell, J. & Deykin, D. Oral anticoagulants: Mechanism of action, clinical effectiveness, and optimal therapeutic range. *CHEST Journal* **119**, 8S-21S, doi:10.1378/chest.119.1_suppl.8S (2001).
- 5 Bonnefont, J., Courade, J.-P., Alloui, A. & Eschalier, A. Mechanism of the Antinociceptive effect of paracetamol. *Drugs* **63**, 1-4 (2003).
- 6 Sheen, C. L., Dillon, J. F., Bateman, D. N., Simpson, K. J. & Macdonald, T. M. Paracetamol toxicity: epidemiology, prevention and costs to the health - care system. *Quarterly Journal of Medicine* **95**, 609-619, doi:10.1093/qjmed/95.9.609 (2002).
- 7 Thomas, G. *Medicinal Chemistry an Introduction*. Second edn, (John Wiley & Sons Ltd, 2008).
- 8 Drews, J. Drug Discovery: A Historical Perspective. *Science* **287**, 1960-1964, doi:10.1126/science.287.5460.1960 (2000).
- 9 Kubinyi, H. Drug research: myths, hype and reality. *Nature Reviews Drug Discovery* **2**, 665-668, doi:10.1038/nrd1156 (2003).
- 10 Mah, R., Thomas, J. R. & Shafer, C. M. Drug discovery considerations in the development of covalent inhibitors. *Bioorganic & Medicinal Chemistry Letters* **24**, 33-39, doi:10.1016/j.bmcl.2013.10.003 (2014).
- 11 Singh, J., Petter, R. C., Baillie, T. A. & Whitty, A. The resurgence of covalent drugs. *Nature Reviews Drug Discovery* **10**, 307-317, doi:10.1038/nrd3410 (2011).
- 12 Gibson, G. G. & Skett, P. *Introduction to Drug Metabolism*. Third edn, (Nelson Thornes Publishers, 2001).
- 13 Park, B. K., Kitteringham, N. R., Maggs, J. L., Pirmohamed, M. & Williams, D. P. The role of metabolic activation in drug-induced hepatotoxicity. *Annual Review of Pharmacology and Toxicology* **45**, 177-202, doi:10.1146/annurev.pharmtox.45.120403.100058 (2005).
- 14 Housecroft, E. C. & Constable, C. E. *Chemistry*. 3rd edn, (Pearson Education Limited, 2006).
- 15 Clayden, J., Greeves, N., Warren, S. & Wothers, P. *Organic Chemistry*. 1st edn, (Oxford University Press, 2005).
- 16 Frieden, E. Non-covalent interactions: Key to biological flexibility and specificity. *Journal of Chemical Education* **52**, 754, doi:10.1021/ed052p754 (1975).

- 17 Rang, H. P., Dale, M. M., Ritter, J. M. & Moore, P. K. *Pharmacology*. Fifth edn, (Elsevier, 2006).
- 18 Johnson, D. S., Weerapana, E. & Cravatt, B. F. Strategies for discovering and derisking covalent, irreversible enzyme inhibitors. *Future Medicinal Chemistry* **2**, 949-964, doi:10.4155/fmc.10.21 (2010).
- 19 Ariëns, E. J., van Rossum, J. M. & Simonis, A. M. Affinity, intrinsic activity and drug interactions. *Pharmacological Reviews* **9**, 218-236 (1957).
- 20 Bunnage, M. E., Chekler, E. L. P. & Jones, L. H. Target validation using chemical probes. *Nature Chemical Biology* **9**, 195-199, doi:10.1038/nchembio.1197 (2013).
- 21 Gibbs, J. B. Mechanism-Based Target Identification and Drug Discovery in Cancer Research. *Science* **287**, 1969-1973, doi:10.1126/science.287.5460.1969 (2000).
- 22 Bantscheff, M., Scholten, A. & Heck, A. J. R. Revealing promiscuous drug–target interactions by chemical proteomics. *Drug Discovery Today* **14**, 1021-1029, doi:10.1016/j.drudis.2009.07.001 (2009).
- 23 Schenone, M., Dancik, V., Wagner, B. K. & Clemons, P. A. Target identification and mechanism of action in chemical biology and drug discovery. *Nature Chemical Biology* **9**, 232-240, doi:10.1038/nchembio.1199 (2013).
- 24 Ong, S.-E., Schenone, M., Margolin, A. A., Li, X., Do, K., Doud, M. K., Mani, D. R., Kuai, L., Wang, X., Wood, J. L., Tolliday, N. J., Koehler, A. N., Marcaurelle, L. A., Golub, T. R., Gould, R. J., Schreiber, S. L. & Carr, S. A. Identifying the proteins to which small-molecule probes and drugs bind in cells. *Proceedings of the National Academy of Sciences* **106**, 4617-4622, doi:10.1073/pnas.0900191106 (2009).
- 25 Ahn, Y.-H., Hwang, Y., Liu, H., Wang, X. J., Zhang, Y., Stephenson, K. K., Boronina, T. N., Cole, R. N., Dinkova-Kostova, A. T., Talalay, P. & Cole, P. A. Electrophilic tuning of the chemoprotective natural product sulforaphane. *Proceedings of the National Academy of Sciences* **107**, 9590-9595, doi:10.1073/pnas.1004104107 (2010).
- 26 WHO. *Malaria*, <http://www.who.int/mediacentre/factsheets/fs094/en/> Last updated: March 2013, Access date: **July 2013**.
- 27 WHO. *Do all mosquitoes transmit malaria?*, <http://www.who.int/features/ga/10/en/> Last updated: December 2009, Access date: **July 2013**.
- 28 WHO. *Factsheet on the World Malaria Report 2013*, http://www.who.int/malaria/media/world_malaria_report_2013/en/ Last updated: December 2013, Access date: **May 2014**.
- 29 Wells, T. N. C., Alonso, P. L. & Gutteridge, W. E. New medicines to improve control and contribute to the eradication of malaria. *Nature Reviews Drug Discovery* **8**, 879-891, doi:10.1038/nrd2972 (2009).
- 30 O'Neill, P. M., Amewu, R. K., Nixon, G. L., Bousejra ElGarah, F., Mungthin, M., Chadwick, J., Shone, A. E., Vivas, L., Lander, H., Barton, V., Muangnoicharoen, S., Bray, P. G., Davies, J., Park, B. K., Wittlin, S., Brun, R., Preschel, M., Zhang, K. & Ward, S. A. Identification of a 1,2,4,5-Tetraoxane Antimalarial Drug-Development Candidate (RKA 182) with Superior Properties to the

- Semisynthetic Artemisinins. *Angewandte Chemie International Edition* **49**, 5693-5697, doi:10.1002/anie.201001026 (2010).
- 31 Klayman, D. Qinghaosu (artemisinin): an antimalarial drug from China. *Science* **228**, 1049-1055, doi:10.1126/science.3887571 (1985).
- 32 Wang, X., Dong, Y., Wittlin, S., Charman, S. A., Chiu, F. C. K., Chollet, J., Katneni, K., Mannila, J., Morizzi, J., Ryan, E., Scheurer, C., Steuten, J., Santo Tomas, J., Snyder, C. & Vennerstrom, J. L. Comparative Antimalarial Activities and ADME Profiles of Ozonides (1,2,4-trioxolanes) OZ277, OZ439, and Their 1,2-Dioxolane, 1,2,4-Trioxane, and 1,2,4,5-Tetraoxane Isosteres. *Journal of Medicinal Chemistry* **56**, 2547-2555, doi:10.1021/jm400004u (2013).
- 33 Bousejra-El Garah, F., Wong, M. H.-L., Amewu, R. K., Muangnoicharoen, S., Maggs, J. L., Stigliani, J.-L., Park, B. K., Chadwick, J., Ward, S. A. & O'Neill, P. M. Comparison of the Reactivity of Antimalarial 1,2,4,5-Tetraoxanes with 1,2,4-Trioxolanes in the Presence of Ferrous Iron Salts, Heme, and Ferrous Iron Salts/Phosphatidylcholine. *Journal of Medicinal Chemistry* **54**, 6443-6455, doi:10.1021/jm200768h (2011).
- 34 O'Neill, P. M., Barton, V. E. & Ward, S. A. The Molecular Mechanism of Action of Artemisinin—The Debate Continues. *Molecules* **15**, 1705-1721, doi:10.3390/molecules15031705 (2010).
- 35 Tang, Y., Dong, Y. & Vennerstrom, J. L. Synthetic peroxides as antimalarials. *Medicinal Research Reviews* **24**, 425-448, doi:10.1002/med.10066 (2004).
- 36 Kaiser, M., Wittlin, S., Nehrbass-Stuedli, A., Dong, Y., Wang, X., Hemphill, A., Matile, H., Brun, R. & Vennerstrom, J. L. Peroxide Bond-Dependent Antiplasmodial Specificity of Artemisinin and OZ277 (RBx11160). *Antimicrobial Agents and Chemotherapy* **51**, 2991-2993, doi:10.1128/aac.00225-07 (2007).
- 37 Posner, G. H., Wang, D., Cumming, J. N., Oh, C. H., French, A. N., Bodley, A. L. & Shapiro, T. A. Further Evidence Supporting the Importance of and the Restrictions on a Carbon-Centered Radical for High Antimalarial Activity of 1,2,4-Trioxanes Like Artemisinin. *Journal of Medicinal Chemistry* **38**, 2273-2275, doi:10.1021/jm00013a001 (1995).
- 38 Wu, Y. How Might Qinghaosu (Artemisinin) and Related Compounds Kill the Intraerythrocytic Malaria Parasite? A Chemist's View. *Accounts of Chemical Research* **35**, 255-259, doi:10.1021/ar000080b (2002).
- 39 Kannan, R., Sahal, D. & Chauhan, V. S. Heme-Artemisinin Adducts Are Crucial Mediators of the Ability of Artemisinin to Inhibit Heme Polymerization. *Chemistry & Biology* **9**, 321-332, doi:10.1016/S1074-5521(02)00117-5 (2002).
- 40 Wu, Y., Yue, Z.-Y. & Liu, H.-H. New Insights into the Degradation of Qinghaosu (Artemisinin) Mediated by Non-Heme-Iron Chelates, and Their Relevance to the Antimalarial Mechanism. *Helvetica Chimica Acta* **84**, 928-932, doi:10.1002/1522-2675(20010418)84:4<928::AID-HLCA928>3.0.CO;2-I (2001).
- 41 Fairhurst, R. M., Nayyar, G. M. L., Breman, J. G., Hallett, R., Vennerstrom, J. L., Duong, S., Ringwald, P., Wellems, T. E., Plowe, C. V. & Dondorp, A. M. Artemisinin-Resistant Malaria: Research Challenges, Opportunities, and Public Health Implications. *The American Journal of Tropical Medicine and Hygiene* **87**, 231-241, doi:10.4269/ajtmh.2012.12-0025 (2012).

- 42 Meshnick, S. R. Artemisinin: mechanisms of action, resistance and toxicity. *International Journal for Parasitology* **32**, 1655-1660, doi:10.1016/S0020-7519(02)00194-7 (2002).
- 43 Vennerstrom, J. L., Arbe-Barnes, S., Brun, R., Charman, S. A., Chiu, F. C. K., Chollet, J., Dong, Y., Dorn, A., Hunziker, D., Matile, H., McIntosh, K., Padmanilayam, M., Santo Tomas, J., Scheurer, C., Scorneaux, B., Tang, Y., Urwyler, H., Wittlin, S. & Charman, W. N. Identification of an antimalarial synthetic trioxolane drug development candidate. *Nature* **430**, 900-904, doi:10.1038/nature02779 (2004).
- 44 MMV. OZ439, <http://www.mmv.org/research-development/project-portfolio/oz439> Last updated: 2013, Access date: **October 2013**.
- 45 Ellis, G. L., Amewu, R., Sabbani, S., Stocks, P. A., Shone, A., Stanford, D., Gibbons, P., Davies, J., Vivas, L., Charnaud, S., Bongard, E., Hall, C., Rimmer, K., Lozanom, S., Jesús, M., Gargallo, D., Ward, S. A. & O'Neill, P. M. Two-Step Synthesis of Achiral Dispiro-1,2,4,5-tetraoxanes with Outstanding Antimalarial Activity, Low Toxicity, and High-Stability Profiles. *Journal of Medicinal Chemistry* **51**, 2170-2177, doi:10.1021/jm701435h (2008).
- 46 Honda, T., Honda, Y., Favaloro Jr, F. G., Gribble, G. W., Suh, N., Place, A. E., Rendi, M. H. & Sporn, M. B. A novel dicyanotriterpenoid, 2-cyano-3,12-dioxooleana-1,9(11)-dien-28-onitrile, active at picomolar concentrations for inhibition of nitric oxide production. *Bioorganic & Medicinal Chemistry Letters* **12**, 1027-1030, doi:10.1016/S0960-894X(02)00105-1 (2002).
- 47 Honda, T., Rounds, B. V., Gribble, G. W., Suh, N., Wang, Y. & Sporn, M. B. Design and synthesis of 2-cyano-3,12-dioxoolean-1,9-dien-28-oic acid, a novel and highly active inhibitor of nitric oxide production in mouse macrophages. *Bioorganic & Medicinal Chemistry Letters* **8**, 2711-2714, doi:10.1016/S0960-894X(98)00479-X (1998).
- 48 Coussens, L. M. & Werb, Z. Inflammation and cancer. *Nature* **420**, 860-867, doi:10.1038/nature01322 (2002).
- 49 Reuter, S., Gupta, S. C., Chaturvedi, M. M. & Aggarwal, B. B. Oxidative stress, inflammation, and cancer: How are they linked? *Free Radical Biology and Medicine* **49**, 1603-1616, doi:10.1016/j.freeradbiomed.2010.09.006 (2010).
- 50 Yore, M. M., Liby, K. T., Honda, T., Gribble, G. W. & Sporn, M. B. The synthetic triterpenoid 1-[2-cyano-3,12-dioxooleana-1,9(11)-dien-28-oyl]imidazole blocks nuclear factor- κ B activation through direct inhibition of I κ B kinase β . *Molecular Cancer Therapeutics* **5**, 3232-3239, doi:10.1158/1535-7163.mct-06-0444 (2006).
- 51 Wilson, A. J., Kerns, J. K., Callahan, J. F. & Moody, C. J. Keep Calm, and Carry on Covalently. *Journal of Medicinal Chemistry* **56**, 7463-7476, doi:10.1021/jm400224q (2013).
- 52 Liby, K. T. & Sporn, M. B. Synthetic Oleanane Triterpenoids: Multifunctional Drugs with a Broad Range of Applications for Prevention and Treatment of Chronic Disease. *Pharmacological Reviews* **64**, 972-1003, doi:10.1124/pr.111.004846 (2012).
- 53 Sies, H. Oxidative stress: oxidants and antioxidants. *Experimental Physiology* **82**, 291-295 (1997).

- 54 Giudice, A., Arra, C. & Turco, M. in *Transcription Factors* Vol. 647 *Methods in Molecular Biology* (ed Paul J. Higgins) Ch. 3, 37-74 (Humana Press, 2010).
- 55 Bryan, H. K., Olayanju, A., Goldring, C. E. & Park, B. K. The Nrf2 cell defence pathway: Keap1-dependent and -independent mechanisms of regulation. *Biochemical Pharmacology* **85**, 705-717, doi:10.1016/j.bcp.2012.11.016 (2013).
- 56 Takaya, K., Suzuki, T., Motohashi, H., Onodera, K., Satomi, S., Kensler, T. W. & Yamamoto, M. Validation of the multiple sensor mechanism of the Keap1-Nrf2 system. *Free Radical Biology and Medicine* **53**, 817-827, doi:10.1016/j.freeradbiomed.2012.06.023 (2012).
- 57 Kensler, T. W., Wakabayashi, N. & Biswal, S. Cell Survival Responses to Environmental Stresses Via the Keap1-Nrf2-ARE Pathway. *Annual Review of Pharmacology and Toxicology* **47**, 89-116, doi:10.1146/annurev.pharmtox.46.120604.141046 (2007).
- 58 Zhang, D. D. Mechanistic Studies of the Nrf2-Keap1 Signaling Pathway. *Drug Metabolism Reviews* **38**, 769-789, doi:10.1080/03602530600971974 (2006).
- 59 Baird, L. & Dinkova-Kostova, A. The cytoprotective role of the Keap1-Nrf2 pathway. *Arch Toxicol* **85**, 241-272, doi:10.1007/s00204-011-0674-5 (2011).
- 60 Klaassen, C. D. & Reisman, S. A. Nrf2 the rescue: Effects of the antioxidative/electrophilic response on the liver. *Toxicology and Applied Pharmacology* **244**, 57-65, doi:10.1016/j.taap.2010.01.013 (2010).
- 61 Liby, K., Hock, T., Yore, M. M., Suh, N., Place, A. E., Risingsong, R., Williams, C. R., Royce, D. B., Honda, T., Honda, Y., Gribble, G. W., Hill-Kapturczak, N., Agarwal, A. & Sporn, M. B. The Synthetic Triterpenoids, CDDO and CDDO-Imidazolide, Are Potent Inducers of Heme Oxygenase-1 and Nrf2/ARE Signaling. *Cancer Research* **65**, 4789-4798, doi:10.1158/0008-5472.can-04-4539 (2005).
- 62 Couch, R. D., Browning, R. G., Honda, T., Gribble, G. W., Wright, D. L., Sporn, M. B. & Anderson, A. C. Studies on the reactivity of CDDO, a promising new chemopreventive and chemotherapeutic agent: implications for a molecular mechanism of action. *Bioorganic & Medicinal Chemistry Letters* **15**, 2215-2219, doi:10.1016/j.bmcl.2005.03.031 (2005).
- 63 Egger, A. L., Small, E., Hannink, M. & Mesecar, A. D. Cul3-mediated Nrf2 ubiquitination and antioxidant response element (ARE) activation are dependent on the partial molar volume at position 151 of Keap1. *Biochemical Journal* **422**, 171-180, doi:10.1042/bj20090471 (2009).
- 64 Ichikawa, T., Li, J., Meyer, C. J., Janicki, J. S., Hannink, M. & Cui, T. Dihydro-CDDO-Trifluoroethyl Amide (dh404), a Novel Nrf2 Activator, Suppresses Oxidative Stress in Cardiomyocytes. *PLoS ONE* **4**, e8391, doi:10.1371/journal.pone.0008391 (2009).
- 65 Pharmaceuticals, R. *Reata Pharmaceuticals Completes \$78 Million Equity Financing for Second Pivotal Trial of Bardoxolone Methyl*, [http://www.reatapharma.com/investors-media/news/news-timeline/archive/reata-pharmaceuticals-completes-\\$78-million-equity-financing-for-second-pivotal-trial-of-bardoxolone-methyl.aspx](http://www.reatapharma.com/investors-media/news/news-timeline/archive/reata-pharmaceuticals-completes-$78-million-equity-financing-for-second-pivotal-trial-of-bardoxolone-methyl.aspx) Last updated: 2013, Access date: **July 2013**.

- 66 Pharmaceuticals, R. *Company Statement: Termination of the BEACON Trial*, <http://www.reatapharma.com/investors-media/news/news-timeline/2012/company-statement-termination-of-beacon-trial.aspx> Last updated: 2013, Access date: **July 2013**.
- 67 de Zeeuw, D., Akizawa, T., Audhya, P., Bakris, G. L., Chin, M., Christ-Schmidt, H., Goldsberry, A., Houser, M., Krauth, M., Lambers Heerspink, H. J., McMurray, J. J., Meyer, C. J., Parving, H.-H., Remuzzi, G., Toto, R. D., Vaziri, N. D., Wanner, C., Wittes, J., Wrolstad, D. & Chertow, G. M. Bardoxolone Methyl in Type 2 Diabetes and Stage 4 Chronic Kidney Disease. *New England Journal of Medicine* **369**, 2492-2503, doi:10.1056/NEJMoa1306033 (2013).

CHAPTER 2

The synthesis and biological profiling of CDDO derivatives

Chapter 2

2.1. Introduction	47
2.1.1. Aims	49
2.2. Results and discussion	50
2.2.1. Chemical synthesis of CDDO and derivatives	50
2.2.2. Biological analysis	60
2.3. Conclusion	69
2.4. Chemistry Experimental	70
2.4.1. General	70
2.4.2. Purification of solvents and reagents	70
2.4.2.1. Purification of <i>meta</i> -chloroperoxybenzoic acid	70
2.4.3. Stains	71
2.4.4. Purification of products	71
2.4.5. Analysis	71
2.4.6. Numbering	72
2.4.7. Synthesis	73
2.5. Biological experimental	90
2.5.1. Materials	90
2.5.2. Cell culture	91
2.5.3. Plating	91
2.5.4. Treatment of cells for Nrf2 western blot analysis	92
2.5.5. Treatment of cells for luciferase activity assay.	92
2.5.6. Preparation of cells for luciferase reporter assay	93

Chapter 2 – The synthesis and biological profiling of CDDO derivatives

2.5.7. Preparation of cells for Nrf2 western blot analysis	93
2.5.8. Protein determination	93
2.5.9. Western blot analysis	94
2.5.9.1. 3-(<i>N</i> -morpholino)propanesulphonic acid (MOPS) running buffer	94
2.5.9.2. Transfer buffer	94
2.5.9.3. Tris-buffered saline solution (TBS-Tween)	94
2.5.9.4. Method	94
2.6. References	97

2.1. Introduction

CDDO and its methyl ester CDDO-Me (bardoxolone methyl) are well known potent inducers of Nrf2 (Figure 2.1). Both compounds were originally synthesised from oleanolic acid by the Sporn group.¹⁻⁵

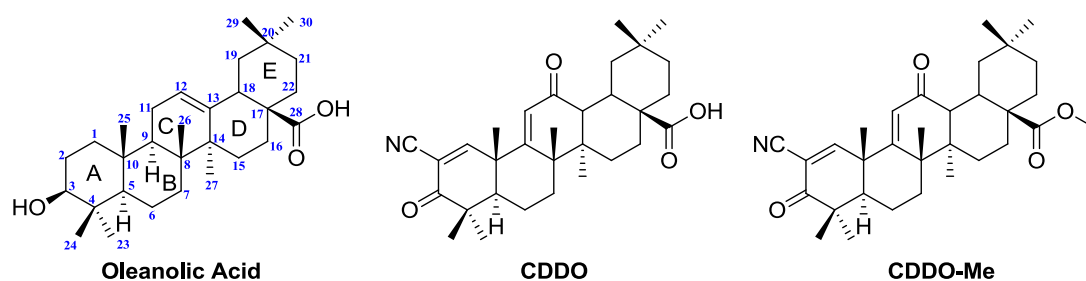


Figure 2.1: Chemical structure of Oleanolic acid, CDDO and CDDO-Me including the carbon numbering sequence.

As described in chapter 1, CDDO-Me is one of the most potent inducers of Nrf2 currently known. Unfortunately, the molecular mechanisms that underlie its potency are not completely understood. CDDO-Me was withdrawn from phase III clinical trials for the treatment of advanced chronic kidney disease due to cardiovascular adverse events and mortality. Therefore, a better understanding of the pharmacological and toxicological targets of CDDO-Me is required to prevent toxicity from occurring.⁶ The interaction of CDDO-Me with protein targets is hypothesised to be through reversible conjugation to thiols *via* a 1,4 conjugate addition process. The reversibility of CDDO-Me makes it more difficult to detect conjugate adducts yet most chemical biological techniques for detecting drug protein adducts deal with reversible acting drugs. Based on the chemical structure, there are two possible thiol reactive groups in the A ring and the C ring. It has been

suggested that the presence of the cyano group facilitates the reversible addition through increased acidity of the enolate intermediate.

The cyano group is a highly electron withdrawing group. The electron withdrawing effect pulls electrons from the double bond within the α,β unsaturated ketone. This enables weaker nucleophiles to attack at the α,β unsaturated ketone *via* a 1,4 conjugate addition. The cyano group can also stabilise a negative charge more effectively therefore enabling reversibility. Without the cyano group an intermediate enol is formed that can readily tautomerise into a ketone.⁷ The mechanism is shown in Figure 2.2.

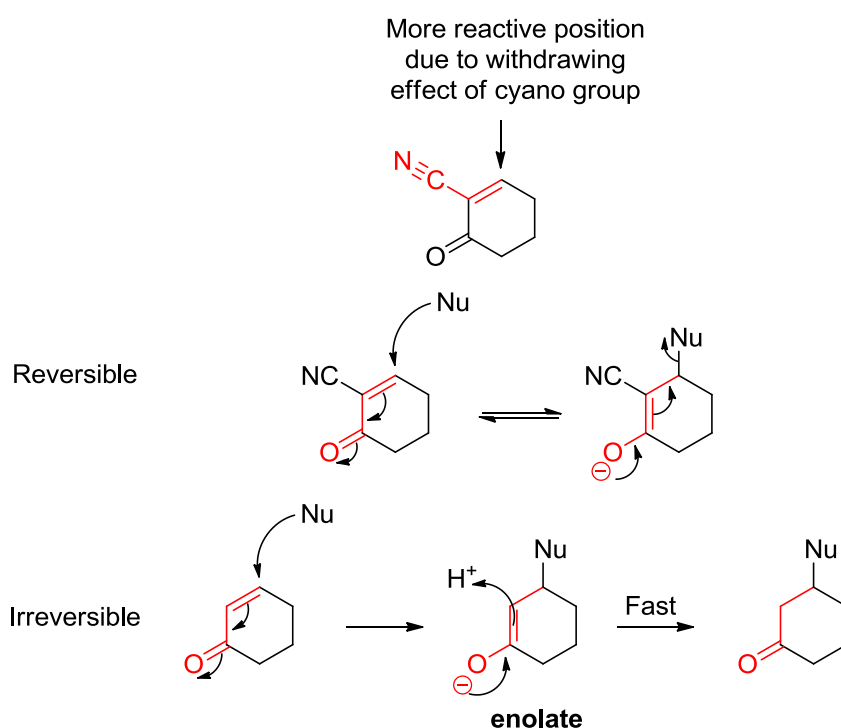


Figure 2.2: Reversible and irreversible nucleophilic attack and the effect of a withdrawing group.

2.1.1. Aims

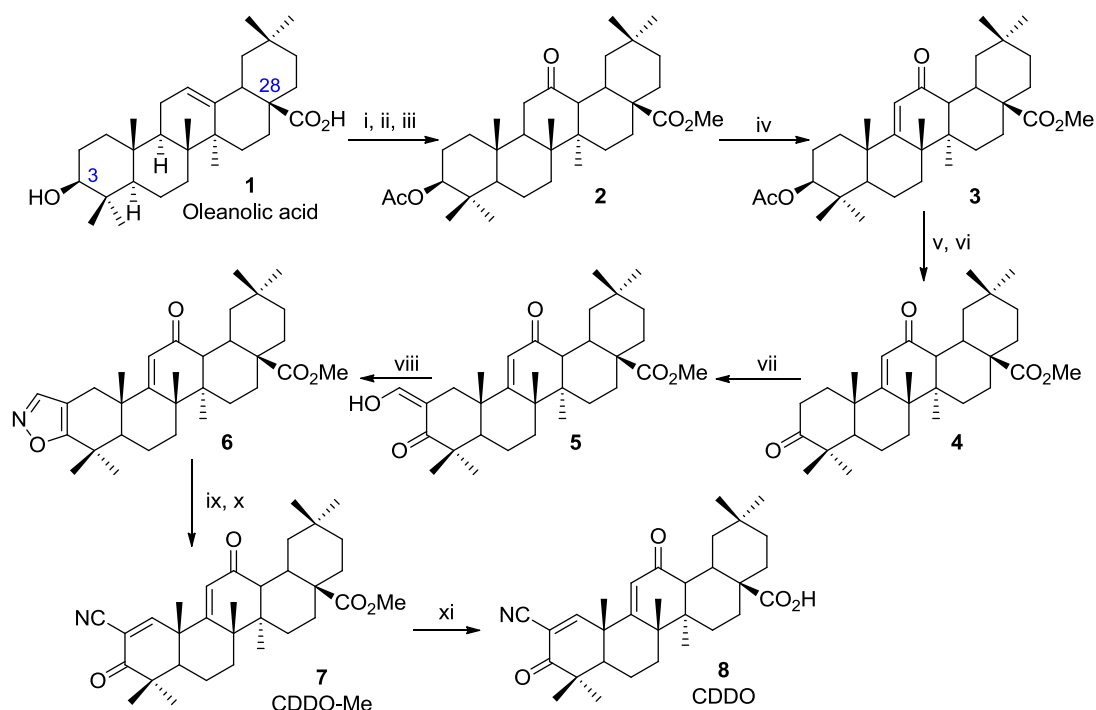
By understanding the chemistry of these compounds, it will be possible to design a compound capable of a non-reversible thiol reaction whilst maintaining biological activity. Such a compound would represent a novel tool with which to explore the critical targets of CDDO and its derivatives in relevant biological contexts. The aim of this section is to enable the production of such a compound by synthesising CDDO derivatives.

In addition, biological tests will involve screening for the induction of Nrf2 using western blotting and a high throughput screening assay based on H4IIE cells stably expressing the ARE8L-reporter. These will be conducted to ensure that the compounds are pharmacologically active.

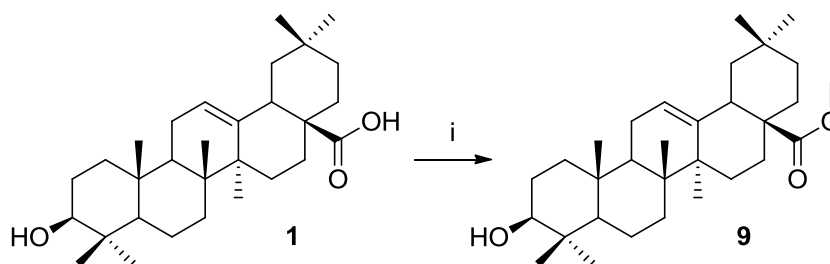
2.2. Results and discussion

2.2.1. Chemical synthesis of CDDO and derivatives

Synthesis of CDDO (**8**) from commercially available oleanolic acid (**1**) involves an eleven step process established by Sporn *et al.*¹⁻⁵ (Scheme 2.1) The initial reactions involve the protection of the carboxylic acid group at C-28 by methylation followed by the protection of the alcohol group at the C-3 position by acetylation with acetic anhydride to form an acetoxy group. The literature procedure employed diazomethane for the methylation of the carboxylic acid group. Due to the explosive properties of diazomethane and the need for a large scale reaction to protect the carboxylic acid, the less reactive trimethylsilyldiazomethane (TMS diazomethane) was used as an alternative.⁸ This reaction gave a 51% yield of **9** (Scheme 2.2). Although TMS diazomethane is safer to handle than diazomethane, scaling up the reaction can prove expensive due to the cost of TMS diazomethane. The TMS diazomethane route was used to provide authentic methyl ester protected material for subsequent spectral analysis.



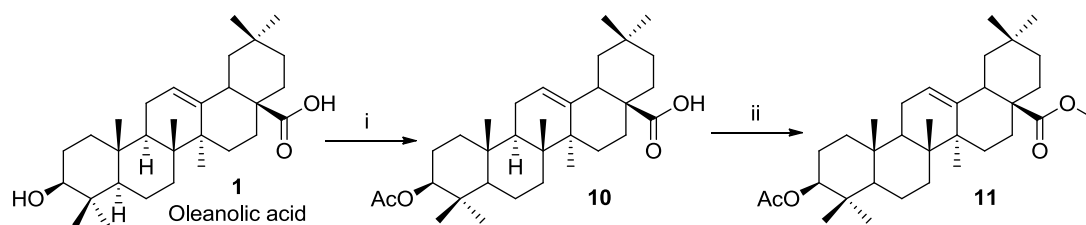
Scheme 2.1: Reagents and conditions: (i) CH_2N_2 , Et_2O , THF; (ii) Ac_2O , Pyr; (iii) 30% H_2O_2 , AcOH; (iv) Br_2 , HBr, AcOH; (v) KOH (aq) MeOH; (vi) 0°C , CrO_3 (2.5M) in $\text{H}_2\text{SO}_4:\text{H}_2\text{O}$ (1:4); (vii) HCO_2Et , MeONa, PhH; (viii) $\text{NH}_2\text{OH}\cdot\text{HCl}$, EtOH; (ix) MeONa, MeOH, Et_2O ; (x) DDQ, PhH; (xi) LiI, DMF.



Scheme 2.2: Reagents and conditions: (i) THF, MeOH, N_2 (g), TMS diazomethane (2.0M) (1.1 equiv) 51%.

Alternative routes were explored for the protection of the carboxylic acid group as well as the alcohol group. Protection of the alcohol group was achieved by acetylation of oleanolic acid. Triethylamine, acetic anhydride and 4-(dimethylamino) pyridine were the reagents used to obtain **10** in 95% yield (Scheme 2.3).

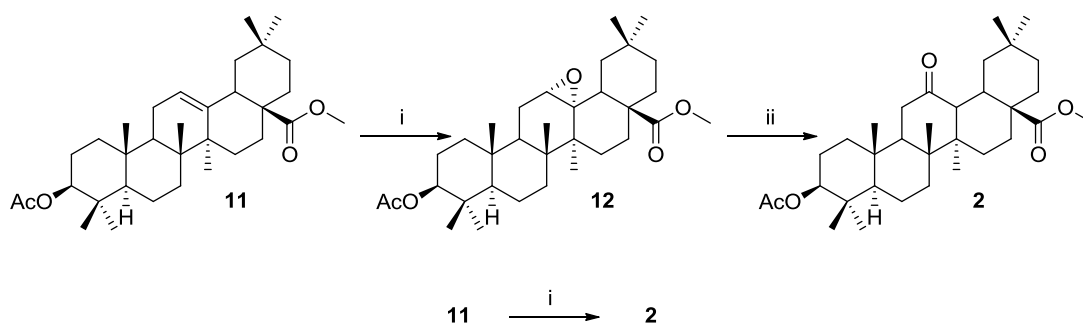
Methylation of **10** to protect the carboxylic acid using iodomethane and potassium carbonate⁹ gave a 97% yield of **11** (Scheme 2.3). By changing the initial reagents and sequence of protection, an alternative synthetic route was produced. This provided a safer solution during scale up unlike diazomethane which is toxic, expensive and potentially explosive in nature.



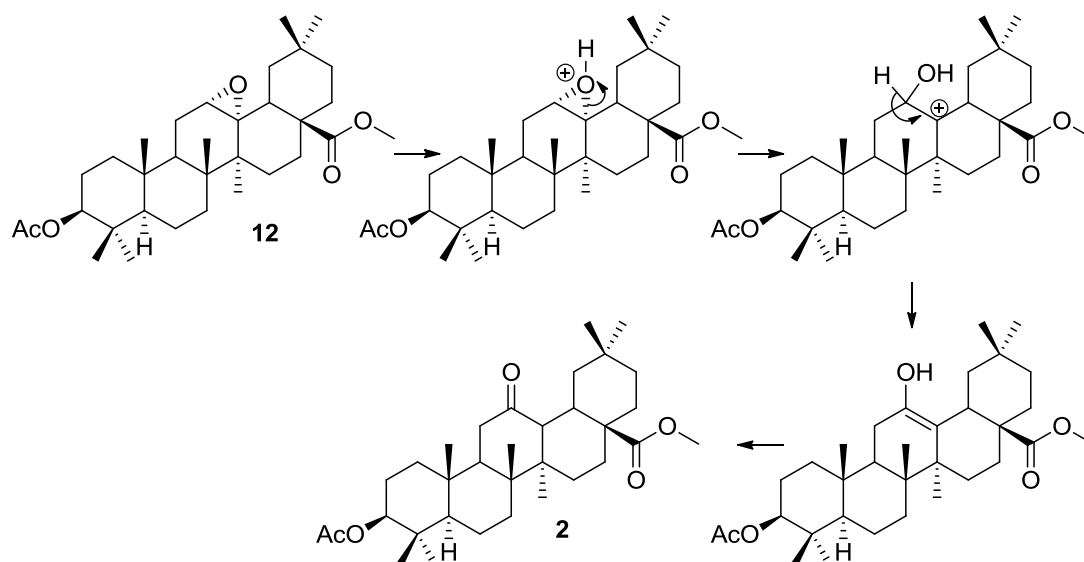
Scheme 2.3: Reagents and conditions: (i) DCM, NEt_3 (2 equiv), acetic anhydride (2.5 equiv), 4-(dimethylamino)pyridine (0.01 equiv), N_2 (g), 12 hours, 95%; (ii) MeI (4 equiv) K_2CO_3 (4 equiv), acetone, r.t., 24 hours, 97%.

Formation of **2** (Scheme 2.4) involves the epoxidation of **11** to **12** using *meta*-chloro-peroxybenzoic acid (*m*CPBA).¹⁰ The intermediate epoxide **12** was not isolated during the purification procedure. The reaction proceeded to give methyl 3-acetoxy-12-oxo-13-oleanolate (**2**) directly in 99% yield. This was confirmed by comparison with the ^{13}C NMR reported in the literature and mass spectrometry. The epoxide (**12**) is prone to ring opening to form a highly stabilised tertiary carbocation and upon loss of a proton, leads to the formation of the ketone (Scheme 2.5). During subsequent scale up of this step, the epoxide (**12**) was isolated and full analysis later matched published literature.¹¹ However, during purification by column chromatography, the epoxide was no longer observed. One explanation is that the acidic nature of the silica used for chromatographic purification, could have caused the epoxide to rearrange to form **2**. The literature preparation

required the use of $\text{BF}_3 \cdot \text{OEt}_2$ to cause the rearrangement of the epoxide, but this step was not required as the epoxide also proceeded to form **2** during the purification *via* flash column chromatography.



Scheme 2.4: Reagents and conditions: (i) mCPBA (1.2 equiv), DCM, 0°C to r.t. overnight; (ii) $\text{BF}_3 \cdot \text{OEt}_2$, benzene.

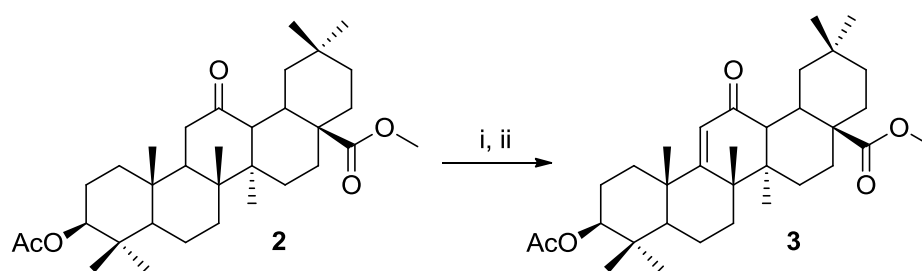


Scheme 2.5: Rearrangement of the epoxide to the target ketone.

The dehydrogenation of **2** to obtain **3** (Scheme 2.1) was initially unsuccessful leading to an unknown compound. Mass spectroscopy and NMR indicated hydrolysis of the methyl ester to a carboxylic acid had occurred. (Singlet peak located at $\delta 3.62$ in the ^1H NMR was no longer present). As well as dehydrogenation,

addition of hydrogen bromide was also observed. The exact structure could not be determined due to the overlapping of proton signals. However, mass spectrometry indicated the presence of bromine due to the bromine isotope peaks.

The most likely explanation for ester hydrolysis is the nature of the harsh reaction conditions used. The acetic acid was replaced with acetonitrile as the solvent, resolving the issue and producing the desired product in excellent yield.¹² Purification by recrystallisation from methanol gave compound **3** in 99% yield.



Scheme 2.6: Reagents and conditions: (i) HBr 48% (0.38 equiv), Br₂ [1.0M in MeCN] (1.08 equiv), MeCN, 35°C, 16 hr; (ii) Br₂ [1.0M in MeCN] over 5 mins, 1 hour, 99%.

The stereochemistry at C-18 was difficult to determine by NMR spectroscopy due to overlapping of proton signals in the ¹H NMR. The C-18 can have two configurations and the stereochemistry of this position has been shown to have an effect on anti-inflammatory activity.¹³ The *cis* isomer **1a** is the naturally occurring isomer for oleanolic acid. During the synthesis of CDDO derivatives, there is a possibility that the C-18 proton may change in configuration giving the *trans* isomer **1b**.

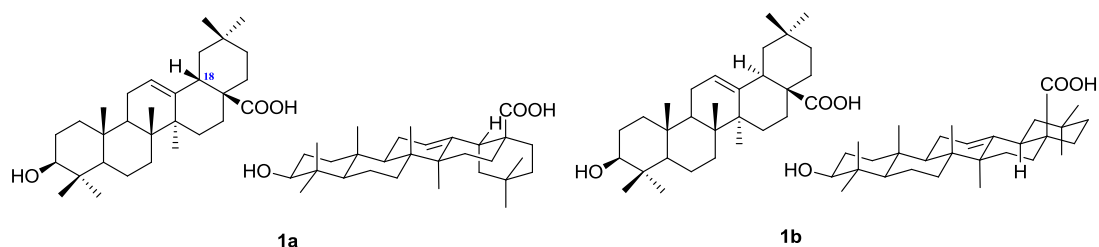


Figure 2.3: Stereochemistry of the C-18 proton from oleanolic acid.

An X-ray crystal structure of **3** was obtained (Figure 2.4) and confirmed that the configuration of the proton located on C-18 was as depicted (**3a**) i.e. *cis* and the stereochemistry from oleanolic acid was maintained (**1a**).

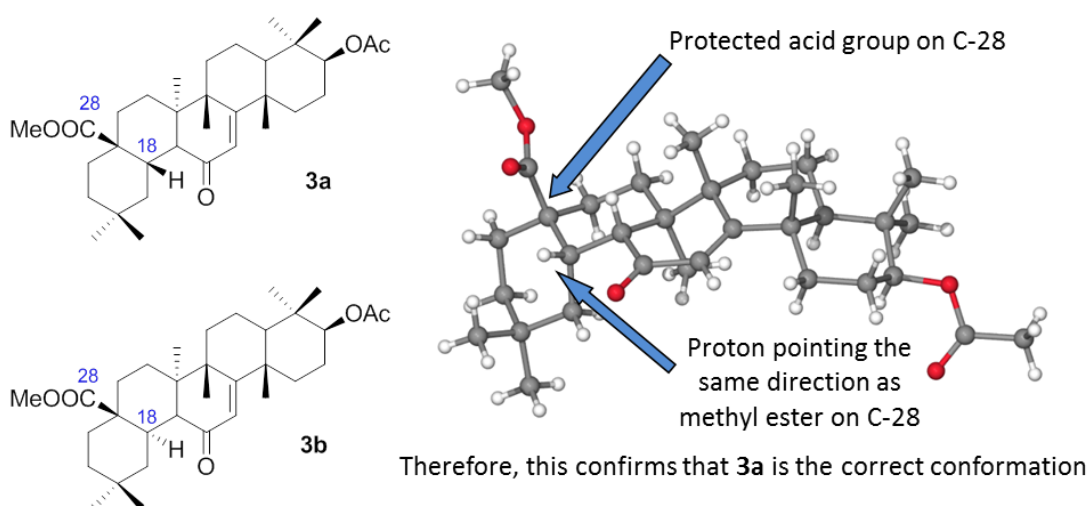
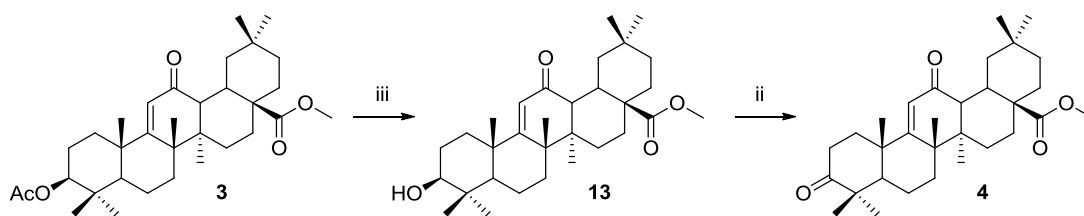


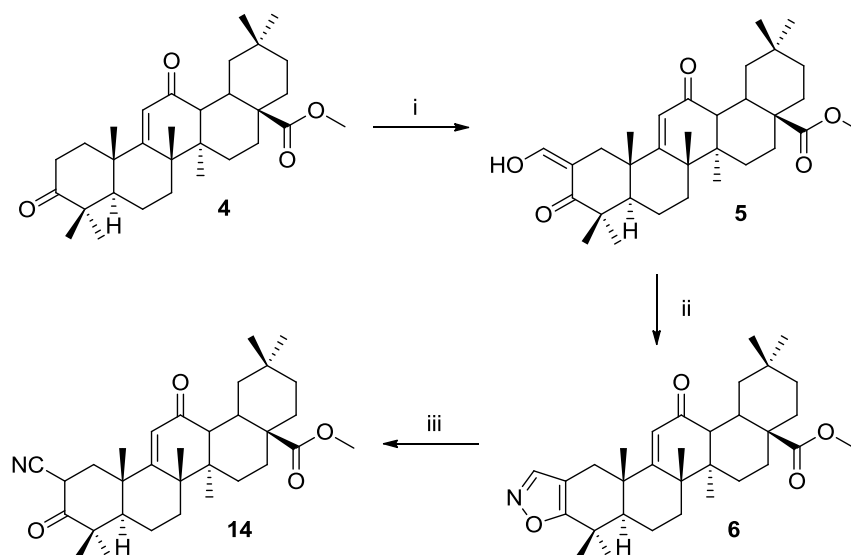
Figure 2.4: Chemical structures of two possible diastereoisomers and the X-ray crystal of intermediate **3**.

Deprotection of **3** to obtain the alcohol by refluxing with potassium hydroxide in methanol gave **13** in 99% yield.³ Oxidation of the alcohol at the C-3 position using the Jones reagent gave **4** in 99% yield. (Scheme 2.7)

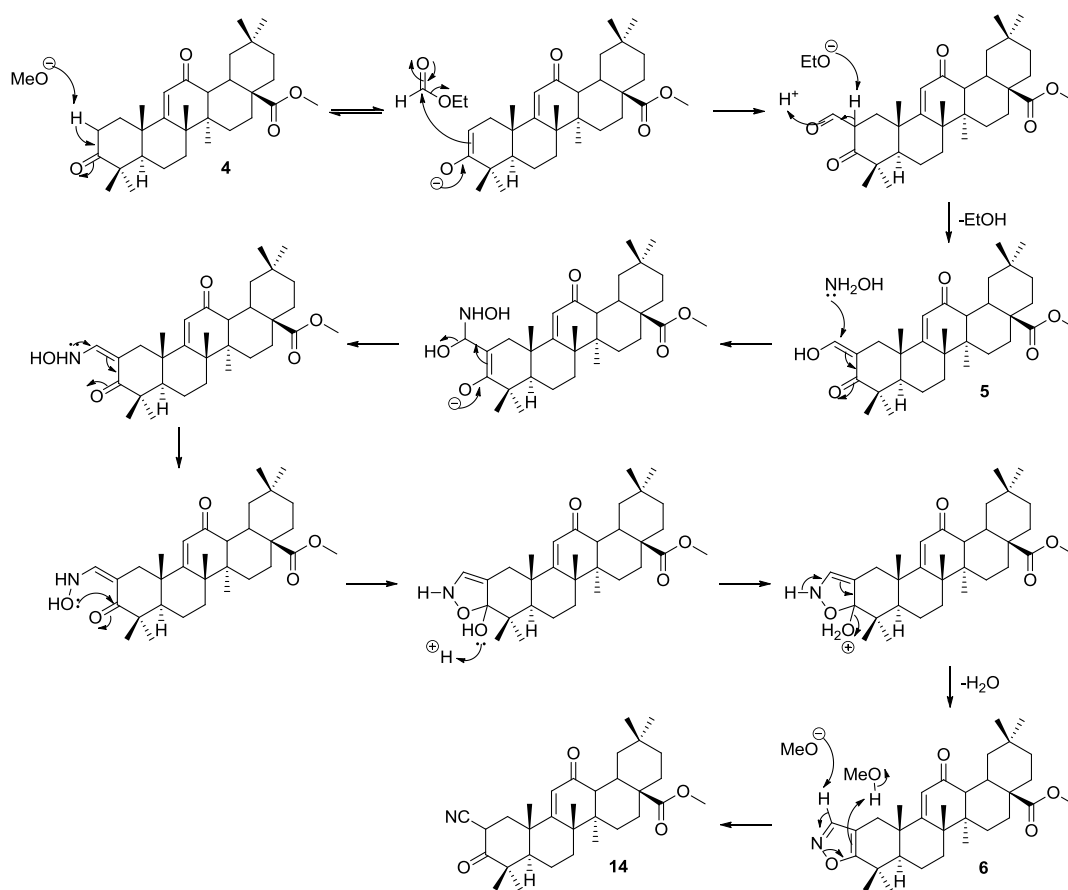


Scheme 2.7: Reagents and conditions: (i) KOH, MeOH, reflux, 30 mins, 99%; (ii) acetone, Jones reagent, 0°C stir, r.t. 10 mins, 99%.

Synthesis of **5** involved the use of sodium methoxide, ethyl formate and toluene under anhydrous conditions. The literature procedure used benzene as the solvent,² however, since toluene is less toxic and has similar properties to benzene, we utilised toluene for this reaction. Initially this reaction failed and the starting material **4** was obtained (confirmed by NMR). Utilising a fresh batch of sodium methoxide proved successful and yielded **5** in 98% yield (Scheme 2.8). The seven steps from oleanolic acid to **5** were also performed on a larger scale (4 g scale). During the scale up, the reactions were higher yielding than on a smaller scale. Cyclization of **5** involved refluxing in 9:1 ethanol:water with $\text{NH}_2\text{OH}\cdot\text{HCl}$ to obtain **6** in 86% yield.³ In order to prepare **14**, compound **6** was allowed to react with sodium methoxide in methanol and diethyl ether. The reaction was initially at 0°C then room temperature for 45 minutes to give **14** in 70% yield.³ (Scheme 2.8) The chemical mechanism to convert compound **4** to **14** is shown in Scheme 2.9.

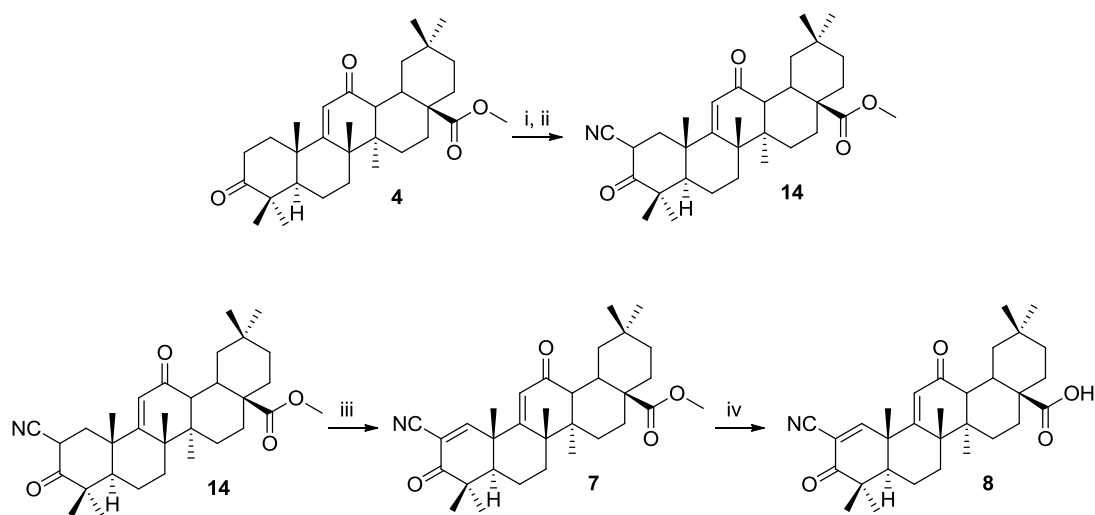


Scheme 2.8: *Reagents and conditions:* (i) MeONa (6.05 equiv), toluene, ethyl formate (4.5 equiv), r.t., 2 hours, 98%; (ii) EtOH:H₂O (9:1), NH₂OH·HCl (10 equiv), reflux, 1 hour, 86%; (iii) MeOH, Et₂O, NaOMe (34 equiv), 0°C to r.t. 45 mins, 70%.



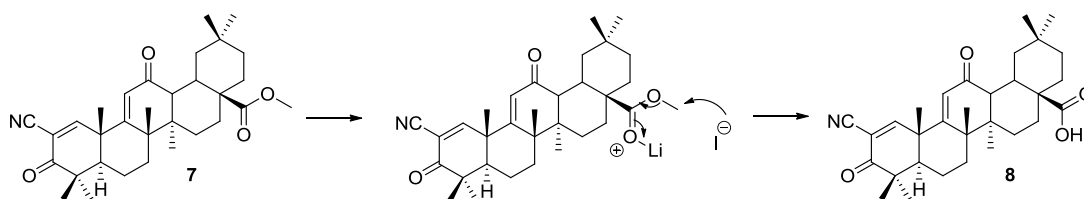
Scheme 2.9: Synthesis of **4** to **14** and their chemical mechanism of action.

Compound **14** could be obtained from compound **4** using an alternative reaction shown in Scheme 2.10. The synthetic step involved an addition reaction. Here a nitrile functional group was added onto C-2 and reduced the synthetic pathway to nine steps. Compound **4** was treated with LDA at -78°C to form an intermediate enolate anion which was treated with *p*-TscN to obtain **14** in 88% yield.



Scheme 2.10: *Reagents and conditions:* (i) LDA (1.5 equiv) [2.0M heptane/THF/ethyl benzene], THF, N_{2(g)}, -78°C to r.t., 20 mins; (ii) *p*-TsCN (2 equiv), -78°C, 5 mins; (iii) DDQ (1.72 equiv), anhydrous benzene, reflux, 15 mins, 87%; (iv) LiI (19 equiv), anhydrous DMF, N_{2(g)}, reflux, overnight.

Dehydrogenation of **14** required refluxing with 2,3-dichloro-5,6-dicyano-*p*-benzoquinone (DDQ) in anhydrous benzene for 1 hour gave **7** in 87% yield. Initially anhydrous toluene was also utilised as an alternative for benzene for this step, however, only starting material was obtained. The final step involved the hydrolysis of the methyl ester on C-28 to obtain the carboxylic acid functional group. Formation of CDDO (**8**) involved the use of lithium iodide in anhydrous DMF at reflux overnight to give CDDO in 44% yield. The mechanism is shown in Scheme 2.11. A side product was also obtained during this reaction (**15**) where NMR and mass spectra confirmed the side product. This could have been caused by a small amount of **14** being present during this reaction. This compound is useful for the SAR studies to compare the importance of CDDO (**8**) and CDDO without the double bond (**15**) located on the A ring.



Scheme 2.11: Chemical mechanism of lithium iodide hydrolysis

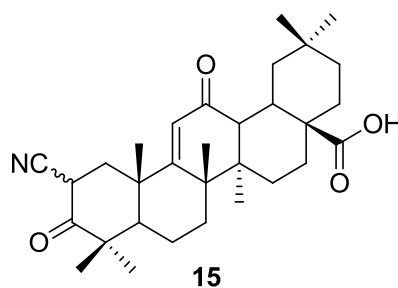


Figure 2.5: Side product obtained when using LiI in DMF.

2.2.2. Biological analysis

Following the chemical synthesis of CDDO and derivatives, SAR studies were performed to ensure the compounds that were synthesised were biologically active. As reported in the literature, CDDO derivatives provoke the accumulation of Nrf2 which induces the expression of phase II enzymes containing the ARE motifs in their promoter region.¹⁴

In order to determine the potency of CDDO and its derivatives, H4IIE rat hepatoma cells, stably transfected with a Nrf2-sensitive luciferase reporter transgene,¹⁵ were exposed to the compounds for 24 hours. Binding of Nrf2 to the ARE motifs located within the reporter transgene causes an increase in the expression of luciferase, which catalyses the conversion of luciferin to oxyluciferin with visible light

produced as a by-product. (Figure 2.6). H4IIE cell are known to express functional Nrf2 and down-stream regulated enzymes.¹⁵⁻¹⁷ Therefore, the amount of light produced is proportional to the amount of Nrf2 present.

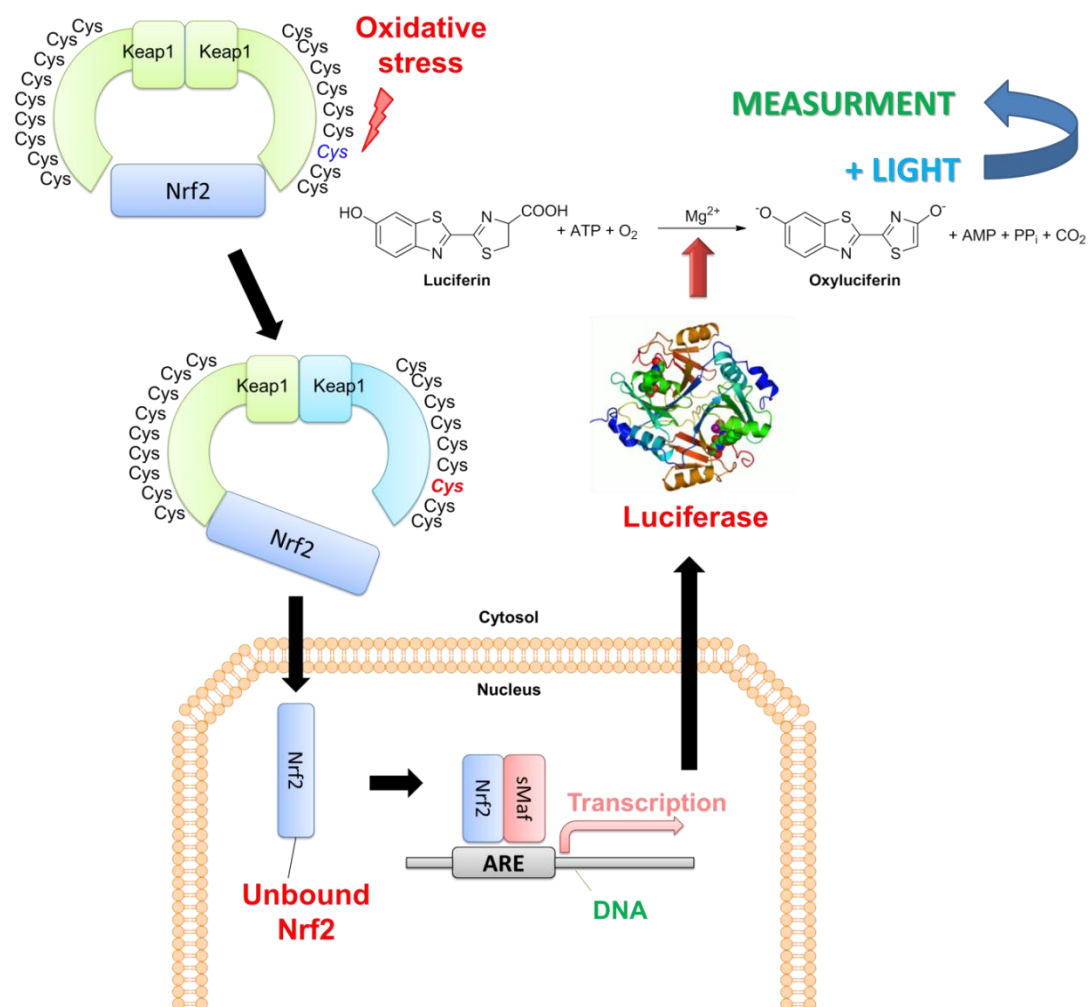


Figure 2.6: Schematic overview of the principle of the luciferase reporter assay for determination of Nrf2 activity in H4IIE-ARE cells. Oxidative stress modifies key cysteine residues located on Keap1. Nrf2 is no longer regulated by Keap1 and Nrf2 enters the nucleus. Binding of Nrf2 to the ARE motifs located within the reporter transgene causes an increase in the expression of luciferase, which catalyses the conversion of luciferin to oxyluciferin with visible light produced as a by-product. This light can be measured and directly correlates to the amount of Nrf2 present.

In order to confirm that CDDO-Me (**7**) was capable of inducing the accumulation of Nrf2 *per se*, H4IIE-ARE cells were exposed to increasing concentrations of CDDO-Me for 1 hour, and Nrf2 levels were determined by western blot. The data demonstrates that CDDO-Me provoked a concentration dependant accumulation of Nrf2 (Figure 2.7). CDDO-Me was also screened using the Luciferase reporter assay and compared to the western blot data. (Graph 2.2)

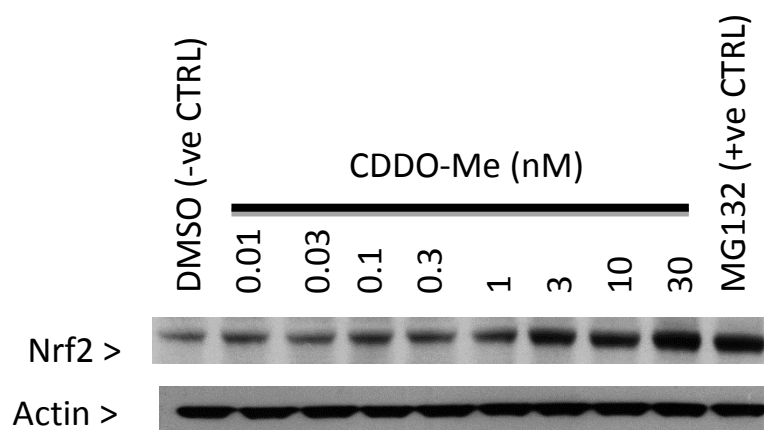
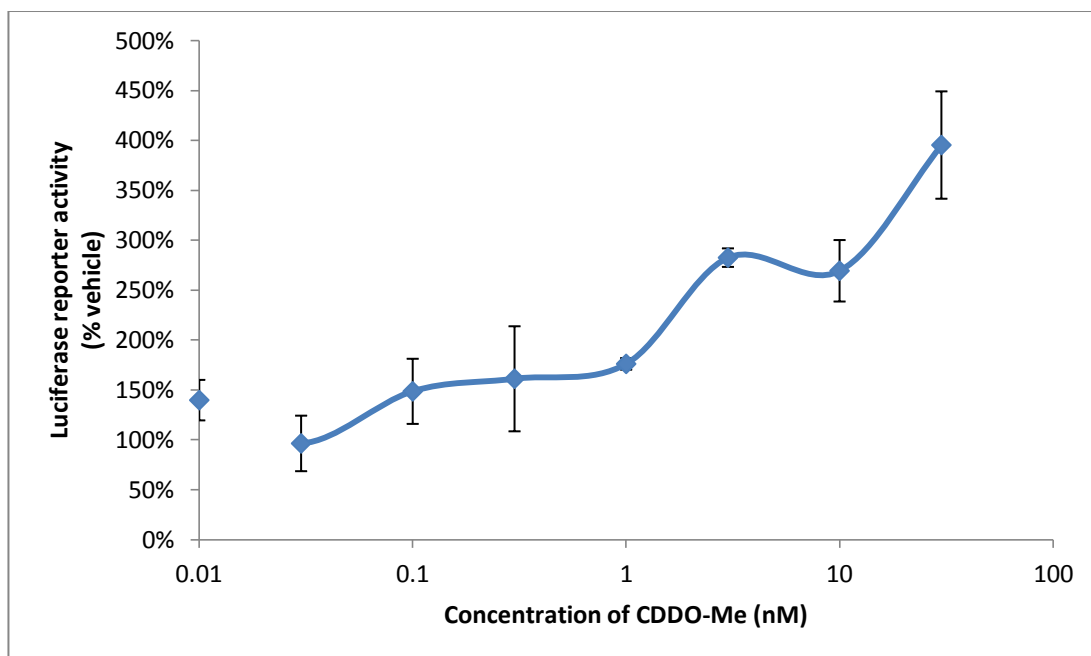


Figure 2.7: Western blot for Nrf2 and actin. CDDO-Me exposed to H4IIE-ARE cells for 1 hour over a range of concentrations.



Graph 2.1: Densitometry data from western blot. CDDO-Me was exposed to H4IIE-ARE cells for 1 hour. Data shown is the average of n=3 where Nrf2 values are normalised against actin.

The luciferase reporter assay was compared with the Nrf2 western blot data. The concentrations that were required to provoke a concentration dependent accumulation of Nrf2 also provoked an increase in luciferase activity.

Altogether fifteen intermediates were prepared during the synthesis of CDDO, of which seven were selected for screening using the luciferase reporter assay. The concentration range that was selected for the screening of these compounds is explained as followed. The highest concentration with no observable effect in luciferase activity was 0.001 nM during the screening of CDDO-Me, therefore this is kept as the lowest concentration range. Above 20 mM, most of these compounds are insoluble in DMSO, and maintaining a 0.5% DMSO content in each well will give a final concentration of 100 μ M. The 0.5% DMSO content in each well will ensure

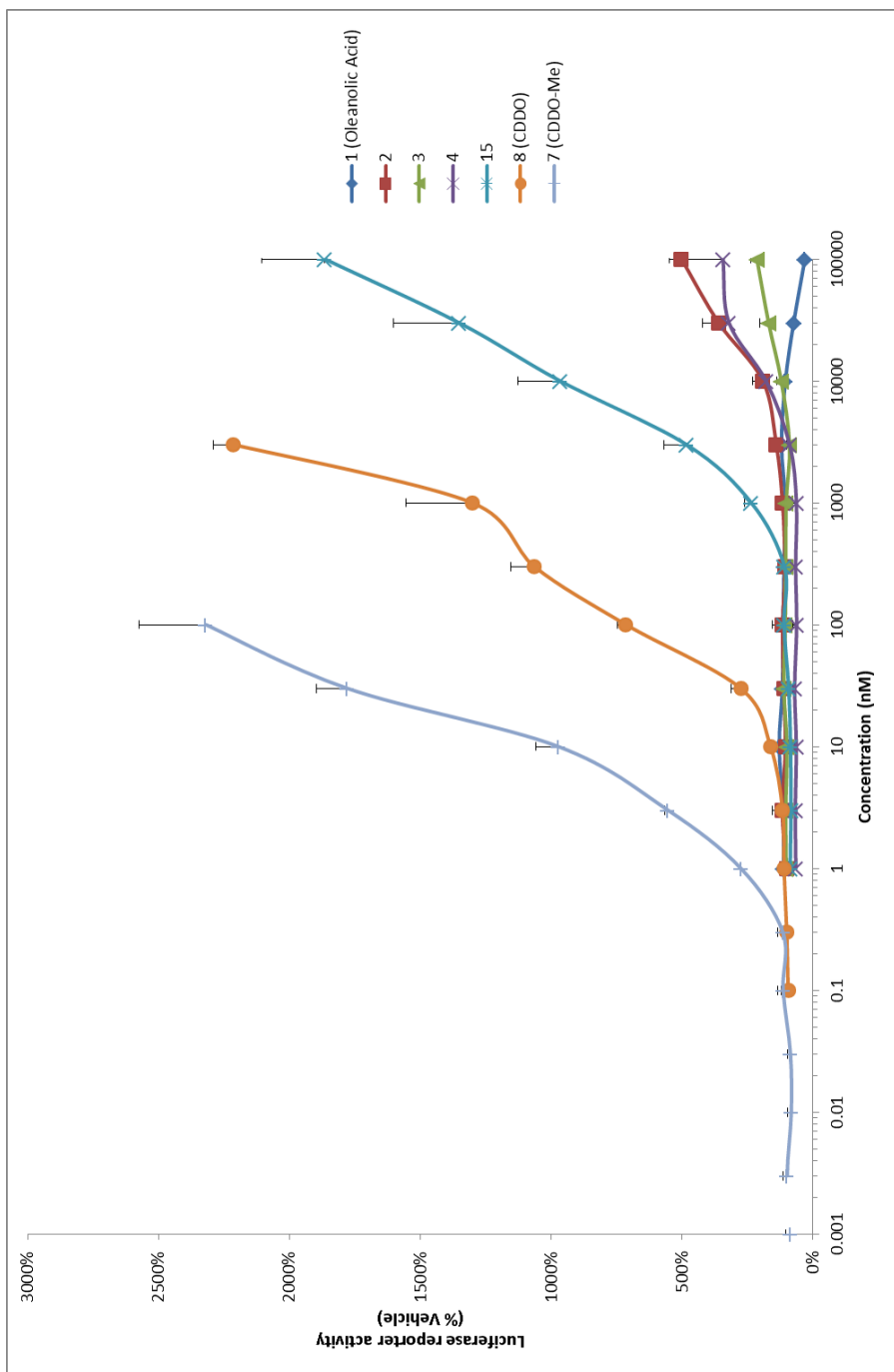
that no toxicity is observed from DMSO. Therefore, the range selected for the luciferase reporter assay is between 0.001 nM – 100 µM. The intermediates were measured based on their effective concentration to double luciferase activity (EC_{200}).

This screening of the seven compounds is used to provide data that will help to further understand the SAR (Graph 2.2 and Figure 2.8).

In this assay, luciferase activity was not observed when exposed to oleanolic acid at the concentration range set.

NAD(P)H:quinone oxidoreductase 1 (NQO1) is a cytoplasmic 2-electron reductase that is involved in chemoprotection. NQO1 is mediated by the ARE-promoter region within DNA. Activation of Nrf2 induces phase 2 genes *via* induction of ARE-dependent genes. NQO1 is a phase 2 gene and therefore an increase in NQO1 results in cell defence mechanism.¹⁸ Dinkova-Kostova *et al*, has demonstrated that there is a clear correlation between potencies of compounds that are able to induce the phase 2 enzyme NQO1 and the suppression of interferon gamma (IFN- γ) dependent transcriptional activation of inducible nitric oxide synthase (iNOS).¹⁹ Therefore, the induction of Nrf2 is also highly linked to the activation of iNOS.

Oleanolic acid has been shown to inhibit iNOS production induced by IFN- γ in mouse macrophages.³ However, it was inactive when tested for its ability to induce NQO1.¹⁹ Oleanolic acid has also demonstrated its ability to induce Nrf2 *in vivo*.²⁰ This suggests that the concentration range used within our assay may not be within the range where Nrf2 is accumulated.



Graph 2.2: Seven compounds selected for the luciferase reporter assay were exposed to H4IIE-ARE cells for 24 hours prior to obtaining the luminescence data. Data points were normalised to a negative control treated well of DMSO. Data shown is the average of n=3 and the error bars are plus or minus the standard deviation.

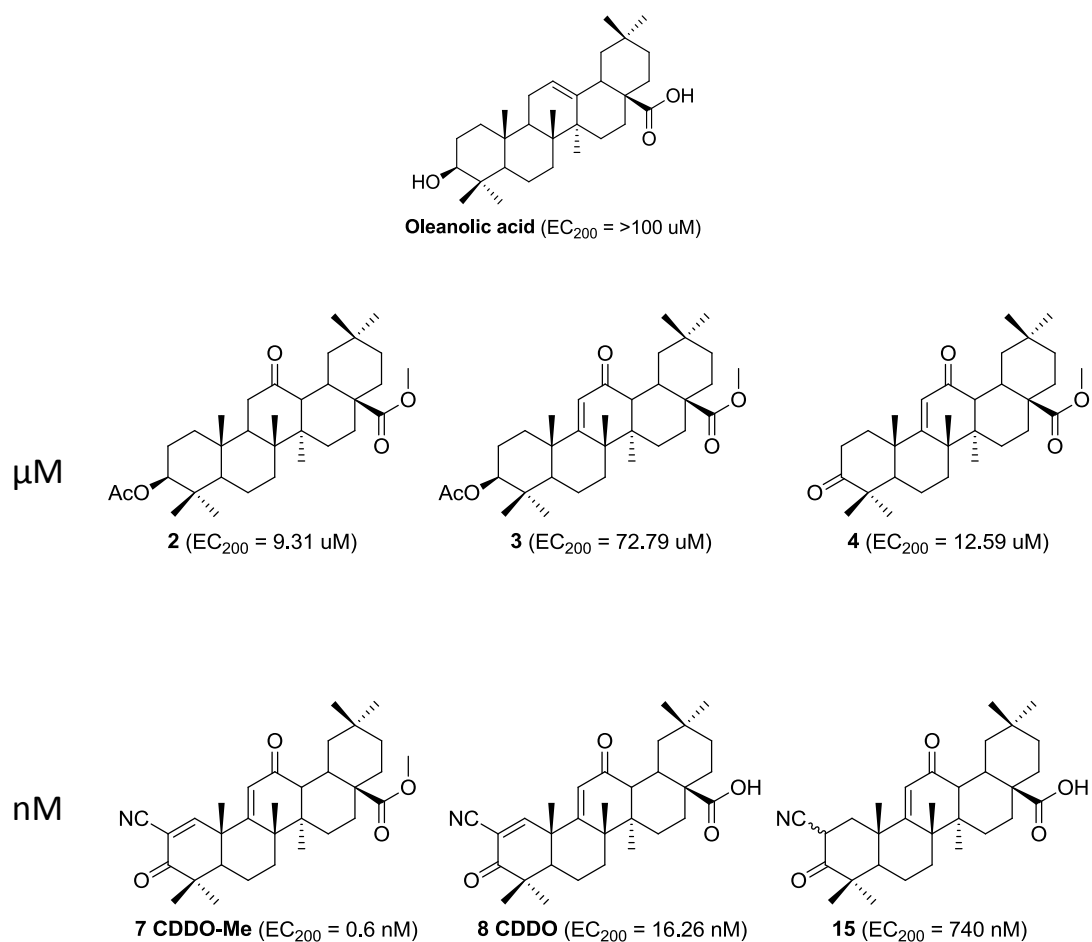


Figure 2.8: Seven compounds that were tested using the luciferase activity assay. Their EC_{200} values were calculated based on their ability to increase luciferase activity. They were grouped based on their EC_{200} values being in micromolar or nanomolar concentrations.

Compound **2**, **3** and **4** are the intermediate products from steps 3, 4 and 6 for the synthesis of CDDO respectively. Their ability to induce Nrf2 was increased compared to oleanolic acid ranging in the micromolar range. However, these three compounds lack the pharmacophore located in the A ring (Figure 2.8). This is the α,β unsaturated ketone along with the incorporation of an electron withdrawing cyano group in the C-2 position within the A ring. Compound **2** was more active than compounds **3** and **4**. SAR studies by Sporn *et al* suggested that the α,β unsaturated ketone located on the A and C rings are vital for nanomolar activity and

the lack of this functional group decreases activity.^{2,3} Surprisingly, introduction of a double bond in the C ring (compound **2** vs. compound **3**) which converts the ketone to the α,β unsaturated ketone decreased activity. This suggests that the Michael acceptor in the C ring is not of great importance. Converting the acetate group to a ketone within the A ring (compound **3** vs. compound **4**) resulted in an increase in EC_{200} but only to similar levels to compound **2**.

Compound **7** is CDDO-Me, the most active compound within the series giving an EC_{200} at 0.62 nM. This was followed by compound **8** (CDDO) with an EC_{200} at 16.26 nM. Compound **15** also gave nanomolar activity, however, unlike CDDO and CDDO-Me this was at 740 nM. Compound **15** lacked the double bond in the A ring which suggests that this is an important pharmacophore in order to obtain low nanomolar activity.

Structural comparison of CDDO with CDDO-Me showed that the difference in SAR was the conversion from methyl ester of CDDO-Me to carboxylic acid CDDO. This renders CDDO-Me more lipophilic in nature than CDDO and therefore may contribute to the increase in potency. Keap1 is a known cytoplasmic Nrf2 repressor. The increase in lipophilicity of CDDO-Me might enable the drug to enter cells more readily and therefore results in an increase in drug concentration within cells. If Keap1 is indeed the target protein for CDDO derivatives then the increase in concentrations within the cells will result in more drug being available for drug target interactions and therefore will result in an increase in potency. Other literature examples that adopt similar structural conversions from a carboxylic acid

group to an ester group to increase lipophilicity and hence potency are shown in Table 2.1.

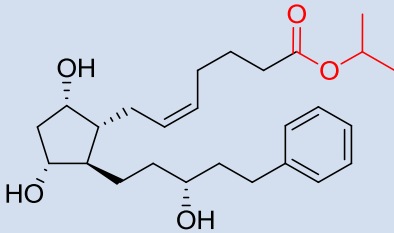
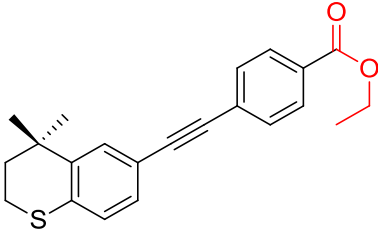
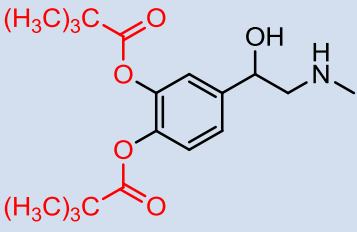
Name, conversion from (therapeutic area)	Chemical structure and highlighted functional group	Detail of potency
<p>Latanoprost from Lantaoprost acid (Glaucoma)</p>		<p>Improved lipophilicity resulting in increase absorption and safety</p>
<p>Tazarotene from Tazarotene acid (psoriasis, acne and tropical skin disorders)</p>		<p>Improved lipophilicity but maintains adequate aqueous solubility resulting in improved skin permeation</p>
<p>Dipivefrin from adrenaline (Glaucoma)</p>		<p>600 fold increase in lipophilicity compared to dipivefrin enabling dipivefrin to permeate the human cornea 17 times faster than adrenaline</p>

Table 2.1: Table contains examples of drugs resulting in improved potency by converting the carboxylic acid groups to esters (highlighted in red). Adapted from Rautio *et al.*²¹

CDDO-Me and CDDO have also been tested for the inhibition of INF- γ dependent transcriptional activation of iNO in mouse macrophages as an anti-inflammatory.³ The IC₅₀ values were 0.1 and 0.2 nM respectively. Hence, CDDO-Me is more active than CDDO in its ability to inhibit INF- γ .³ Currently, there are no other

biological/pharmacological literature data for the other compounds shown in Figure 2.8.

2.3. Conclusion

The synthesis of CDDO was a success. Initially the synthesis involved eleven steps, some of which involved toxic and explosive reagents. Through the use of alternative reagents and conditions, some of the hazards were minimised and the synthesis was reduced to nine steps. In total, fifteen compounds were obtained during this synthesis. The pharmacological potency of six of these compounds was determined in H4IIE-ARE cells. CDDO-Me was found to be the most active compound followed by CDDO, with both compounds inducing Nrf2 signalling at low nanomolar concentrations. This is consistent with literature data currently available for both compounds.^{2,3}

2.4. Chemistry Experimental

2.4.1. General

Reactions that were air and moisture sensitive were performed under a nitrogen atmosphere. This was achieved with oven dried or flame dried glassware sealed with a rubber septa. Dry nitrogen gas was introduced *via* a manifold or balloon.

Reactions were stirred using Teflon-coated magnetic stir bars. Organic solutions were concentrated using a Büchi rotary evaporator with a diaphragm vacuum pump. Anhydrous solutions and sensitive liquids were transferred *via* syringe.

2.4.2. Purification of solvents and reagents

Anhydrous solvents were obtained from commercial sources or dried and distilled prior to use. The distillation was under the flow of dry nitrogen. THF was distilled from sodium. Dichloromethane was distilled from calcium hydride. Oleanolic acid was obtained from Toronto Research Chemicals Inc. and Indofine Chemical Company Inc. All reagents were purchased from Sigma Aldrich or Alfa Aesar and were used without purification unless otherwise indicated.

2.4.2.1. Purification of *meta*-chloroperoxybenzoic acid

m-Chloroperbenzoic acid (~45%) was purified prior to use. Disodium hydrogen phosphate (4.32 g, 30.0 mmol) and potassium dihydrogen phosphate (1.18 g, 8.7 mmol) were dissolved in 1 L of distilled water. 500 mL of buffer was added to commercial *m*CPBA (25 g). The mixture was stirred and the solid filtered off. The filtered solid was washed with the rest of the buffer (500 mL) and was dissolved in dichloromethane (200 mL). The solution was dried over anhydrous magnesium

sulfate, filtered and the solvent removed *in vacuo*. *m*CPBA was left to dry under reduced pressure overnight to give approximately 95-100% pure *m*CPBA as a white flocculent solid.

2.4.3. Stains

p-Anisaldehyde stain

Concentrated sulphuric acid (2.5 mL) was added to *p*-anisaldehyde (15 g) in ethanol (250 mL) to give a clear solution of *p*-anisaldehyde stain.

2.4.4. Purification of products

Analytical thin layer chromatography (TLC) was performed with 0.25 mm Merck silica gel 60 F254 plates with 254 nm fluorescent indicator. Plates were visualised by U.V. at 254 nm or treated with *p*-anisaldehyde solution followed by gentle heating. Chromatographic purification of products was accomplished by flash column chromatography unless otherwise indicated.

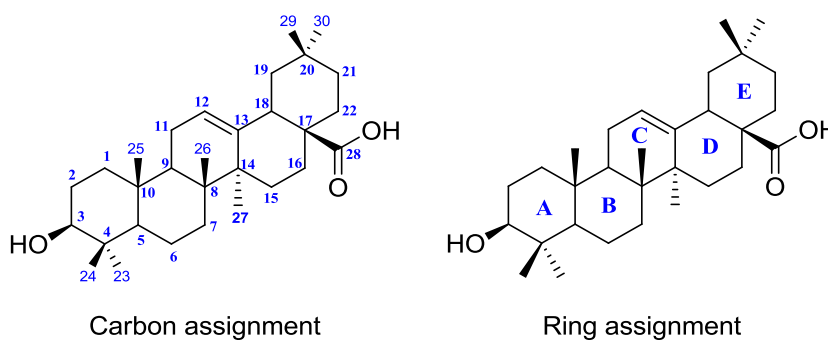
2.4.5. Analysis

¹H NMR spectra were measured on a Bruker AMX400 (400 MHz) nuclear magnetic resonance spectrometer. Solvents are indicated in the text. The data for ¹H NMR spectra are reported as follows: chemical shifts were described in parts per million (δ , ppm) downfield from an internal reference of trimethylsilane. Integration. Multiplicities: (s = singlet, d = doublet, t = triplet, q = quartet, dd = doublet of doublets, dt = doublet of triplets, td = triplet of doublets and m = multiplet). Coupling (*J*, Hz). ¹³C NMR spectra were measured on a Bruker AMX400 (100 MHz) and are reported in terms of chemical shift (δ , ppm) relative to residual solvent

peak. Mass spectrometry (MS) and High Resolution Mass Spectrometry (HRMS) were recorded on a VG analytical 7070E machine, Frisons TRIO spectrometers or Agilent QTOF 7200 using chemical ionisation (CI) or electron ionisation (EI). Micromass LCT mass spectrometer used electron spray ionisation (ESI). Reported mass values are within error limits of ± 5 ppm. Elemental analysis (%C, %H, %N) were determined by the University of Liverpool Microanalysis Laboratory. The reported atomic percentages are within error limits of $\pm 0.5\%$. Melting points were determined on a Gallenkamp melting point apparatus in degrees Celsius and are uncorrected. Infrared spectra were recorded on either a Jasco FT/IR-4200 fourier transform infrared spectrometer or a Bruker Alpha platinum ART and are reported in wavenumbers (cm^{-1}). Single crystal X-ray data were collected on a Bruker D8 diffractometer with an APEX CCD detector.

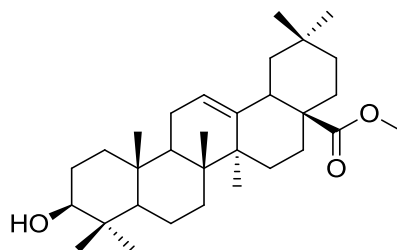
2.4.6. Numbering

Oleanolic acid

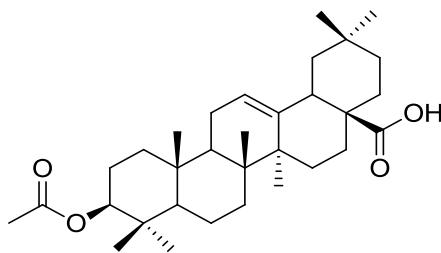


2.4.7. Synthesis

Preparation of methyl 3 β -hydroxy-olean-12-en-28-oate (**9**)²²⁻²⁴

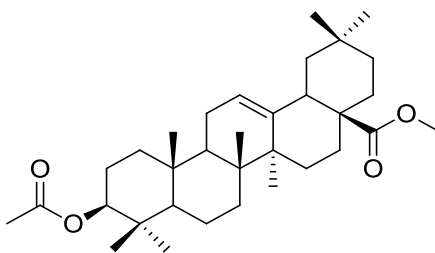


Oleanolic acid (**1**) (0.2 g, 0.44 mmol) was dissolved in tetrahydrofuran (2 mL) and methanol (0.5 mL). The solution was cooled to 0°C and (trimethylsilyl)diazomethane (2.0 M in hexanes, 76.6 μ L, 0.48 mmol) was added slowly to the reaction. The reaction mixture was allowed to warm to room temperature and left to stir for 1 hour. The solvent was removed and concentrated *in vacuo* and purified by flash column chromatography using 5% ethyl acetate in dichloromethane to give the title compound **9** (105 mg, 51%) as a white solid; R_f = 0.7, 20% ethyl acetate in dichloromethane; ^1H NMR (400 MHz, CDCl_3) δ 5.28 (t, J = 3.6 Hz, 1H), 3.62 (s, 3H), 3.21 (dd, J = 11.1, 4.7 Hz, 1H), 2.86 (dd, J = 13.8, 4.2 Hz, 1H), 2.03 – 1.83 (m, 3H), 1.74 – 1.26 (m, 16H), 1.22 – 1.14 (m, 2H), 1.13 (s, 3H), 1.05 (dd, J = 11.4, 3.9 Hz, 1H), 0.99 (s, 3H), 0.97 (s, 1H), 0.92 (s, 3H), 0.90 (s, 3H), 0.90 (s, 3H), 0.78 (s, 3H) and 0.72 (s, 3H); ^{13}C NMR (100 MHz, CDCl_3) δ 178.5, 143.9, 122.5, 79.2, 55.4, 51.7, 47.8, 46.9, 46.0, 41.8, 41.4, 39.4, 38.9, 38.6, 37.2, 34.0, 33.3, 32.8, 32.5, 30.8, 28.2, 27.8, 27.3, 26.1, 23.8, 23.6, 23.2, 18.5, 17.0, 15.7 and 15.4; HRMS (ESI) calculated for $\text{C}_{31}\text{H}_{50}\text{O}_3$ $[\text{M}+\text{Na}]^+$ 493.3658 found 493.3668.

Preparation of 3 β -acetoxy-olean-12-en-28-oic acid (**10**)^{1,10}

Under an atmosphere of nitrogen, oleanolic acid (**1**) (4 g, 8.76 mmol) was dissolved in dichloromethane (100 mL). Triethylamine (2.44 mL, 17.52 mmol), acetic anhydride (2.07 mL, 21.9 mmol) and 4-(dimethylamino)pyridine (10.7 mg, 87.6 μ mol) were added to the reaction and left to stir at room temperature for 12 hours. 2 M hydrochloric acid solution was added to the reaction. The reaction mixture was washed with dichloromethane (3 x 100 mL). The combined organic layers were washed with water, brine and dried over magnesium sulfate. The solution was concentrated *in vacuo* to give crude product in which purification by flash chromatography using 20% ethyl acetate in hexane gave the title compound **10** (4.13 g, 95%) as a white powder; $R_f = 0.4$, 20% ethyl acetate in hexane; mp = lit²⁵ 254.2-257.8°C found 255-257°C; ¹H NMR (400 MHz, CDCl₃) δ 5.27 (t, $J = 3.3$ Hz, 1H), 4.59 – 4.39 (m, 1H), 2.82 (dd, $J = 13.4, 3.7$ Hz, 1H), 2.05 (s, 3H), 2.03 – 1.85 (m, 3H), 1.82 – 1.16 (m, 18H), 1.12 (s, 3H), 1.10 – 1.02 (m, 2H), 0.94 (s, 3H), 0.93 (s, 3H), 0.90 (s, 3H), 0.86 (s, 3H), 0.85 (s, 3H) and 0.74 (s, 3H); ¹³C NMR (100 MHz, CDCl₃) δ 184.6, 171.2, 143.7, 122.7, 81.1, 55.4, 47.7, 46.7, 45.9, 41.6, 41.0, 39.4, 38.2, 37.8, 37.1, 33.9, 33.2, 32.6, 32.6, 30.8, 28.2, 27.8, 26.0, 23.7, 23.6, 23.5, 23.0, 21.5, 18.3, 17.3, 16.8 and 15.5; IR ν_{max} (neat)/cm⁻¹ 3178 (OH), 2943 (CH), 1726 (C=O) and 1680 (C=C); HRMS (ESI) calculated for C₃₂H₅₀O₄ [M+Na]⁺ 521.3607 found 521.3618.

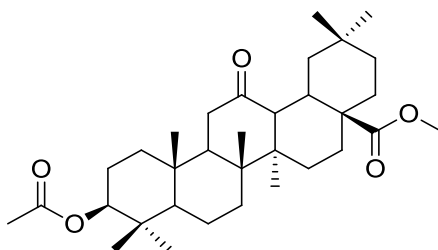
Preparation of 3 β -acetyloleanolic acid methyl ester (**11**)⁹



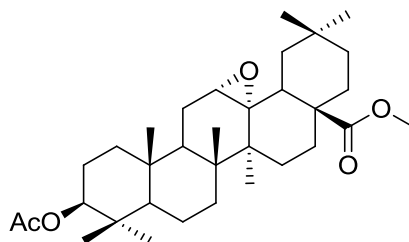
10 (6.47 g, 12.97 mmol) was dissolved in acetone (100 mL). Potassium carbonate (7.17 g, 51.89 mmol) and iodomethane (3.23 mL, 51.89 mmol) were added to the reaction and left to stir at room temperature for 24 hours. The reaction was concentrated *in vacuo* and the residue was dissolved in dichloromethane. The organic layer was washed with water, brine and dried over magnesium sulfate. The solution was concentrated *in vacuo* to give crude product in which purification by flash chromatography using 5% ethyl acetate in hexane gave the title compound **11** (6.48 g, 97%) as a white powder; $R_f = 0.8$, 20% ethyl acetate in hexane

9 (100 mg, 212 μ mol) was dissolved in anhydrous dichloromethane (50 mL) and purged with nitrogen. Triethylamine (59.22 μ L, 425 μ mol), acetic anhydride (50.2 μ L, 531 μ mol) and 4-(dimethylamino)pyridine (259 μ g, 2.12 μ mol) were added to the reaction and left to stir at room temperature overnight. The reaction was concentrated *in vacuo* and the residue was dissolved in dichloromethane. The organic layer was washed with 2 M hydrochloric acid, water, brine and dried over magnesium sulfate. The solution was concentrated to give crude product which was purified by flash chromatography using 10% ethyl acetate in hexane to give the title compound **11** (99.1 mg, 91%) as a white powder; $R_f = 0.8$, 20% ethyl acetate in hexane.

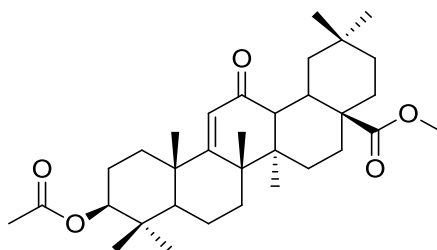
mp = lit⁹ 219-221°C found 218-219°C; ¹H NMR (400 MHz, CDCl₃) δ 5.28 (t, *J* = 3.6 Hz, 1H), 4.49 (dd, *J* = 8.9, 7.1 Hz, 1H), 3.62 (s, 3H), 2.86 (dd, *J* = 13.8, 4.2 Hz, 1H), 2.05 (s, 3H), 2.02 – 1.83 (m, 3H), 1.74 – 1.25 (m, 15H), 1.22 – 1.15 (m, 2H), 1.12 (s, 3H), 1.10 – 0.99 (m, 2H), 0.93 (s, 3H), 0.92 (s, 3H), 0.90 (s, 3H), 0.86 (s, 3H), 0.85 (s, 3H) and 0.72 (s, 3H); ¹³C NMR (100 MHz, CDCl₃) δ 178.4, 171.2, 143.9, 122.4, 81.0, 55.4, 51.7, 47.7, 46.8, 46.0, 41.7, 41.4, 39.4, 38.2, 37.8, 37.0, 34.0, 33.2, 32.7, 32.5, 30.8, 28.2, 27.8, 26.0, 23.8, 23.6, 23.5, 23.2, 21.5, 18.3, 17.0, 16.8 and 15.5; IR ν_{max} (neat)/cm⁻¹ 2937 (CH), 2862 (COCH₃) and 1726 (C=O); HRMS (ESI) calculated for C₃₃H₅₂O₄ [M+Na]⁺ 535.3763 found 535.3758; Microanalysis calculated for C₃₃H₅₂O₄ requires C 77.30%, H 10.22% found C 77.396%, H 10.161%

Preparation of methy-3 β -acetoxy-12-oxo-olean-28-oate (**2**)¹⁰

11 (3.85 g, 7.51 mmol) was dissolved in dry dichloromethane (50 mL) and cooled to 0°C. Pre-purified *meta*-chloroperoxybenzoic acid (1.55 g, 9.01 mmol) (see section 2.4.2.1) was added to this reaction and left to stir for 12 hours at room temperature. The reaction was washed with sodium hydrogen carbonate solution and dichloromethane. The organic layer was washed with water, brine, dried over magnesium sulfate and filtered. The filtrate was concentrated *in vacuo* to obtain the crude product. The crude product was purified by flash chromatography using 5% ethyl acetate in hexane to give the title compound **2** (3.93 g, 99%) as a white powder; $R_f = 0.56$, 20% ethyl acetate in hexane; mp = lit²⁶ 189-191°C found 187-189°C; ¹H NMR (400 MHz, CDCl₃) δ 4.47 (dd, $J = 11.1, 5.0$ Hz, 1H), 3.68 (s, 3H), 2.79 (dt, $J = 13.5, 3.4$ Hz, 1H), 2.60 (d, $J = 4.3$ Hz, 1H), 2.28 – 2.07 (m, 2H), 2.05 (s, 3H), 1.97 – 1.73 (m, 3H), 1.69 – 1.14 (m, 15H), 1.13 – 0.99 (m, 2H), 0.98 (s, 3H), 0.96 (s, 3H), 0.94 (s, 3H), 0.90 (s, 3H), 0.87 (s, 3H), 0.87 (s, 2H) and 0.86 (s, 3H); ¹³C NMR (100 MHz, CDCl₃) δ 211.9, 178.5, 171.1, 80.5, 55.3, 52.0, 49.7, 47.5, 41.9, 41.3, 38.6, 37.9, 37.7, 36.9, 36.3, 34.6, 33.5, 33.1, 32.1, 31.8, 30.8, 28.0, 27.6, 23.5, 23.3, 22.8, 21.4, 20.7, 18.3, 16.6, 16.2 and 15.4; IR ν_{max} (neat)/cm⁻¹ 2927 (CH), 2858 (COCH₃) and 1724 (C=O); HRMS (ESI) calculated for C₃₃H₅₂O₅ [M+Na]⁺ 551.3712 found 551.3711.

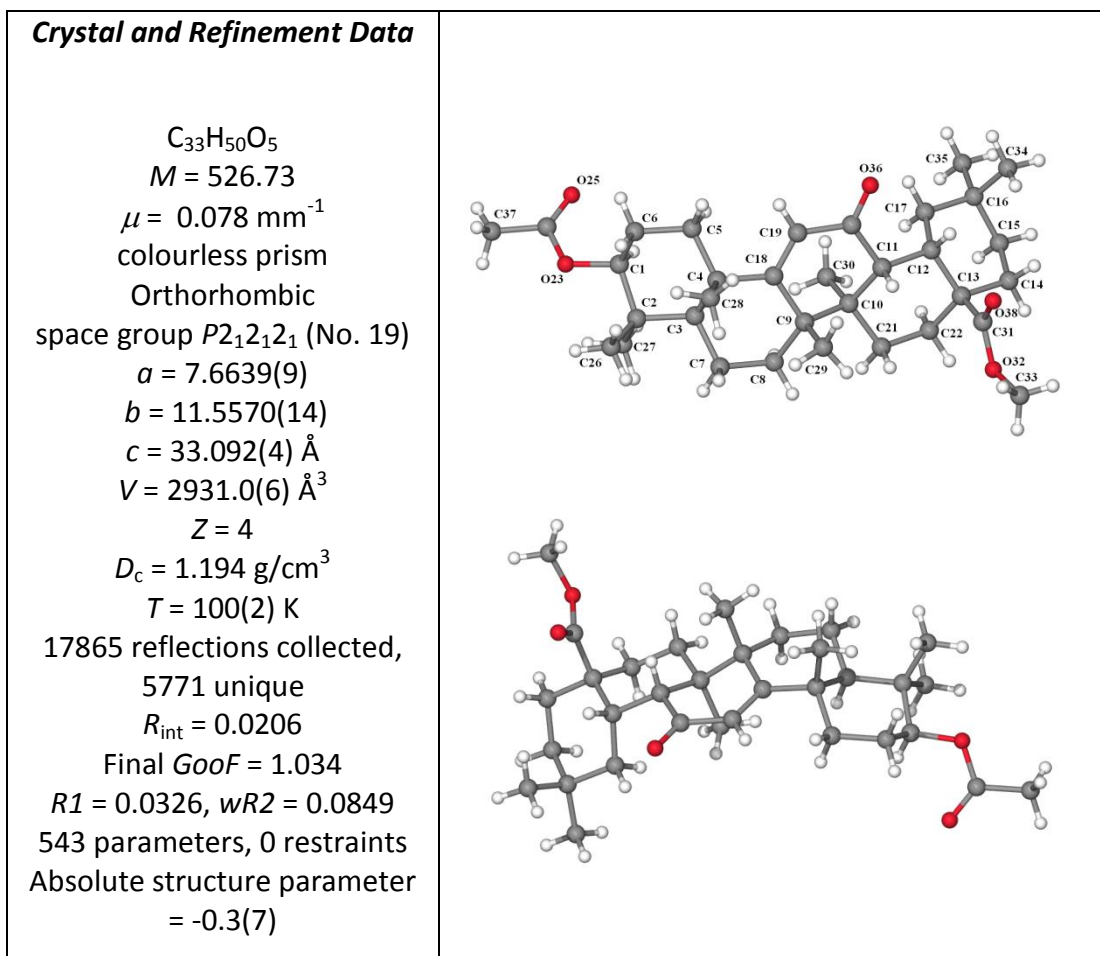
Intermediate methyl 3 β -acetoxy-12,13-epoxyoleanolate (**12**)^{10,11}

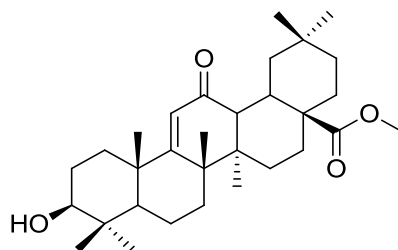
11 (6.48 g, 12.64 mmol) was dissolved in dry dichloromethane (50 mL) and cooled to 0°C. Pre-purified *meta*-chloroperoxybenzoic acid (2.62 g, 2.62 mmol) (see section 2.4.2.1) was added to this reaction and left to stir for 12 hours at room temperature. The reaction was washed with sodium hydrogen carbonate solution and dichloromethane. The organic layer was washed with water, brine, dried over magnesium sulfate and filtered. The filtrate was concentrated *in vacuo* to obtain the crude product. The crude product was purified by flash chromatography using 5% ethyl acetate in hexane to give the title minor compound **12** (153 mg, 2%) as a white compound; $R_f = 0.46$, 20% ethyl acetate in hexane; $^1\text{H NMR}$ (400 MHz, CDCl_3) δ 4.47 (dd, $J = 10.5, 5.9$ Hz, 1H), 3.68 (s, 3H), 3.16 (s, 1H), 2.04 (s, 3H), 2.06 – 1.91 (m, 2H), 1.85 – 1.55 (m, 11H), 1.49 – 1.13 (m, 10H), 1.11 (s, 3H), 0.94 (s, 3H), 0.93 (s, 3H), 0.84 (s, 3H), 0.82 (s, 3H), 0.81 (s, 3H) and 0.80 (s, 3H); $^{13}\text{C NMR}$ (100 MHz, CDCl_3) δ 178.5, 171.1, 80.8, 67.4, 63.8, 55.3, 51.9, 47.9, 43.9, 41.0, 40.4, 39.3, 38.5, 38.1, 37.8, 36.7, 34.2, 33.3, 32.7, 30.5, 29.4, 28.3, 23.9, 23.7, 23.5, 22.8, 22.8, 21.4, 20.0, 18.0, 17.1, and 16.7; IR ν_{max} (neat)/ cm^{-1} 2949 (CH), 2862 (COCH₃) and 1730 (C=O); HRMS (ESI) calculated for $\text{C}_{33}\text{H}_{52}\text{O}_5$ $[\text{M}+\text{Na}]^+$ 551.3712 found 551.3727.

Preparation of methyl 3 β -acetoxy-12-oxoolean-9(11)-en-28-oate (**3**)^{27,28}

Ketone **2** (12.31 g, 23.28 mmol) was dissolved in acetonitrile (100 mL). 48% Hydrobromic acid (1.0 mL, 8.85 mmol) was then added to the reaction. The reaction mixture was heated to 35°C and 1.0 M of bromine in acetonitrile (25.14 mL, 25.14 mmol) was added to the reaction and left to stir at 35°C for 18 hours. A further 1.0 M of bromine in acetonitrile (25.14 mL, 25.14 mmol) was added dropwise to the reaction mixture and left to stir for a further 1 hour at 35°C. The reaction was cooled to room temperature and the reaction was diluted with ethyl acetate. The solution was worked up with water and sodium bicarbonate. The organic layer was then washed with saturated sodium sulfite in water, brine and dried over magnesium sulfate. The solution was filtered and dried *in vacuo* to give the crude product. The crude product was re-crystallised using methanol and water to obtain title compound **3** (12.11 g, 99%) as a white solid; $R_f = 0.33$, 20% ethyl acetate in hexane; mp = lit²⁸ 208-209 found 207-208°C; ¹H NMR (400 MHz, CDCl₃) δ 5.74 (s, 1H), 4.48 (dd, $J = 11.7, 4.7$ Hz, 1H), 3.68 (s, 3H), 3.02 (dt, $J = 13.6, 3.6$ Hz, 1H), 2.84 (d, $J = 4.7$ Hz, 1H), 2.06 (s, 3H), 1.99 – 1.56 (m, 12H), 1.55 – 1.11 (m, 7H), 1.24 (s, 3H), 1.21 (s, 3H), 1.00 (s, 3H), 0.99 (s, 3H), 0.91 (s, 3H), 0.90 (s, 3H) and 0.90 (s, 3H); ¹³C NMR (100 MHz, CDCl₃) δ 200.6, 178.4, 178.0, 171.0, 123.0, 79.8, 51.9, 50.4, 49.5, 47.4, 45.3, 41.7, 39.9, 38.3, 36.2, 35.9, 34.6, 33.4, 33.0, 32.9, 31.6, 30.7, 28.1, 28.1, 24.0, 24.0, 23.8, 23.2, 22.7, 21.8, 21.4, 17.9 and 16.8; IR ν_{max} (neat)/cm⁻¹ 2946 (CH),

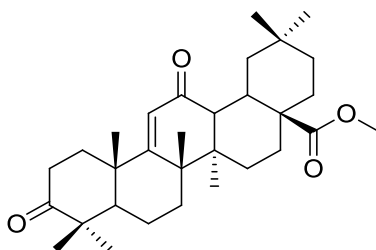
2862 (COCH₃), 1734 (C=O), 1720 (C=O) and 1663 (C=C); HRMS (ESI) calculated for C₃₃H₅₀O₅ [M+Na]⁺ 549.3556 found 549.3561; Microanalysis Calculated for C₃₃H₅₀O₅ requires C 75.25%, H 9.57% found C 75.15%, H 9.505%



Preparation of methyl 3 β -hydroxy-12-oxoolean-9(11)-en-28-oate (**13**)²⁸

Acetyl **3** (1.7 g, 3.23 mmol) was dissolved in methanol (50 mL). Potassium hydroxide (5 g, 90.33 mmol) was added to the reaction mixture and refluxed for 1 hour. The reaction was cooled to room temperature and 6.0 M hydrochloric acid was used for the work up and extracted three times in dichloromethane: diethyl ether (1:2, 3 x 50 mL). The combined organic layers were washed with water, brine and dried over magnesium sulfate. The solution was filtered and the solvent was removed under reduced pressure to give the title compound **13** (1.55 g, 99%) as a white solid; $R_f = 0.11$, 20% ethyl acetate in hexane; mp = lit²⁸ 233°C found 232-233°C; ¹H NMR (400 MHz, CDCl₃) δ 5.75 (s, 1H), 3.68 (s, 3H), 3.22 (dd, $J = 11.6, 4.6$ Hz, 1H), 3.02 (dt, $J = 13.7, 3.6$ Hz, 1H), 2.84 (d, $J = 4.7$ Hz, 1H), 2.00 – 1.56 (m, 14H), 1.53 – 1.25 (m, 6H), 1.24 (s, 3H), 1.18 (s, 3H), 1.03 (s, 3H), 1.00 (s, 3H), 0.99 – 0.97 (m, 2H), 0.89 (s, 4H) and 0.83 (s, 3H); ¹³C NMR (100 MHz, CDCl₃) δ 200.8, 178.5, 178.5, 122.9, 78.1, 52.0, 50.3, 49.6, 47.4, 45.4, 41.8, 40.1, 39.4, 36.5, 35.9, 34.6, 33.4, 33.0, 32.9, 31.6, 30.8, 28.2, 27.6, 24.0, 23.8, 23.2, 22.8, 21.9, 18.1 and 15.7; IR ν_{max} (neat)/cm⁻¹ 3299 (OH), 2943 (CH), 2867 (COCH₃), 1721 (C=O) and 1658 (C=C); HRMS (ESI) calculated for C₃₁H₄₈O₄ [M+Na]⁺ 507.3450 found 507.3445.

Preparation of methyl 3,12-dioxoolean-9(11)-en-28-oate (**4**)³

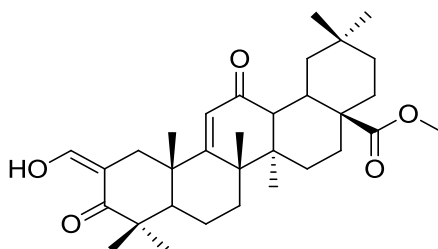


Preparation of Jones reagent: 2.5 g of CrO₃ was dissolved in 2.5 mL of conc. H₂SO₄. The mixture was cooled to 0°C and 75 mL of cold water was added drop wise to obtain a maroon coloured solution.

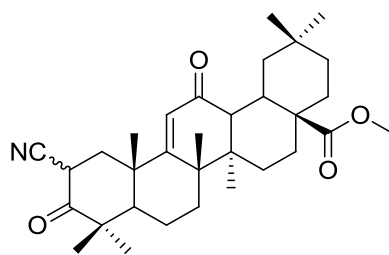
Alcohol **13** (2.6 g, 5.36 mmol) was dissolved in acetone (50 mL). The reaction mixture was cooled to 0°C. The Jones reagent was added drop wise to the reaction until a colour change from green to light orange/brown colour was observed. The mixture was stirred at room temperature for 10 minutes. The acetone was removed by *vacuo* and worked up in dichloromethane:diethyl ether (1:2, 3 x 50 mL) and water. The combined organic layers were washed with water, brine, dried over magnesium sulfate and filtered. The solvent was removed *in vacuo* to give the title compound **4** (2.57 g, 99%) as a white solid product; R_f = 0.22, 20% ethyl acetate in hexane; mp = 102-105°C; ¹H NMR (400 MHz, CDCl₃) δ 5.79 (s, 1H), 3.69 (s, 3H), 3.03 (dt, *J* = 13.6, 3.5 Hz, 1H), 2.89 (d, *J* = 4.7 Hz, 1H), 2.65 (ddd, *J* = 15.8, 11.0, 7.2 Hz, 1H), 2.48 (ddd, *J* = 15.8, 7.0, 3.8 Hz, 1H), 2.21 (ddd, *J* = 13.3, 7.3, 3.9 Hz, 1H), 1.95 – 1.56 (m, 10H), 1.54 – 1.43 (m, 3H), 1.31 (s, 3H), 1.28 (s, 3H), 1.26 – 1.15 (m, 3H), 1.13 (s, 3H), 1.09 (s, 3H), 1.01 (s, 3H), 1.00 (s, 3H) and 0.89 (s, 3H); ¹³C NMR (100 MHz, CDCl₃) δ 216.0, 200.2, 178.4, 176.7, 124.2, 52.0, 51.1, 49.7, 47.7, 47.4, 45.5, 41.9, 39.6, 37.2, 36.0, 34.6, 34.3, 33.4, 33.0, 32.1, 31.7, 30.8, 28.3, 26.4, 23.9, 23.7, 23.2, 22.9,

21.8, 21.6 and 19.3; IR ν_{\max} (neat)/ cm^{-1} 2945 (CH), 2870 (COCH₃), 1720 (C=O), 1709 (C=O) and 1659 (C=C); HRMS (ESI) calculated for C₃₁H₄₆O₄ [M+Na]⁺ 505.3294 found 505.3282;

Preparation of methyl 2-hydroxymethylene-3,12-dioxoolean-9(11)-en-28-oate (5)³



4 (1.34 g, 2.78 mmol) dissolved in anhydrous toluene (10 mL). Ethyl formate (1 mL, 12.49 mmol) and sodium methoxide (907.34 mg, 16.80 mmol) were added to the reaction and stirred at room temperature for 2 hours. The reaction was diluted with dichloromethane: diethyl ether (1:2, 50 mL) and washed with 5% hydrochloric acid (3 x 50 mL). The combined aqueous layers were washed with dichloromethane: diethyl ether (1:2, 3 x 50 mL). The combined organic layers were washed with water, brine, dried over magnesium sulfate and filtered. The solution was concentrated *in vacuo* and purified by flash chromatography using 2% ethyl acetate in hexane to give the title compound **5** (1.39 g, 98%) as a white powder; $R_f = 0.37$, 20% ethyl acetate in hexane; ¹H NMR (400 MHz, CDCl₃) δ 8.77 (d, $J = 2.5$ Hz, 1H), 5.90 (s, 1H), 3.70 (s, 3H), 3.04 (dt, $J = 13.4, 3.4$ Hz, 1H), 2.92 (d, $J = 4.7$ Hz, 1H), 2.62 (d, $J = 14.4$ Hz, 1H), 2.29 (d, $J = 14.4$ Hz, 1H), 1.97 – 1.79 (m, 3H), 1.77 – 1.58 (m, 7H), 1.56 – 1.30 (m, 6H), 1.28 (s, 3H), 1.26 (s, 3H), 1.18 (s, 3H), 1.17 (s, 3H), 1.02 (s, 3H), 1.01 (s, 3H) and 0.90 (s, 3H); ¹³C NMR (100 MHz, CDCl₃) δ 200.2, 190.2, 188.2, 178.4, 175.8, 171.3, 124.4, 105.1, 52.0, 49.6, 48.2, 47.4, 45.5, 41.9, 40.5, 39.2, 37.1, 35.9, 34.6,

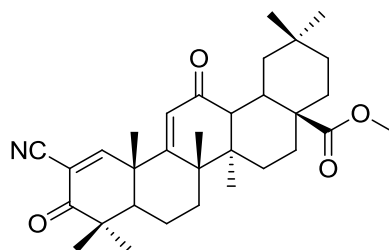
Preparation of methyl 2-cyano-3,12-dioxoolean-9(11)-en-28-oate (**14**)^{3,29}

4 (0.2 g, 414 μmol) was dissolved in dry tetrahydrofuran. The solution was cooled to -78°C , flushed with nitrogen and nitrogen balloon attached. Lithium diisopropylamide (66.58 mg, 0.31 mL, 621 μmol , 2.0 M in heptanes/THF/ethyl benzene) was added drop wise to the reaction and left to stir at room temperature for 20 minutes. *p*-toluenesulfonyl cyanide (150 mg, 828 μmol) was dissolved in dry tetrahydrofuran in a dry flask. The flask was cooled to -78°C and the solution containing **4** was transferred drop wise to the flask. The reaction was left to stir for 5 minutes and quenched with ammonia solution. The solution was acidified with 5% hydrogen chloride solution and extracted with ethyl acetate (3 x 50 mL). Combined organic layers were washed with water brine and dried over magnesium sulfate. Solvent was removed *in vacuo* and purified by flash chromatography using 5% ethyl acetate in hexane to give the title compound **14** (185 mg, 88%) as a white powder; $R_f = 0.3$, 30% ethyl acetate in hexane.

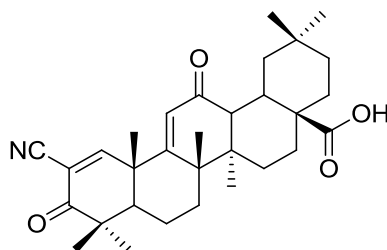
6 (0.938 g, 1.85 mmol) was dissolved in methanol (40 mL) and diethyl ether (160 mL). The solution was cooled to 0°C and sodium methoxide (3.40 g, 62.84 mmol) was added to reaction. The reaction was left to stir at room temperature for 45 minutes. The mixture was diluted in dichloromethane:diethyl ether (1:2, 50 mL) and washed with 5% HCl (3 x 50 mL). The combined acidic washings were extracted with

dichloromethane:diethyl ether (1:2, 3 x 50 mL). The combined organic layers were washed with water, brine, dried over magnesium sulfate and filtered. The solvent was removed *in vacuo* and purified by flash chromatography using 2% ethyl acetate in hexane to give the title compound **14** (653.9 mg, 70%) as a white powder. $R_f = 0.09$, 20% ethyl acetate in hexane.

^1H NMR (400 MHz, CDCl_3) δ 5.80 – 5.70 (m, 1H), 3.69 (s, 3H), 3.08 – 2.98 (m, 1H), 2.95 – 2.86 (m, 1H), 2.43 (d, $J = 15.3$ Hz, 1H), 2.25 (d, $J = 15.3$ Hz, 1H), 1.94 – 1.55 (m, 12H), 1.53 – 1.37 (m, 4H), 1.25 (s, 3H), 1.22 (s, 3H), 1.20 (s, 3H), 1.12 (s, 3H), 1.00 (s, 6H) and 0.90 (s, 3H); ^{13}C NMR (100 MHz, CDCl_3) δ 200.0, 178.4, 175.1, 124.5, 52.0, 49.7, 48.5, 47.4, 45.5, 42.3, 41.9, 39.6, 38.7, 38.6, 38.1, 37.5, 36.0, 34.6, 33.4, 33.0, 32.9, 31.6, 31.3, 30.8, 28.3, 28.0, 24.1, 23.2, 23.1, 21.7, 20.0 and 18.9; IR ν_{max} (neat)/ cm^{-1} 2949 (CH), 2869 (COCH_3), 2207 (CN), 1722 (C=O) and 1659 (C=C); HRMS (ESI) calculated for $\text{C}_{32}\text{H}_{45}\text{NO}_4$ $[\text{M}+\text{Na}]^+$ 530.3246 found 530.3233.

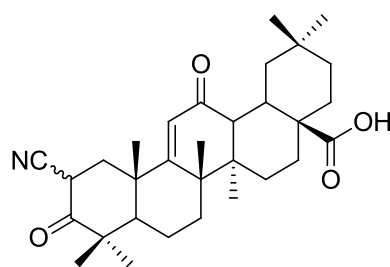
Preparation of methyl 2-cyano-3,12-dioxooleana-1,9(11)-dien-28-oate (**7**)^{3,30}

14 (2.6 g, 5.13 mmol) was dissolved in anhydrous benzene. 2,3-Dichloro-5,6-dicyanobenzoquinone (2.0 g, 8.82 mmol) was added to the solution of **14** and refluxed for 30 minutes. The solution was cooled and the insoluble matter was filtered. Benzene was removed *in vacuo* and the crude product was recrystallised from methanol and water to obtain the title compound **7** (2.25 g, 87%) as a white solid product; $R_f = 0.3$, 30% ethyl acetate in hexane; mp = lit³⁰ 228°C found 228-230°C; ¹H NMR (400 MHz, CDCl₃) δ 8.05 (s, 1H), 5.97 (s, 1H), 3.70 (s, 3H), 3.04 (dt, $J = 13.6, 3.7$ Hz, 1H), 2.94 (d, $J = 4.7$ Hz, 1H), 1.96 – 1.63 (m, 9H), 1.60 – 1.50 (m, 3H), 1.49 (s, 3H), 1.33 (s, 3H), 1.30 – 1.20 (m, 3H), 1.26 (s, 3H), 1.17 (s, 3H), 1.01 (s, 3H), 1.00 (s, 3H) and 0.90 (s, 3H); ¹³C NMR (100 MHz, CDCl₃) δ 199.0, 196.7, 178.3, 168.5, 165.9, 124.1, 114.7, 114.5, 52.0, 49.8, 47.8, 47.3, 45.8, 45.1, 42.6, 42.2, 35.8, 34.5, 33.3, 32.8, 31.7, 31.6, 30.7, 28.1, 27.1, 26.7, 24.7, 23.2, 22.7, 21.7, 21.7 and 18.3; IR ν_{\max} (neat)/cm⁻¹ 2947 (CH), 2868 (COCH₃) 2234 (CN), 1720 (CO), 1688 (C=C) and 1663 (C=C); HRMS (ESI) calculated for C₃₂H₄₃NO₄ [M+Na]⁺ 528.3090 found 528.3101.

Preparation of 2-cyano-3,12-dioxooleana-1,9(11)-dien-28-oic acid (**8**)^{3,31}

7 (1.26 g, 2.49 mmol) was dissolved in anhydrous DMF (20 mL). Lithium iodide was added to the reaction and left to reflux overnight. The reaction was cooled and water (50 mL) was added. 5% HCl was added to the solution and washed with ethyl acetate (3 x 50 mL). The combined organic layers were washed with water (3 x 50 mL), brine (3 x 50 mL) and dried over magnesium sulfate. The solution was filtered and the solvent was removed under vacuum. The crude product was purified by flash chromatography using 5% ethyl acetate in hexane to give the title compound **8** (538.5 mg, 44%); $R_f = 0.08$, 1:1 ethyl acetate in hexane; mp = lit³¹ 283-288°C found 296-298°C; $^1\text{H NMR}$ (400 MHz, CDCl_3) δ 8.07 (s, 1H), 6.01 (s, 1H), 3.08 – 2.95 (m, 2H), 2.00 – 1.87 (m, 2H), 1.83 – 1.68 (m, 6H), 1.62 – 1.51 (m, 3H), 1.49 (s, 3H), 1.35 (s, 3H), 1.32 – 1.19 (m, 4H), 1.26 (s, 3H), 1.17 (s, 3H), 1.03 (s, 3H), 1.00 (s, 3H), 0.91 (s, 3H); $^{13}\text{C NMR}$ (100 MHz, CDCl_3) δ 198.9, 196.7, 183.9, 168.7, 165.9, 124.1, 114.6, 114.5, 49.8, 47.7, 47.1, 45.8, 45.1, 42.6, 42.2, 35.7, 34.4, 33.3, 33.0, 31.7, 31.4, 30.7, 28.0, 27.0, 26.7, 24.7, 23.1, 22.5, 21.7 and 18.3; IR ν_{max} (neat)/ cm^{-1} 2944, 1723, 1688 and 1663; HRMS (ESI) calculated for $\text{C}_{31}\text{H}_{41}\text{NO}_4$ $[\text{M}+\text{Na}]^+$ 514.2933 found 514.2916.

Preparation of 2-cyano-3,12-dioxooleana-9(11)-en-28-oic acid (**15**)



Isolated from previous procedure to give the title compound **15** (95 mg, 6%); ^1H NMR (400 MHz, CDCl_3) δ 5.79 – 5.70 (m, 1H), 3.03 – 2.96 (m, 1H), 2.93 (d, $J = 4.7$ Hz, 1H), 2.42 (d, $J = 15.2$ Hz, 1H), 2.25 (d, $J = 15.2$ Hz, 1H), 2.00 – 1.86 (m, 3H), 1.82 – 1.54 (m, 11H), 1.52 – 1.40 (m, 3H), 1.26 (s, 3H), 1.22 (s, 3H), 1.21 (s, 3H), 1.12 (s, 3H), 1.00 (s, 6H) and 0.90 (s, 3H); ^{13}C NMR (100 MHz, CDCl_3) δ 199.7, 175.1, 171.6, 124.5, 49.7, 48.6, 48.5, 47.2, 45.6, 41.9, 39.6, 38.8, 38.7, 38.1, 37.5, 35.9, 34.6, 33.3, 33.1, 33.0, 31.6, 31.3, 30.8, 28.2, 28.0, 24.1, 23.20, 23.16, 21.7, 20.0 and 18.9; HRMS (ESI) calculated for $\text{C}_{31}\text{H}_{43}\text{NO}_4$ $[\text{M}+\text{Na}]^+$ 516.3090 found 516.3113.

2.5. Biological experimental

2.5.1. Materials

H4IIE cells stably expressing the ARE8L-reporter, were provided by Prof. Alex Odermatt (Department of Pharmaceutical Sciences, University of Basel, Switzerland). Nunclon Δ cell culture flasks and multiwall plates were from Nalge-Nunc International (c/o VWR International, Lutterworth, UK). Precision Plus Protein Kaleidoscope standards, non-fat dry milk, the GS-800 calibrated imaging densitometer were from Bio-Rad (Hemel Hempstead, UK).

Fetal bovine serum (FBS), trypsin 0.25% EDTA, The XCell Sure Lock mini-cell, NuPAGE Novex 4-12% Bis-Tris gels, NuPAGE LDS sample buffer and sample reducing agent were from Life Technologies (Paisley, UK). TotalLab Quantity One software was from TotalLab Ltd (Newcastle Upon Tyne, UK). The MRX microplate reader was from Dynatech Laboratories (Billingshort, UK). The Varioskan Flash and SkanIT software were from Thermo Scientific (Hemel Hempstead, UK). Western Lightening chemiluminescence reagents were from PerkinElmer (Beaconsfield, UK). Hyperfilm ECL and nitrocellulose blotting membrane (Hybond ECL) were from Amersham (Little Chalfont, UK). The rabbit anti-Nrf2 antibody was from Abcam (Cambridge, UK). Bright-Glo luciferase assay system and glo lysis buffer were from Promega (Southampton, UK). Dulbecco's modified eagle medium (DMEM), penicillin-streptomycin solution, dimethyl sulfoxide (DMSO), 3-(*N*-morpholino)propanesulfonic acid (MOPS), mouse anti-actin primary antibody, rabbit anti-mouse HRP conjugated secondary antibody, goat anti-rabbit Horseradish peroxidase (HRP) conjugated secondary antibody, Kodak developer and fixer

solutions, bicinchoninic acid solution, copper(II) sulphate solution, Bovine serum albumin, ponceau S solution, Tween 20, phosphate buffered saline (PBS) tablets, radioimmunoprecipitation assay (RIPA) buffer solution, MEM non-essential amino acid solution and 4-(2-hydroxyethyl)piperazine-1-ethanesulfonic acid (HEPES) buffer 100X were from Sigma-Aldrich (Poole, UK). All other reagents were of analytical or molecular grade, and were from Sigma-Aldrich.

2.5.2. Cell culture

H4IIE-ARE cells were maintained in a humidified incubator, at 37°C, in a 5% carbon dioxide (CO₂) atmosphere. The cells were incubated in Dulbecco's modified eagle's medium (DMEM) supplemented with 10% heat-inactivated fetal bovine serum (FBS), 1mM HEPES and 1 x non-essential amino acids. The culture medium was antibiotic free.

75 cm² Nunclon Δ culture flasks were used and cells were passaged at approximately 80% confluence, every 3-4 days. Unsupplemented DMEM was used to wash the cells prior to 1 minute incubation at room temperature with 5 mL trypsin. The trypsin was removed and the cells were further incubated for 5 minutes at 37°C, facilitating detachment from the flask surface. Cells were re-suspended in 5 mL growth media and passed through a 21-gauge needle several times to ensure cells were individually suspended. For continuation, cells were re-seeded at a cells:growth medium ratio of 2:10.

2.5.3. Plating

For the analysis of Nrf2 levels by Western blot or luciferase reporter activity, a 10 μL aliquot of the cell suspension was transferred to the edge of a haemocytometer

and allowed to spread evenly across the surface by capillary action. Cells were visualised using the 20 X objective of a light microscope. The cells were counted within the central 5 x 5 square (equivalent to 0.1 mm³). The original cell density was calculated as follows:

$$\text{Number of cells counted} = \text{cells per } 0.1 \text{ mm}^3 \times 10,000 = \text{cells per } 1 \text{ cm}^3 = \text{cells per } 1 \text{ mL}$$

For the analysis of Nrf2 levels by western blot, H4IIE-ARE cells were seeded in a sterile Nunclon Δ flat bottom 12 well plate (3.2 cm²), at 300,000 cells/well, in a total volume of 2 mL growth medium and allowed to grow overnight.

For the analysis of luciferase reporter activity, H4IIE-ARE cells were seeded in sterile Nunclon Δ flat bottom 98 well plates, at 20,000 cells/well, in a total volume of 0.2 mL growth medium and allowed to grow overnight.

2.5.4. Treatment of cells for Nrf2 western blot analysis

CDDO-Me was dissolved in DMSO at 200x the required final concentration. Under sterile conditions, H4IIE-ARE cells were exposed to 10 μL of DMSO, 10 μL of MG132 at 2 mM (giving final concentration of 10 μM) or 10 μL of CDDO-Me concentrations (i.e. 1:200 dilution) to give the required final concentrations as indicated. The concentration of DMSO in the cell culture medium was 0.5% (volume/volume; v/v). The cells were returned to a humidified incubator (37°C, 5% CO₂) for one hour.

2.5.5. Treatment of cells for luciferase activity assay.

CDDO derivatives were dissolved in DMSO at 200x the required final concentration. Under sterile conditions, H4IIE-ARE cells were exposed to 1 μL of DMSO or 1 μL of CDDO derivatives (i.e. 1:200 dilution). The concentration of DMSO in the cell culture

medium was 0.5% (v/v). The cells were returned to a humidified incubator (37°C, 5% CO₂) for 24 hours.

2.5.6. Preparation of cells for luciferase reporter assay

Following compound exposure, the media was removed and 100 µL of 1x Glo Lysis Buffer was added to each well. The plate was shaken for 5 minutes at 700 rpm to promote cell lysis. 80 µL of the cell lysate was transferred to a white 96 well flat bottom microplate and 20 µL of Bright-Glo luciferase reagent was added to each well. The Plate was shaken at 700 rpm for 15 seconds prior to quantification of luminescence on a Varioskan Flash Spectra Luminometer.

2.5.7. Preparation of cells for Nrf2 western blot analysis

Following compound exposure, the media was removed and 500 µL of phosphate buffered saline pH 7 (PBS) was added to each well. The cells were dislodged from the well surface by pipetting PBS several times. The cell suspension was transferred into 0.5 mL microcentrifuge tubes and centrifuged at 1000 g, room temperature, for 5 minutes. The pellet was washed in 200 µL PBS, centrifuged at 1000 g, room temperature for 5 minutes and resuspended in 40 µL RIPA buffer per sample. All samples were stored at -80°C.

2.5.8. Protein determination

The protein content of the cell lysates was determined using the bicinchoninic acid (BCA) protein assay. The BCA assay involves the reduction of Cu(II) to Cu(I) by proteins in a concentration dependent manner. Two molecules of bicinchoninic acid chelates the Cu(I) ion, forming a purple Cu(I) complex. This complex has a maximum absorbance at 562 nm in which the absorbance is directly proportional to protein

concentration.³² A stock solution of (2 mg/mL) bovine serum albumin (BSA) was diluted in water to give 2000, 1500, 1000, 750, 500, 250 and 125 µg/mL where 9 µL was used in a 96 well plate for a standard curve. 2 µL of cell lysate was used per sample and 250 µL of BCA assay solution (1:50 solution of copper(II) sulphate: bicinchoninic acid) was added to each well. The plate was incubated at 37°C for 30 minutes prior to absorption measurement at 570 nm.

2.5.9. Western blot analysis

2.5.9.1. 3-(*N*-morpholino)propanesulphonic acid (MOPS) running buffer

50 mM MOPS, 50 mM tris base, 3.5 mM sodium dodecyl sulphate and 1 mM EDTA.

2.5.9.2. Transfer buffer

0.2 M glycine and 25 mM Tris base in 20% methanol

2.5.9.3. Tris-buffered saline solution (TBS-Tween)

0.15 M NaCl, 25 mM tris base, 3 mM KCl, pH 7.0 supplemented with 0.1% v/v Tween 20

2.5.9.4. Method

Whole cell lysates (20 µg) were denatured with the addition of 5 µL loading buffer (70% (v/v) NuPAGE sample loading buffer, 30% (v/v) NuPAGE reducing agent) and incubated at 80°C for 5 minutes. The samples were loaded onto pre-cast 4-12% NuPAGE Novex bis-tris polyacrylamide gels, alongside 3 µL of PrecisionPlus protein Kaleidoscope standards. The samples were resolved by electrophoresis in an XCell Surelock mini-cell, using MOPS running buffer, at 90 V for 10 minutes, followed by

60 minutes at 170 V. The separated proteins were transferred to a nitrocellulose membrane in a transfer apparatus, using transfer buffer, at 230 mA for 1 hour.

Membranes were stained for 10 seconds with Ponceau S solution to ensure that the transfer was successful. The membrane was cut across the 50 kDa marker (membrane containing protein >50 kDa is referred to as top half of membrane) and the top half of the membrane was blocked overnight at 4°C on an orbital shaker in TBS-Tween and 10% (weight/volume; w/v) non-fat dry milk. The bottom half of the membrane was left in TBS-Tween overnight at 4°C on an orbital shaker. The blocked top half of the membrane was sealed in bag at 4°C on an orbital shaker for 3 hours with rabbit anti-mouse Nrf2 antibody (1:400 in 2 mL TBS-Tween containing 2% (w/v) non-fat dry milk). The bottom half of the membrane was blocked for 1 hour as described above and was exposed to rabbit anti- β -actin antibody (1:200,000 in TBS-Tween containing 2% (w/v) non-fat dry milk) for 1 hour. Following 12 washes in TBS-Tween (5 minute intervals), the membranes were probed for 1 hour with goat anti-rabbit (1:10,000 in TBS-Tween containing 2% (w/v) non-fat dry milk), or rabbit anti-mouse (1:10,000 in TBS-Tween containing 2% (w/v) non-fat dry milk) horseradish peroxidase (HRP) -conjugated secondary antisera. A further 6 washes in TBS-Tween (10 minute intervals) was performed prior to visualisation with Western Lightning chemiluminescence reagents and exposure to Hyperfilm ECL under darkroom conditions, using a Kodak BioMax MS intensifying screen. Films were developed using Kodak developer and fixer solutions. Films were scanned using a GS-800 calibrated imaging densitometer, immunoreactive band volumes were quantified using TotalLab Quantity One software, in accordance with the

manufacturer's instructions, and normalised to β -actin, which was probed as a loading control.

2.6. References

- 1 Honda, T., Finlay, H. J., Gribble, G. W., Suh, N. & Sporn, M. B. New enone derivatives of oleanolic acid and ursolic acid as inhibitors of nitric oxide production in mouse macrophages. *Bioorganic & Medicinal Chemistry Letters* **7**, 1623-1628, doi:10.1016/S0960-894X(97)00279-5 (1997).
- 2 Honda, T., Gribble, G. W., Suh, N., Finlay, H. J., Rounds, B. V., Bore, L., Favalaro, F. G., Wang, Y. & Sporn, M. B. Novel Synthetic Oleanane and Ursane Triterpenoids with Various Enone Functionalities in Ring A as Inhibitors of Nitric Oxide Production in Mouse Macrophages†. *Journal of Medicinal Chemistry* **43**, 1866-1877, doi:10.1021/jm000008j (2000).
- 3 Honda, T., Rounds, B. V., Bore, L., Finlay, H. J., Favalaro, F. G., Suh, N., Wang, Y., Sporn, M. B. & Gribble, G. W. Synthetic Oleanane and Ursane Triterpenoids with Modified Rings A and C: A Series of Highly Active Inhibitors of Nitric Oxide Production in Mouse Macrophages†. *Journal of Medicinal Chemistry* **43**, 4233-4246, doi:10.1021/jm0002230 (2000).
- 4 Honda, T., Rounds, B. V., Gribble, G. W., Suh, N., Wang, Y. & Sporn, M. B. Design and synthesis of 2-cyano-3,12-dioxoolean-1,9-dien-28-oic acid, a novel and highly active inhibitor of nitric oxide production in mouse macrophages. *Bioorganic & Medicinal Chemistry Letters* **8**, 2711-2714, doi:10.1016/S0960-894X(98)00479-X (1998).
- 5 Honda, T.-i., Rounds, B. V., Bore, L., Favalaro Jr, F. G., Gribble, G. W., Suh, N., Wang, Y. & Sporn, M. B. Novel synthetic oleanane triterpenoids: A series of highly active inhibitors of nitric oxide production in mouse macrophages. *Bioorganic & Medicinal Chemistry Letters* **9**, 3429-3434, doi:10.1016/S0960-894X(99)00623-X (1999).
- 6 Pharmaceuticals, R. *Company Statement: Termination of the BEACON Trial*, <http://www.reatapharma.com/investors-media/news/news-timeline/2012/company-statement-termination-of-beacon-trial.aspx> Last updated: 2013, Access date: **July 2013**.
- 7 Clayden, J., Greeves, N., Warren, S. & Wothers, P. *Organic Chemistry*. (Oxford University Press, 2005).
- 8 Rice, K. D., Aay, N., Anand, N. K. & Arcalas, A. *Tropane Compounds*. (2009).
- 9 Niesen, A., Barthel, A., Kluge, R., Köwitzsch, A., Ströhl, D., Schwarz, S. & Csuk, R. Antitumoractive Endoperoxides from Triterpenes. *Archiv der Pharmazie* **342**, 569-576, doi:10.1002/ardp.200900051 (2009).
- 10 Zhu, Y.-M., Shen, J.-K., Wang, H.-K., Cosentino, L. M. & Lee, K.-H. Synthesis and anti-HIV activity of oleanolic acid derivatives. *Bioorganic & Medicinal Chemistry Letters* **11**, 3115-3118, doi:10.1016/S0960-894X(01)00647-3 (2001).
- 11 Okamoto, I., Takeya, T., Kagawa, Y. & Kotani, E. Iron(III)picolinate-induced oxygenation and subsequent rearrangement of triterpenoid derivatives with hydrogen peroxide. *Chemical & Pharmaceutical Bulletin* **48**, 120-125, doi:10.1248/cpb.48.120 (2000).
- 12 Jiang, X., Greiner, J., Maravetz, L. L., Szucs, S. S. & Visnick, M. Antioxidant inflammation modulators: Novel derivatives of oleanolic acid. United states patent US 2010/0048911 A1(2009).

- 13 Sugishita, E., Amagaya, S. & Ogihara, Y. Structure-Activity studies of some oleanane triterpenoid glycosides and their related compounds from the leaves of *tetrapanax papyriferum* on anti-inflammatory activities. *Journal of Pharmacobio-Dynamics* **5**, 379-387, doi:10.1248/bpb1978.5.379 (1982).
- 14 Itoh, K., Chiba, T., Takahashi, S., Ishii, T., Igarashi, K., Katoh, Y., Oyake, T., Hayashi, N., Satoh, K., Hatayama, I., Yamamoto, M. & Nabeshima, Y.-i. An Nrf2/Small Maf Heterodimer Mediates the Induction of Phase II Detoxifying Enzyme Genes through Antioxidant Response Elements. *Biochemical and Biophysical Research Communications* **236**, 313-322, doi:10.1006/bbrc.1997.6943 (1997).
- 15 Kratschmar, D. V., Calabrese, D., Walsh, J., Lister, A., Birk, J., Appenzeller-Herzog, C., Moulin, P., Goldring, C. E. & Odermatt, A. Suppression of the Nrf2-Dependent Antioxidant Response by Glucocorticoids and 11 β -HSD1-Mediated Glucocorticoid Activation in Hepatic Cells. *PLoS ONE* **7**, e36774, doi:10.1371/journal.pone.0036774 (2012).
- 16 Ki, S. H., Cho, I. J., Choi, D. W. & Kim, S. G. Glucocorticoid Receptor (GR)-Associated SMRT Binding to C/EBP β TAD and Nrf2 Neh4/5: Role of SMRT Recruited to GR in GSTA2 Gene Repression. *Molecular and Cellular Biology* **25**, 4150-4165, doi:10.1128/mcb.25.10.4150-4165.2005 (2005).
- 17 Nguyen, T., Nioi, P. & Pickett, C. B. The Nrf2-Antioxidant Response Element Signaling Pathway and Its Activation by Oxidative Stress. *Journal of Biological Chemistry* **284**, 13291-13295, doi:10.1074/jbc.R900010200 (2009).
- 18 Ross, D., Kepa, J. K., Winski, S. L., Beall, H. D., Anwar, A. & Siegel, D. NAD(P)H:quinone oxidoreductase 1 (NQO1): chemoprotection, bioactivation, gene regulation and genetic polymorphisms. *Chemico-Biological Interactions* **129**, 77-97, doi:10.1016/S0009-2797(00)00199-X (2000).
- 19 Dinkova-Kostova, A. T., Liby, K. T., Stephenson, K. K., Holtzclaw, W. D., Gao, X., Suh, N., Williams, C., Risingsong, R., Honda, T., Gribble, G. W., Sporn, M. B. & Talalay, P. Extremely potent triterpenoid inducers of the phase 2 response: Correlations of protection against oxidant and inflammatory stress. *Proceedings of the National Academy of Sciences of the United States of America* **102**, 4584-4589, doi:10.1073/pnas.0500815102 (2005).
- 20 Reisman, S. A., Aleksunes, L. M. & Klaassen, C. D. Oleanolic acid activates Nrf2 and protects from acetaminophen hepatotoxicity via Nrf2-dependent and Nrf2-independent processes. *Biochemical Pharmacology* **77**, 1273-1282, doi:10.1016/j.bcp.2008.12.028 (2009).
- 21 Rautio, J., Kumpulainen, H., Heimbach, T., Oliyai, R., Oh, D., Jarvinen, T. & Savolainen, J. Prodrugs: design and clinical applications. *Nature Reviews Drug Discovery* **7**, 255-270, doi:10.1038/nrd2468 (2008).
- 22 Takeoka, G., Dao, L., Teranishi, R., Wong, R., Flessa, S., Harden, L. & Edwards, R. Identification of Three Triterpenoids in Almond Hulls. *Journal of Agricultural and Food Chemistry* **48**, 3437-3439, doi:10.1021/jf9908289 (2000).
- 23 Seo, S., Tomita, Y. & Tori, K. Biosynthesis of oleanene- and ursene-type triterpenes from [4-¹³C]mevalonolactone and sodium [1,2-¹³C₂]acetate in tissue cultures of *Isodon japonicus* Hara. *Journal of the American Chemical Society* **103**, 2075-2080, doi:10.1021/ja00398a034 (1981).

- 24 Seo, S., Tomita, Y., Tori, K. & Yoshimura, Y. Determination of the absolute configuration of a secondary hydroxy group in a chiral secondary alcohol using glycosidation shifts in carbon-13 nuclear magnetic resonance spectroscopy. *Journal of the American Chemical Society* **100**, 3331-3339, doi:10.1021/ja00479a014 (1978).
- 25 Leal, A. S., Wang, R., Salvador, J. A. R. & Jing, Y. Synthesis of novel heterocyclic oleanolic acid derivatives with improved antiproliferative activity in solid tumor cells. *Organic & Biomolecular Chemistry* **11**, 1726-1738, doi:10.1039/C3OB00011G (2013).
- 26 Siewert, B., Wiemann, J., Köwitsch, A. & Csuk, R. The chemical and biological potential of C ring modified triterpenoids. *European Journal of Medicinal Chemistry* **72**, 84-101, doi:10.1016/j.ejmech.2013.11.025 (2014).
- 27 Jiang, X., Greiner, J., Maravetz, L. L., Szucs, S. S. & Visnick, M. (Google Patents, 2010).
- 28 McKean, L. C., Manson, W. & Spring, F. S. 84. Triterpene resinols and related acids. Part XXV. Ketoisoleanolic acid and isoleanolic acid. *Journal of the Chemical Society (Resumed)*, 432-437, doi:10.1039/JR9520000432 (1952).
- 29 Honda, T., Favaloro, J. F. G., Janosik, T., Honda, Y., Suh, N., Sporn, M. B. & Gribble, G. W. Efficient synthesis of (-)- and (+)-tricyclic compounds with enone functionalities in rings A and C. A novel class of orally active anti-inflammatory and cancer chemopreventive agents. *Organic & Biomolecular Chemistry* **1**, 4384-4391, doi:10.1039/B307491A (2003).
- 30 Walling, J., Parent, S. D., Jonaitis, D. T. & Kral, R. M. (Google Patents, 2009).
- 31 Inc., T. R. C. *Bardoxolone*, [http://www.trc-canada.com/detail.php?CatNum=B118660&CAS=%20218600-44-3&Chemical Name=Bardoxolone&Mol Formula=C31H41O4&Synonym=CDDO;%20RTA%20401;%20-Cyano-3,12-dioxooleana-1,9\(11\)-dien-28-oic%20Acid](http://www.trc-canada.com/detail.php?CatNum=B118660&CAS=%20218600-44-3&Chemical%20Name=Bardoxolone&Mol%20Formula=C31H41O4&Synonym=CDDO;%20RTA%20401;%20-Cyano-3,12-dioxooleana-1,9(11)-dien-28-oic%20Acid)
Last updated: 2014, Access date: **January 2014**.
- 32 Smith, P. K., Krohn, R. I., Hermanson, G. T., Mallia, A. K., Gartner, F. H., Provenzano, M. D., Fujimoto, E. K., Goeke, N. M., Olson, B. J. & Klenk, D. C. Measurement of protein using bicinchoninic acid. *Analytical Biochemistry* **150**, 76-85, doi:10.1016/0003-2697(85)90442-7 (1985).

CHAPTER 3

Design and synthesis of irreversible analogues of CDDO

Chapter 3

3.1 Introduction	103
3.1.1 Aims	108
3.2 Results and discussion	109
3.2.1 NMR evidence for the reversible interaction of CDDO-Me with β -mercaptoethanol or <i>N</i> -acetyl cysteine	109
3.2.2 Mass spectrometric evidence for the interaction of CDDO-Me with thiols	116
3.2.3 Synthesis of an irreversible analogue of CDDO-Me	118
3.2.4 Synthesis of epoxide derivatives of CDDO-Me and DDO-Me	128
3.2.5 Confirming the stereochemistry of CDDO-Epoxide and DDO-Epoxide	129
3.2.6 NMR evidence for the interaction of CDDO-Epoxide with β -mercaptoethanol	135
3.2.7 Mass spectrometry evidence for the interaction of CDDO-Epoxide with GSTP1	142
3.3 Conclusion	146
3.4 Chemistry Experimental	150
3.4.1 General	150
3.4.2 Purification of solvents and reagents	150
3.4.3 Purification of products	150
3.4.4 Analysis	151
3.4.5 Numbering	151
3.4.6 Synthesis	152
	101

Chapter 3 – Design and synthesis of irreversible analogues of CDDO

3.4.7	NMR and VT-NMR experiments	155
3.4.8	Mass spectra analysis for NMR samples	156
3.4.9	Molecular modelling experiments	156
3.5	Biological experimental	157
3.5.1	Materials	157
3.5.2	Cell culture	158
3.5.3	Plating	158
3.5.4	Treatment of cells for luciferase activity assay	158
3.5.5	Preparation of cells for luciferase reporter assay	158
3.5.6	LCMS with recombinant His-GSTP with CDDO-Epoxyde	159
3.6	Reference	163

3.1 Introduction

As discussed in the previous chapter, CDDO-Me is one of the most potent activators of the transcription factor, Nrf2. However, the molecular mechanisms that underly its potency are still unknown. As detailed in chapter 1, Nrf2 is regulated by Keap1. In the presence of chemical/oxidative stress, Keap1 undergoes redox modifications that render it unable to repress Nrf2, culminating in the induction of Nrf2 regulated genes. The currently accepted mechanism of action for CDDO-Me and its derivatives as inducers of Nrf2 is that reversible interactions *via* 1,4 conjugate addition to cysteine residues within Keap1 triggers the up-regulation of cell defence signalling.

SAR studies by the Sporn group led to the identification and optimization of important pharmacophores in oleanolic acid, and ultimately led to the discovery of CDDO. This involved the optimisation of both A and C rings with the introduction of α,β unsaturated ketones (also known as Michael acceptors) at essential positions.¹⁻⁵ An electron withdrawing group within the A ring at the C-2 position was also found to be important. Different derivatives of CDDO were also discovered following SAR studies on the carboxylic acid group, yielding CDDO-Me and CDDO-Im⁶ (Figure 3.1). These compounds were initially tested as anti-inflammatory agents and specifically for their ability to block IFN- γ -dependent induction of inducible nitric oxide synthase (iNOS).^{1-5,7} It was later recognised that these compounds could also induce phase 2 cell defence responses.⁷ Phase 2 responses are highly associated with the Keap1-Nrf2 pathway (as explained in previous chapters) and biological experiments confirmed that these compounds are potent inducers of Nrf2.⁷

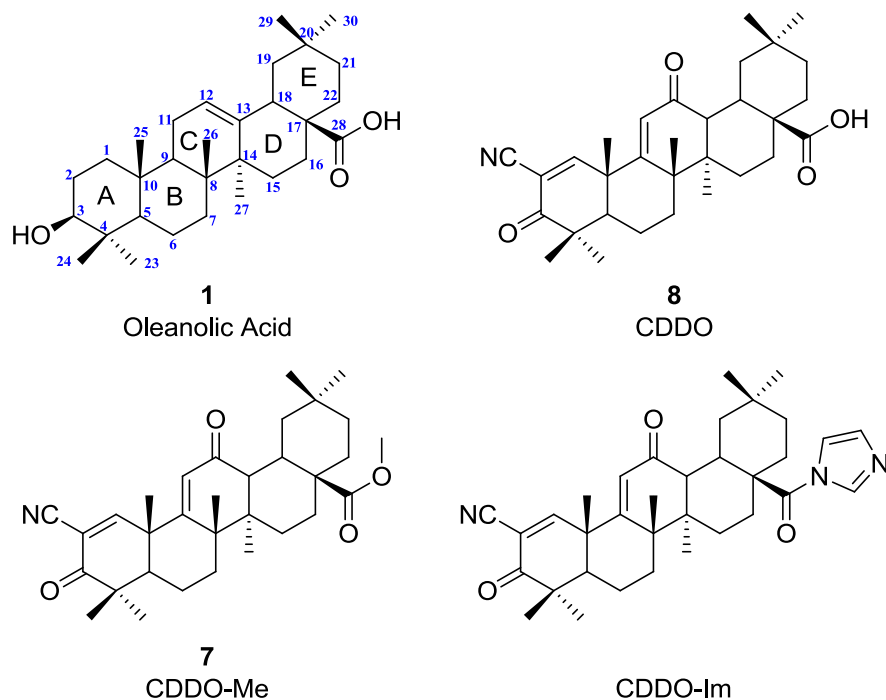


Figure 3.1: Chemical structure of oleanolic acid along with carbon and ring assignment. Important CDDO derivatives CDDO-Me and CDDO-Im.

NMR and UV studies have demonstrated that CDDO can potentially react with thiols *via* 1,4 conjugate addition.⁸ There are two potential pharmacophores that may facilitate this reaction, both being the α,β unsaturated ketones. Variable temperature NMR experiments have demonstrated that these reactions are also highly reversible in nature.⁸

Radiolabelled dexamethasone 21-mesylate (Dex-mes) **16** (Figure 3.2) has previously been shown to directly modify Keap1 cysteines 257, 273, 288, 297 and 613 *in vitro*.⁷ Importantly, pre-incubation of Keap1 with CDDO inhibits labelling of the protein by **16**, indicating, albeit indirectly, that CDDO is capable of modifying Keap1. Other competition experiments with Keap1 involve an analogue of sulforaphane **18**, which enables covalent binding to cysteine residues within Keap1. This will be discussed in more detail below.

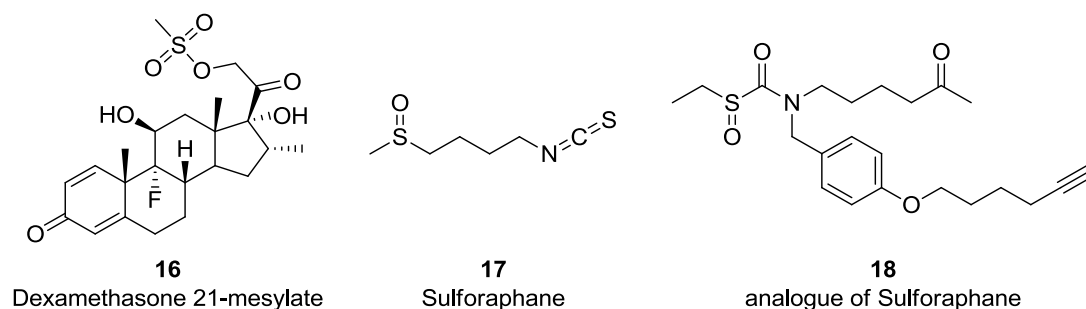


Figure 3.2: Chemical structures of dexamethasone 21-mesylate, sulforaphane and analogue of sulforaphane.

The strategy used by Ahn *et al* to produce an irreversible analogue of sulforaphane involved the identification of the potential active pharmacophore(s) and an understanding of the chemical mechanism of action. In this case, the active pharmacophore of sulforaphane is the highly reactive isothiocyanate that forms dithiocarbamate products with sulfhydryl groups. This is through an enzyme catalysed reaction by glutathione transferase or *via* a non-enzymatic route with sulfhydryl nucleophiles (Figure 3.3).^{9,10} The formation with dithiocarbamate is kinetically labile thus rendering the adduct formation of potential targets reversible. This reversibility therefore hinders the isolation and characterisation of modifications of these compounds.

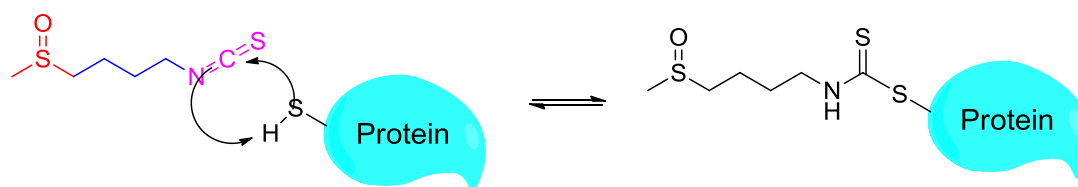


Figure 3.3: Reversible chemical mechanism of sulforaphane. The reversible mechanism between the isothiocyanate group and a thiol on a protein is due to kinetic labile formation of dithiocarbamate. The sulfoxide group is highlighted in red. The isothiocyanate group is highlighted in purple and the four carbon length chain separating the isothiocyanate group and the sulfoxide group is highlighted in blue.

SAR studies with sulforaphane have revealed that the sulfoxide group and the length of the chain separating the sulfoxide and isothiocyanate groups are important in retaining their ability to induce the phase II cytoprotective enzyme, NAD(P)H:quinone oxidoreductase (NQO1).¹¹

Mass spectroscopy experiments have revealed that a sulfoxythiocarbamate CoA analogue (**19**) selectively targets cysteine residues to form stable thiocarbamate adducts that can be readily isolated. Ahn *et al* therefore replaced the reversible isothiocyanate functional group of sulforaphane with an irreversible sulfoxythiocarbamate group which enabled retention of the natural products chemoprotective properties as well as facilitating mechanistic analysis. However, unlike the isothiocyanate, the sulfoxythiocarbamate group requires alkyl substitution on the sulphur atom (R^1 group, Figure 3.4) and to the nitrogen atom located in the sulfoxythiocarbamate (R^2 group, Figure 3.4). These substitutions provide chemical stability and reduce hydrolytic cleavage. This chemical approach

led to the design and synthesis of **18**, which was shown to be capable of binding to cysteine 273, 288 and 613 of Keap1.¹¹

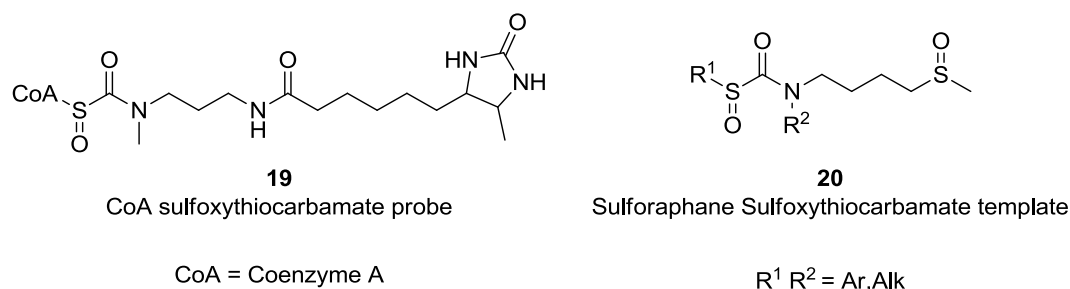


Figure 3.4: Chemical structure of the CoA sulfoxythiocarbamate and the template for the sulforaphane sulfoxythiocarbamate.

Studies by Dinkova-Kostova *et al*, using a UV spectroscopic method, have demonstrated that CDDO (**8**) derivatives react with Keap1 which result in a red shift from 256 to 266 nm.⁷ Despite this spectroscopic evidence, attempts to obtain an adduct from the interaction between CDDO (**8**) and Keap1 have been unsuccessful, which is possibly due to the reversible nature of these compounds.

Site directed mutagenesis of cysteine 151 of Keap1 has been shown to diminish the ability of CDDO derivatives to induce Nrf2 in cells indicating that cysteine 151 of Keap1 plays an important role in transducing the signal for activation of Nrf2 signalling by these compounds.^{12,13} However, the ability of CDDO-Im to induce Nrf2 is unaltered in embryonic fibroblasts derived from transgenic mice expressing a Keap1-Cys-151 mutant.¹⁴ As a result of this conflicting data, the precise nature of the interaction between CDDO derivatives and components of the Keap1-Nrf2 pathway requires clarification in order to support the ongoing optimisation of these compounds as therapeutic agents.

3.1.1 Aims

Experiments have demonstrated that CDDO undergoes highly reversible interactions with thiols and potentially bind to Keap1 as discussed above. It is currently unclear if the ability of CDDO to induce Nrf2 is due to its reversibility or its high affinity for a currently unknown molecular target(s).

Inspired by the strategy used by Ahn *et al*,¹¹ the aim of this chapter is to exploit the known SAR of CDDO and its derivatives to design and synthesize a novel analogue capable of undergoing irreversible reaction with thiols. Such a compound would represent an excellent tool with which to examine the ability of this compound class to modify Keap1, and potentially identify other molecular targets.

3.2 Results and discussion

3.2.1 NMR evidence for the reversible interaction of CDDO-Me with β -mercaptoethanol or *N*-acetyl cysteine

CDDO-Me contains two α,β unsaturated ketones that can potentially react with thiols *via* 1,4-conjugate addition as shown in Figure 3.5.

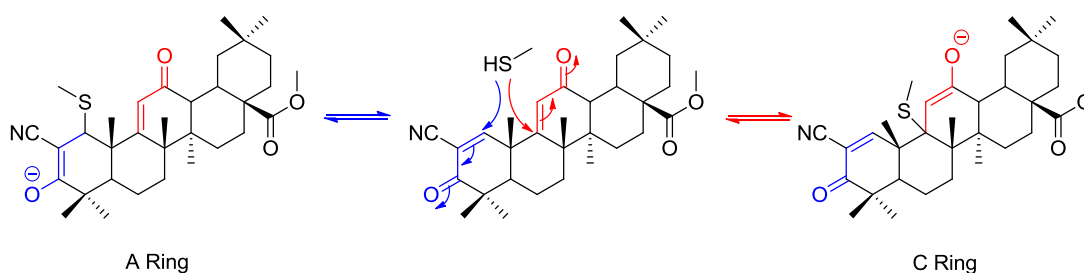


Figure 3.5: Chemical reaction of CDDO-Me with a simple thiol *via* conjugate addition on A or C rings

To further examine the above mechanism, proton NMR coupled with temperature variation was utilised to determine if one Michael acceptor is more susceptible to attack over the other.

The experiment involved the use of deuterated dimethyl sulfoxide (DMSO- d_6), CDDO-Me and the addition of varying amounts of β -mercaptoethanol (β -ME) or *N*-acetyl cysteine (NAC) (up to 2 equivalents). As shown in Figure 3.6, CDDO-Me reacts *via* conjugate addition with β -ME and NAC. Initially, both Michael acceptors appear to react with β -ME and NAC, due to the equal loss of the proton signals with increasing amounts of β -ME or NAC. However, closer observation indicates that the Michael acceptor in the C ring does not react with the thiol. This is indicated by an upfield shift of the vinylic proton on the C ring, giving a singlet at 5.85 ppm or 5.81

ppm respectively. The lack of reaction between β -ME or NAC on the C ring could be due to steric hindrance as the double bond is less susceptible to thiol attack at the C ring compared to the A ring.

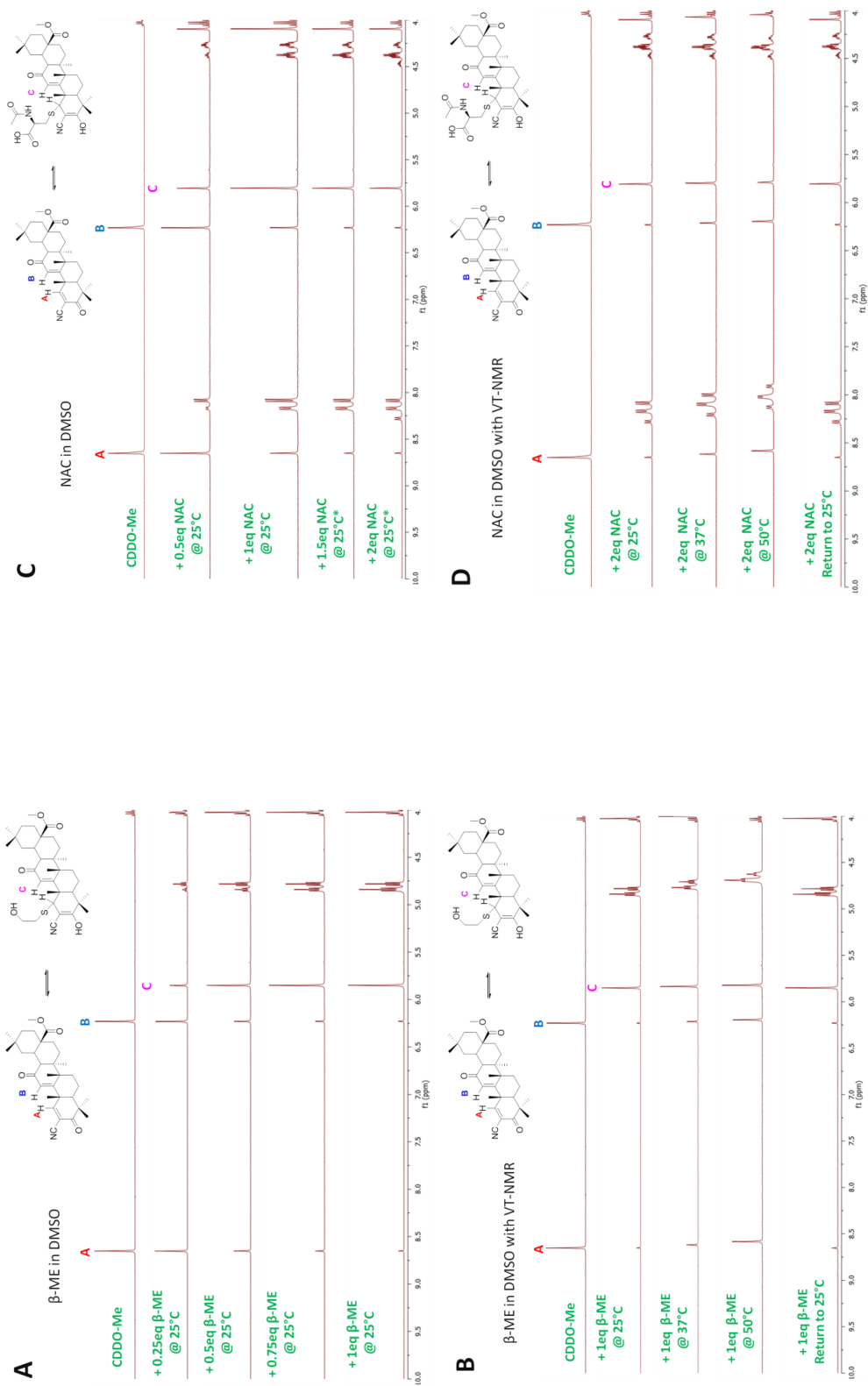


Figure 3.6: (A) CDDO-Me in DMSO- d_6 with increasing equivalent of β -mercaptoethanol; (B) VT-NMR spectra for A; (C) CDDO-Me in DMSO- d_6 with increasing equivalent of *N*-acetyl cysteine; (D) VT-NMR spectra for C

To further investigate the type of interaction causing the up-field shift of the vinylic proton, molecular modelling was adopted for this study. Molecular models can give an indication of bond distance between two atoms and can predict NMR proton shifts for the vinylic proton. To simplify the model, the D and E rings were removed from the modelling experiments. Figure 3.7 shows the simplified structure and space filled model. The sulphur and vinylic proton are in close proximity such that the van der Waals radius of the sulphur (highlighted in yellow in Figure 3.7) interacts with the vinylic proton (highlighted in purple in Figure 3.7) causing a shielding effect. Due to this shielding effect an up-field shift of the vinylic proton is observed.

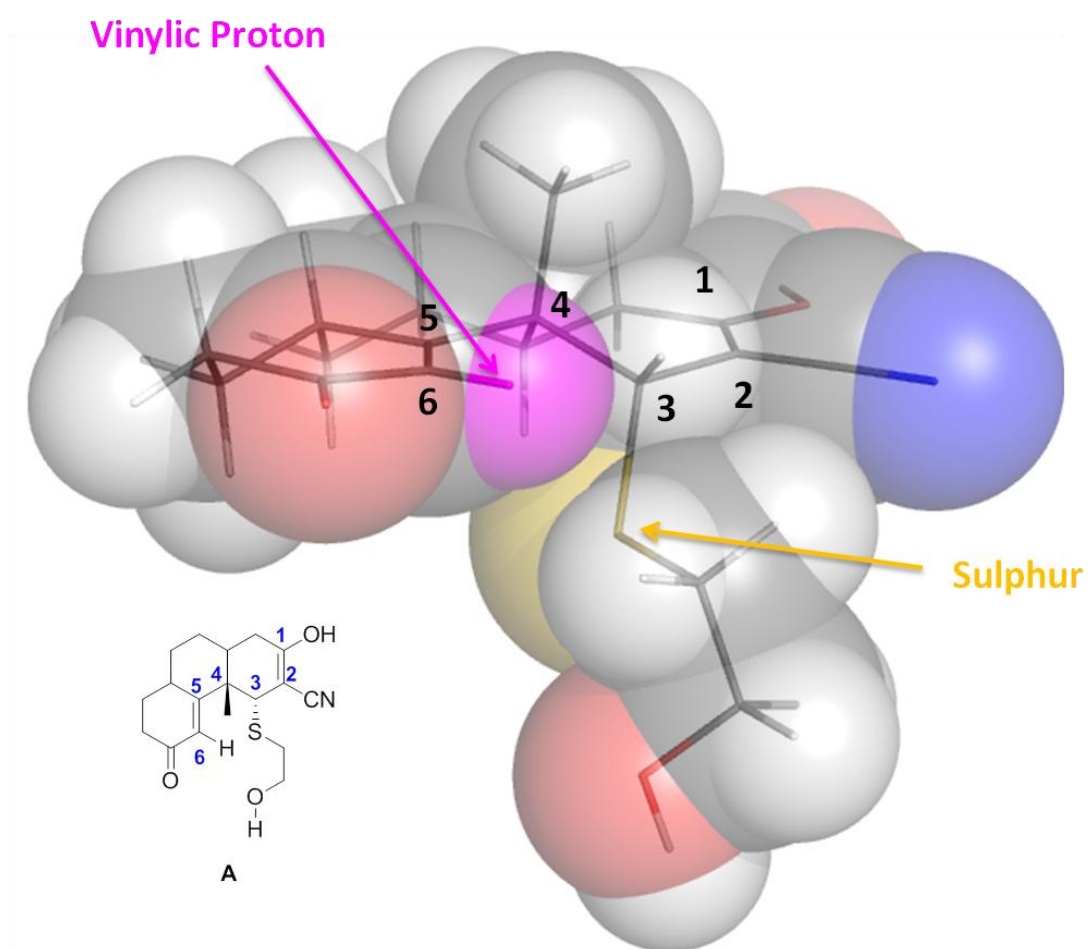


Figure 3.7: Molecule **A** (see Table 3.1) rendered as sticks with transparent spheres (carbon – grey, hydrogen – white, nitrogen – blue, oxygen – red, vinylic proton – purple, sulphur – yellow). Images generated by PyMol (<http://pymol.org>)

Since the site of thiol addition is uncertain (ie α and β attack) all possible products were modelled including the enol intermediates. In total, six possible thiol addition products were modelled (two enol [**A** and **B**] and four ketone [**C-F**]); the results are presented in Table 3.1. The bond distances between the sulphur-hydrogen (vinylic) atoms are between 3.2-2.5 Å. The vinylic proton from experimental NMR is located at 5.85 ppm. From the modelling experiments, the enol form (Table 3.1, **A** and **B**) is predicted as the closer set out of the six possible products. The predicted NMR proton shift for the vinylic proton is closer to the enol which results from an alpha thiol attack (**A**) giving a predicted NMR proton shift at 5.66 ppm. Although the modelling data suggests that **A** is the major product due to thiol attack, it cannot rule out the other potential products as the molecular model is a guide and cannot give experimental value.

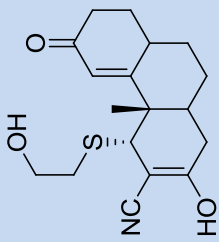
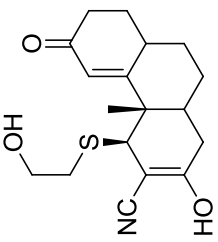
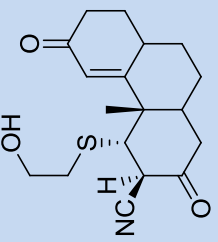
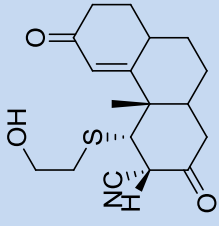
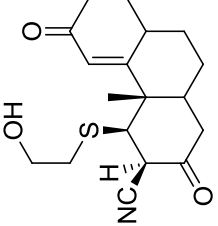
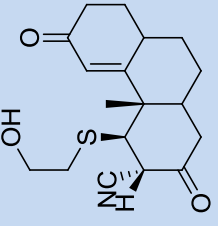
Structure		Calculated vinylic proton (ppm)	S-H vinylic distance (Å)
A		5.66	3.007
B		5.62	2.611
C		5.44	3.048
D		5.51	3.236
E		5.54	2.580
F		5.64	2.597
Experimental vinylic proton			5.66 ppm

Table 3.1: The Molecular modelling data for six potential thiol products from the reaction of CDDO-Me and β -mercaptoethanol. Data includes experimental vinylic proton shift, predicted proton shift for the vinylic proton and the distance between the hydrogen and sulphur atom.

Variable temperature NMR (VT-NMR) was used to determine if the interaction between CDDO-Me and the model thiols was reversible. The temperature of the NMR sample was increased to 37°C and then to 50°C. The sample was left to stabilise prior to spectra analysis at the two temperature points (Figure 3.6B and Figure 3.6D). The data demonstrates that CDDO-Me is a reversible thiol modifier as peaks A and B increase in signal intensity, while peak C decreases upon heating. Upon cooling the reaction back to room temperature (25°C), CDDO-Me was capable of reacting with β -ME or NAC once again. These results are consistent with published literature.⁸

3.2.2 Mass spectrometric evidence for the interaction of CDDO-Me with thiols

In order to confirm the NMR data, aliquot of the reactions was analysed by direct infusion mass spectrometry (MS). The data presented in Figure 3.8 confirms that one thiol addition is present between CDDO-Me and β -ME or NAC. This is shown at peaks 583.9 m/z (Figure 3.8A) and 669.4 m/z (Figure 3.8B) respectively. The abundance of the two adducts were low, which is possibly due to the reversible nature of the reactions, consistent with the NMR data. A mass corresponding to a double thiol adduct was not detected in either reaction.

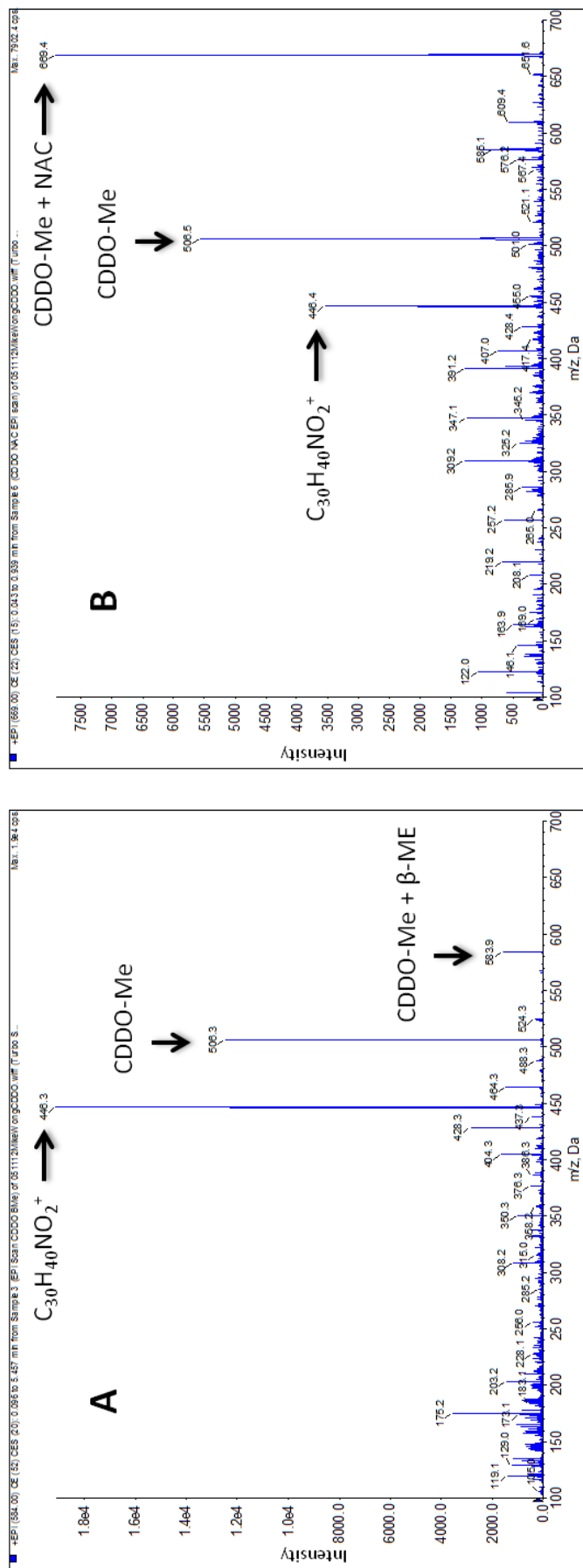


Figure 3.8: Direct infusion mass spectrometry of NMR experiments containing CDDO-Me and β -mercaptoethanol **A** or *N*-acetyl cysteine **B**; **(A)** confirms that CDDO-Me conjugated with β -mercaptoethanol was present at 583.9 m/z; **(B)** confirms that CDDO-Me conjugated with *N*-acetyl cysteine was present at 669.4 m/z. The observed mass of 446.4 m/z corresponds to fragmentation of CDDO-Me and the loss of the methyl ester group.

3.2.3 Synthesis of an irreversible analogue of CDDO-Me

3.2.3.1 Methyl 3,12-dioxooleana-1,9(11)-dien-28-oate (DDO-Me)

The cyano group is a highly electron withdrawing group and renders the α,β unsaturated ketone more susceptible to nucleophilic attack. In addition, the cyano group can also stabilise a negative charge more effectively following reversibility. As a result, removal of the cyano group should enable the irreversible formation of a ketone shown in Figure 3.9.

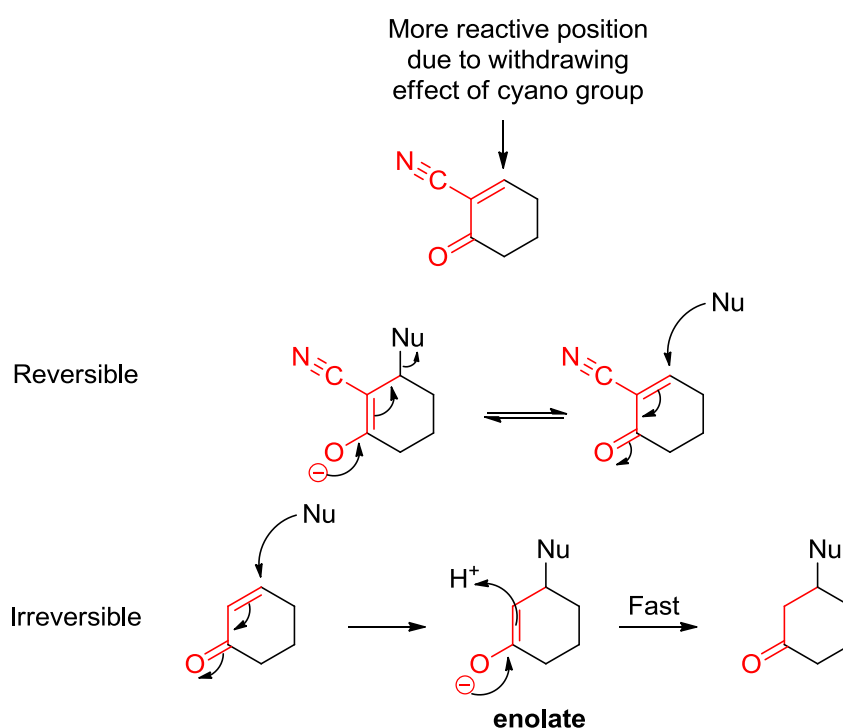
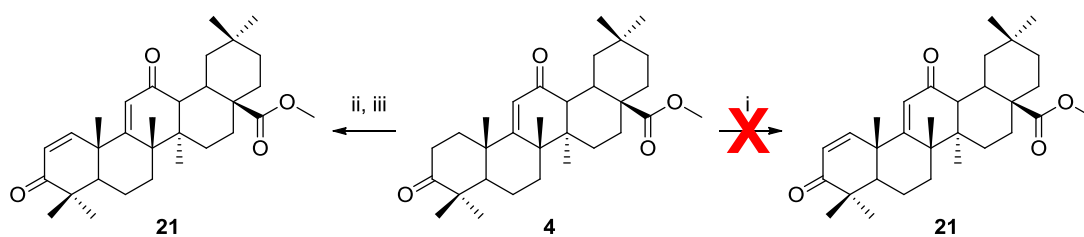


Figure 3.9: Reversible and irreversible nucleophilic attack and the effect of a cyano withdrawing group.

The SAR defined as a result of the full synthesis of CDDO (chapter two) has enabled the development and synthesis of **21**.



Scheme 3.1: *Reagents and conditions:* (i) DDQ (1.7 equiv), Benzene, reflux, 15 mins; (ii) phenylselenenyl chloride, ethyl acetate, r.t., 2.5 hours; (iii) THF with H₂O, 30% H₂O₂

Initial synthesis of **21** involved intermediate **4** and 2,3-dichloro-5,6-dicyano-1,4-benzoquinone (DDQ). (Detailed synthesis of **4** can be found in chapter two). Unfortunately, only starting material was recovered from the reaction. However, the use of phenylselenenyl chloride followed by oxidation with hydrogen peroxide gave a 57% yield of **21** (Scheme 3.1).

The ability of **21** to induce Nrf2 signalling was determined with the Nrf2-sensitive luciferase reporter assay described in chapter two. The EC₂₀₀ for DDO-Me (**21**) was shown to be 1500 x less potent than the parent compound CDDO-Me. This data highlights the importance of the cyano group within ring A for driving the high potency of CDDO-Me as an inducer of Nrf2.

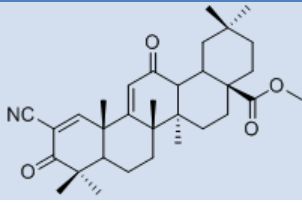
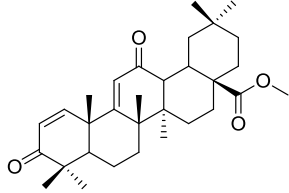
Compound	Structure	Concentration that induces Nrf2 reporter to 200% (EC ₂₀₀)
CDDO-Me		0.62 nM ± 0.02
DDO-Me (21)		0.90 μM ± 0.08

Table 3.2: Relative potencies of CDDO-Me and DDO-Me as inducers of an Nrf2-regulated luciferase reporter transgene in H4IIE-ARE cells

3.2.3.2 NMR evidence for the irreversible interaction of DDO-Me with β-mercaptoethanol or *N*-acetyl cysteine

The incubation of DDO-Me in DMSO-d⁶ and up to 2 equivalents of β-ME or NAC resulted in no reaction after 5 days (data not shown). Given that CDDO-Me reacted readily with thiols at room temperature, this data indicates that the loss of the cyano group at C-2 renders these compounds incapable of reacting with thiol groups under the conditions described. Despite this, DDO-Me is able to induce Nrf2 signalling albeit less potently than CDDO-Me. The full crystal structure of Keap1 is currently unknown, however, important cysteine residues could be in close proximity to basic amino acids, enabling deprotonation of cysteine thiols and allowing the formation of a thiolate anion. The thiolate anion is more nucleophilic in nature than that of a general thiol group and therefore should attack Michael acceptors more readily. An example of such a case is the cysteine protease enzyme of the papain family where Cys-25 and His-159 are present in the active site. The

His-159 deprotonates the cysteine forming a thiolate anion and both Cys-25 and His-159 are present as an ion pair.^{15,16}

To confirm if an anion is required for a thiol to react with DDO-Me, 1 equivalent of an organic base, in this case triethylamine (TEA), was added to the NMR reactions. The samples were left at room temperature and proton NMR spectra were taken at set time intervals. For β -ME the reaction reached equilibrium after 2 days (Figure 3.10A), while for NAC the time taken for the sample to reach a stable equilibrium was up to 4 days (Figure 3.10B). The upfield shift of proton labelled as D in Figure 3.10A and Figure 3.10B was used as a reference for the progression of the reaction with thiols. This data further confirms that the C ring is not reactive with thiols, and that a more reactive thiolate anion is required for a reaction with DDO-Me to be observed. The data show that the A ring reacts with the thiolate anions, whilst VT-NMR at 37°C and 50°C confirmed that these reactions were not reversible.

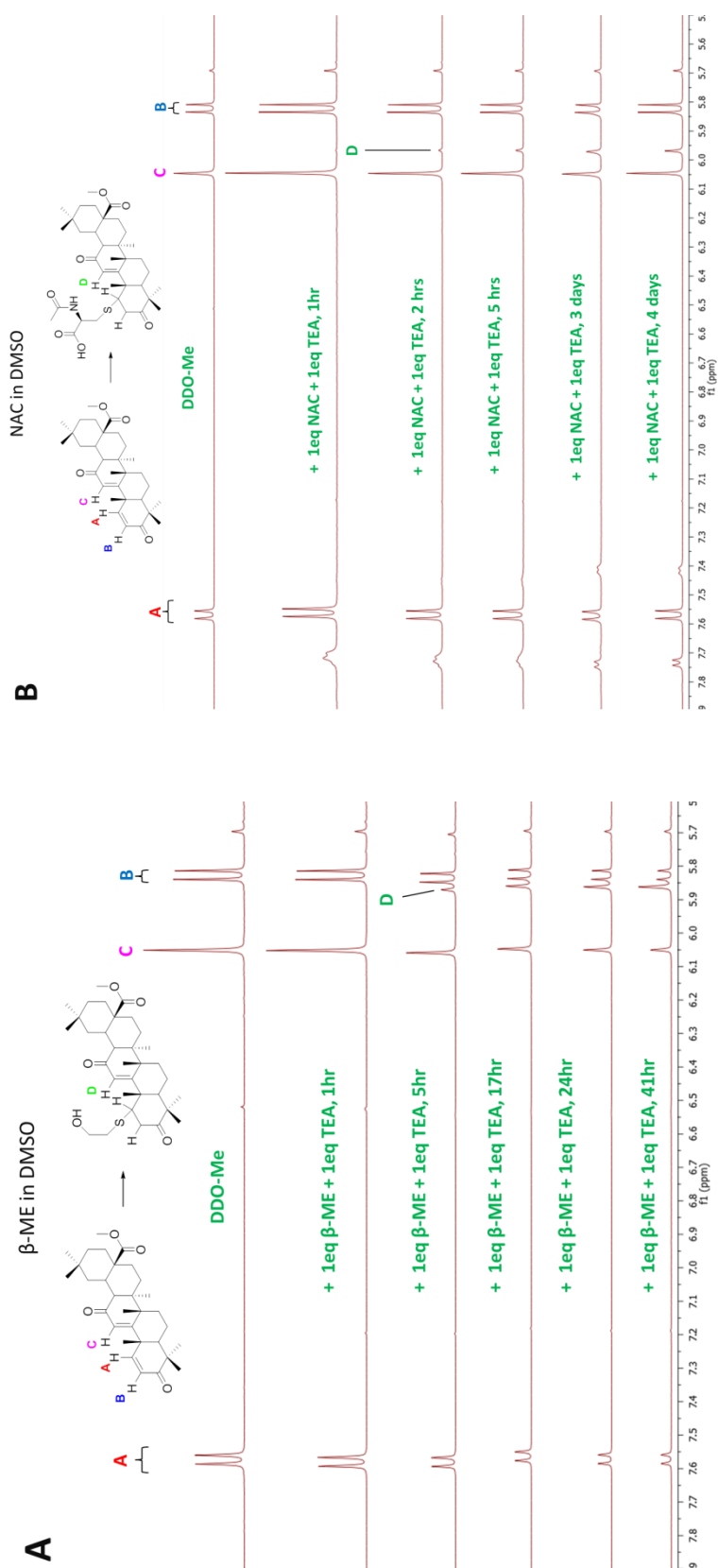


Figure 3.10: (A) DDO-Me in DMSO- d_6 with 1 equivalent of β -mercaptoethanol and 1 equivalent of triethylamine; proton spectra were taken at the indicated time intervals, and the stable thiol adduct is monitored by the appearance of peak D; (B) DDO-Me in DMSO- d_6 with 1 equivalent of *N*-acetylcysteine and 1 equivalent of triethylamine; proton spectra were taken at the indicated time intervals and is monitored by the appearance of peak D.

3.2.3.3 Molecular modelling for the irreversible interaction of DDO-Me with β -mercaptoethanol

As observed in the NMR experiments with CDDO-Me, van der Waals interaction between the sulphur and hydrogen located on the Michael acceptor in the C ring resulted in an up-field shift in proton signal. The model image is shown in Figure 3.11. Similar to CDDO-Me, molecular modelling was utilised to provide an understanding of which product is formed (Table 3.3). The experimental proton shift is located at 5.86 ppm. Comparing the predicted proton shifts in Table 3.3 to those observed in the experiment, it is clear that **K** and **I** are the closer match compared to **H** and **J**. The reactive point in which thiol addition occurs contains an adjacent beta methyl. This causes a steric hindrance and therefore the thiol addition occurs from the alpha face. Similar reactions with steroidal compounds also produce selective alpha additions due to an adjacent beta methyl.¹⁷

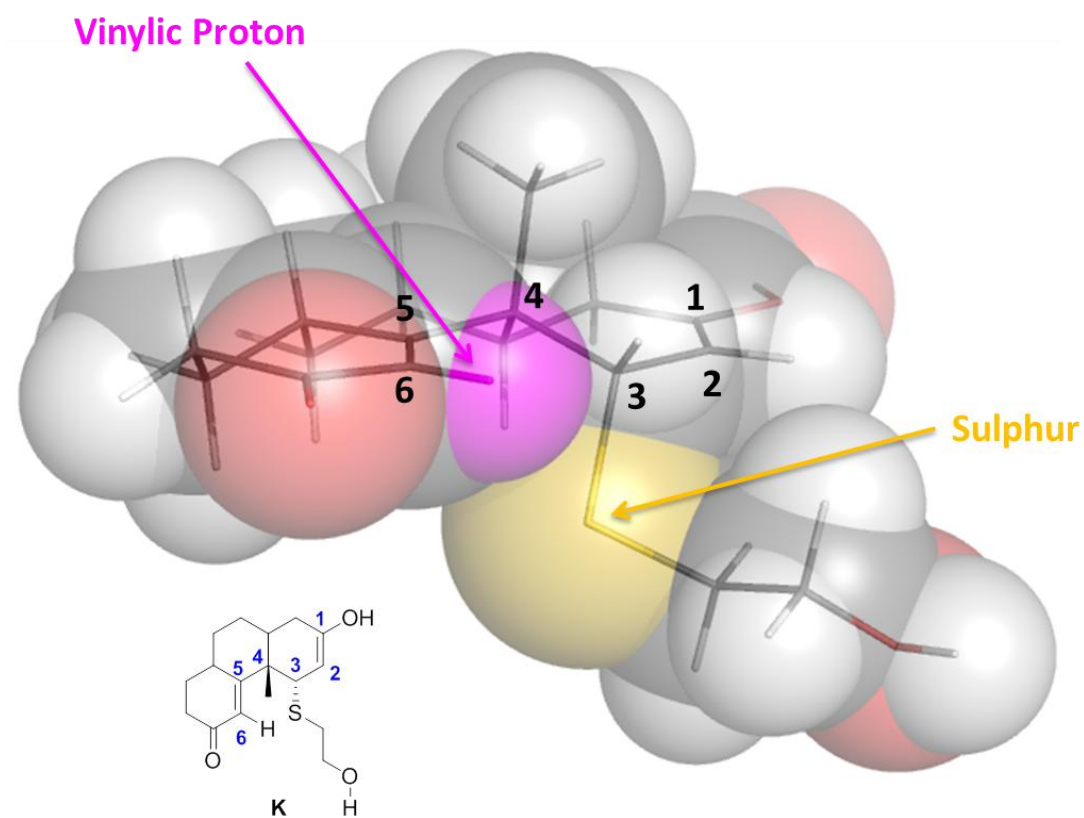


Figure 3.11: Molecule K (see Table 3.3) rendered as sticks with transparent spheres (carbon – grey, hydrogen – white, nitrogen – blue, oxygen – red, vinylic proton – purple, sulphur – yellow). Images generated by PyMol (<http://pymol.org>)

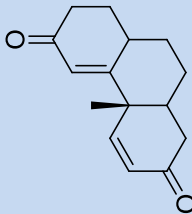
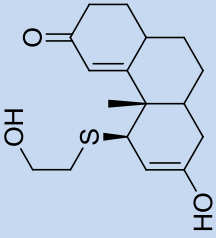
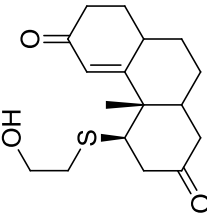
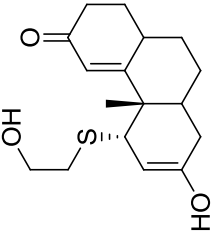
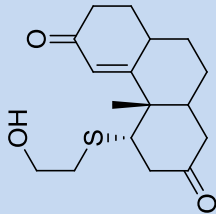
Experimental vinylic proton		5.86 ppm			
Structure	Calculated vinylic proton (ppm)	S-H vinylic distance (Å)	Structure	Calculated vinylic proton (ppm)	S-H vinylic distance (Å)
G 	5.78	-	J 	5.65	2.636
H 	5.58	2.573	K 	5.92	2.845
I 	5.91	2.927			

Table 3.3: Molecular modelling data for four potential thiol products and parent compound DDO-Me (**21**). Data includes experimental vinylic proton shift, predicted proton shift for the vinylic proton and the distance between the hydrogen and sulphur atom.

3.2.3.4 Mass Spectrometry evidence for the interaction of DDO-Me with thiols

An aliquot of the NMR samples was analysed by MS. The NMR data presented in Figure 3.10 confirms that only one thiol addition is present between DDO-Me and β -ME or NAC. The DDO-Me- β -ME adduct was detected at peak 559.6 m/z (Figure 3.12A) and the DDO-Me-NAC adduct at 644.6 m/z (Figure 3.12B). As for reactions with CDDO-Me (see 3.2.2) and consistent with the NMR data, a mass corresponding to a double thiol adduct was not detected in either reaction.

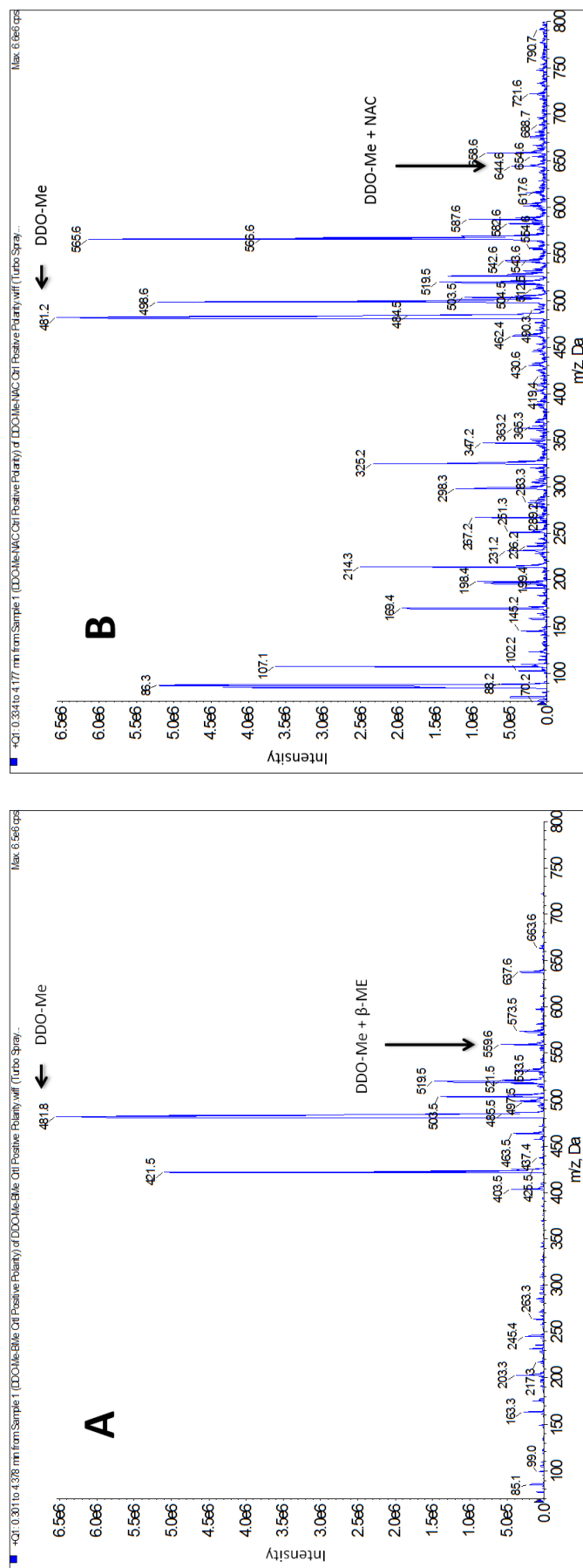


Figure 3.12: Direct infusion mass spectrometry of NMR reactions containing DDO-Me and β -mercaptoethanol **A** or N-acetyl cysteine **B**. **(A)** confirms that DDO-Me conjugated with β -mercaptoethanol was present at 559.6 m/z; **(B)** confirms that CDDO-Me conjugated with N-acetyl cysteine was present at 644.6 m/z.

3.2.4 Synthesis of epoxide derivatives of CDDO-Me and DDO-Me

In light of the relatively poor thiol reactivity of DDO-Me and its low potency as a Nrf2 inducer, and in order to diversify the overall chemical strategy, an alternative irreversible analogue of CDDO-Me was designed, based on the introduction of an epoxide functional group. The angles of the bonds within the three membered ring (60° compared with 109.5° for standard tetrahedral geometry) renders this functional group highly strained (Figure 3.13).^{18,19} The mechanism by which this functional group interacts with a thiol is shown below, with the highly strained epoxide opened up by nucleophilic attack. The resulting alkoxide can then be protonated to give a stable alcohol group, and as such, an irreversible thiol adduct is formed.

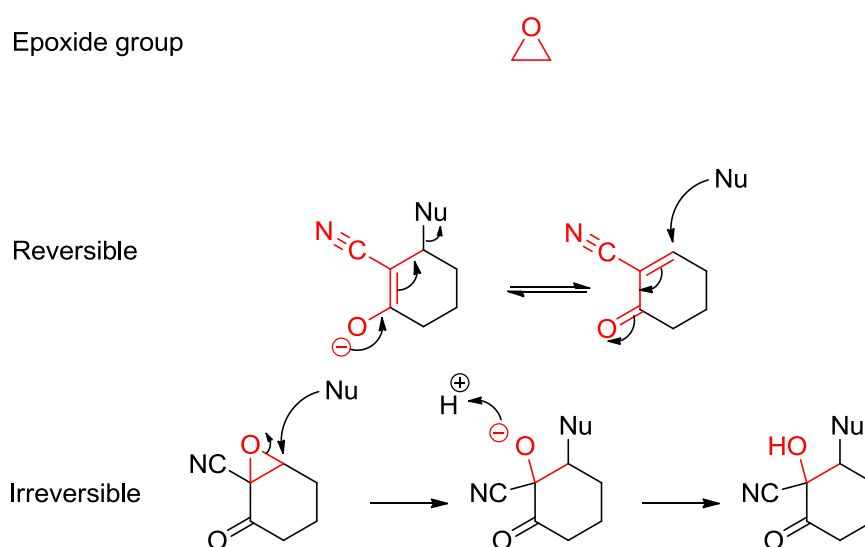
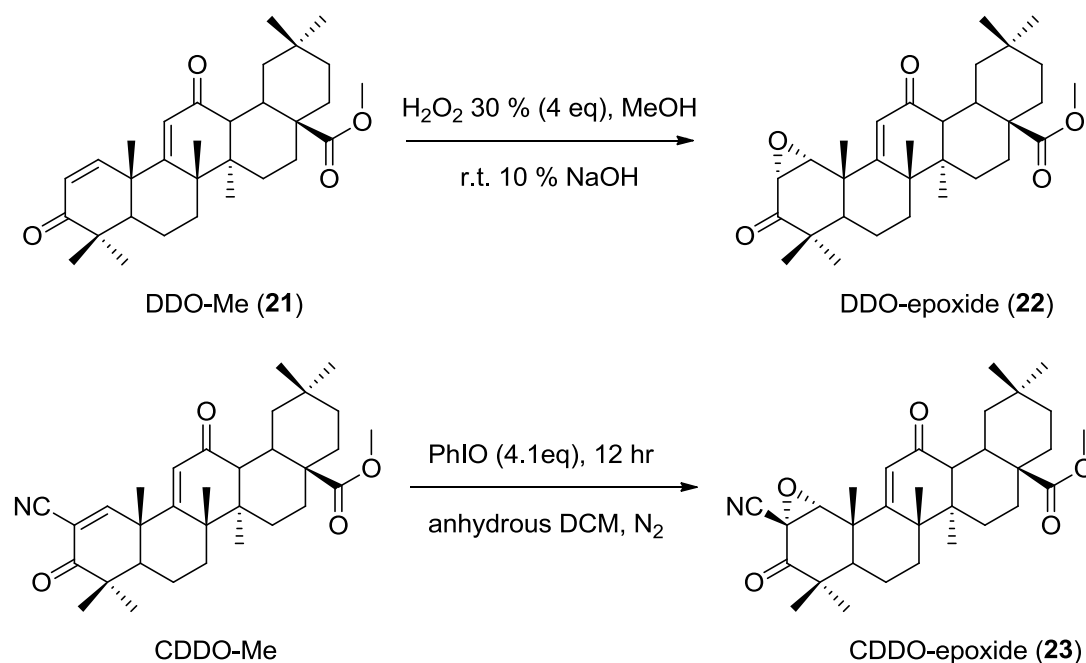


Figure 3.13: Chemical mechanism of an epoxide functional group during nucleophilic attack.

Incorporation of the epoxide functional group was attempted using DDO-Me and CDDO-Me as starting materials. DDO-Epoxide (**22**) required the use of hydrogen

peroxide and a base, giving **22** in a 49% yield. In an attempt to form CDDO-Epoxyde (**23**) hydrogen peroxide and a base were utilized, however, this approach did not yield the required product, and therefore an alternative procedure was required. The use of iodosobenzene in anhydrous dichloromethane (DCM) yielded CDDO-Epoxyde in 75% (Scheme 3.2).



Scheme 3.2: Chemical conditions and reagents required for the synthesis of DDO-Epoxyde and CDDO-Epoxyde.

The stereochemistry of the epoxide located on **22** and **23** is uncertain despite comparing proton and carbon NMR to patent literature data.²⁰

3.2.5 Confirming the stereochemistry of CDDO-Epoxyde and DDO-Epoxyde

It is currently assumed that the epoxide is in the alpha position as shown in Scheme 3.2 (**22** and **23**). However, patent literature did not provide detailed evidence for the assignment of the epoxides stereochemistry. NMR Nuclear Overhauser Effect (nOe) has been used to confirm the stereochemistry of the epoxides. nOe

experiments measure interactions through space between close range nuclei (2-4 Å).²¹ Assuming that the proton on C-1 is in the beta position (epoxide in the alpha), NMR nOe experiments between C-25 β -methyl protons and C-1 β -proton would produce an nOe signal when the protons on the methyl are irradiated (Figure 3.14, **22a** and **23a**). However, if the proton on C-1 is in the alpha position and the epoxide is in the beta, then no nOe signal will be observed as the distance between the C-25 protons and C-1 exceed the 2-4 Å distance required for an interaction to occur (Figure 3.14, **22b** and **23b**).

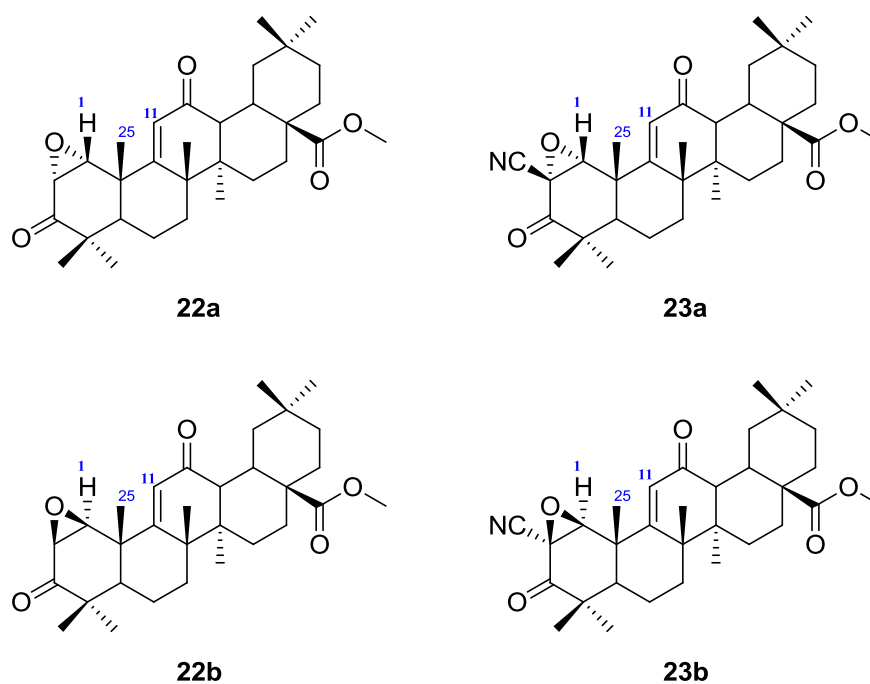


Figure 3.14: DDO-Epoxy and CDDO-Epoxy and the possible stereochemistry of the epoxides including numbering of the protons of interest. **22a** and **23a** represent the epoxide in the alpha position while **22b** and **23b** represent the epoxide in the beta position.

nOe experiments require a viscous solvent; therefore DMSO- d_6 was used for these experiments. The C-25 methyl protons and the C-1 proton were identified for both

DDO-Epoxyde and CDDO-Epoxyde. The C-25 methyl protons were irradiated and an nOe signal for the C-1 and C-11 protons were observed (Figure 3.15, blue spectra). This confirms that the alpha epoxydes were obtained. To further confirm this result, the C-1 proton was irradiated. nOe signals were observed for C-11 and C-25 methyl protons (Figure 3.15, green spectra).

Similar epoxydes have also been synthesised containing a steroidal back bone. This reaction also yielded the alpha epoxyde due to the adjacent beta methyl group.²²

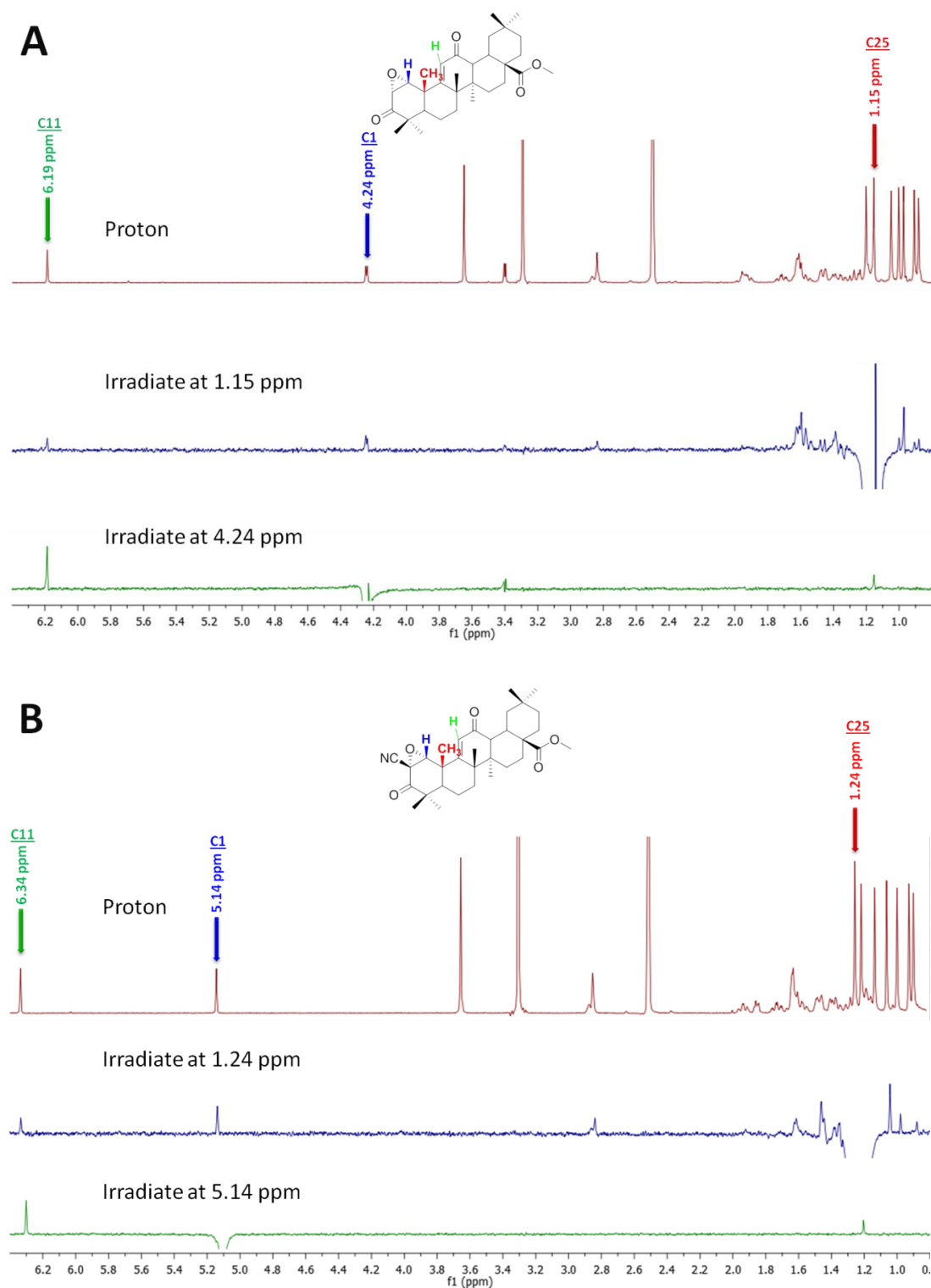


Figure 3.15: nOe experiments for DDO-Epoxyde (**A**) and CDDO-Epoxyde (**B**). Irradiation at C-25 demonstrates that C-1 is in the beta position (blue spectra). Irradiation of the C-1 nuclei further confirms that C-1 proton is in the beta position due to the nOe signal of C-25 (green spectra).

The ability of **22** and **23** to induce Nrf2 signalling was determined using the Nrf2 sensitive luciferase reporter assay. The data is shown in Table 3.4 and Graph 3.1, along with CDDO-Me and **21**. The EC₂₀₀ values for **21** and **22** were in the micromolar range, while those for CDDO-Me and **23** were in the nanomolar range. **22** was approximately 17 times less active than **21** as an inducer of Nrf2. Surprisingly, **23** was approximately 3 times less potent than CDDO-Me. This questions whether the formation of a reversible covalent bond *via* the α,β unsaturated ketone located on the A ring is the primary determinant of the potency of these compounds as inducers of Nrf2. **23** was selected for NMR studies as this was the most active of the two epoxide containing compounds.

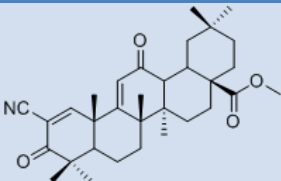
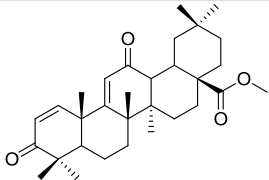
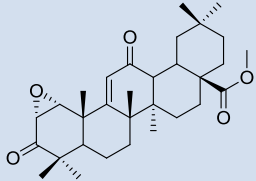
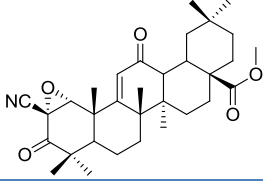
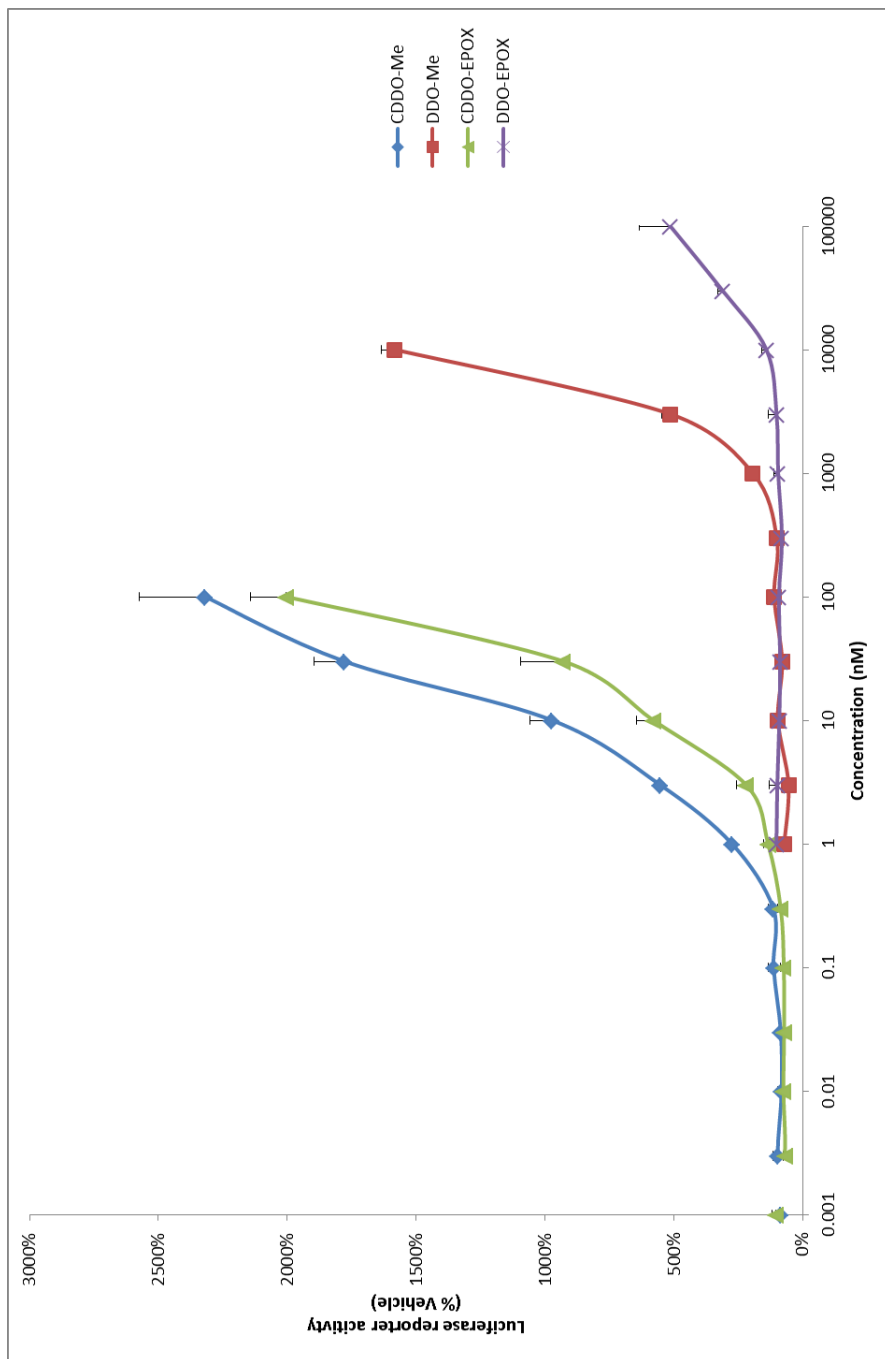
Compound	Structure	Concentration that induces Nrf2 reporter to 200% (EC ₂₀₀)
CDDO-Me (7)		0.62 nM ± 0.02
DDO-Me (21)		0.90 μM ± 0.08
DDO-Epoxyde (22)		15.42 μM ± 0.58
CDDO-Epoxyde (23)		2.11 nM ± 0.24

Table 3.4: Relative potencies of CDDO-Me, DDO-Me, DDO-Epoxyde and CDDO-Epoxyde as inducers of an Nrf2-regulated luciferase reporter transgene in H4IIE-ARE cells.



Graph 3.1: Relative abilities of CDDO-Me, DDO-Me, CDDO-Epoxyde and DDO-Epoxyde to induce an Nrf2-regulated luciferase transgene in H4IIE-ARE cells over 24h. Data points were normalised to the vehicle control (DMSO) n=3.

3.2.6 NMR evidence for the interaction of CDDO-Epoxyde with β -mercaptoethanol

A proton NMR was obtained for CDDO-Epoxyde in DMSO- d^6 following the addition of β -ME and triethylamine, as shown in Figure 3.16A. In contrast to CDDO-Me, CDDO-Epoxyde did not react instantly and required addition of triethylamine to promote covalent interaction with β -ME. However, the reaction proceeded relatively quickly compared to DDO-Me. Once equilibrium was reached, proton VT-NMR (Figure 3.16B) was performed. Heating of the sample did not result in the reversion of the reaction, indicating its stability.

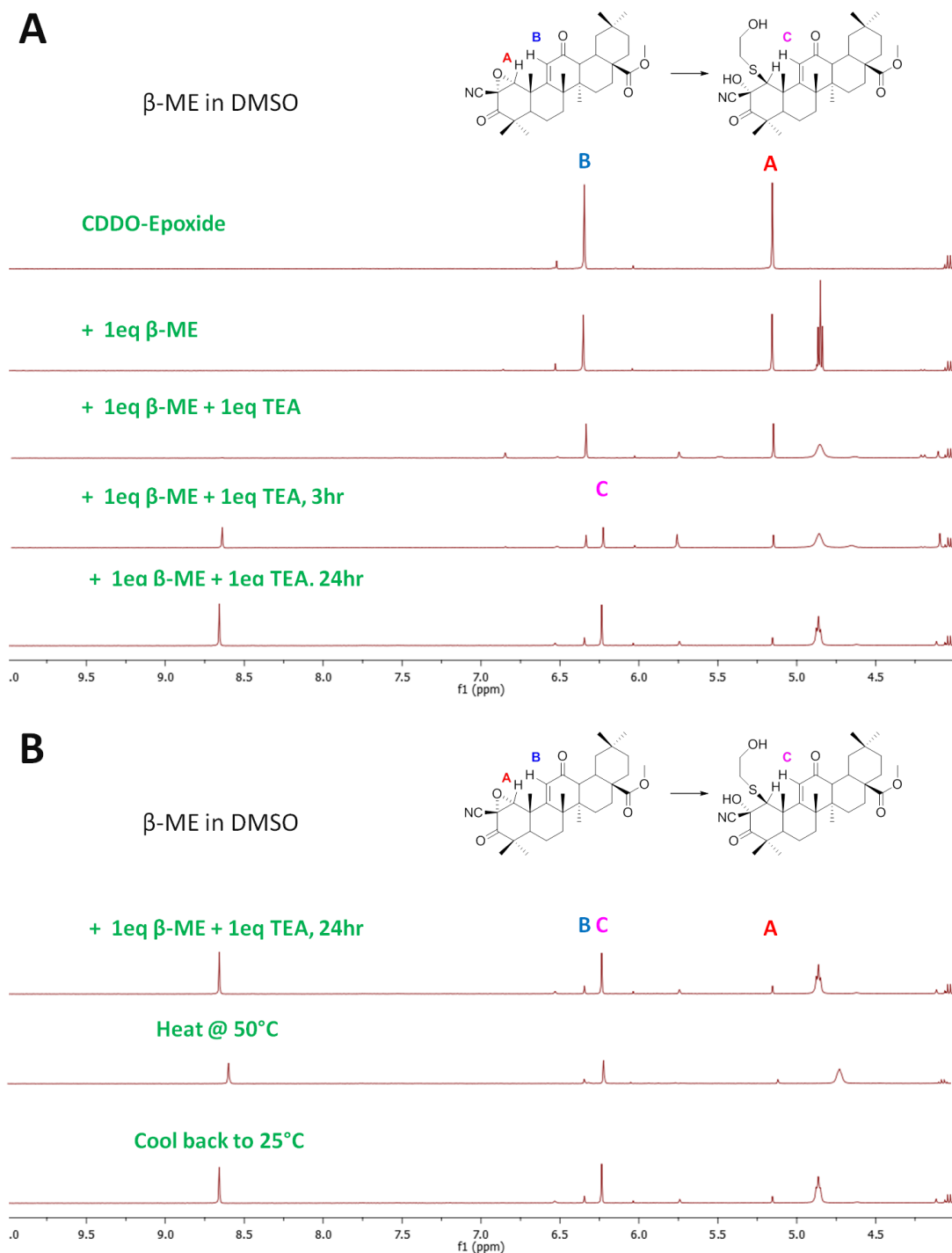


Figure 3.16: Proton NMR and proton VT-NMR; **(A):** 24 hours monitoring of the reaction of CDDO-Epoxy (**23**) and β -mercaptoethanol in the presence of triethylamine; **(B):** Heating of the sample did not reverse thiol addition.

3.2.6.1 Molecular modelling for the interaction of CDDO-Epoxyde with β -mercaptoethanol

Similar to the previous NMR experiments, the vinylic proton is shifted upfield from 6.34 ppm to 6.23 ppm. This interaction between vinylic proton and sulphur was modelled and the results are shown in Table 3.5. The exact confirmation of the epoxyde is in the alpha position as determined earlier in the chapter. However, for completeness, both alpha and beta CDDO-Epoxydes were modelled (**L** and **K** from Table 3.5). The experimental vinylic proton is located at 6.34 ppm. Comparing this with the model, this value is closest to the alpha epoxyde model **L**. If this is true, the addition of a thiol will result in the beta addition of the thiol (**N**). Both alpha and beta addition of the compounds are modelled. The experimental proton shift (6.23 ppm) is closest to **N** (5.59 ppm) giving further confidence that the CDDO-Epoxyde assignment, along with the predicted thiol adducts, are correct.

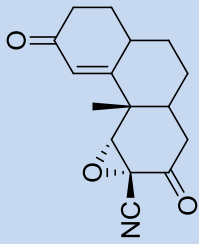
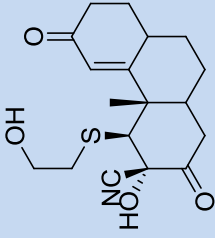
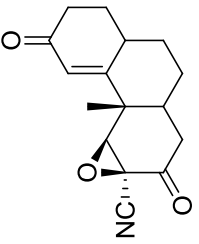
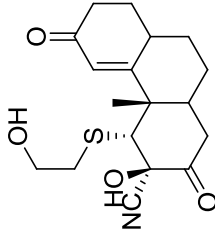
Structure	Calculated vinylic proton (ppm)	S-H vinylic distance (Å)	Structure	Calculated vinylic proton (ppm)	S-H vinylic distance (Å)
L 	6.00	-	N 	5.59	3.264
M 	5.78	-	O 	5.47	2.591
			Experimental vinylic proton	6.23 ppm	

Table 3.5: Molecular modelling data for two potential thiol products and parent compounds CDDO-Epoxyde (**23**). Data includes experimental vinylic proton shift, predicted proton shift for the vinylic proton and the distance between the hydrogen and sulphur atom.

3.2.6.2 nOe experiments for the interaction of CDDO-Epoxyde with β -mercaptoethanol

In addition to the molecular modelling, nOe experiments were performed. The C-25 β -methyl protons were located at similar chemical shifts to pure CDDO-Epoxyde. (Figure 3.17)

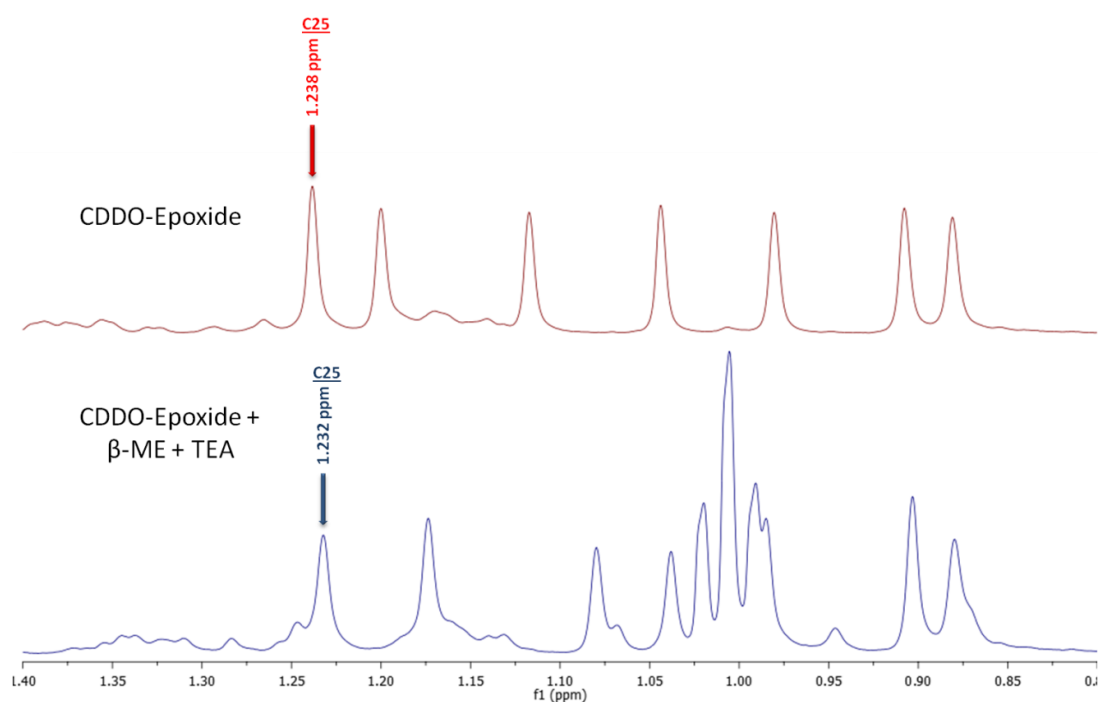


Figure 3.17: Proton NMR for CDDO-Epoxyde compared with the CDDO-Epoxyde- β -mercaptoethanol reaction mixture. The C-25 methyl proton signal is highlighted.

The irradiation of the C-25 methyl proton signal did not produce a nOe signal (data not shown). This further supports the model predictions where β -mercaptoethanol attacks from the opposite side of the epoxide resulting in a beta addition of the thiol.

3.2.6.3 Mass Spectrometry evidence for the interaction of CDDO-Epoxyde with β -mercaptoethanol

An aliquot of the sample was analysed by MS. A peak corresponding to the CDDO-Epoxyde- β -Me adduct was detected at 602.39 m/z, as opposed to the expected 600 m/z (Figure 3.18). The reaction was performed in deuterated DMSO, therefore, a possible explanation is the addition of deuterium during the rearrangement of the epoxyde and deuterium exchange between the hydroxyl group located on β -mercaptoethanol. The mass spectra data also confirmed the starting material was detected at 522.41 m/z. Mass spectrometry confirmed that a stable CDDO-Epoxyde-thiol adduct was formed, justifying further experimentation to define the value of CDDO-Epoxyde as a chemical tool for defining the target(s) of this compound class in cells.

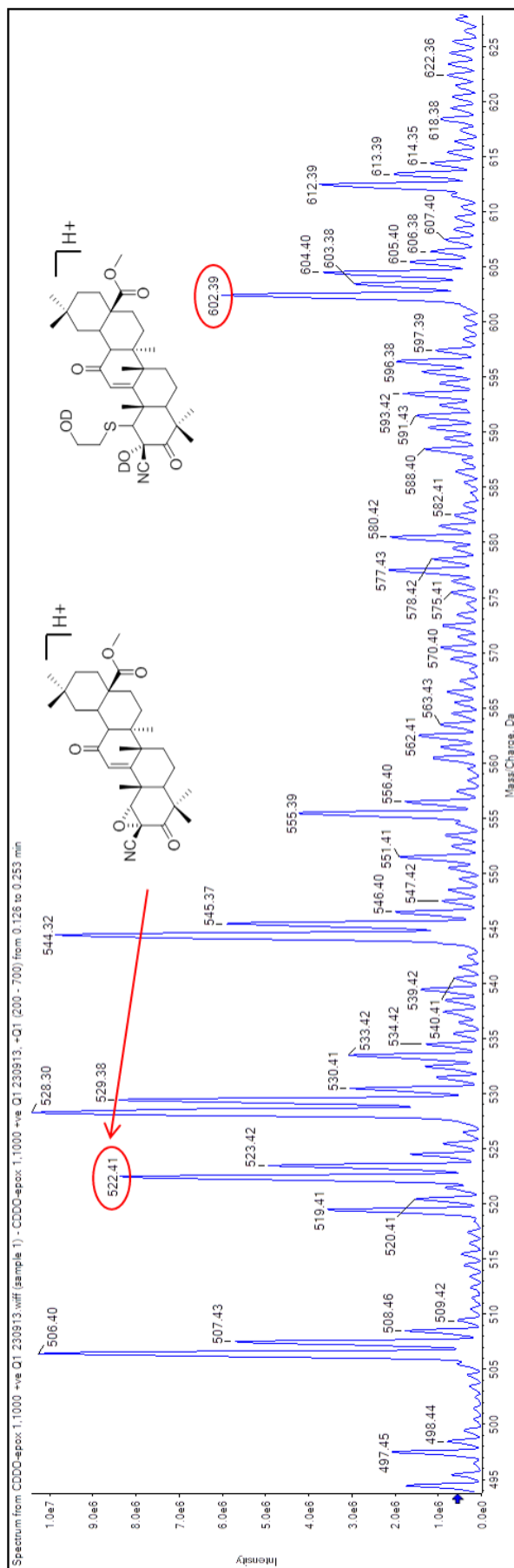


Figure 3.18: Direct infusion mass spectrometry of NMR reactions containing CDDO-Epoxyde and β -mercaptoethanol in the presence of triethylamine. CDDO-Epoxyde-thiol adduct was present at 602.3 m/z.

3.2.7 Mass spectrometry evidence for the interaction of CDDO-Epoxyde with GSTP1

Glutathione-S-transferase pi (GSTP1) catalyses the conjugation of glutathione to xenobiotic substrates therefore facilitating their detoxification. GSTP1 contains four cysteine residues with divergent reactivity, and thus represents a model protein for characterising site specific modification, especially for soft electrophiles.²³ GSTP1 was therefore used to determine the capacity of CDDO-Epoxyde to form stable and detectable adducts with a protein.

Tandem MS, in which molecules are fragmented by collision induced dissociation, is a powerful tool for identifying proteins and peptide sequencing. Fragmentation of peptide lengths can be predicted due to the typical fragmentation pattern.²⁴ There are 6 fragmentation patterns along the peptide backbone and are each labelled a, b, c along with their respected counterpart x, y, z as shown in Figure 3.19.

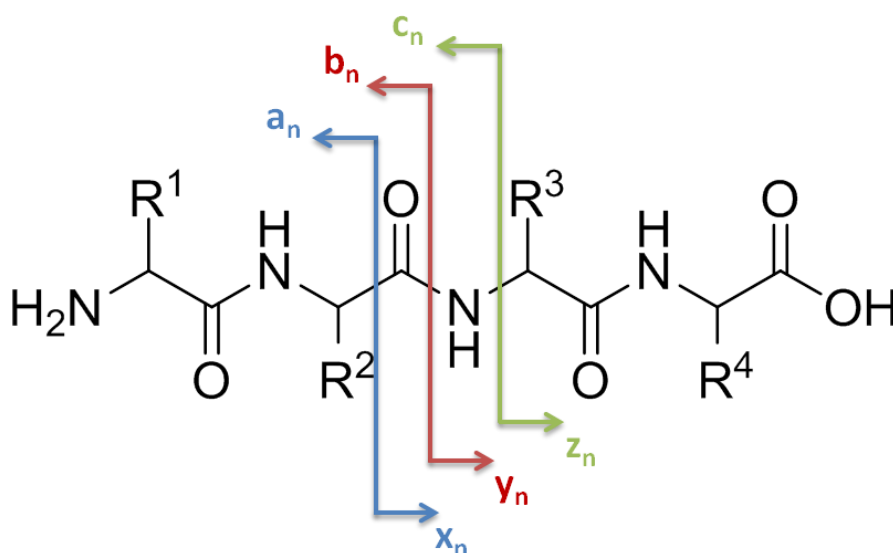


Figure 3.19: Nomenclature of fragment ions observed along the peptide backbone during tandem MS.²⁴

The peptide sequence of GSTP1 is known and therefore small peptide sequences can be predicted during tryptic digestion. To determine if an amino acid has been modified within a peptide sequence, the small peptide must contain an additional mass similar to that of the compound used. This modified peptide is subjected to tandem MS revealing the individual amino acids and hence revealing the modified amino acid.²⁴ In this case, the fragmentation of the peptide observed is the b and y ions as shown in Figure 3.20.

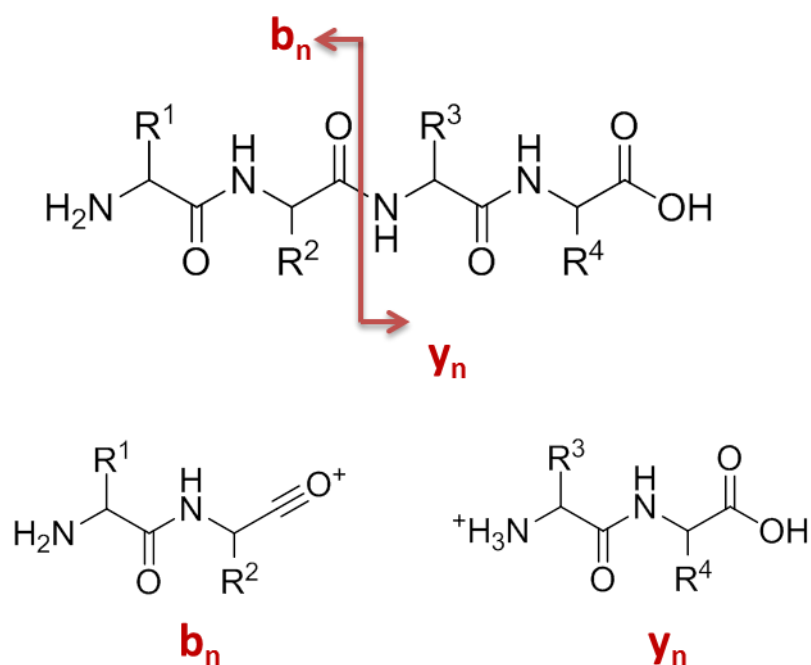


Figure 3.20: Fragmentation of the amide bond revealing the b and y ions.

Following incubation of GSTP1-His with CDDO-Epoxyde for 24h, the reaction mixture was subjected to tandem MS. CDDO-Epoxyde was found to have modified Cys-47 and Cys-14 of the protein. Cys-101 and Cys-169 may have also been modified by CDDO-Epoxyde, however, they could not be detected due to the size of the peptide fragments resulting from tryptic digestion. This was due to Cys-101 being too small

and Cys-169 too large for detection on the LCMS). (Figure 3.21) This data provides proof of principle that CDDO-Epoxyde can be used to identify the site(s) of modification of proteins by this compound class.

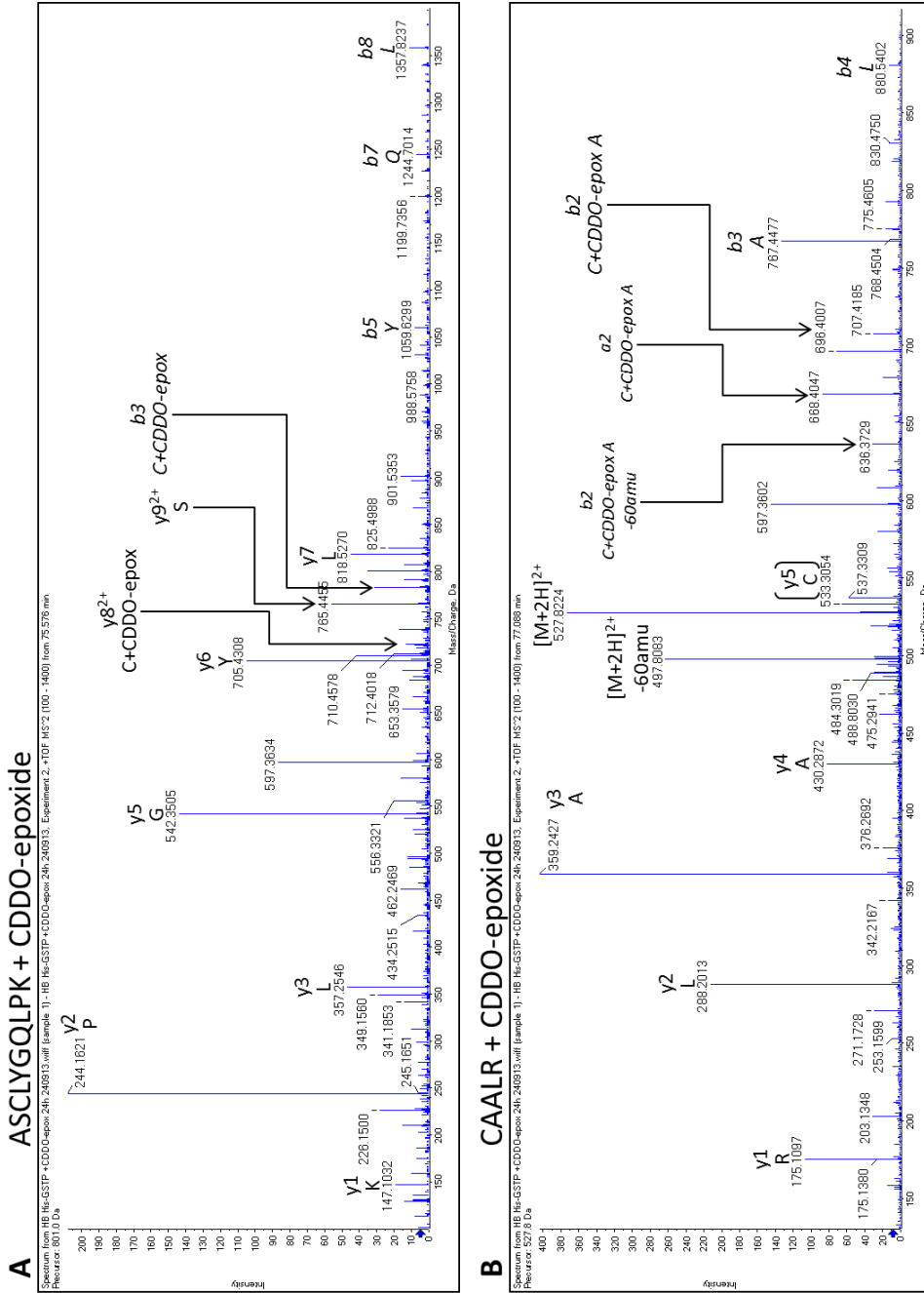


Figure 3.21: LCMS evidence for the modification of GSTP1 with CDDO-Epoide. (A) CDDO-Epoide bound to Cys-47 (B) CDDO-Epoide bound to Cys-14.

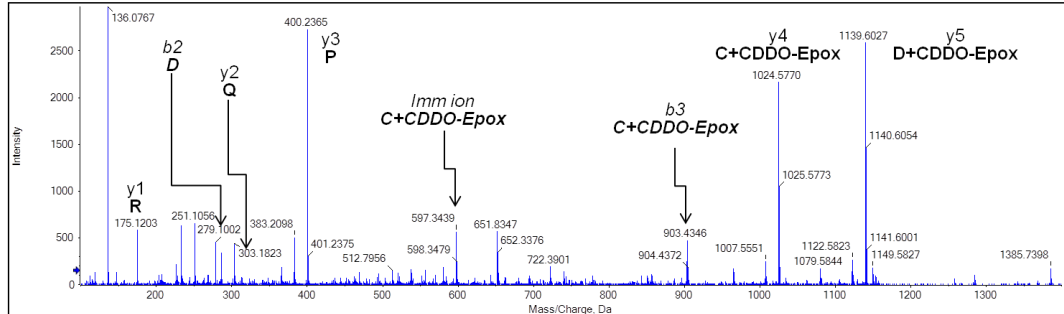
3.3 Conclusion

NMR and VT-NMR analysis has provided a detailed insight into the chemical mechanism of action of CDDO-Me as a reversible thiol modifier. Chemical manipulation of key functional groups has enabled the synthesis of the irreversible analogues, DDO-Me and CDDO-Epoxyde. In particular, CDDO-Epoxyde exhibits relatively high potency as an inducer of Nrf2 and undergoes stable thiol addition readily in the presence of base. Additional evidence of irreversible binding of DDO-Me and CDDO-Epoxyde has been generated following reaction with the model protein GSTP1, further supporting the use of these probes to define the molecular targets of CDDO-Me and its derivatives in cells.

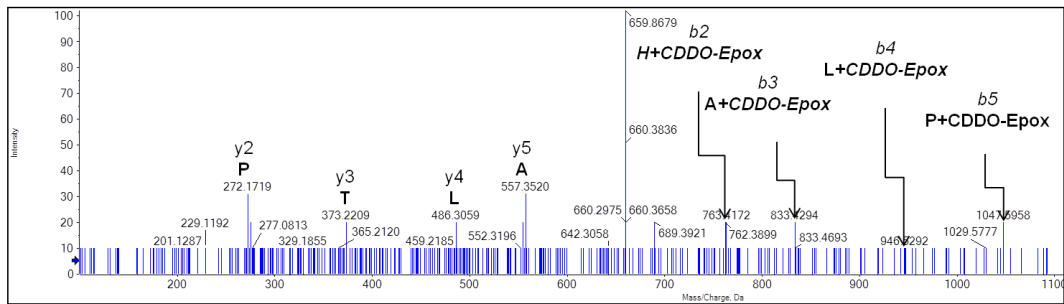
The epoxyde probe is currently being used by collaborators to determine the site(s) of modification following incubation of the compound with purified recombinant Keap1 protein *in vitro*. Preliminary data indicates that Cys-257, Cys-273, Cys-288, Cys-434, Cys-489 and Cys-613 of Keap1 are modified by CDDO-Epoxyde under these conditions. The preliminary results are shown in Figure 3.22 A to F respectively. This is the first time that the specific sites of interaction of a triterpenoid with components of the Nrf2 pathway have been identified. Importantly, previous work has shown that site-direct mutagenesis of Cys-273 and Cys-288 renders Keap1 unable to repress Nrf2, leading to an induction of Nrf2 signalling.^{25,26} Therefore, it is plausible that the direct modification of these cysteine residues underlies the ability of CDDO-Epoxyde and other triterpenoids, to activate Nrf2.

This future work will reveal whether these important cysteines located on Keap1 is a molecular target for CDDO-Me and its derivatives. If Keap1 is not the molecular target, CDDO-Epoxy can be used to identify alternative cysteine containing targets due to its capacity to undergo irreversible interaction with thiols.

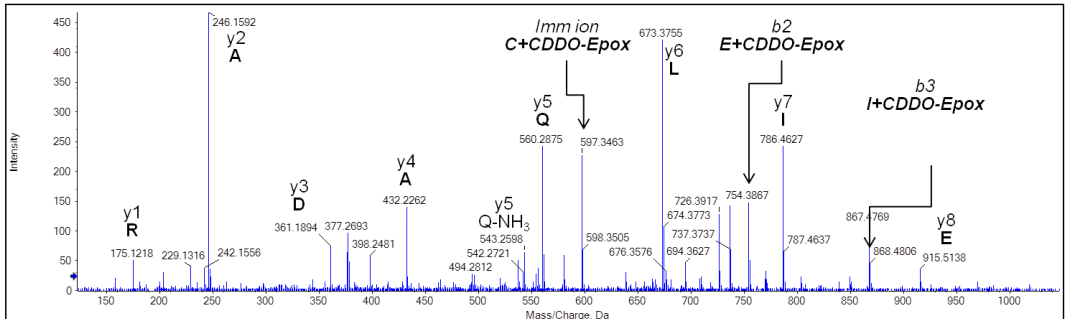
A $^{255}\text{YDC}(+\text{CDDO-EpoX})\text{PQR}^{260}$



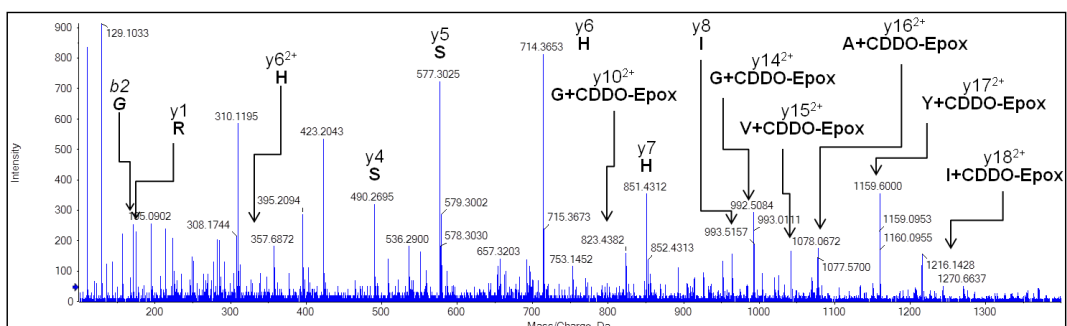
B Keap1 $^{273}\text{C}(+\text{CDDO-EpoX})\text{HALTPR}^{279}$



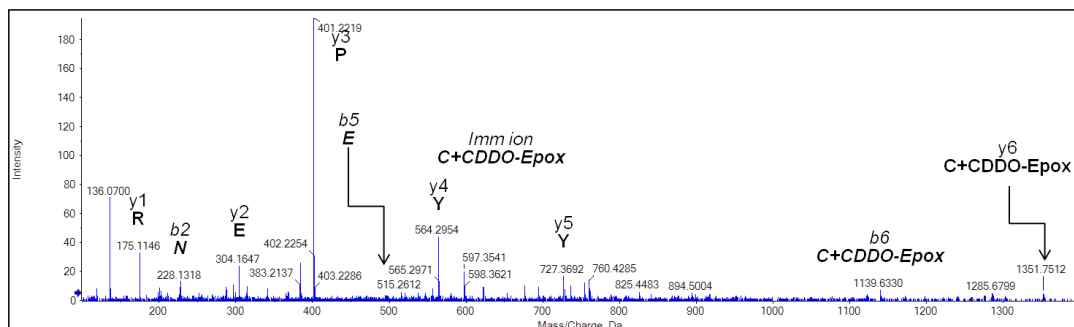
C Keap1 $^{288}\text{C}(+\text{CDDO-EpoX})\text{EILQADAR}^{296}$



D Keap1 $^{416}\text{IGVGVIDGHYAVGGSHGC}(+\text{CDDO-EpoX})\text{IHHSSVER}^{442}$



E 484LNSAEC(+CDDO-Epox)YYPER494



F Keap1⁶⁰²SGVGVAVTMEPC(+CDDO-Epox [521])RK⁶¹⁵

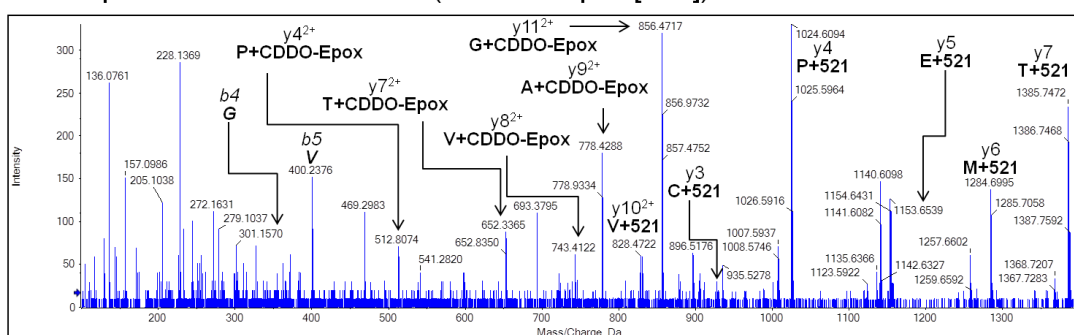


Figure 3.22: Preliminary LCMS evidence for the modification of Keap1 with CDDO-Epoxide. CDDO-Epoxide bound to (A) Cys-257; (B) Cys-273; (C) Cys-288; (D) Cys-434; (E) Cys-489 and (F) Cys-613.

3.4 Chemistry Experimental

3.4.1 General

See section 2.4.1

3.4.2 Purification of solvents and reagents

Anhydrous solvents were obtained from commercial sources or dried and distilled prior to use. The distillation was under the flow of dry nitrogen. THF was distilled from sodium and benzophenone. Dichloromethane was distilled from calcium hydride. Oleonic acid was obtained from Toronto Research Chemicals Inc. and Indofine chemical company Inc. HPLC or LCMS grade solvents were purchased from Fisher. All reagents were purchased from Sigma Aldrich or Alfa Aesar and were used without any purification unless otherwise indicated.

3.4.2.1 Stains

p-Anisaldehyde stain

Concentrated sulphuric acid (2.5 mL) was added to *p*-anisaldehyde (15 g) in ethanol (250 mL) to give a clear solution of *p*-anisaldehyde stain.

Potassium permanganate

Potassium permanganate (3 g) and potassium carbonate (20 g) were dissolved in 5% sodium hydroxide (5 mL) and water (300 mL).

3.4.3 Purification of products

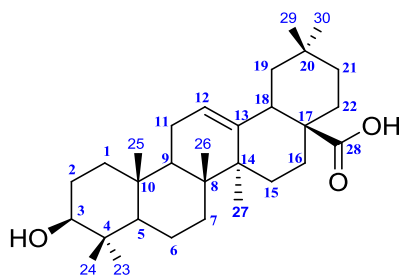
See section 2.4.4

3.4.4 Analysis

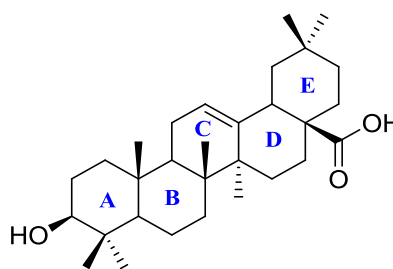
See section 2.4.5

3.4.5 Numbering

Oleanolic acid



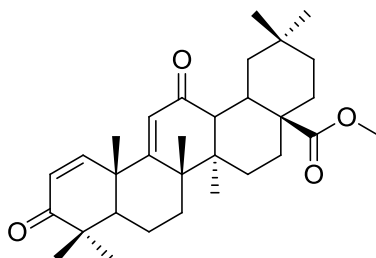
Carbon assignment



Ring assignment

3.4.6 Synthesis

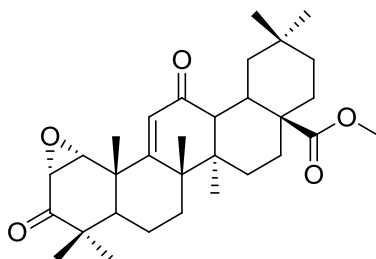
Preparation of methyl 3,12-dioxooleana-1,9(11)-dien-28-oate (21)³



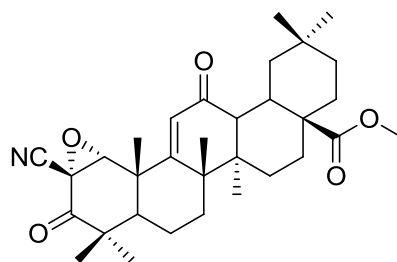
For the synthesis of **4** see section 2.4.7. **4** (200 mg, 414 μmol) was dissolved in ethyl acetate (25 mL). Phenylselenenyl chloride (87 mg, 456 μmol) was added to the reaction and left to stir at room temperature for 2.5 hours. 5 mL of water was added to the reaction. The water was removed *via* a separating funnel and THF (15 mL) was added to the organic layer along with hydrogen peroxide (30%, 0.33 mL). The reaction was left to stir for a further hour at room temperature. The reaction was washed with water (3 x 50 mL), brine (50 mL) and dried over magnesium sulfate. The solvent was removed *in vacuo* and purified by flash chromatography using 2% ethyl acetate in hexane to give the title compound **21** (114.5 mg, 57%) as a white powder; $R_f = 0.19$, 20% ethyl acetate in hexane; mp = 182-183°C; ^1H NMR (400 MHz, CDCl_3) δ 7.33 (d, $J = 10.5$ Hz, 1H), 6.00 (s, 1H), 5.92 (d, $J = 10.5$ Hz, 1H), 3.70 (s, 3H), 3.04 (dt, $J = 13.4, 3.5$ Hz, 1H), 2.92 (d, $J = 4.7$ Hz, 1H), 2.02 – 1.64 (m, 10H), 1.62 – 1.44 (m, 5H), 1.42 (s, 3H), 1.31 (s, 3H), 1.19 (s, 3H), 1.12 (s, 3H), 1.01 (s, 3H), 1.00 (s, 3H) and 0.89 (s, 3H); ^{13}C NMR (100 MHz, CDCl_3) δ 203.6, 199.7, 178.4, 171.6, 154.9, 126.0, 123.8, 52.0, 49.8, 48.5, 47.4, 45.8, 44.8, 42.2, 41.9, 36.0, 34.6, 33.4, 33.0, 32.2, 31.7, 30.8, 28.2, 27.3, 27.0, 24.7, 23.2, 22.8, 21.8, 21.7 and 18.5; IR

ν_{\max} (neat)/ cm^{-1} 2945 (CH), 2861 (COCH_3), 1716 (CO), 1673(C=C) and 1654 (C=C);
 HRMS (ESI) calculated for $\text{C}_{31}\text{H}_{44}\text{O}_4$ $[\text{M}+\text{Na}]^+$ 503.3137 found 503.3138.

Preparation of methyl 3,12-dioxo-1,2-epoxyolean-9(11)-en-28-oate (**22**)²⁰



21 (200 mg, 416 μmol) was dissolved in methanol (5 mL). Hydrogen peroxide (30%, 200 μL , 2.0 mmol) and sodium hydroxide (10% w/v) were added successively and monitored using TLC analysis. The reaction was completed in 4 hours. Ethyl acetate (100 mL) was added to the reaction mixture and washed with water, sodium thiosulfate solution (5% w/v, 100 mL) and dried over magnesium sulfate. The solution was concentrated to give a crude product in which purification by flash chromatography using 20% ethyl acetate in hexane to give the title compound **22** (101.2 mg, 49%) as a white powder; mp = 116-118°C; ^1H NMR (400 MHz, CDCl_3) δ 6.12 (s, 1H), 3.92 (d, $J = 4.5$ Hz, 1H), 3.70 (s, 3H), 3.44 (d, $J = 4.5$ Hz, 1H), 3.05 (dt, $J = 7.3, 3.9$ Hz, 1H), 2.93 (d, $J = 4.5$ Hz, 1H), 2.13 – 2.06 (m, 1H), 1.98 – 1.79 (m, 2H), 1.77 – 1.40 (m, 9H), 1.40 – 1.27 (m, 3H), 1.26 (s, 3H), 1.20 (s, 3H), 1.14 (s, 3H), 1.10 (s, 3H), 1.05 (s, 3H), 1.00 (s, 3H) and 0.90 (s, 3H); ^{13}C NMR (100 MHz, CDCl_3) δ 211.2, 199.6, 178.4, 171.2, 124.5, 62.6, 56.6, 52.0, 49.8, 47.4, 45.7, 44.8, 42.4, 42.0, 41.1, 35.9, 34.6, 33.4, 32.9, 31.8, 31.6, 30.8, 28.3, 28.0, 23.9, 23.2, 23.0, 22.8, 21.8, 21.2 and 18.5; IR ν_{\max} (neat)/ cm^{-1} 2946 (CH), 2870 (COCH_3), 1721 (CO), 1704 (C=C) and 1661 (C=C); HRMS (ESI) calculated for $\text{C}_{31}\text{H}_{44}\text{O}_5$ $[\text{M}+\text{Na}]^+$ 519.3086 found 519.3086.

Preparation of methyl 2β-cyano-3,12-dioxo-1,2-epoxyolean-9(11)-en-28-oate(23)^{20,27}

Preparation of Iodosylbenzene²⁷: Sodium hydroxide (1.88 M, 532 mL) was added drop wise to (diacetoxyiodo)benzene (1.19 g, 4.09 mmol) at room temperature. The yellow mixture was stirred for three hours at room temperature and filtered under vacuum. The filtrate was washed with water until the washings were neutral. The yellow solid was dried and stored at room temperature until required.

CDDO-Me (50.0 mg, 98.9 μmol) was dissolved in chloroform (50 mL). Iodosylbenzene (89.2 mg, 405.4 μmol) was added to the reaction and left to stir for 12 hours. The reaction mixture was washed with water (50 mL), brine and dried over magnesium sulfate. The solution was concentrated to give crude product in which purification by flash chromatography using 30% ethyl acetate in hexane gave the title compound **23** (38.8 mg, 75%) as a white powder; $R_f = 0.21$, 20% ethyl acetate in hexane; mp = 142-143°C; $^1\text{H NMR}$ (400 MHz, CDCl_3) δ 6.08 (s, 1H), 4.35 (s, 1H), 3.70 (s, 3H), 3.04 (dt, $J = 6.7, 3.7$ Hz, 1H), 2.94 (d, $J = 4.6$ Hz, 1H), 2.02 – 1.79 (m, 3H), 1.77 – 1.44 (m, 10H), 1.39 – 1.28 (m, 2H), 1.27 (s, 6H), 1.19 (s, 3H), 1.12 (s, 3H), 1.08 (s, 3H), 1.00 (s, 3H) and 0.90 (s, 3H); $^{13}\text{C NMR}$ (100 MHz, CDCl_3) δ 202.5, 198.9, 178.3, 168.7, 125.0, 113.7, 69.2, 53.3, 52.0, 49.8, 47.3, 45.7, 45.2, 42.6, 42.1, 41.0, 35.9, 34.6, 33.4, 32.9, 31.6, 31.5, 30.8, 28.3, 28.1, 24.0, 23.2, 22.9, 22.8, 21.7, 21.5

and 18.4; IR ν_{max} (neat)/ cm^{-1} 2947 (CH), 2870 (COCH₃), 1715 (CO), 1663 (C=C), 1242, 906 and 810; HRMS (ESI) calculated for C₃₂H₄₃NO₅ [M+Na]⁺ 544.3039 found 544.3047.

3.4.7 NMR and VT-NMR experiments

For NMR and VT-NMR experiments with simple thiols, proton NMR spectra were obtained on a Bruker DPX400 (¹H, 400 MHz). Deuterated DMSO (DMSO-d⁶) was obtained from Cambridge Isotope Laboratories Inc (Leicestershire, UK).

Proton spectras were acquired at 25°C unless stated otherwise. NMR samples were locked and shimmed for each addition of thiol or base prior to obtaining a proton spectrum. CDDO derivatives were weighed out exactly between 5-10 mg and 750 μL of DMSO-d⁶ was added. The required equivalent of thiol (β -mercaptoethanol or *N*-acetyl cysteine) was added to the NMR reaction and proton NMR spectra were obtained. If required, one equivalent of triethylamine was added and proton spectras were acquired at set time points at 25°C. VT-NMR required heating of the probe and sample to 37°C or 50°C. Once the required temperature was reached, the sample was left for 3 minutes to equilibrate prior to obtaining a proton spectrum. Cooling of the sample from 50°C required setting the probe to 25°C and leaving the sample to reach the required temperature prior to obtaining a proton spectrum.

3.4.8 Mass spectra analysis for NMR samples

β -mercaptoethanol or *N*-acetyl cysteine adducts were dissolved in 50% methanol/0.1% formic acid to a concentration of between 0.25 and 25 μ M and infused at 5 μ l/min directly into a QTRAP 4000 hybrid quadrupole-linear ion trap mass spectrometer (AB Sciex, Foster City, CA, USA) fitted with a turboion source. The ionspray potential was set to 5500 V in positive ion mode and the interface heater was turned off. Ions of m/z 583.9, 559.6 and 601.2 (ion found at 602.4) corresponding to the β -mercaptoethanol adducts of CDDO-Me, DDO-Me and CDDO-Epoxyde respectively, were selected manually for fragmentation to generate full product ion scans (EPI) to aid structure confirmation. Ions of m/z 669.4 and 644.6 corresponded to the *N*-acetyl cysteine adducts of CDDO-Me, and DDO-Me respectively.

3.4.9 Molecular modelling experiments

Calculations were performed using Spartan14 (<http://wavefun.com/products/spartan.html>). Structure optimisations were carried out using density functional theory (DFT) in the gas phase using the B3LYP functional. For all the optimisations the 6-31G* basis set were used for all atoms.

3.5 Biological experimental

3.5.1 Materials

H4IIE cells stably expressing the ARE8L-reporter were provided by Prof. Alex Odermatt (Department of Pharmaceutical Sciences, University of Basel, Switzerland). Nunclon Δ cell culture flasks and multiwall plates were from Nalge-Nunc International (c/o VWR International, Lutterworth, UK). Fetal bovine serum (FBS) and trypsin 0.25% EDTA were from Life Technologies (Paisley, UK). The MRX microplate reader was from Dynatech Laboratories (Billingshort, UK). The Varioskan Flash and SkanIT software were from Thermo Scientific (Hemel Hempstead, UK). Bright-Glo luciferase assay system, glo lysis buffer and isopropyl β -D-1-thiogalactopyranoside were from Promega (Southampton, UK).

Soniprep 150 was from MSE (London, UK). Beckman DU 640 spectrophotometer was from Beckman Coulter (High Wycombe, UK). Dulbecco's modified Eagle medium (DMEM), Dimethyl Sulfoxide (DMSO), Phosphate buffered saline (PBS) tablets, LB broth, Minimum essential Medium (MEM) non-essential amino acid solution, 4-(2-hydroxyethyl)piperazine-1-ethanesulfonic acid (HEPES) buffer 100X and HIS-beads were from Sigma-Aldrich (Poole, UK). All other reagents were of analytical or molecular grade, and were from Sigma-Aldrich.

3.5.2 Cell culture

See section 2.5.2

3.5.3 Plating

See section 2.5.3

3.5.4 Treatment of cells for luciferase activity assay

See section 2.5.5

3.5.5 Preparation of cells for luciferase reporter assay

See section 2.5.6

3.5.6 LCMS with recombinant His-GSTP with CDDO-Epoxyde

3.5.6.1 Isopropyl β -D-1-thiogalactopyranoside solution (IPTG)

476.6 mg of Isopropyl β -D-1-thiogalactopyranoside was dissolved in 20 mL of distilled water to obtain 100 mM

3.5.6.2 6 x His Buffer

0.5 M sodium chloride, 20 mM disodium phosphate and 20 mM imidazole dissolved up in distilled water.

3.5.6.3 Preparation of His-GSTP

BL21 *E. Coli* cells expressing His-GSTP were obtained from co-workers and used as described previously.²³ A starter culture of 50 μ L of glycerol stock and 20 mL lysogeny broth (LB) supplemented with 100 μ g/mL ampicillin was incubated in a shaking incubator at 220 rpm at 37°C overnight. The following day, the culture volume was adjusted to 1 L with LB supplemented with 100 μ g/mL ampicillin and incubated at 220 rpm at 37°C for 2-3 hours. Bacterial growth was determined using optical density readings measured at 600 nm (OD_{600}). Aliquot samples were taken from the culture every hour and OD_{600} readings were compared to a blank LB sample. The OD_{600} measurement identifies which stage of growth the bacteria are in, with 0.4 indicating that the cells are in an exponential growth phase. When an OD_{600} reading of 0.4 was reached, 10 mL of 100 mM of IPTG was added to induce the expression of GSTP1 which is under the control of the lac operator. The culture was left to shake at 150 rpm at room temperature for 24 hours.

The bacteria were pelleted in 50 mL tubes at 5000 g for 5 minutes and LB broth removed. Pellets were vortexed in 10 mL 6x HIS buffer and 4 mL aliquots were subjected to sonication (3 x 1 min with 30 sec rest between sonications) to lyse cells. The supernatant was aliquoted into 1.5 mL tubes and pelleted at 18,000 g for 10 minutes. Pellets were collected, pooled and subjected to freeze thaw at -80°C for 2-3 hours. The supernatant was again aliquoted into 1.5 mL tubes, pelleted at 18,000 g for 10 mins and pellets were collected and pooled. The supernatant was passed through a 0.45 µm filter. The lysate was aliquoted in 1.5 mL and frozen at -80°C until required.

3.5.6.4 Incubation of GSTP1 with CDDO-Epoxyde

The 6X histidine residues on GSTP1 enabled protein purification *via* the affinity for nickel beads. Nickel beads were washed in triplicate with 6X His buffer. The bacterial lysate was added to the beads to give a 1:1 ratio and left to rotate at room temperature for 15 mins. A blank sample (nickel beads plus 6X His buffer) was used as a negative control for protein determination. Beads were pelleted and washed with 1 mL 6X His buffer five times to remove bacterial lysate. A BCA assay was used to determine the amount of GSTP1 bound to 10 µL of beads *via* referenced to a BSA standard curve.

Using 50 µL of beads, the GSTP1 protein was exposed to a 100:1 molar excess of CDDO-Epoxyde in PBS (pH 8.4) made up to 1 mL. Samples were rotated at 37°C for 24 hours. Following this incubation, the beads were washed twice with PBS (pH 8.4) to remove all traces of CDDO-Epoxyde, and then washed twice with 0.5 mL 25 mM ammonium bicarbonate, before being resuspended in 90 µL 25 mM ammonium

bicarbonate. A 400 µg/µL stock solution of sequence-grade modified trypsin was diluted 1:10 with 25 mM ammonium bicarbonate and 10 µL was added to the beads to a final concentration of 4 µg/µL. Trypsin digestion of the sample was performed overnight at 37°C.

The tryptic digest was vortexed and centrifuged at 14,000rpm for 1 minute. The supernatant containing GSTP1 peptides was removed into a new eppendorf and dried using a speedvac at 37°C for 90 minutes. The samples were then re-suspended in 20 µL 0.1% trifluoroacetic acid (TFA) and prepared using ZipTips.

3.5.6.5 ZipTip protocol

C₁₈ tips were wet in 2 x 10 µL 100% acetonitrile (ACN), followed by washing in 4 x 10 µL 0.1% TFA, 10 µL of the samples was then drawn up and released 10 times. Following this, the tip was washed again in 3 x 10 µL 0.1% TFA and the sample was eluted into a fresh eppendorf in 10 µL 50% ACN/0.1% TFA. This was repeated in triplicate with fresh C₁₈ tips per sample. The samples were then dried again with a speedvac at 37°C for 30 minutes.

3.5.6.6 LCMS analysis

Following protein reduction, alkylation and digestion, samples were de-salted by reversed phase chromatography using ZipTips (Millipore). Samples were delivered into a Triple TOF 5600 mass spectrometer (AB Sciex) by automated in-line reversed phase liquid chromatography (LC) using an Eksigent NanoUltra cHiPLC System mounted with microfluidic trap and analytical column (15 cm x 75 µm) packed with ChromXP C18-CL 3µm. A NanoSpray III source was fitted with a 10 µm inner

diameter PicoTip emitter (New Objective). Samples were loaded in 0.1% formic acid onto the trap which was then washed with 2% ACN/0.1% FA for 10mins at 2 μ L/min before switching in-line with the analytical column. A gradient of 2-50% (v/v) ACN, 0.1% (v/v) FA over 90 min was applied to the column at a flow rate of 300 nL/min. Spectra were acquired automatically in positive ion mode using information-dependent acquisition powered by Analyst TF 1.5.1 software, using mass ranges of 400-1600 atomic mass units (amu) in MS and 100-1400 amu in MS/MS. Up to 25 MS/MS spectra were acquired per cycle (approx 10 Hz) using a threshold of 100 counts per sec, with dynamic exclusion for 12 secs and rolling collision energy. The instrument was automatically calibrated after every fifth sample using a beta-galactosidase digest. Protein sequence coverage was determined using ProteinPilot software v4.0 using the ParagonTM algorithm²⁸ and the most recent version of the SwissProt database. Carboxyamidomethyl (+57.0 amu) was selected as a variable modification. Drug-modified peptides were identified using PeakView software to extract parent ions of the appropriate peptide plus drug m/z (extracted ion count, XIC).

3.6 Reference

- 1 Honda, T., Finlay, H. J., Gribble, G. W., Suh, N. & Sporn, M. B. New enone derivatives of oleanolic acid and ursolic acid as inhibitors of nitric oxide production in mouse macrophages. *Bioorganic & Medicinal Chemistry Letters* **7**, 1623-1628, doi:10.1016/S0960-894X(97)00279-5 (1997).
- 2 Honda, T., Gribble, G. W., Suh, N., Finlay, H. J., Rounds, B. V., Bore, L., Favalaro, F. G., Wang, Y. & Sporn, M. B. Novel Synthetic Oleanane and Ursane Triterpenoids with Various Enone Functionalities in Ring A as Inhibitors of Nitric Oxide Production in Mouse Macrophages†. *Journal of Medicinal Chemistry* **43**, 1866-1877, doi:10.1021/jm000008j (2000).
- 3 Honda, T., Rounds, B. V., Bore, L., Finlay, H. J., Favalaro, F. G., Suh, N., Wang, Y., Sporn, M. B. & Gribble, G. W. Synthetic Oleanane and Ursane Triterpenoids with Modified Rings A and C: A Series of Highly Active Inhibitors of Nitric Oxide Production in Mouse Macrophages†. *Journal of Medicinal Chemistry* **43**, 4233-4246, doi:10.1021/jm0002230 (2000).
- 4 Honda, T., Rounds, B. V., Gribble, G. W., Suh, N., Wang, Y. & Sporn, M. B. Design and synthesis of 2-cyano-3,12-dioxolean-1,9-dien-28-oic acid, a novel and highly active inhibitor of nitric oxide production in mouse macrophages. *Bioorganic & Medicinal Chemistry Letters* **8**, 2711-2714, doi:10.1016/S0960-894X(98)00479-X (1998).
- 5 Honda, T.-i., Rounds, B. V., Bore, L., Favalaro Jr, F. G., Gribble, G. W., Suh, N., Wang, Y. & Sporn, M. B. Novel synthetic oleanane triterpenoids: A series of highly active inhibitors of nitric oxide production in mouse macrophages. *Bioorganic & Medicinal Chemistry Letters* **9**, 3429-3434, doi:10.1016/S0960-894X(99)00623-X (1999).
- 6 Samudio, I., Konopleva, M., Hail, N., Shi, Y.-X., McQueen, T., Hsu, T., Evans, R., Honda, T., Gribble, G. W., Sporn, M., Gilbert, H. F., Safe, S. & Andreeff, M. 2-Cyano-3,12-dioxoleana-1,9-dien-28-imidazolide (CDDO-Im) Directly Targets Mitochondrial Glutathione to Induce Apoptosis in Pancreatic Cancer. *Journal of Biological Chemistry* **280**, 36273-36282, doi:10.1074/jbc.M507518200 (2005).
- 7 Dinkova-Kostova, A. T., Liby, K. T., Stephenson, K. K., Holtzclaw, W. D., Gao, X., Suh, N., Williams, C., Risingsong, R., Honda, T., Gribble, G. W., Sporn, M. B. & Talalay, P. Extremely potent triterpenoid inducers of the phase 2 response: Correlations of protection against oxidant and inflammatory stress. *Proceedings of the National Academy of Sciences* **102**, 4584-4589, doi:10.1073/pnas.0500815102 (2005).
- 8 Couch, R. D., Browning, R. G., Honda, T., Gribble, G. W., Wright, D. L., Sporn, M. B. & Anderson, A. C. Studies on the reactivity of CDDO, a promising new chemopreventive and chemotherapeutic agent: implications for a molecular mechanism of action. *Bioorganic & Medicinal Chemistry Letters* **15**, 2215-2219, doi:10.1016/j.bmcl.2005.03.031 (2005).
- 9 Zhang, Y. & Talalay, P. Anticarcinogenic Activities of Organic Isothiocyanates: Chemistry and Mechanisms. *Cancer Research* **54**, 1976s-1981s (1994).
- 10 Zhang, Y. S., Kolm, R. H., Mannervik, B. & Talalay, P. Reversible Conjugation of Isothiocyanates with Glutathione Catalyzed by Human Glutathione

- Transferases. *Biochemical and Biophysical Research Communications* **206**, 748-755, doi:10.1006/bbrc.1995.1106 (1995).
- 11 Ahn, Y.-H., Hwang, Y., Liu, H., Wang, X. J., Zhang, Y., Stephenson, K. K., Boronina, T. N., Cole, R. N., Dinkova-Kostova, A. T., Talalay, P. & Cole, P. A. Electrophilic tuning of the chemoprotective natural product sulforaphane. *Proceedings of the National Academy of Sciences* **107**, 9590-9595, doi:10.1073/pnas.1004104107 (2010).
- 12 Egger, A. L., Small, E., Hannink, M. & Mesecar, A. D. Cul3-mediated Nrf2 ubiquitination and antioxidant response element (ARE) activation are dependent on the partial molar volume at position 151 of Keap1. *Biochemical Journal* **422**, 171-180, doi:10.1042/BJ20090471 (2009).
- 13 Ichikawa, T., Li, J., Meyer, C. J., Janicki, J. S., Hannink, M. & Cui, T. Dihydro-CDDO-Trifluoroethyl Amide (dh404), a Novel Nrf2 Activator, Suppresses Oxidative Stress in Cardiomyocytes. *PLoS ONE* **4**, e8391, doi:10.1371/journal.pone.0008391 (2009).
- 14 Takaya, K., Suzuki, T., Motohashi, H., Onodera, K., Satomi, S., Kensler, T. W. & Yamamoto, M. Validation of the multiple sensor mechanism of the Keap1-Nrf2 system. *Free Radical Biology and Medicine* **53**, 817-827, doi:10.1016/j.freeradbiomed.2012.06.023 (2012).
- 15 Mladenovic, M., Schirmeister, T., Thiel, S., Thiel, W. & Engels, B. The Importance of the Active Site Histidine for the Activity of Epoxide- or Aziridine-Based Inhibitors of Cysteine Proteases. *ChemMedChem* **2**, 120-128, doi:10.1002/cmdc.200600159 (2007).
- 16 Otto, H.-H. & Schirmeister, T. Cysteine Proteases and Their Inhibitors. *Chemical Reviews* **97**, 133-172, doi:10.1021/cr950025u (1997).
- 17 Campbell, M. M., Jigajinni, V. B. & Wightman, R. H. Michael additions to steroidal 1-ene-3-ones. *Tetrahedron Letters* **20**, 2455-2456, doi:10.1016/S0040-4039(01)86319-X (1979).
- 18 Clayden, J., Greeves, N., Warren, S. & Wothers, P. *Organic Chemistry*. (Oxford University Press, 2005).
- 19 Housecroft, E. C. & Constable, C. E. *Chemistry*. 3rd edn, (Pearson Education Limited, 2006).
- 20 Anderson, E., CBender, C. F., Jiang, X., Liu, X., Sun, H. & Visnic, m. A-Ring epoxidized triterpenoid-based anti-inflammation modulators and methods of use thereof. United States patent WO 2013/188818 A1(2013).
- 21 Williams, D. H. & Fleming, I. *Spectroscopic Methods in Organic Chemistry*. Sixth edn, (McGraw-Hill Higher Education, 2008).
- 22 Powell, H., Williams, D. H., Budzikiewicz, H. & Djerassi, C. Mass Spectrometry in Structural and Stereochemical Problems. XLVIII.1 A Study of the Hydrogen Transfer Reactions Accompanying Fragmentation Processes of 1-Keto Steroids. Synthesis of Deuterated 5 α -Androstan-1-ones². *Journal of the American Chemical Society* **86**, 2623-2628, doi:10.1021/ja01067a021 (1964).
- 23 Jenkins, R. E., Kitteringham, N. R., Goldring, C. E. P., Dowdall, S. M. J., Hamlett, J., Lane, C. S., Boerma, J.-S., Vermeulen, N. P. E. & Park, B. K. Glutathione-S-transferase pi as a model protein for the characterisation of chemically reactive metabolites. *Proteomics* **8**, 301-315, doi:10.1002/pmic.200700843 (2008).

- 24 Hardouin, J. Protein sequence information by matrix-assisted laser desorption/ionization in-source decay mass spectrometry. *Mass Spectrometry Reviews* **26**, 672-682, doi:10.1002/mas.20142 (2007).
- 25 Kobayashi, M., Li, L., Iwamoto, N., Nakajima-Takagi, Y., Kaneko, H., Nakayama, Y., Eguchi, M., Wada, Y., Kumagai, Y. & Yamamoto, M. The Antioxidant Defense System Keap1-Nrf2 Comprises a Multiple Sensing Mechanism for Responding to a Wide Range of Chemical Compounds. *Molecular and Cellular Biology* **29**, 493-502, doi:10.1128/mcb.01080-08 (2009).
- 26 Yamamoto, T., Suzuki, T., Kobayashi, A., Wakabayashi, J., Maher, J., Motohashi, H. & Yamamoto, M. Physiological Significance of Reactive Cysteine Residues of Keap1 in Determining Nrf2 Activity. *Molecular and Cellular Biology* **28**, 2758-2770, doi:10.1128/mcb.01704-07 (2008).
- 27 McQuaid, K. M. & Pettus, T. R. R. Chemoselective Epoxidation of Electron Deficient Enones with Iodosylbenzene. *Synlett* **2004**, 2403-2405, doi:10.1055/s-2004-832814 (2004).
- 28 Shilov, I. V., Seymour, S. L., Patel, A. A., Loboda, A., Tang, W. H., Keating, S. P., Hunter, C. L., Nuwaysir, L. M. & Schaeffer, D. A. The Paragon Algorithm, a Next Generation Search Engine That Uses Sequence Temperature Values and Feature Probabilities to Identify Peptides from Tandem Mass Spectra. *Molecular & Cellular Proteomics* **6**, 1638-1655, doi:10.1074/mcp.T600050-MCP200 (2007).

CHAPTER 4

Examination of the role of ferrous iron and phosphatidylcholine in the
bioactivation of novel tetraoxane antimalarials

Chapter 4

4.1 Introduction	168
4.1.1 Aims	173
4.2 Results and discussion	174
4.2.1 Chemical synthesis of unsymmetrical dispiro-1,2,4,5-tetraoxanes	174
4.2.2 Investigating the radical pathway of tetraoxanes	181
4.2.3 Reactivity of tetraoxanes with iron(II) and phosphatidylcholine (PC)	186
4.3 Conclusion	195
4.4 Chemistry Experimental	197
4.4.1 General	197
4.4.2 Purification of solvents and reagents	197
4.4.2.1 Stains	197
4.4.3 Purification of products	197
4.4.3.1 General	197
4.4.3.2 HPLC-UV purification	198
4.4.4 Analysis	198
4.4.5 Synthesis of unsymmetrical dispiro-1,2,4,5-tetraoxanes	199
4.4.6 Determination of <i>P. falciparum</i> IC ₅₀ values	213
4.4.7 Degradation of unsymmetrical dispiro-1,2,4,5-tetraoxanes with iron(II) salts	213
4.4.8 Reactions of PC with tetraoxane and iron(II) salt	217
4.4.8.1 LCMS analysis	217
4.5 Reference	218

4.1 Introduction

In 2012, an estimated 207 million cases of malaria and 627,000 associated deaths were thought to have occurred.¹ Many of these deaths were among children under the age of five.¹ Malaria is a preventable and treatable mosquito borne disease. However, the suboptimal use of traditional drugs such as chloroquine and sulfadoxine-pyrimethamine based antimalarials has led to the emergence of resistant strains of the parasite and the re-emergence of malaria in areas where the disease had previously been eradicated.² Artemisinin based combination therapies (ACT) are now recommended as the first line treatment for malaria in many endemic regions.³⁻⁵ Artemisinin is a sesquiterpene lactone extracted from the Chinese herb *Artemisia annua*. The key pharmacophore of artemisinin is the endoperoxide containing 1,2,4-trioxane unit.² (Figure 4.1).

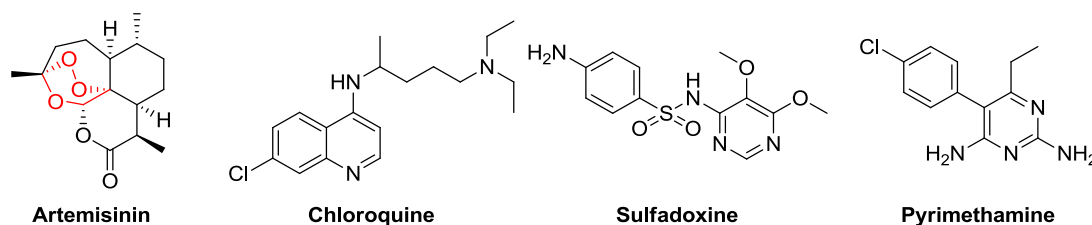


Figure 4.1: Structure of artemisinin, chloroquine, sulfadoxine and pyrimethamine. Artemisinin contains the active pharmacophore endoperoxide bridge highlighted in red.

As discussed in chapter 1, it has been established that iron(II) salts reductively activate the peroxide bond within artemisinin. The activation of the peroxide bond leads to the formation of oxy radical intermediates that undergo rearrangement to form primary or/and secondary carbon centred radicals (Figure 4.2). It has been

Chapter 4 – Examination of the role of ferrous iron and phosphatidylcholine in the bioactivation of novel tetraoxane antimalarials proposed that the carbon-centred radicals interact with vital cellular components within the malaria parasite, resulting in its death.

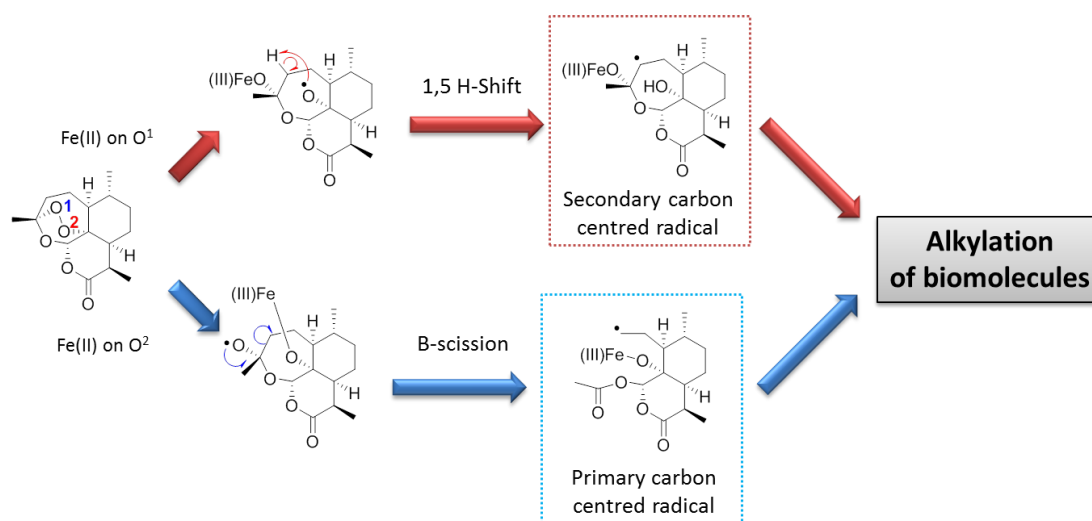


Figure 4.2: Suggested chemical mechanism underlying the antimalarial action of artemisinin, based on the formation of the primary and secondary carbon-centred radicals.

Artemisinin is a highly active antimalarial drug. However, there are many disadvantages to the use of artemisinin, including poor bioavailability, high cost of synthesis and the recent emergence of resistance.^{5,6} A great deal of effort to develop synthetic alternatives to the artemisinin class of antimalarials has resulted in the discovery of the trioxolane and tetraoxane classes. Structure relationship activity (SAR) studies of both trioxolanes and tetraoxanes have identified a stable general template. Both classes contain an adamantyl group to stabilise the endoperoxide as well as a variable polar or non-polar group⁷ (Figure 4.3). Compounds in both classes, including OZ277 trioxolane and RKA182 tetraoxane (Figure 4.3) have shown impressive antimalarial activities in pre-clinical tests.⁸⁻¹⁰

Chapter 4 – Examination of the role of ferrous iron and phosphatidylcholine in the bioactivation of novel tetraoxane antimalarials

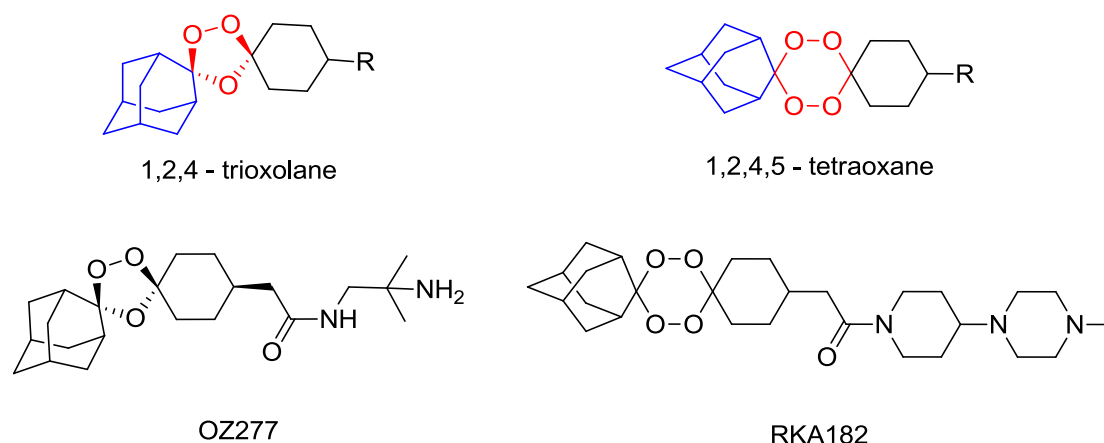
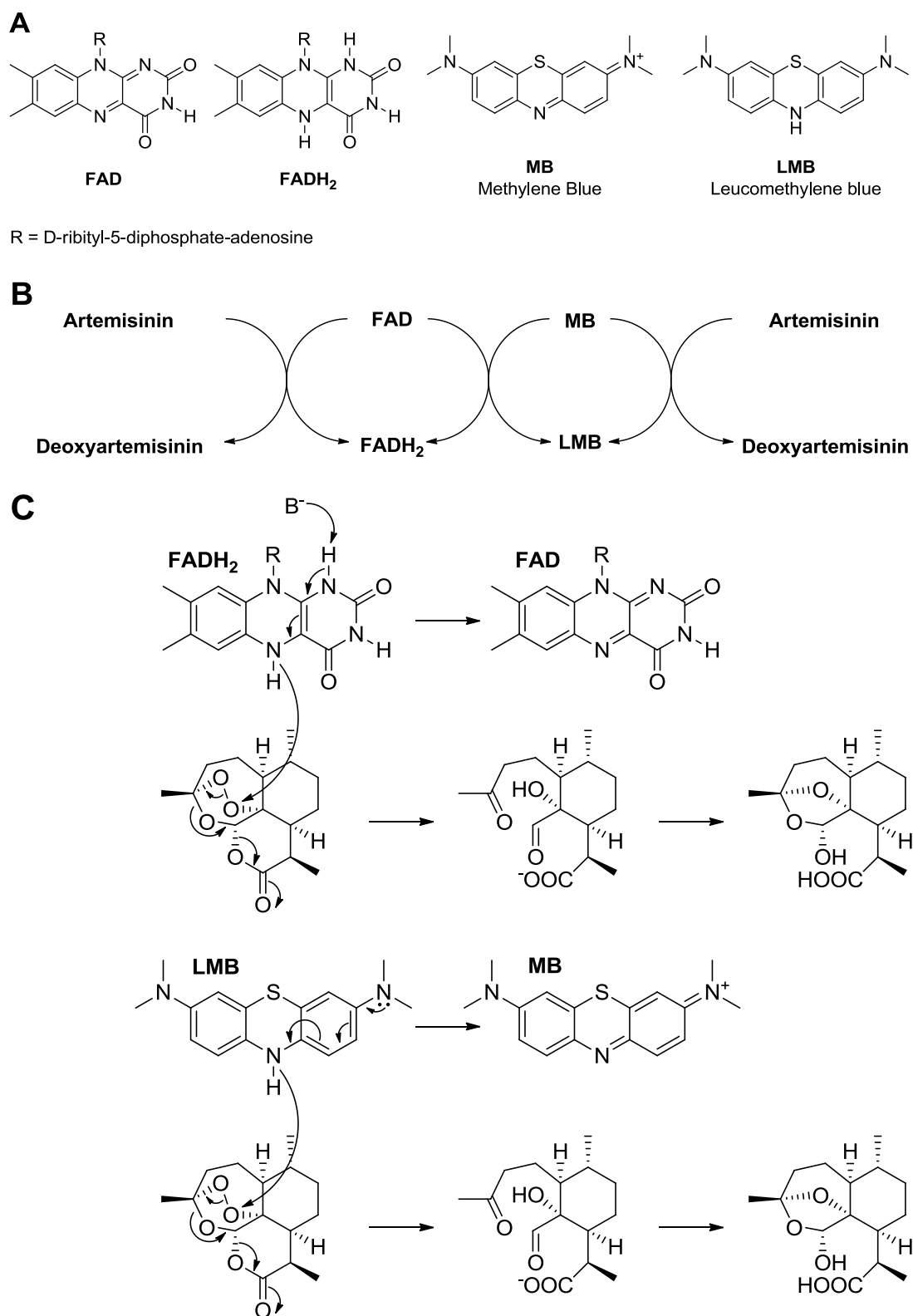


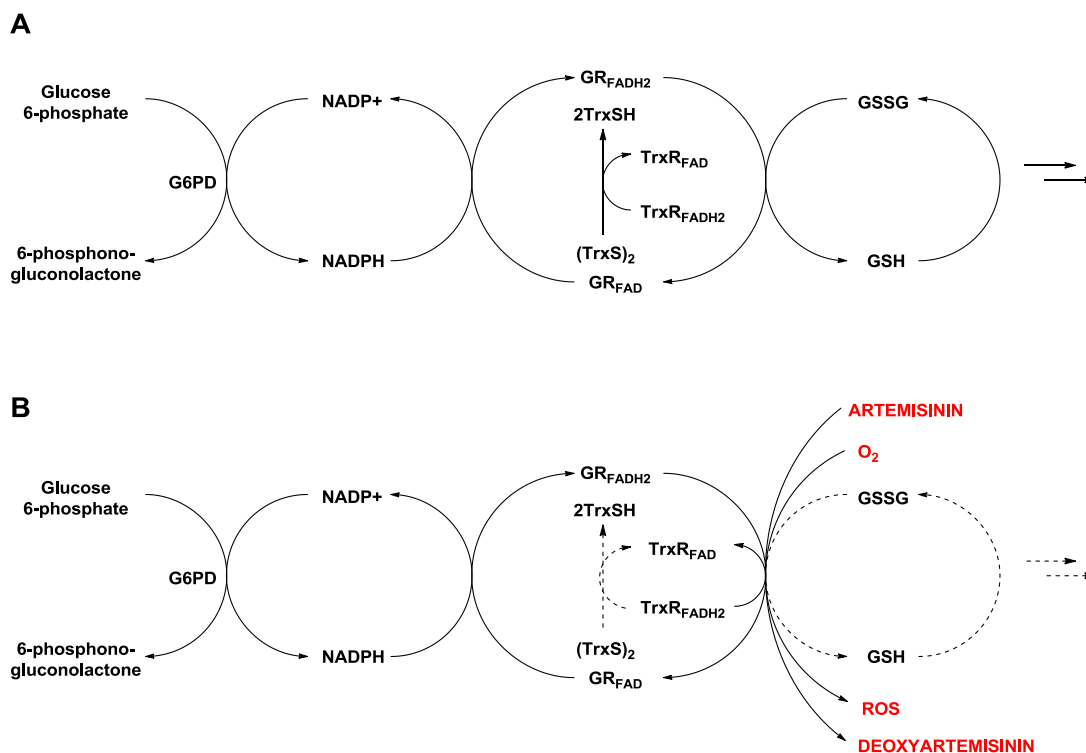
Figure 4.3: Trioxolane and tetraoxane template. Adamantyl group highlighted in blue, endoperoxide pharmacophore highlighted in red and the variable group in black. Chemical structure for trioxolane OZ277 and tetraoxane RKA182 are also shown.

Despite their impressive antimalarial activity, the mechanism of action and molecular targets of trioxolanes and tetraoxanes are still unclear. For example, there is conflicting evidence for the role of sarco/endoplasmic reticulum calcium ATPase of *P. falciparum* (PfATP6).¹¹⁻¹³ Recent studies by Haynes and Monti have proposed a non-iron mediated mechanism of bioactivation.^{14,15} This involves the flavin adenine dinucleotide (FAD), which is reduced by NADPH flavin reductase to give FADH₂. This in turn reduces the antimalarial drug methylene blue (MB) to leucomethylene blue (LMB). MB has a synergistic pharmacological effect when administered in combination with artemisinin. Therefore, it is suggested that artemisinins/endoperoxides oxidise LMB or FADH₂ to give MB or FAD. It is postulated that this interferes with the NADPH reduction of flavin cofactors in parasite flavin disulphide reductases, thus generating lethal ROS.^{14,15} A summary of this mechanism is shown in Scheme 4.1 and Scheme 4.2

Chapter 4 – Examination of the role of ferrous iron and phosphatidylcholine in the bioactivation of novel tetraoxane antimalarials



Scheme 4.1: (A) Chemical structures for FAD, FADH₂, MB and LMB; (B) The overall schematic mechanism of MB and artemisinin; (C) Chemical mechanism of FADH₂ or LMB with artemisinin.^{14,15}



Scheme 4.2: Scheme is adapted from Haynes *et al.*¹⁵ **(A) Normal process:** As part of the pentose phosphate pathway, glucose 6-phosphate is converted to 6-phosphono-gluconolactone by glucose-6-phosphate dehydrogenase (G6PD), with NADPH generated from NADP+. Glutathione reductase (GR) converts oxidised glutathione (GSSH) to its reduced form (GSH) and NADPH to NADP+, whilst converting the cofactor FAD to FADH₂. Thioredoxin in its oxidised state (TrxS)₂ is reduced to TrxSH *via* thioredoxin reductase, using FAD and FADH₂ as cofactors; **(B) Endoperoxide conditions:** Artemisinins/endoperoxides are proposed to interfere with the NADPH pathway by disrupting the equilibrium of the flavin cofactors resulting in elevated ROS generation and subsequently oxidative stress.

This provides an alternative mechanism of activation for the endoperoxide classes; however, further additional biological support for this proposal is required. It is suggested that both trioxolane and tetraoxane classes have a similar mechanism of

Chapter 4 – Examination of the role of ferrous iron and phosphatidylcholine in the bioactivation of novel tetraoxane antimalarials action to that of artemisinin.² Studies with artemisinin and trioxolanes have revealed that primary and secondary carbon-centred radicals can be produced when activated with iron(II) salts.¹⁶ However, the artemisinin and trioxolane classes have also been shown to react with heme and tetraphenylporphyrins.¹⁷ Adducts detected were formed *via* the primary carbon-centred radical pathway and no adducts for the secondary radical pathway were detected.

Kumura *et al* have shown a requirement for oxygen in the oxidative degradation of unsaturated phospholipids in the presence of iron(II) salt with artemisinins but not with tetraoxanes.¹⁸ This suggests that the two endoperoxide classes may have different modes of action despite their similar antimalarial activities. The chemical mechanism of action for the tetraoxane class of antimalarials therefore requires further investigation. The importance of understanding the ferrous ion reactivity of these important classes of antimalarials will be key for the production of new endoperoxide derivatives that can provide good exposures in malaria infected patients and exhibit improved safety profiles.

4.1.1 Aims

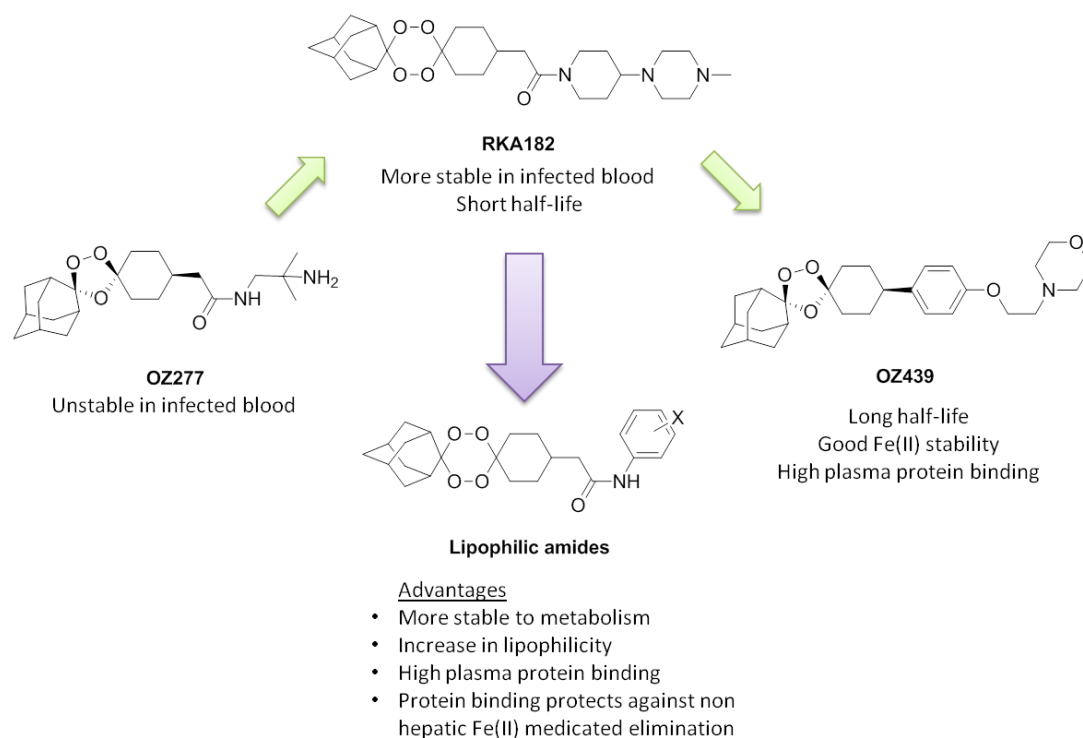
The aims of the project were to prepare a range of tetraoxane analogues and subsequently assess their activity in malaria parasites *in vitro*. In addition to establishing the antimalarial profile in *P. falciparum*, we also planned to investigate the biomimetic Fe(II) chemistry of key exemplar molecules. The final aim was to investigate the oxidative degradation of phospholipids by the Fe(II) / tetraoxane combination.

4.2 Results and discussion

4.2.1 Chemical synthesis of unsymmetrical dispiro-1,2,4,5-tetraoxanes

As discussed in chapter 1, OZ277 is a 1,2,4-trioxolane derivative with impressive antimalarial activity but poor stability in the plasma of malaria patients, resulting in a short half-life.⁸ OZ439 is a second generation trioxolane with improved pharmacokinetics and *in vivo* antimalarial activity due to enhanced lipophilicity and stability.¹⁹ As a result of the unacceptable short half-life of OZ277, OZ439 was favoured as a lead compound. The enhanced stability of OZ439 may be due to its lipophilicity, which has the potential to promote plasma protein binding. Based on this information, it was hypothesised that the synthesis of a phenyl amide tetraoxane would yield a compound with increased lipophilicity and stability. The phenyl amide also provides an active ultra violet (UV) chromophore, which is useful for aiding product identification during degradation studies. The overall rationale is highlighted in Scheme 4.3.

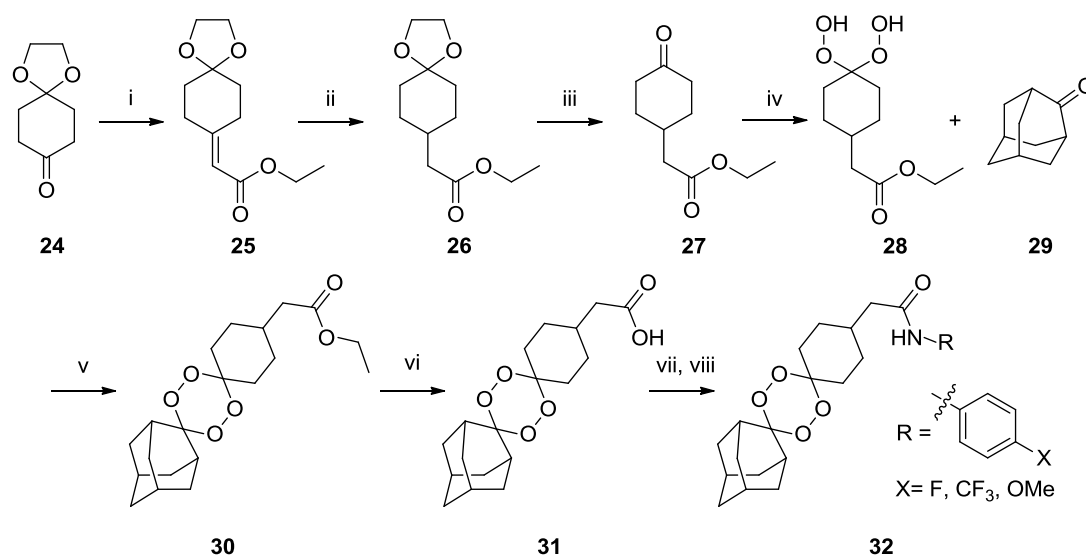
Chapter 4 – Examination of the role of ferrous iron and phosphatidylcholine in the bioactivation of novel tetraoxane antimalarials



Scheme 4.3: Overall rationale for the synthesis of lipophilic phenyl amide tetraoxanes, inspired by OZ277, RKA182 and OZ439.

Chapter 4 – Examination of the role of ferrous iron and phosphatidylcholine in the bioactivation of novel tetraoxane antimalarials

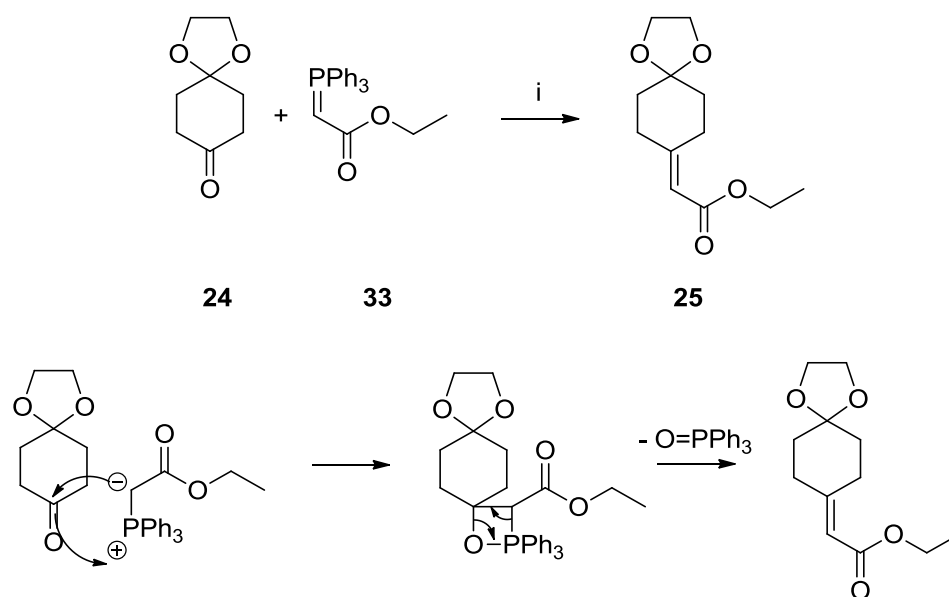
The synthesis of unsymmetrical dispiro-1,2,4,5-tetraoxanes involves a seven step synthesis (Scheme 4.4).



Scheme 4.4: Reagents and conditions: (i) Toluene, Ph₃P=CHCO₂Et reflux 18 hours, 87%; (ii) H₂, Pd/C (1.1 equiv), EtOAc, 91%; (iii) 1M HCl 56%; (iv) H₂O₂, acetonitrile, Formic acid, 0°C, 30 mins; (v) Re₂O₇ (2%), H₂O₂, DCM, r.t., 37%; (vi) MeOH, KOH, 1 hour, 70°C, H₂O, HCl, DCM, 98%; (vii) NEt₃ (1.5 equiv), ClCO₂Me (1.1 equiv), DCM, 0°C, 1 Hour; (viii) HNR¹ (1.1 equiv), 30 mins 0°C to r.t.

The first step involves a Wittig reaction between 1,4-cyclohexanedione monoethylketal acetal (**24**) and ethyl (triphenylphosphoranylidene)acetate (**33**) resulting in the formation of **25** with a 87% yield (Scheme 4.5). Hydrogenation of **25** in the presence of palladium on carbon gives compound **26** in a 91% yield. Hydrolysis with 1 M hydrochloric acid gives ethyl 2-(4-oxocyclohexyl)acetate (**27**) in a 56% yield.

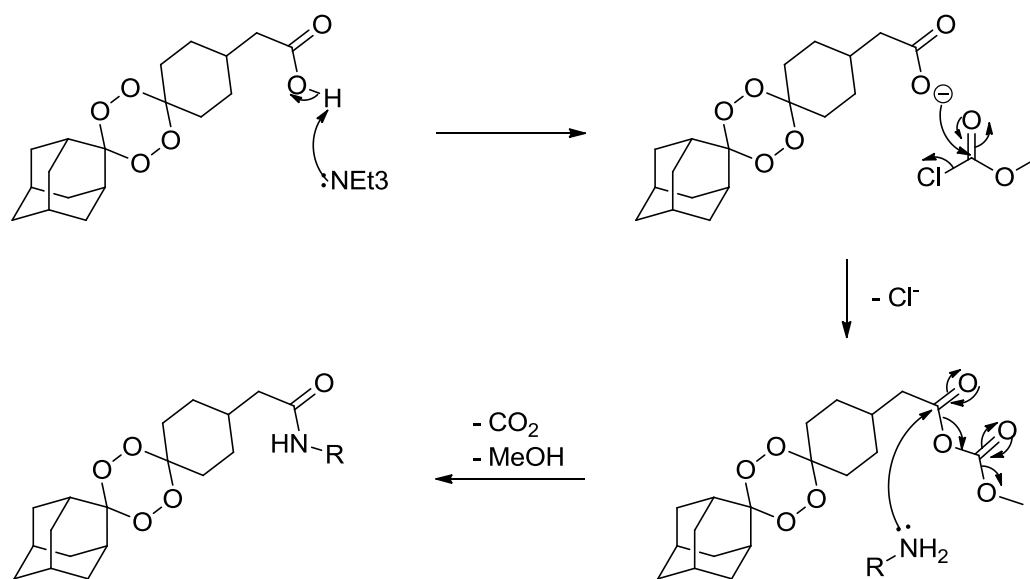
Chapter 4 – Examination of the role of ferrous iron and phosphatidylcholine in the bioactivation of novel tetraoxane antimalarials



Scheme 4.5: Reagents and conditions: (i) Toluene, $\text{Ph}_3\text{P=CHCO}_2\text{Et}$ reflux 18 hours, 87%; Chemical mechanism for the Wittig reaction.

Formation of the 1,2,4,5-tetraoxanes involves a two step procedure where ethyl 2-(4-oxocyclohexyl)acetate (**27**) is first reacted to form ethyl 2-(4,4-dihydroperoxycyclohexyl)acetate (**28**) using H_2O_2 and formic acid in acetonitrile. **28** was not purified due to instability and was reacted with 2-adamantanone (**29**) and Re_2O_7 in dichloromethane to produce the unsymmetrical dispiro-1,2,4,5-tetraoxane (**30**), in a 37% yield over two steps. Hydrolysis of **30** into the tetraoxane acid (**31**) gave the acid template. A mixed anhydride amide coupling reaction with the corresponding amine gave the required compounds in reasonable yields (Table 4.1). The chemical mechanism of action is shown in Scheme 4.6.

Chapter 4 – Examination of the role of ferrous iron and phosphatidylcholine in the bioactivation of novel tetraoxane antimalarials



Scheme 4.6: Chemical mechanism of action for the mixed anhydride amide coupling reaction

Compound	R	Yield (%)	Compound	R	Yield (%)
34		78	38		70
35		71	39		74
36		40	40		65
37		65	41		75

Table 4.1: Synthesised unsymmetrical dispiro-1,2,4,5-tetraoxanes including percentage yields and chemical structures.

Chapter 4 – Examination of the role of ferrous iron and phosphatidylcholine in the bioactivation of novel tetraoxane antimalarials

Seven of the compounds were submitted to the Liverpool School of Tropical Medicine and were tested for their ability to inhibit the proliferation of *Plasmodium falciparum* 3D7 (chloroquine sensitive) strain *in vitro*. Data generated from this study is presented in Table 4.2

Compound	R	<i>In vitro</i> IC ₅₀ (nM)	Compound	R	<i>In vitro</i> IC ₅₀ (nM)
31	—OH	185.7 ± 34.1	37		5.0 ± 0.5
34		3.8 ± 1.0	38		11.7 ± 2.4
35		3.0 ± 1.3	39		5.0 ± 1.3
36		12.0 ± 3.0	41		17.4 ± 5.5

Table 4.2: The concentrations of unsymmetrical dispiro-1,2,4,5-tetraoxanes that provoke a 50% inhibition (IC₅₀) of the proliferation of *Plasmodium falciparum* 3D7 strain *in vitro*.

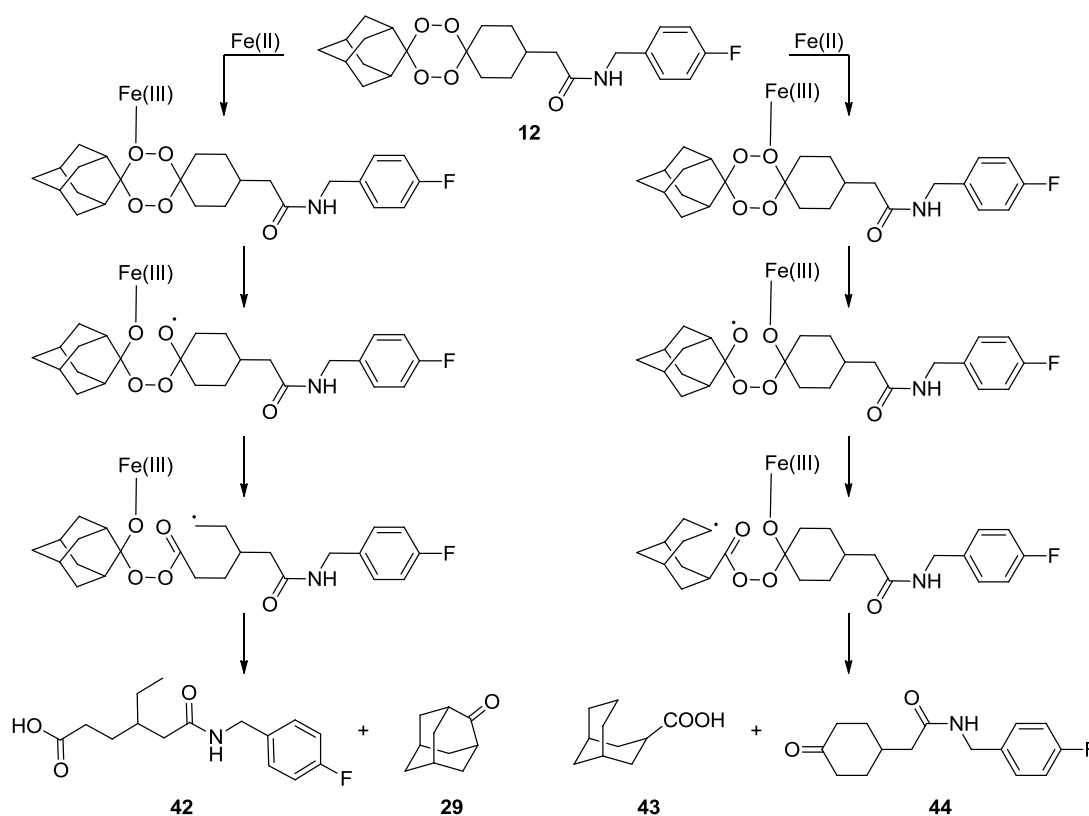
All compounds that were submitted for testing were active against the *P. falciparum* 3D7 strain. The most active compound within this series was compound **35** giving an IC₅₀ of 3.0 ± 1.3 nM. The removal of the carbon linker between the

Chapter 4 – Examination of the role of ferrous iron and phosphatidylcholine in the bioactivation of novel tetraoxane antimalarials

amide and phenyl groups (compound **34**) slightly reduced antimalarial activity compared to compound **35**. Substituting the fluoro group with chlorine (**36** and **37**) reduced antimalarial activity. However, the chlorine derivatives further confirmed that a carbon linker is required between the amide and the phenyl group to obtain greater antimalarial activity. *Para* substituted methoxy, trifluoromethyl and substitution of the phenyl for the cyclohexyl ring did not improve antimalarial activity. Compound **35** was therefore selected for use in experiments designed to examine the radical pathway of tetraoxanes by activation with an inorganic iron(II).

4.2.2 Investigating the radical pathway of tetraoxanes

Activation of the endoperoxide tetraoxane by inorganic ferrous iron (iron(II) salts) is hypothesised to generate primary or secondary carbon-centred radicals. The proposed chemical mechanism is shown in Scheme 4.7.



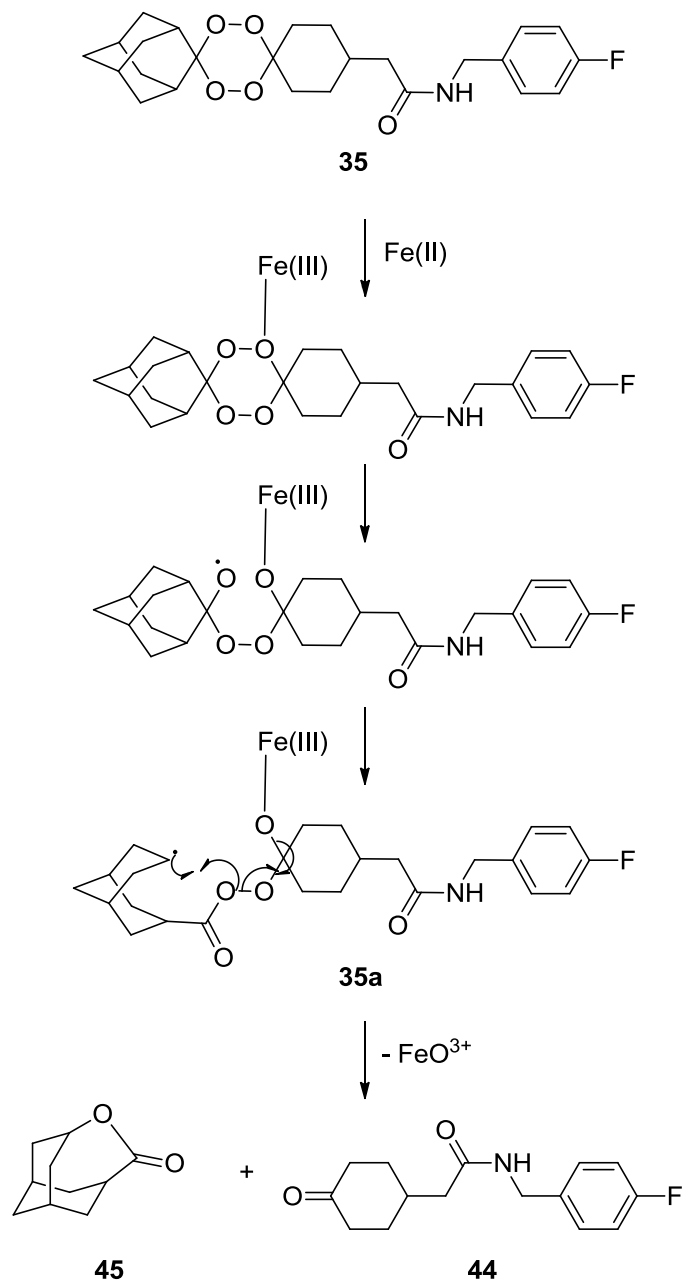
Scheme 4.7: Proposed mechanism of endoperoxide activation by iron(II) for the tetraoxane class. The chemical mechanism for the formation of primary (left route) and secondary (right route) carbon-centred radicals is depicted.

The degradation of the tetraoxane compound **35** was performed in an attempt to isolate products that have resulted from carbon-centred radical formation. A range of iron(II) salts were used under a variety of different conditions to obtain the optimal yield. Iron(II) acetate under two different conditions (DCM/acetonitrile or THF) mainly produced low turnover of the tetraoxane and as a result a different

Chapter 4 – Examination of the role of ferrous iron and phosphatidylcholine in the bioactivation of novel tetraoxane antimalarials

iron salt was explored. The use of iron(II) gluconate or iron(II) sulphate resulted in an improved reaction turnover. For experiments involving iron(II) gluconate, dimethylformamide (DMF) and water were used as the solvent in an attempt to mimic biological conditions. The incubation time was varied in order to determine the optimal conditions for full turnover. The degradation of the tetraoxane was monitored by thin layer chromatography (TLC). The overall turnover (96%) was maintained when the incubation period was reduced from 24 hours to 7 hours. Purification by flash chromatography and HPLC yielded three of the four predicted reaction products (**29**, **42**, and **44**). This suggests that iron(II) salt-mediated degradation of tetraoxanes follows the two proposed chemical routes (Scheme 4.7). The primary and secondary carbon-centred radicals are generated in approximately equal amounts as isolation of **42** and **44** were obtained at approximately 1:1.

The postulated acid product **43** associated with the formation of a secondary carbon-centred radical was not observed under any of the conditions used despite isolation of the predicted ketone counterpart **44**. A lactone product **45** was obtained in similar ratios to the ketone counterpart **44** (Scheme 4.8). Further examination with LCMS revealed that the lactone **45** was indeed generated under these conditions. Such a lactone could be formed *via* intramolecular attack on the peroxy ester function by the C-radical centre of **35a** resulting in the loss of FeO^{3+} and the formation of lactone **45** (Scheme 4.8).



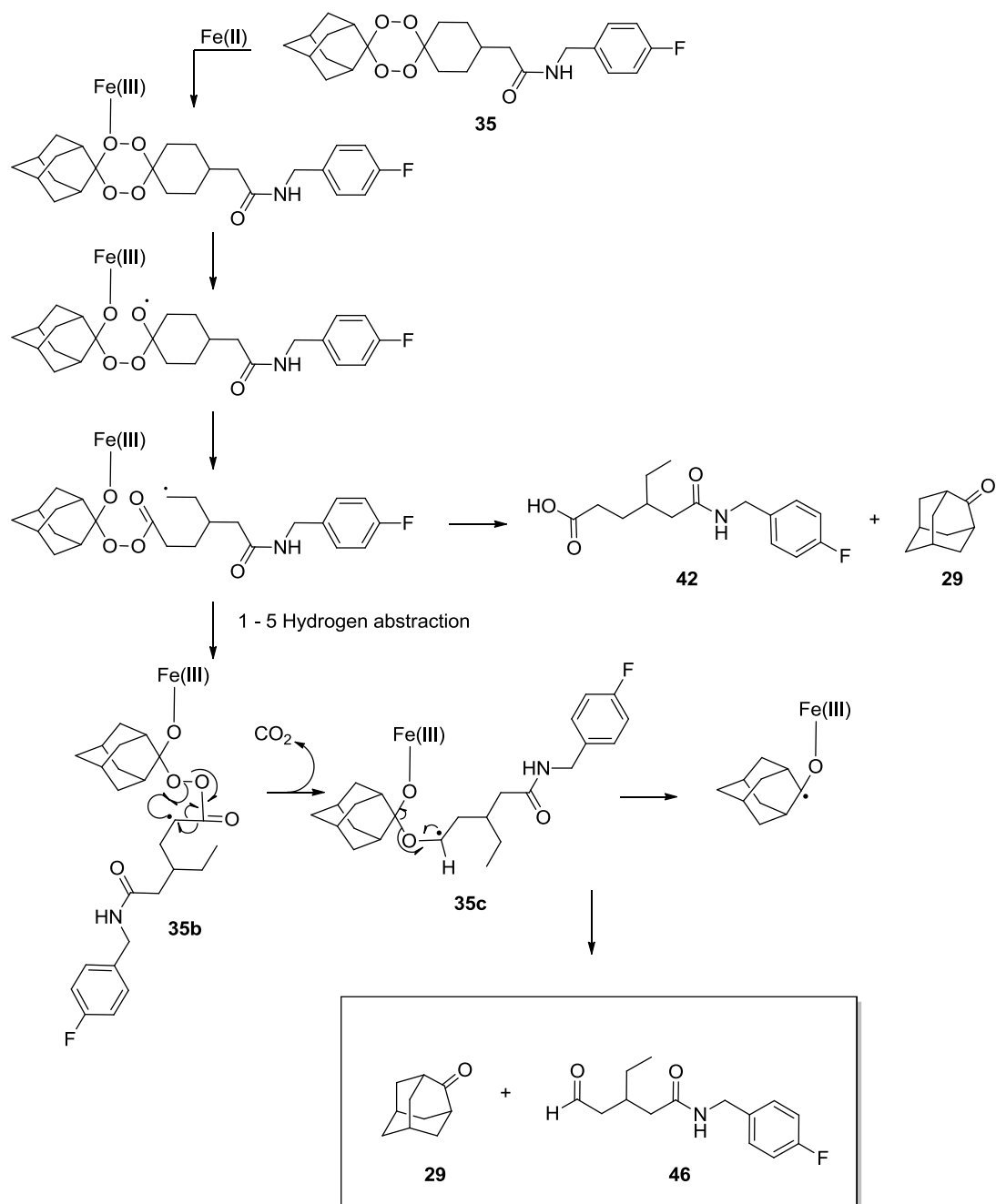
Scheme 4.8: Secondary carbon-centred radical pathway and the mechanism which results in the formation of lactone **45** following iron(II) salt-mediated degradation of tetraoxane **35**.

Chapter 4 – Examination of the role of ferrous iron and phosphatidylcholine in the bioactivation of novel tetraoxane antimalarials

In addition to the four products (**29**, **42**, **44** and **45**) obtained during the degradation experiments, a fifth product was obtained. Chemical analysis suggested that this product was an aldehyde (**46**). Proton NMR indicated that a single proton triplet was located at 9.77 ppm. This represents a de-shielded CH group next to a CH₂. The corresponding carbon NMR along with HMQC and DEPT135 confirmed that the carbon located at 202.2 ppm was that of an aldehyde. Mass spectrometry also confirmed an aldehyde was present. Fragmentation during ionisation on MS resulted in a mass loss of 18 *m/z* which is commonly associated with the presence of aldehydes, ketones and primary alcohols.²⁰ A proposed chemical mechanism is shown in Scheme 4.9 where intramolecular 1-5 hydrogen abstraction of **35b** results in the loss of carbon dioxide and the formation of **35c**. **35c** R5earranges to give compound **29** and the corresponding aldehyde **46**. Although the aldehyde is obtained during the degradation experiments, it may not fully represent the chemical mechanism of action under *in vivo* conditions as 2 equivalents of iron(II) were used during these *in vitro* experiments.

Despite some contention, the radical pathway for the activation of endoperoxide tetraoxanes by iron-mediated decomposition is currently the most convincing mechanism of action for this class of antimalarials. Primary and secondary carbon-centre radicals can alkylate vital parasitic proteins resulting in cell death. However, the identity of such biological targets is currently unclear and requires further examination.

Chapter 4 – Examination of the role of ferrous iron and phosphatidylcholine in the bioactivation of novel tetraoxane antimalarials



Scheme 4.9: Primary carbon-centred radical pathway and the mechanism which results in the formation of lactone **42** and **29**. Further intramolecular 1-5 hydrogen abstraction results in the formation of **35c** and eventually the aldehyde **46**.

4.2.3 Reactivity of tetraoxanes with iron(II) and phosphatidylcholine (PC)

The capacity of the tetraoxanes to alkylate proteins *via* the formation of carbon centred radicals has been met with scepticism. The capacity of the tetraoxanes to react with biologically relevant lipid targets is therefore of interest as an alternative mechanism of action. Tilley *et al* have examined the lipid environment within *Plasmodium falciparum*. The study identified that phosphatidylcholine (PC)(**47**) was present in the parasite food vacuole.²¹ The food vacuole is the site of haemoglobin degradation and the site of heme production.¹¹ The lipid bilayer is a well-known target for many reactive oxygen species (ROS). The generation of ROS can lead to oxidative cleavage and lipid peroxidation, culminating in cell damage and death.² Kumura *et al* have reported that tetraoxane salts (**48**) can induce oxidative degradation of PC in the presence of an iron(II) salt. Several PC degradation products were identified, however, the authors did not propose any chemical mechanisms for their formation.¹⁸ The symmetrical tetraoxane salt (**48**) used by Kumura is structurally different from the unsymmetrical more lipid soluble 1,2,4,5-tetraoxanes. Therefore, examining the reactivity of unsymmetrical tetraoxanes in the presence of biological relevant lipids is vital for understanding the potential mechanism of action of compounds within this class.

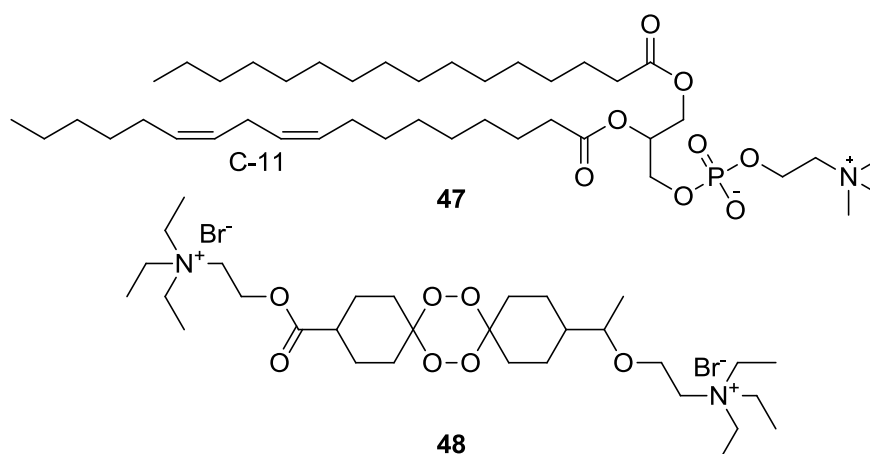


Figure 4.4: Chemical structure of 2-linoleoyl-1-palmitoyl-*sn*-phosphatidylcholine² and the symmetrical salt previously studied by Kumura.¹⁸

During the purification of the degradation products, flash column chromatograph and ultraviolet detection by high performance liquid chromatography (HPLC-UV) was used to obtain analytical standards for compounds **35**, **42**, **44** and **45**. Compound **43** was synthesised and provided by co-workers.² This enabled the use of liquid chromatography with mass spectral analysis (LCMS), and calibration of reverse phase column conditions, by using the standard compounds as references. The retention times of each compound were determined. This data is shown in Figure 4.5.

Chapter 4 – Examination of the role of ferrous iron and phosphatidylcholine in the bioactivation of novel tetraoxane antimalarials

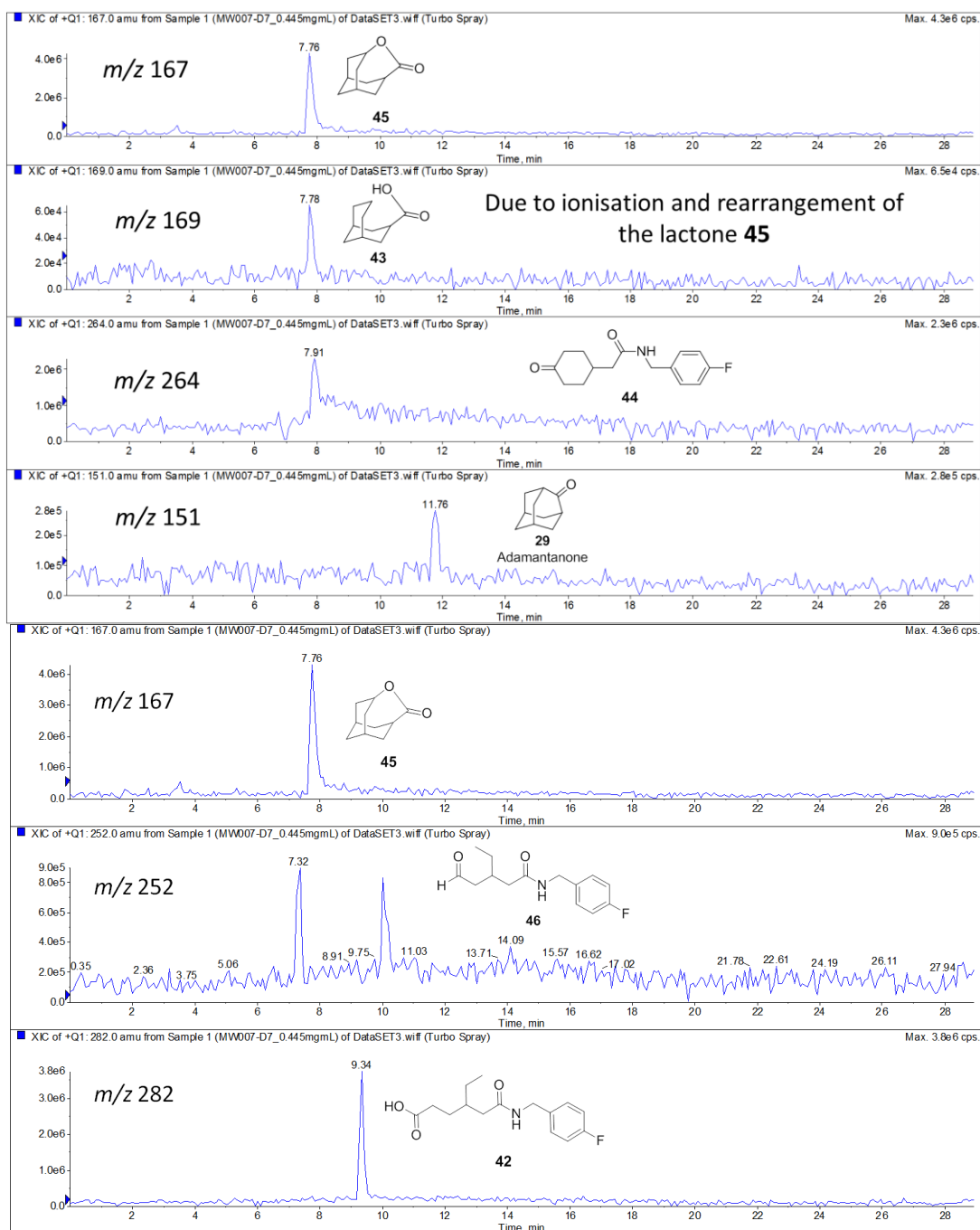


Figure 4.6: LCMS analysis of tetraoxane 35 reacted with FeSO₄. The resulting degradation products had similar retention times to the chemically purified references.

The degradation reaction mixture was produced with iron(II) sulphate in acetonitrile:water. This condition was used by Kumura *et al* for the reaction of PC with the endoperoxides.¹⁸ During LCMS analysis, acid 43 was detected at 7.78

Chapter 4 – Examination of the role of ferrous iron and phosphatidylcholine in the bioactivation of novel tetraoxane antimalarials

minutes. This is also the retention time of the lactone **45** and therefore the observation of **43** is due to ionisation and rearrangement of the lactone. Acid **43** has an expected retention time of 13.70 minutes. Compounds **29**, **42**, **44** and **45** were detected at the expected times compared to standards.

Reactions of 2-linoleoyl-1-palmitoyl-*sn*-glycero-phosphatidylcholine (PC **47**) with tetraoxane **35** in the presence of iron(II) sulphate were analysed using mass spectrometry (MS). MS data was compared to native PC and indicated the formation of several products (Figure 4.7). The predominant degradation products had m/z 622.2, 650.6, 666.5 and 788.6. All of these ions were detected by Kumura *et al.*¹⁸ The bis-allylic hydrogen located at C-11 of the linoleic acid within PC is likely to be abstracted by the tetraoxane radicals formed during activation of iron(II) salt. The proposed mechanisms for the formation of each of the PC oxidation products are depicted in Figure 4.8. This is based on the examination of linoleic acid peroxidation by Spiteller *et al.*²²

Product P1 is derived from the C-9 capture of oxygen followed by peroxy radical H-abstraction from another molecule of PC, which results in a radical chain reaction. Homolytic cleavage of the hydroperoxide followed by fragmentation forms a carbon centred radical on C-8, which is capable of abstracting an hydrogen to produce the product P1. Fragmentation resulting in the loss of the phosphorus group during MS analysis resulted in the fragment P2. The product P4 is formed *via* the Hock rearrangement resulting in the generation of an aldehyde P3. P3 undergoes oxidation under the reaction conditions to provide P4. Product P5 is derived from PC and the C-13 oxygen capture. Reductive activation by ferrous iron produces a

Chapter 4 – Examination of the role of ferrous iron and phosphatidylcholine in the bioactivation of novel tetraoxane antimalarials

peroxy epoxide that can undergo hydrogen abstraction and oxidation to produce a gem dihydroperoxide. The gem dihydroperoxide undergoes rearrangement to release hydrogen peroxide yielding product P5.

As shown earlier, tetraoxane are able to generate primary and secondary carbon centred radicals once exposed to iron(II) salts. To further understand the mechanistic pathway of tetraoxane degradation, LCMS analysis was performed to determine which of the carbon-centred radical species is responsible for hydrogen abstraction of the bis-allylic hydrogen located at C11 of the linoleic acid within PC. This analysis resulted in the detection of the acid **42** and the lactone **45** and their respective counterpart **29** and **44** resulting from the degradation of tetraoxane **35** (Figure 4.9). The acid **43** is only generated if hydrogen abstraction of PC occurs *via* the secondary carbon centred radical pathway, however, **43** was not detected under these reaction conditions and only the lactone **45** was detected. Hence, hydrogen abstraction did not occur. Therefore, the data obtained strongly suggests that the primary carbon-centred radical is primarily responsible for hydrogen abstraction of PC.

Chapter 4 – Examination of the role of ferrous iron and phosphatidylcholine in the bioactivation of novel tetraoxane antimalarials

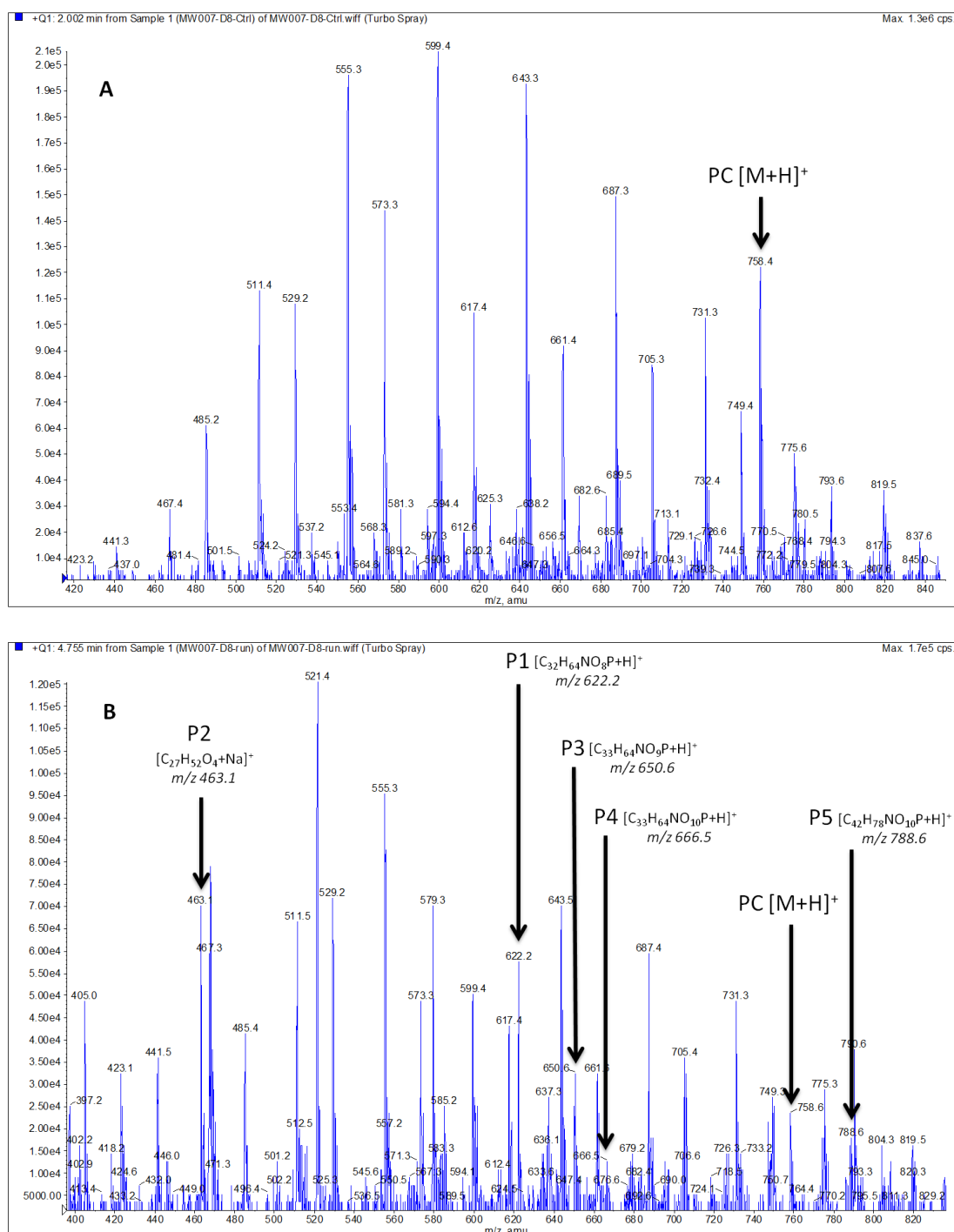


Figure 4.7: (A) MS spectra of the products resulting from the reaction of PC and iron(II) sulphate in the absence of tetraoxane **35**; (B) MS spectra of the products resulting from the reaction of PC, iron(II) sulphate and tetraoxane **35**. The predominant degradation products had m/z 622.2, 666.5 and 788.6.

Chapter 4 – Examination of the role of ferrous iron and phosphatidylcholine in the bioactivation of novel tetraoxane antimalarials

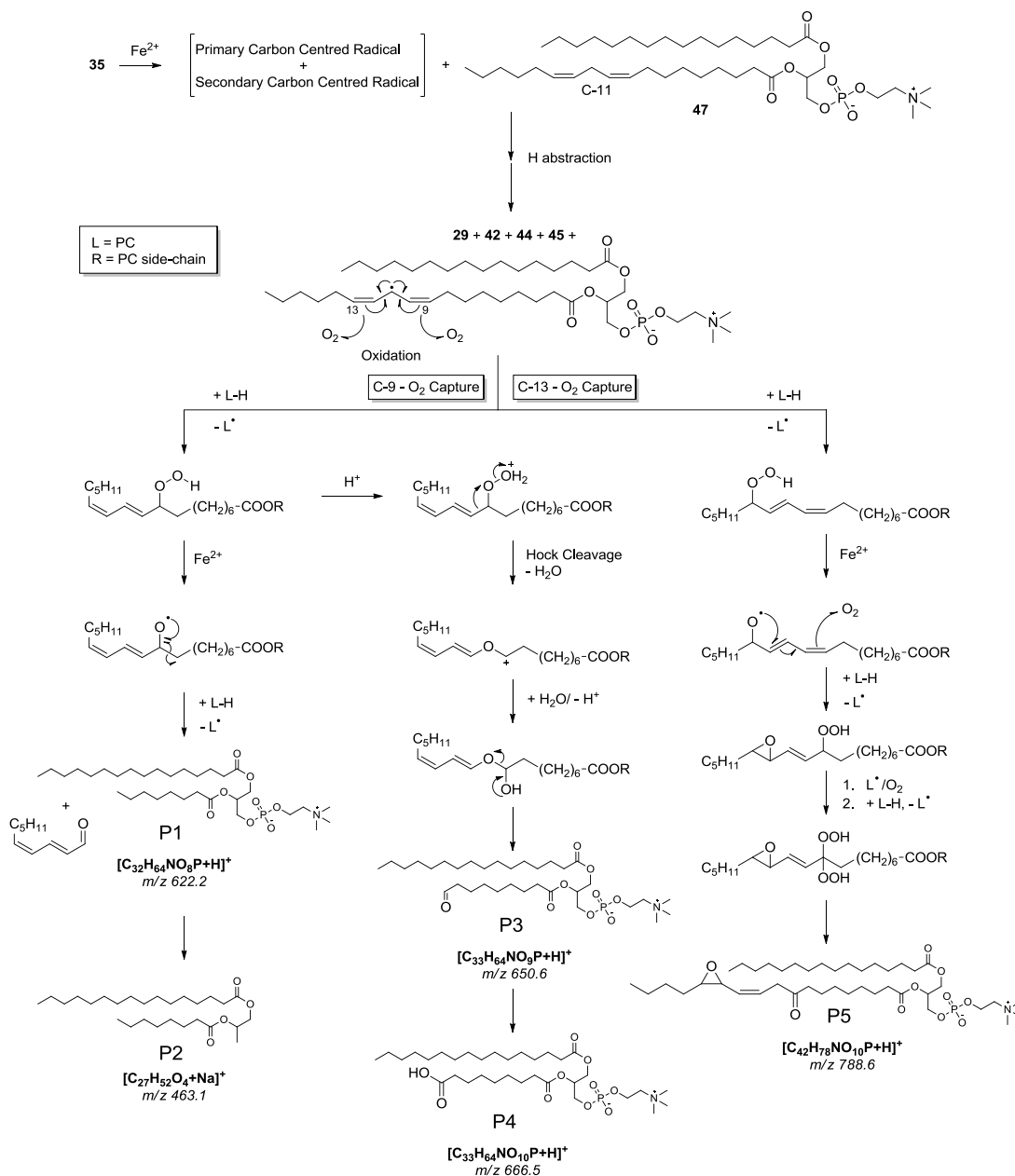


Figure 4.8: Proposed mechanisms for tetraoxane mediated lipid peroxidation, as suggested by Kumura *et al.*¹⁸

Chapter 4 – Examination of the role of ferrous iron and phosphatidylcholine in the bioactivation of novel tetraoxane antimalarials

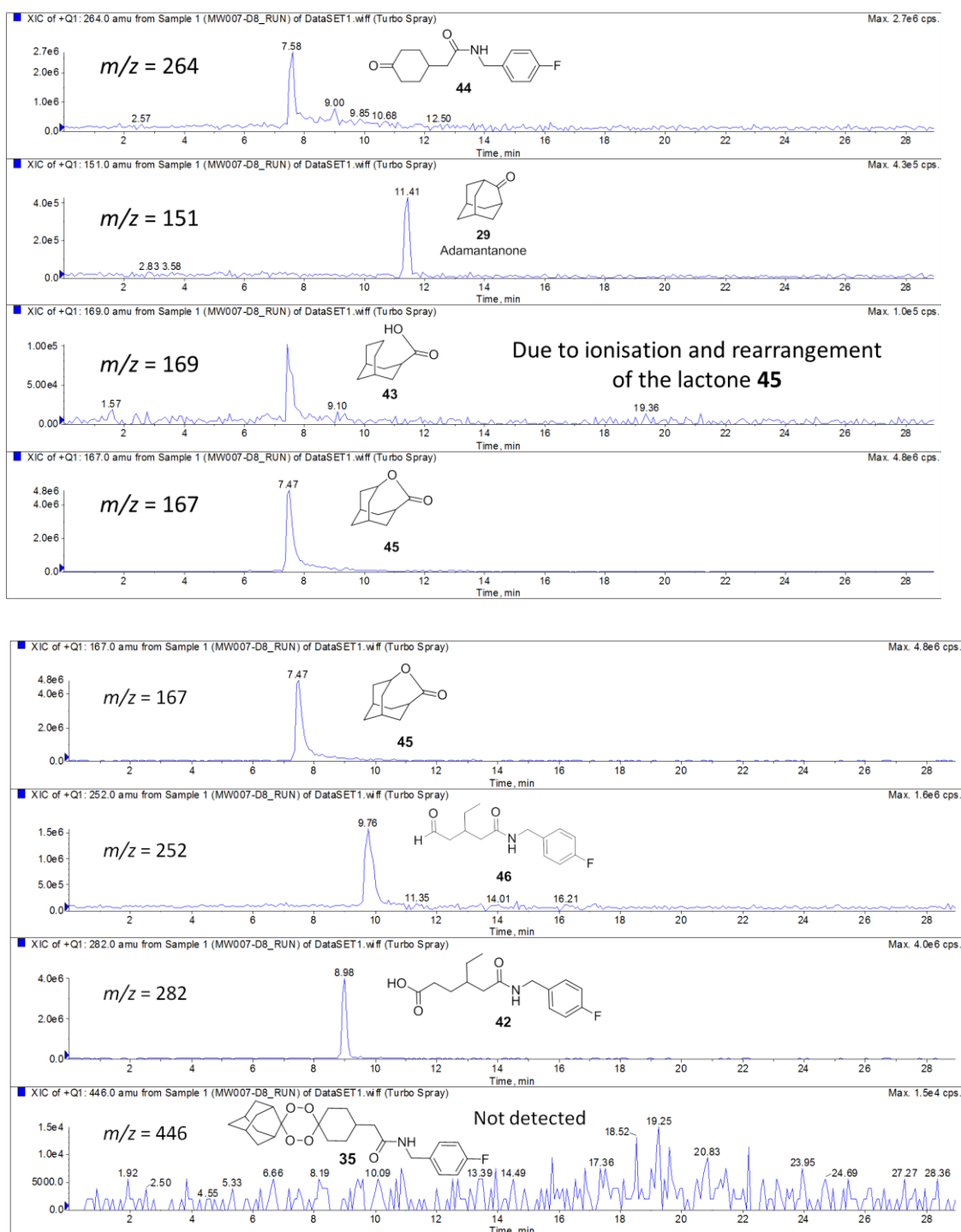


Figure 4.9: LCMS spectra of the products resulting from the reaction of PC, iron(II) sulphate and tetraoxane **35**. The tetraoxane by products resulting from the formation of primary and secondary carbon-centre radicals were detected at the expected retention times.

4.3 Conclusion

The synthesis of unsymmetrical dispiro-1,2,4,5-tetraoxanes has produced seven novel tetraoxane compounds that are active in the low nanomolar range against the 3D7 strain of *P. falciparum*. Degradation studies involving tetraoxanes in the presence of inorganic iron under various conditions have produced three of the predicted degradation products. Two additional degradation products were also obtained. This study has therefore demonstrated that both primary and secondary carbon centred radicals can be formed under such conditions. Reactions of PC with tetraoxane in the presence of iron(II) confirmed that lipids such as PC could be an alternative molecular target for this class of antimalarials.

Secondary carbon-centred radicals derived from an iron(II) activated tetraoxane have been shown to bind to heme porphyrin⁸. Therefore it was of interest to determine if secondary carbon-centred radicals are also responsible for the hydrogen abstraction of PC. Based on this study it is clear that hydrogen abstraction of PC is exclusively mediated through the primary carbon-centred radicals generated by the tetraoxane when exposed to iron(II) salts. Surprisingly, previous work has shown that artemisinins do not provoke lipid peroxidation,² suggesting that tetraoxanes and artemisinins may have different chemical mechanisms of action as antimalarials.

One suggested mechanism of action could be similar to chloroquine, which was developed in the mid 20th century from quinine. Chloroquine accumulates within the parasite food vacuole and inhibits hemozoin biocrystallization, causing an accumulation of cytotoxic heme which kills the parasite *via* an oxidation

Chapter 4 – Examination of the role of ferrous iron and phosphatidylcholine in the bioactivation of novel tetraoxane antimalarials process.^{23,24} Studies by Sugioka *et al* have demonstrated that a ferriprotoporphyrin IX-chloroquine complex promotes heme-catalysed lipid peroxidation.²⁵ Tetraoxanes have been shown to bind to heme porphyrin and could therefore have a similar mechanism to that of chloroquine whereby hemozoin biocrystallization is inhibited, resulting in heme catalysed lipid peroxidation.

4.4 Chemistry Experimental

4.4.1 General

See section 2.4.1

4.4.2 Purification of solvents and reagents

See section 3.4.2

4.4.2.1 Stains

See section 3.4.2.1

4.4.3 Purification of products

4.4.3.1 General

See section 2.4.4

4.4.3.2 HPLC-UV purification

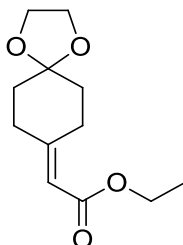
HPLC system consists of Gilson 305 and 306 pumps, 811C low-volume dynamic mixer, 119 UV detector and 805 manometric module (Gilson, Inc. USA). The software used was Clarity version 2.6.5.517 (DataApex Ltd, Prague, The Czech Republic). Samples were dissolved in 70% Methanol, 30% water and filtered using 13 mm 0.2 µm PTFE membrane syringe filters (c/o VWR International, Lutterworth, UK) prior to injection. The solutions (2 mL) were chromatographed at room temperature on an Eurospher 100-5 C18 column (250 × 20 mm i.d.; Knauer advanced scientific instruments, Hegauer Weg, Berlin, Germany) by gradient elution with methanol (70-95% over 15 min; 70% from 15 min to 30 min) in water. The eluent flow rate was 5.0 mL/min using UV detection set at 254 nm.

4.4.4 Analysis

See section 2.4.5

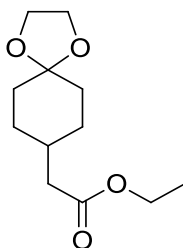
4.4.5 Synthesis of unsymmetrical dispiro-1,2,4,5-tetraoxanes

Preparation of Ethyl 2-(1,4-dioxaspiro[4.5]decan-8-ylidene)acetate (**25**)⁷



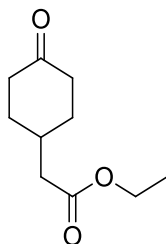
A solution of 1,4-cyclohexanedione monoethylene acetal (**24**)(10 g, 64 mmol) and ethyl 2-(triphenylphosphoranylidene)acetate (**33**)(24.54 g, 70.4 mmol) in toluene was refluxed under nitrogen for 16 hours. The solvent was removed under vacuum and the crude product purified *via* flash column chromatography using 5% ethyl acetate in hexane to give the title compound **25** (12.69 g, 88%) as a colourless oil; $R_f = 0.53$, 20% ethyl acetate in hexane; $^1\text{H NMR}$ (400 MHz, CDCl_3) δ 5.66 (s, 1H), 4.14 (q, $J = 7.1$ Hz, 2H), 3.97 (s, 4H), 3.03 – 2.97 (m, 2H), 2.42 – 2.32 (m, 2H), 1.83 – 1.70 (m, 4H) and 1.27 (t, $J = 7.1$ Hz, 3H); $^{13}\text{C NMR}$ (100 MHz, CDCl_3) δ 166.3, 160.1, 114.2, 107.8, 64.3, 59.4, 35.7, 34.9, 34.5, 25.9 and 14.2; IR ν_{max} (neat)/ cm^{-1} 2934 (CH), 2860 (COCH_2), 1710 (CO) and 1150 (C-O-C); MS (CI) $\text{C}_{12}\text{H}_{18}\text{O}_4$ $[\text{M}+\text{NH}_4]^+$ m/z 244.1.

Preparation of ethyl 2-(1,4-dioxaspiro[4.5]decan-8-yl)acetate (**26**)⁷



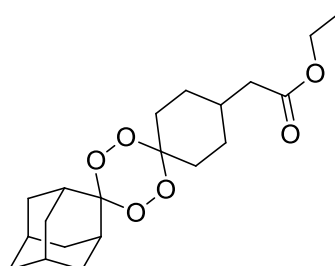
In the absence of light palladium on carbon (10% w/w, 6.56 g, 61.7 mmol) in anhydrous ethyl acetate was added to a solution of **25** (12.7 g, 56.1 mmol) and stirred in a hydrogen atmosphere at room temperature for 16 hours. The reaction was filtered through a pad of celite and washed with ethyl acetate. The solvent was removed under vacuum to give the title compound **26** (11.73 g, 92%) as a clear yellow oil; $R_f = 0.75$, 50% ethyl acetate in hexane; $^1\text{H NMR}$ (400 MHz, CDCl_3) δ 4.13 (d, $J = 7.0$ Hz, 2H), 3.94 (s, 4H), 2.23 (d, $J = 7.0$ Hz, 2H), 1.76 – 1.70 (m, 1H), 1.61 – 1.51 (m, 2H), 1.30 – 1.23 (m, 3H) and 1.26 (t, $J = 7.2$ Hz, 3H); $^{13}\text{C NMR}$ (100 MHz, CDCl_3) δ 173.0, 108.6, 64.2, 60.2, 41.0, 34.2, 33.4, 29.9 and 14.2. MS (CI) $\text{C}_{12}\text{H}_{20}\text{O}_4$ $[\text{M}+\text{H}]^+$ m/z 229.1.

Preparation of ethyl 2-(4-oxocyclohexyl)acetate (**27**)⁸



A solution of hydrochloric acid (1 M, 300 mL) was added to compound **26** (11.73 g, 51.8 mmol) and left to stir at room temperature for 4.5 hours. Saturated sodium carbonate was added to the reaction to neutralise the acid. The resulting solution was worked up with dichloromethane (300 mL), dried over magnesium sulfate and the solvent removed under vacuum. The crude product was purified *via* flash column chromatography using 20% ethyl acetate in hexane to give the title compound **27** (5.33 g, 56%) as a colourless oil; $R_f = 0.5$, 50% ethyl acetate to hexane; $^1\text{H NMR}$ (400 MHz, CDCl_3) δ 4.15 (q, $J = 7.1$ Hz, 2H), 2.41 – 2.33 (m, 5H), 2.32 (s, 2H), 2.15 – 2.06 (m, 2H), 1.56 – 1.43 (m, 2H) and 1.27 (t, $J = 7.1$ Hz, 3H); $^{13}\text{C NMR}$ (100 MHz, CDCl_3) δ 210.8, 172.1, 60.2, 40.3, 40.0, 32.8, 32.2 and 14.0; MS (CI) $\text{C}_{10}\text{H}_{16}\text{O}_3$ $[\text{M}+\text{NH}_4]^+$ m/z 202.1.

Preparation of ethyl dispiro [cyclohexane-1,3'-[1,2,4,5]tetraoxane-6',2''-tricyclo [3.3.1.1^{3,7}] decan]-4-ylacetate (**30**)⁸

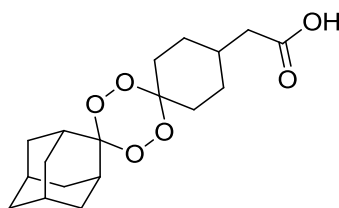


A solution of **26** (1 g, 5.43 mmol) in acetonitrile (50 mL) was cooled on an ice bath to 0°C. Formic acid in acetonitrile (1:1 mix, 10 mL, 133 mmol) along with hydrogen peroxide solution (30% w/w, 6 mL, 59.7 mmol) was added to the reaction and left to stir for 30 minutes. The reaction was monitored by TLC to ensure all starting material was converted. $R_f = 0.65$, 50% ethyl acetate to hexane. The reaction was quenched with water and washed with dichloromethane (3 x 50 mL). The organic layers were combined and the solvent was removed *in vacuo* to obtain intermediate **28**. Under a nitrogen atmosphere, **28** was re-dissolved in anhydrous dichloromethane (50 mL). Adamantanone (**29**) (1.09 g, 7.23 mmol) in anhydrous dichloromethane (50 mL) was added to the stirring reaction containing **5**. Rhenium(VII) oxide (70 mg, 144.58 μmol) was added to the reaction and left to stir for 30 minutes. The solvent was removed *in vacuo* and the crude product was purified *via* flash chromatography using 20% ethyl acetate in hexane to give the title compound **30** (470 mg, 37%) as a white solid; $R_f = 0.85$, 20% ethyl acetate to hexane; mp = lit⁸ 60-62°C found 61-63°C ¹H NMR (400 MHz, CDCl₃) δ 4.12 (q, $J = 7.1$ Hz, 2H), 2.23 (d, $J = 6.7$ Hz, 2H), 2.16 – 1.80 (m, 9H), 1.79 – 1.46 (m, 12H), 1.43 – 1.17 (m, 2H) and 1.25 (t, $J = 7.1$ Hz, 3H); ¹³C NMR (100 MHz, CDCl₃) δ 172.8, 110.6,

Chapter 4 – Examination of the role of ferrous iron and phosphatidylcholine in the bioactivation of novel tetraoxane antimalarials

107.8, 60.4, 40.9, 37.1, 33.8, 33.3, 27.2 and 14.4; HRMS (ESI) calculated for $C_{20}H_{30}O_6$ $[M+Na]^+$ 389.1940 found 389.1920.

Preparation of dispiro[cyclohexane-1,3'-[1,2,4,5]tetraoxane-6',2''-tricyclo[3.3.1.1^{3,7}]decan]-4-ylacetic acid (**31**)⁸

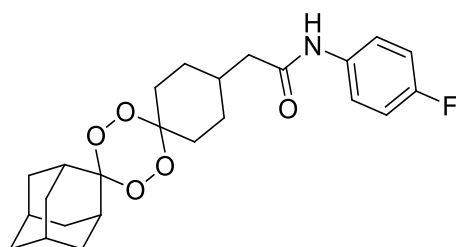


Potassium hydroxide (1.2 g, 21.46 mmol) was dissolved in a small amount of methanol and added to a stirring solution of **30** (1.43 g, 3.90 mmol) in methanol (50 mL) and refluxed for 1 hour. The solution was allowed to cool to room temperature and concentrated under reduced pressure. The resulting residue was dissolved in water (50 mL) and worked up in dichloromethane (150 mL), dried over magnesium sulfate and the solvent was removed under vacuum to give the title compound **31** (1.30 g, 98%) as a white solid; $R_f = 0$, 1:1 Ethyl acetate:hexane; mp = lit²⁶ 119-121°C found 166-170°C; 1H NMR (400 MHz, $CDCl_3$) δ 2.34 – 2.24 (m, 2H), 2.20 – 1.47 (m, 21H) and 1.44 – 1.23 (m, 2H); ^{13}C NMR (100 MHz, $CDCl_3$) δ 178.9, 110.6, 107.7, 40.5, 37.1, 33.6, 33.3 and 27.2; IR ν_{max} (neat)/ cm^{-1} 2930, 2907, 2858 and 1697; HRMS (ESI) calculated for $C_{18}H_{26}O_6$ $[M+Na]^+$ 361.1627 found 361.1609; Microanalysis calculated for $C_{18}H_{26}O_6$ requires C 63.89%, H 7.74%, found C 63.635%, H 7.65%.

General procedure 1

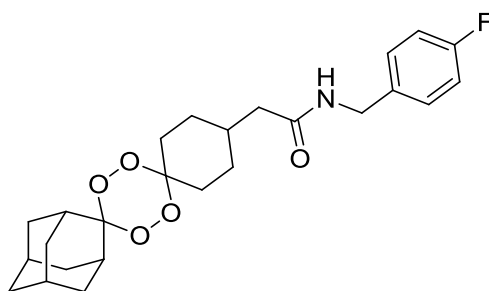
To a dry flask, Compound **31** was dissolved in anhydrous dichloromethane (50 mL) and stirred under a nitrogen atmosphere prior to cooling to 0°C. Triethylamine (1.5 equivalent) and methyl chloroformate (1.1 equivalent) was added to the reaction and left to stir at 0°C for 1 hour. The required amine (1 equivalent) was added to the reaction mixture and left to stir for 30 minutes at 0°C then at room temperature for a further 1 hour. The reaction mixture was washed with dichloromethane (3 x 50 mL), water (50 mL), brine (50 mL) and dried over magnesium sulfate. The reaction was concentrated under reduced pressure and purified *via* flash column chromatography.

Preparation of 2-(dispiro[cyclohexane-1,3'-[1,2,4,5]tetraoxane-6',2''-tricyclo[3.3.1.1^{3,7}]decan]-4-yl)-N-(4-fluorophenyl)acetamide (34)



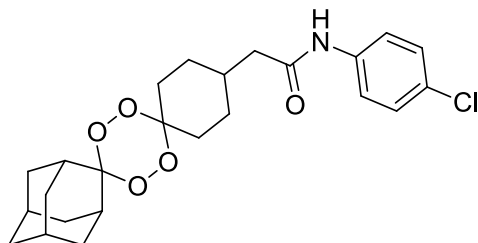
31 (200 mg, 0.6 mmol) was synthesised according to general procedure 1. 4-Fluoroaniline (56 μ L, 0.6 mmol) was used in the coupling step. **34** was purified *via* flash column chromatography using 5% ethyl acetate in dichloromethane to give the title compound **34** (201.7 mg, 79%) as a white solid; $R_f = 1$, 50% ethyl acetate to dichloromethane; mp = 162-163°C; ^1H NMR (400 MHz, CDCl_3) δ 7.50 – 7.43 (m, 2H), 7.15 (s, 1H), 7.01 (t, $J = 8.6$ Hz, 2H), 2.25 (d, $J = 7.0$ Hz, 2H), 2.17 – 1.49 (m, 21H) and 1.33 (s, 2H); ^{13}C NMR (100 MHz, CDCl_3) δ 170.2, 133.8 (d, $J = 2.1$ Hz), 121.8 (d, $J = 7.8$ Hz), 115.8 (d, $J = 22.5$ Hz), 110.6, 107.8, 44.3, 37.1, 34.3, 33.30, 33.27, 27.20 and 27.18; IR ν_{max} (neat)/ cm^{-1} 3292 (CONH), 3267 (CONH), 2920 (Ar-H), 2856 (CH), 1655(C=C), 1543 (C=C) and 1508 (C=C); ERMS (ESI) calculated for $\text{C}_{24}\text{H}_{30}\text{FNO}_5$ $[\text{M}+\text{Na}]^+$ 454.2006 found 454.1992; Microanalysis calculated for $\text{C}_{24}\text{H}_{30}\text{FNO}_5$ requires C 66.80%, H 7.01%, N 3.25%, found C 66.68%, H 7.05%, N 3.21%.

Preparation of 2-(dispiro[cyclohexane-1,3'-[1,2,4,5]tetraoxane-6',2''-tricyclo[3.3.1.1^{3,7}]decan]-4-yl)-N-(4-fluorobenzyl)acetamide (**35**)²



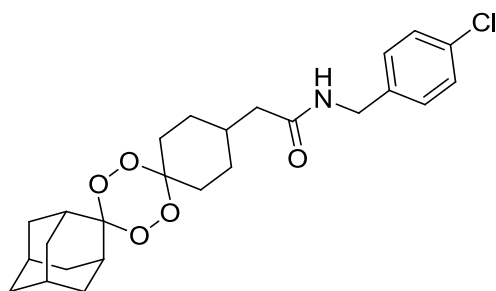
31 (203.4 mg, 601 μmol) was synthesised according to general procedure 1. 4-Fluorobenzylamine (68.7 μL , 601 μmol) was used in the coupling step. **35** was purified *via* flash column chromatography using 3% ethyl acetate in dichloromethane to give the title compound **35** (189.6 mg, 71%) as a white solid: R_f = 0.78, 50% ethyl acetate in dichloromethane; mp = lit² 140°C found 150-152°C; ¹H NMR (400 MHz, CDCl₃) δ 7.36 – 7.20 (m, 2H), 7.16 – 6.98 (m, 2H), 5.70 (s, 1H), 4.41 (d, J = 5.7 Hz, 2H), 2.11 (d, J = 7.1 Hz, 2H), 2.09 – 1.43 (m, 21H) and 1.25 (s, 2H); ¹³C NMR (100 MHz, CDCl₃) δ 171.8, 134.2 (d, J = 3.7 Hz), 129.6 (d, J = 8.1 Hz), 115.7 (d, J = 21.5 Hz), 110.6, 107.8, 43.5, 43.0, 37.1, 34.2, 33.3 and 27.2. IR ν_{max} (neat)/cm⁻¹ 3242 (CONH), 2918 (Ar-H), 2856 (CH), 1631 (C=C), 1545 (C=C), 1510 (C=C) and 1225 (CF); ERMS (ESI) calculated for C₂₅H₃₂FNO₅ [M+Na]⁺ 468.2162 found 468.2149; Microanalysis calculated for C₂₅H₃₂FNO₅ requires C 67.40%, H 7.24%, N 3.14%, found C 67.68%, H 7.27%, N 3.16%.

Preparation of *N*-(4-chlorophenyl)-2-(dispiro[cyclohexane-1,3'-[1,2,4,5]tetraoxane-6',2''-tricyclo[3.3.1.1^{3,7}]decan]-4-yl)acetamide (**36**)



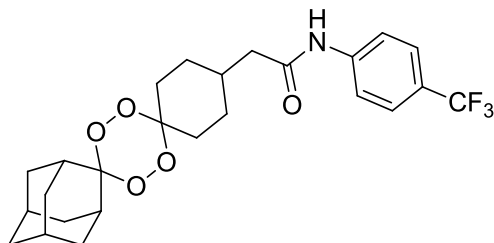
31 (200 mg, 591.02 μmol) was synthesised according to general procedure 1. 4-Chloroaniline (52.7 μL , 591.02 μmol) was used in the coupling step. **36** was purified *via* flash column chromatography using 5% ethyl acetate in dichloromethane to give the title compound **36** (107 mg, 40%) as a white solid: $R_f = 0.95$, 50% ethyl acetate in dichloromethane; mp = 169-171 $^{\circ}\text{C}$; ^1H NMR (400 MHz, CDCl_3) δ 7.46 (d, $J = 8.8$ Hz, 2H), 7.28 (d, $J = 8.8$ Hz, 2H), 2.26 (d, $J = 6.9$ Hz, 2H), 2.11 – 1.46 (m, 21H) and 1.43 – 1.23 (m, 3H); ^{13}C NMR (100 MHz, CDCl_3) δ 170.2, 169.2, 136.4, 129.5, 129.2, 121.1, 110.7, 107.8, 44.4, 37.1, 34.2, 33.3, 27.2 and 27.2; IR ν_{max} (neat)/ cm^{-1} 3232 (CONH), 2931 (Ar-H), 2858 (CH), 1651 (C=C), 1543 (C=C), 1493 (C=C) and 825 (C-Cl); ERMS (ESI) calculated for $\text{C}_{24}\text{H}_{30}\text{ClNO}_5$ $[\text{M}+\text{Na}]^+$ 470.1710 and 472.1681 found 470.1715 and 472.1693; Microanalysis calculated for $\text{C}_{24}\text{H}_{30}\text{ClNO}_5$ requires C 64.35%, H 6.75%, N 3.13%, found C 64.58 %, H 6.83%, N 3.01%.

Preparation of *N*-(4-chlorobenzyl)-2-(dispiro[cyclohexane-1,3'-[1,2,4,5]tetraoxane-6',2''-tricyclo[3.3.1.1^{3,7}]decan]-4-yl)acetamide (**37**)



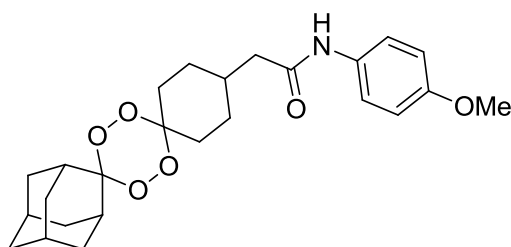
31 (200 mg, 591.02 μmol) was synthesised according to general procedure 1. 4-Chlorobenzylamine (71.9 μL , 591.02 μmol) was used in the coupling step. **37** was purified *via* flash column chromatography using 5% ethyl acetate in dichloromethane to give the title compound **37** (177.9 mg, 65%) as a white solid; R_f = 0.73, 50% ethyl acetate in dichloromethane; mp = 159-160°C; ^1H NMR (400 MHz, CDCl_3) δ 7.33 – 7.28 (m, 2H), 7.20 (d, J = 8.5 Hz, 2H), 4.41 (d, J = 5.8 Hz, 2H), 2.12 (d, J = 7.1 Hz, 2H), 2.07 – 1.43 (m, 21H) and 1.38 – 1.15 (m, 3H); ^{13}C NMR (100 MHz, CDCl_3) δ 171.8, 137.0, 133.5, 129.3, 129.0, 110.6, 107.8, 43.4, 43.0, 37.1, 34.2, 33.3 and 27.2; IR ν_{max} (neat)/ cm^{-1} 3278 (CONH), 2927 (Ar-H), 2862 (CH), 1643 (C=C), 1543 (C=C), 1493 (C=C), and 825 (C-Cl); ERMS (ESI) calculated for $\text{C}_{25}\text{H}_{32}\text{ClNO}_5$ $[\text{M}+\text{Na}]^+$ 484.1867 found 484.1880; Microanalysis calculated for $\text{C}_{25}\text{H}_{32}\text{ClNO}_5$ requires C 65.00%, H 6.98%, N 3.03%, found C 64.60 %, H 6.92%, N 2.88%.

Preparation of 2-(dispiro[cyclohexane-1,3'-[1,2,4,5]tetraoxane-6',2''-tricyclo[3.3.1.1^{3,7}]decan]-4-yl)-N-(4-(trifluoromethyl)phenyl)acetamide (**38**)



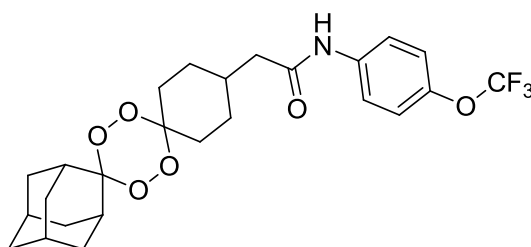
31 (203.3 mg, 601 μmol) was synthesised according to general procedure 1. 4-(Trifluoromethyl)aniline (75.5 μL , 601 μmol) was used in the coupling step. **38** was purified *via* flash column chromatography using 3% ethyl acetate in dichloromethane to give the title compound (203.3 mg, 70%) as a white solid: R_f = 0.95, 50% ethyl acetate in dichloromethane; mp = 157-160°C; ^1H NMR (400 MHz, CDCl_3) δ 7.65 (d, J = 8.5 Hz, 2H), 7.58 (d, J = 8.7 Hz, 2H), 2.30 (d, J = 6.6 Hz, 2H), 2.20 – 1.50 (m, 21H) and 1.34 (s, 2H); ^{13}C NMR (100 MHz, CDCl_3) δ 170.8, 140.9, 126.4 (q, J = 3.5 Hz), 126.1, 123.8 (q, J = 271.8 Hz), 119.6, 110.7, 107.7, 44.4, 37.0, 34.2, 33.3, 33.2 and 27.1; IR ν_{max} (neat)/ cm^{-1} 3359 (CONH), 3309 (CONH), 2920 (Ar-H), 2858 (CH), 1664 (C=C), 1603 (C=C), 1531 (C=C), 1323 (CF), 748 (CF) and 613 (CF); ERMS (ESI) calculated for $\text{C}_{25}\text{H}_{30}\text{F}_3\text{NO}_5$ $[\text{M}+\text{Na}]^+$ 504.1974 found 504.1960.

Preparation of 2-(dispiro[cyclohexane-1,3'-[1,2,4,5]tetraoxane-6',2''-tricyclo[3.3.1.1^{3,7}]decan]-4-yl)-N-(4-methoxyphenyl)acetamide (**39**)



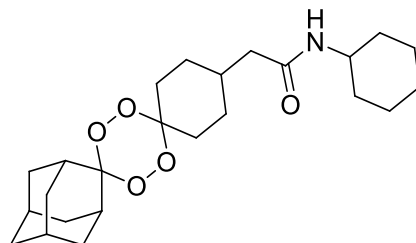
31 (203.3 mg, 599.6 μmol) was synthesised according to general procedure 1. 4-Methoxyaniline (69 μL , 599.6 μmol) was used in the coupling step. **39** was purified *via* flash column chromatography using 3% ethyl acetate in dichloromethane to give the title compound **39** (170.9 mg, 64%) as a white solid: $R_f = 0.83$, 50% ethyl acetate in dichloromethane; mp = 174-175°C; ^1H NMR (400 MHz, CDCl_3) δ 7.40 (d, $J = 8.9$ Hz, 2H), 7.03 (s, 1H), 6.86 (d, $J = 8.9$ Hz, 2H), 3.79 (s, 3H), 2.24 (d, $J = 6.9$ Hz, 2H), 2.15 – 1.47 (m, 21H) and 1.33 (s, 2H); ^{13}C NMR (100 MHz, CDCl_3) δ 170.0, 156.6, 130.9, 121.9, 114.3, 110.6, 107.8, 55.6, 44.3, 37.1, 34.3, 33.3 and 27.2; IR ν_{max} (neat)/ cm^{-1} 3234 (CONH), 2914 (Ar-H), 2856 (CH), 1649 (C=C), 1543 (C=C), 1510 (C=C), 1246 (C-O-C) and 1041 (C-O-C); ERMS (ESI) calculated for $\text{C}_{25}\text{H}_{33}\text{NO}_6$ $[\text{M}+\text{Na}]^+$ 466.2206 found 466.2215; Microanalysis calculated for $\text{C}_{25}\text{H}_{33}\text{NO}_6$ requires C 67.70%, H 7.50%, N 3.16%, found C 67.50%, H 7.51%, N 3.12%.

Preparation of 2-(dispiro[cyclohexane-1,3'-[1,2,4,5]tetraoxane-6',2''-tricyclo[3.3.1.1^{3,7}]decan]-4-yl)-N-(4-(trifluoromethoxy)phenyl)acetamide (**40**)



31 (250.2 mg, 739.37 μmol) was synthesised according to general procedure 1. 4-(Trifluoromethoxy)aniline (99 μL , 739.37 μmol) was used in the coupling step. **40** was purified *via* flash column chromatography using 5% ethyl acetate in dichloromethane to give the title compound **40** (237.5 mg, 65%) as a white solid: R_f = 0.85, 50% ethyl acetate in dichloromethane; mp = 115-118°C; ^1H NMR (400 MHz, CDCl_3) δ 7.54 (d, J = 9.0 Hz, 2H), 7.17 (d, J = 8.4 Hz, 2H), 2.27 (d, J = 6.9 Hz, 2H), 2.12 – 1.47 (m, 21H) and 1.42 – 1.17 (m, 3H); ^{13}C NMR (100 MHz, CDCl_3) δ 170.3, 136.5, 121.9, 121.1, 110.7, 107.7, 44.3, 37.1, 34.2, 33.3, 33.3, 27.2 and 27.2; IR ν_{max} (neat)/ cm^{-1} 3308 (CONH), 2935 (Ar-H), 2860 (CH), 1658 (C=C), 1532 (C=C), 1509 (C=C), 1273 (C-O-C), 1150 (CF) and 685 (CF); ERMS (ESI) calculated for $\text{C}_{25}\text{H}_{30}\text{F}_3\text{NO}_6$ $[\text{M}+\text{Na}]^+$ 520.1923 found 520.1934; Microanalysis calculated for $\text{C}_{25}\text{H}_{30}\text{F}_3\text{NO}_6$ requires C 60.35%, H 6.08%, N 2.82%, found C 60.93 %, H 6.375%, N 2.405%.

Preparation of *N*-cyclohexyl-2-(dispiro[cyclohexane-1,3'-[1,2,4,5]tetraoxane-6',2''-tricyclo[3.3.1.1^{3,7}]decan]-4-yl)acetamide (**41**)



31 (200 mg, 591.02 μmol) was synthesised according to general procedure 1. Cyclohexylamine (68 μL , 591.02 μmol) was used in the coupling step. **41** was purified *via* flash column chromatography using 5% ethyl acetate in dichloromethane to give the title compound **41** (185.8 mg, 75%) as a white solid: R_f = 0.78, 50% ethyl acetate in dichloromethane; mp = 174-176°C; ^1H NMR (400 MHz, CDCl_3) δ 5.31 (d, J = 8.0 Hz, 1H), 4.00 – 3.53 (m, 1H), 2.03 (d, J = 7.1 Hz, 2H) and 2.42 – 1.03 (m, 30H); ^{13}C NMR (100 MHz, CDCl_3) δ 170.9, 110.6, 107.9, 48.2, 43.9, 37.1, 34.3, 33.4, 33.3, 27.2, 25.6 and 25.0; IR ν_{max} (neat)/ cm^{-1} 3246 (CONH), 2925 (Ar-H) and 2854 (CH); ERMS (ESI) calculated for $\text{C}_{24}\text{H}_{37}\text{NO}_5$ $[\text{M}+\text{Na}]^+$ 442.2569 found 442.2565; Microanalysis calculated for $\text{C}_{24}\text{H}_{37}\text{NO}_5$ requires C 68.71%, H 8.89%, N 3.34%, found C 68.60%, H 8.92%, N 3.30%.

4.4.6 Determination of *P. falciparum* IC₅₀ values

This procedure is described in Antoine *et al.*²⁷

4.4.7 Degradation of unsymmetrical dispiro-1,2,4,5-tetraoxanes with iron(II) salts

The tetraoxane that was used for the degradation experiments was **35** unless stated otherwise.

Degradation procedure 1

To a solution of the tetraoxane (200 mg) in anhydrous DCM (50 mL), anhydrous acetonitrile (10 mL) and iron(II) acetate (1.5 equivalent) was added. The reaction was left to stir under nitrogen at 35°C for 24 hours. The solvent was removed to give crude product. Purification *via* flash column chromatography using 10% ethyl acetate in dichloromethane to give the desired product.

Degradation procedure 2

To a solution of the tetraoxane (200 mg) in anhydrous THF (25 mL), Fe(OAc)₂ (2 equivalents) was added to the reaction and left to stir under nitrogen at room temperature for 24 hours. Water and DCM was added to the reaction. The organic layer was washed with water, brine and dried over magnesium sulfate. The solution was filtered and solvent removed to give crude product. Purification *via* flash column chromatography using 10% ethyl acetate in dichloromethane to give the desired product.

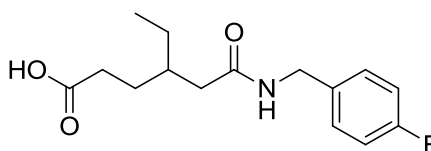
Degradation procedure 3

To a solution of the tetraoxane (200 mg) in DMF (75 mL), iron(II) gluconate was added. The reaction was left to stir under nitrogen for 7-24 hours at room temperature. DMF was removed *in vacuo* and the crude product was extracted with dichloromethane (3 x 20 mL). The combined organic extracts were washed with brine, dried over magnesium sulfate, and concentrated *in vacuo* to give the crude product. Purification *via* flash column chromatography using 10% ethyl acetate in dichloromethane to give the desired product.

Degradation procedure 4

Tetraoxane (100 mg) was dissolved in a 1:1 mixture of acetonitrile:water (30 mL). Iron(II) sulphate heptahydrate (18 eq) was added to the mixture and left to stir under nitrogen for 24 hours. The solvent was removed and re-dissolved in ethyl acetate and DCM and dried over magnesium sulfate. The solution was filtered, solvent removed and purified *via* flash column chromatography using 10% ethyl acetate in dichloromethane.

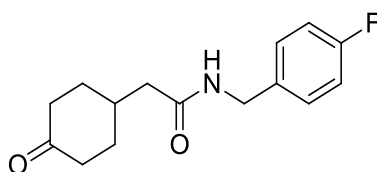
Preparation of 4-ethyl-6-((4-fluorobenzyl)amino)-6-oxohexanoic acid (**42**)



Tetraoxane **35** (201.4 mg, 452 μ mol) was used with degradation procedure 1, 2, 3 and 4. An analytically pure sample was further purified using HPLC-UV to obtain the title compound **42** (56.4 mg) as a hygroscopic white solid; R_f = 0.05, 50% ethyl

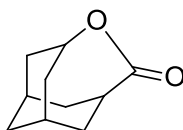
Chapter 4 – Examination of the role of ferrous iron and phosphatidylcholine in the bioactivation of novel tetraoxane antimalarials acetate in dichloromethane; HPLC-UV retention time = 14.5 minutes; ^1H NMR (400 MHz, CD_3OD) δ 7.35 – 7.25 (m, 2H), 7.08 – 6.98 (m, 2H), 4.34 (s, 2H), 2.23 (s, 2H), 2.18 (d, $J = 7.0$ Hz, 2H), 1.90 – 1.79 (m, 1H), 1.67 – 1.54 (m, 2H), 1.41 – 1.26 (m, 3H) and 0.89 (t, $J = 7.4$ Hz, 3H); ^{13}C NMR (100 MHz, MD_3OD) δ 198.7, 175.6, 163.5 (d, $J = 243.7$ Hz), 136.2 (d, $J = 3.1$ Hz), 130.6 (d, $J = 8.2$ Hz), 116.1 (d, $J = 21.6$ Hz), 43.4, 41.4, 37.8, 30.4, 27.0 and 11.0; IR ν_{max} (neat)/ cm^{-1} 3295 (CONH), 2923 (Ar-H), 2880 (CH), 1685 (CONH), 1630 (C=C), 1545 (C=C), 1510 (C=C), 1218 (CF) and 677 (CF); ERMS (ESI) calculated for $\text{C}_{15}\text{H}_{20}\text{FNO}_3$ $[\text{M}+\text{Na}]^+$ 304.1325 found 304.1319.

Preparation of *N*-(4-fluorobenzyl)-2-(4-oxocyclohexyl)acetamide (**44**)



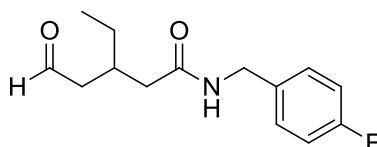
Tetraoxane **35** (201.4 mg, 452 μmol) was used with degradation procedure 1, 2, 3 and 4. An analytically pure sample was further purified using HPLC-UV to obtain the title compound **44** (61.2 mg) as a white solid; $R_f = 0.28$, 50% ethyl acetate in dichloromethane; HPLC-UV retention time = 15.8 minutes; mp = 149°C; ^1H NMR (400 MHz, CDCl_3) δ 7.31 – 7.20 (m, 2H), 7.07 – 6.97 (m, 2H), 5.89 (s, 1H), 4.42 (d, $J = 5.8$ Hz, 2H), 2.45 – 2.31 (m, 5H), 2.20 (d, $J = 7.1$ Hz, 2H), 2.13 – 2.05 (m, 2H) and 1.51 – 1.35 (m, 2H); ^{13}C NMR (100 MHz, CDCl_3) δ 211.6, 171.5, 162.3 (d, $J = 246.1$ Hz), 134.1 (d, $J = 3.2$ Hz), 129.6 (d, $J = 8.0$ Hz), 115.7 (d, $J = 21.5$ Hz), 43.1, 42.8, 40.8, 33.6 and 32.7; IR ν_{max} (neat)/ cm^{-1} 3251 (CONH), 3074 (Ar-H), 2937 (CH), 1710 (C=O), 1635 (C=C), 1559 (C=C), 1508 (C=C), 1218 (CF) and 747 (CF); ERMS (ESI) calculated for $\text{C}_{15}\text{H}_{18}\text{FNO}_2$ $[\text{M}+\text{Na}]^+$ 286.1219 found 286.1216;

Preparation of 4-oxatricyclo[4.3.1.1^{3,8}]undecan-5-one (45)



Degradation procedure 1 was used along with (diadamanetetraoxane) (204.3 mg, 614.6 μmol) as the tetraoxane to give the title compound **(45)** (91 mg, 89%) as a white solid; Tetraoxane **35** was used in degradation procedures 2, 3 and 4 to give the title compound **45** as a white solid. $R_f = 0.19$, 50% ethyl acetate in dichloromethane; $^1\text{H NMR}$ (400 MHz, CDCl_3) δ 4.49 (s, 1H), 3.08 (s, 1H) and 2.20 – 1.63 (m, 12H); $^{13}\text{C NMR}$ (100 MHz, CDCl_3) δ 179.2, 73.3, 41.3, 35.9, 33.9, 31.0 and 25.9; ; IR ν_{max} (neat)/ cm^{-1} 2919 (C-H), 2860, 1824 (C=O); MS (CI) $\text{C}_{10}\text{H}_{14}\text{O}_2$ $[\text{M}+\text{NH}_4]^+$ m/z 184.1.

Preparation of 3-ethyl-N-(4-fluorobenzyl)-5-oxopentanamide (46)



Tetraoxane **35** (201.4 mg, 452 μmol) was used with degradation procedure 1, 2, 3 and 4. An analytically pure sample was further purified *via* column chromatography to obtain the title compound (20 mg) as a white solid; $R_f = 0.5$, 50% ethyl acetate in dichloromethane, stain yellow in *p*-anisaldehyde; $^1\text{H NMR}$ (400 MHz, CDCl_3) δ 9.77 (t, $J = 1.9$ Hz, 1H), 7.28 – 7.22 (m, 2H), 7.03 – 6.95 (m, 2H), 5.07 (d, $J = 14.8$ Hz, 1H), 4.95 – 4.90 (m, 1H), 4.25 (d, $J = 14.8$ Hz, 1H), 2.64 (ddd, $J = 17.3, 4.7, 2.1$ Hz, 1H), 2.05 – 1.95 (m, 3H), 1.50 – 1.40 (m, 1H), 1.37 – 1.29 (m, 2H) and 0.92 (t, $J = 7.4$ Hz,

Chapter 4 – Examination of the role of ferrous iron and phosphatidylcholine in the bioactivation of novel tetraoxane antimalarials

3H); ^{13}C NMR (100 MHz, CDCl_3) δ 202.2, 170.7, 162.3 (d, $J = 245.6$ Hz), 133.4 (d, $J = 3.1$ Hz), 130.0 (d, $J = 8.0$ Hz), 115.6 (d, $J = 21.4$ Hz), 46.7, 38.8, 36.9, 28.8, 28.6 and 11.0; ERMS (ESI) calculated for $\text{C}_{14}\text{H}_{18}\text{FNO}_2$ $[\text{M}+\text{Na}]^+$ 274.1219 found 274.1227.

4.4.8 Reactions of PC with tetraoxane and iron(II) salt

A solution of 2-linoleoyl-1-palmitoyl-*sn*-glycero-phosphatidylcholine (PC) in water (1 mL, 0.83 μmol) was added to an aqueous solution of iron(II) gluconate (1 mL, 7.2 μmol) and tetraoxane **35** in ethanol (1 mL, 6.81 μmol). [Note: for the control sample, absolute ethanol (1 mL) was added]. Solutions were stirred for 24 hours at 38°C. Reactions were quenched with 50% phatic acid (20 μL) and 1 μL of butylated hydroxytoluene was added. The reaction was extracted in chloroform:methanol mixture (1:2, 2 mL) and the chloroform layer was analysed using electrospray ionisation mass spectra analysis. The organic layer was concentrated under reduced pressure and LCMS analysis was performed to obtain degradation data.

4.4.8.1 LCMS analysis

Aliquots of the solutions (10-20 μL) were chromatographed at room temperature on an Agilent 5- μm ZORBAX Eclipse XDB-C18 column (150 \times 4.6 mm i.d.; Agilent Technologies, Santa Clara, CA, USA) by gradient elution with acetonitrile (20-60% over 15 min; 60% for 10 min) in 0.1% formic acid (v/v). The eluent flow rate was 1.0 mL/min. Full-scanning positive-ion spectra were acquired with an AB Sciex 2000 mass spectrometer.

4.5 Reference

- 1 WHO. *Factsheet on the World Malaria Report 2013*, http://www.who.int/malaria/media/world_malaria_report_2013/en/ Last updated: December 2013, Access date: **May 2014**.
- 2 Bousejra-El Garah, F., Wong, M. H.-L., Amewu, R. K., Muangnoicharoen, S., Maggs, J. L., Stigliani, J.-L., Park, B. K., Chadwick, J., Ward, S. A. & O'Neill, P. M. Comparison of the Reactivity of Antimalarial 1,2,4,5-Tetraoxanes with 1,2,4-Trioxolanes in the Presence of Ferrous Iron Salts, Heme, and Ferrous Iron Salts/Phosphatidylcholine. *Journal of Medicinal Chemistry* **54**, 6443-6455, doi:10.1021/jm200768h (2011).
- 3 Shandilya, A., Chacko, S., Jayaram, B. & Ghosh, I. A plausible mechanism for the antimalarial activity of artemisinin: A computational approach. *Scientific Reports* **3**, doi:10.1038/srep02513 (2013).
- 4 Greenwood, B. M., Fidock, D. A., Kyle, D. E., Kappe, S. H. I., Alonso, P. L., Collins, F. H. & Duffy, P. E. Malaria: progress, perils, and prospects for eradication. *The Journal of Clinical Investigation* **118**, 1266-1276, doi:10.1172/JCI33996 (2008).
- 5 Dondorp, A. M., Nosten, F., Yi, P., Das, D., Phyto, A. P., Tarning, J., Lwin, K. M., Ariey, F., Hanpithakpong, W., Lee, S. J., Ringwald, P., Silamut, K., Imwong, M., Chotivanich, K., Lim, P., Herdman, T., An, S. S., Yeung, S., Singhasivanon, P., Day, N. P. J., Lindegardh, N., Socheat, D. & White, N. J. Artemisinin Resistance in Plasmodium falciparum Malaria. *New England Journal of Medicine* **361**, 455-467, doi:doi:10.1056/NEJMoa0808859 (2009).
- 6 Ellis, G. L., Amewu, R., Hall, C., Rimmer, K., Ward, S. A. & O'Neill, P. M. An efficient route into synthetically challenging bridged achiral 1,2,4,5-tetraoxanes with antimalarial activity. *Bioorganic & Medicinal Chemistry Letters* **18**, 1720-1724, doi:10.1016/j.bmcl.2008.01.053 (2008).
- 7 Amewu, R., Stachulski, A. V., Ward, S. A., Berry, N. G., Bray, P. G., Davies, J., Labat, G., Vivas, L. & O'Neill, P. M. Design and synthesis of orally active dispiro 1,2,4,5-tetraoxanes; synthetic antimalarials with superior activity to artemisinin. *Organic & Biomolecular Chemistry* **4**, 4431-4436, doi:10.1039/B613565J (2006).
- 8 O'Neill, P. M., Amewu, R. K., Nixon, G. L., Bousejra ElGarah, F., Mungthin, M., Chadwick, J., Shone, A. E., Vivas, L., Lander, H., Barton, V., Muangnoicharoen, S., Bray, P. G., Davies, J., Park, B. K., Wittlin, S., Brun, R., Preschel, M., Zhang, K. & Ward, S. A. Identification of a 1,2,4,5-Tetraoxane Antimalarial Drug-Development Candidate (RKA 182) with Superior Properties to the Semisynthetic Artemisinins. *Angewandte Chemie International Edition* **49**, 5693-5697, doi:10.1002/anie.201001026 (2010).
- 9 Wang, X., Dong, Y., Wittlin, S., Charman, S. A., Chiu, F. C. K., Chollet, J., Katneni, K., Mannila, J., Morizzi, J., Ryan, E., Scheurer, C., Steuten, J., Santo Tomas, J., Snyder, C. & Vennerstrom, J. L. Comparative Antimalarial Activities and ADME Profiles of Ozonides (1,2,4-trioxolanes) OZ277, OZ439, and Their 1,2-Dioxolane, 1,2,4-Trioxane, and 1,2,4,5-Tetraoxane Isosteres. *Journal of Medicinal Chemistry* **56**, 2547-2555, doi:10.1021/jm400004u (2013).

Chapter 4 – Examination of the role of ferrous iron and phosphatidylcholine in the bioactivation of novel tetraoxane antimalarials

- 10 Vennerstrom, J. L., Arbe-Barnes, S., Brun, R., Charman, S. A., Chiu, F. C. K., Chollet, J., Dong, Y., Dorn, A., Hunziker, D., Matile, H., McIntosh, K., Padmanilayam, M., Santo Tomas, J., Scheurer, C., Scorneaux, B., Tang, Y., Urwyler, H., Wittlin, S. & Charman, W. N. Identification of an antimalarial synthetic trioxolane drug development candidate. *Nature* **430**, 900-904, doi:10.1038/nature02779 (2004).
- 11 O'Neill, P. M., Barton, V. E. & Ward, S. A. The Molecular Mechanism of Action of Artemisinin—The Debate Continues. *Molecules* **15**, 1705-1721, doi:10.3390/molecules15031705. (2010).
- 12 Cardi, D., Pozza, A., Arnou, B., Marchal, E., Clausen, J. D., Andersen, J. P., Krishna, S., Møller, J. V., le Maire, M. & Jaxel, C. Purified E255L Mutant SERCA1a and Purified PfATP6 Are Sensitive to SERCA-type Inhibitors but Insensitive to Artemisinins. *Journal of Biological Chemistry* **285**, 26406-26416, doi:10.1074/jbc.M109.090340 (2010).
- 13 Garah, F. B.-E., Stigliani, J.-L., Coslédan, F., Meunier, B. & Robert, A. Docking Studies of Structurally Diverse Antimalarial Drugs Targeting PfATP6: No Correlation between in silico Binding Affinity and in vitro Antimalarial Activity. *ChemMedChem* **4**, 1469-1479, doi:10.1002/cmdc.200900200 (2009).
- 14 Haynes, R. K., Chan, W.-C., Wong, H.-N., Li, K.-Y., Wu, W.-K., Fan, K.-M., Sung, H. H. Y., Williams, I. D., Prosperi, D., Melato, S., Coghi, P. & Monti, D. Facile Oxidation of Leucomethylene Blue and Dihydroflavins by Artemisinins: Relationship with Flavoenzyme Function and Antimalarial Mechanism of Action. *ChemMedChem* **5**, 1282-1299, doi:10.1002/cmdc.201000225 (2010).
- 15 Haynes, R. K., Cheu, K.-W., Tang, M. M.-K., Chen, M.-J., Guo, Z.-F., Guo, Z.-H., Coghi, P. & Monti, D. Reactions of Antimalarial Peroxides with Each of Leucomethylene Blue and Dihydroflavins: Flavin Reductase and the Cofactor Model Exemplified. *ChemMedChem* **6**, 279-291, doi:10.1002/cmdc.201000508 (2011).
- 16 Tang, Y., Dong, Y., Wang, X., Sriraghavan, K., Wood, J. K. & Vennerstrom, J. L. Dispiro-1,2,4-trioxane Analogues of a Prototype Dispiro-1,2,4-trioxolane: Mechanistic Comparators for Artemisinin in the Context of Reaction Pathways with Iron(II). *The Journal of Organic Chemistry* **70**, 5103-5110, doi:10.1021/jo050385+ (2005).
- 17 Laurent, S. A. L., Loup, C., Mourgues, S., Robert, A. & Meunier, B. Heme Alkylation by Artesunic Acid and Trioxaquine DU1301, Two Antimalarial Trioxanes. *ChemBioChem* **6**, 653-658, doi:10.1002/cbic.200400249 (2005).
- 18 Kumura, N., Furukawa, H., Onyango, A. N., Izumi, M., Nakajima, S., Ito, H., Hatano, T., Kim, H.-S., Wataya, Y. & Baba, N. Different behavior of artemisinin and tetraoxane in the oxidative degradation of phospholipid. *Chemistry and Physics of Lipids* **160**, 114-120, doi:10.1016/j.chemphyslip.2009.04.005 (2009).
- 19 MMV. OZ439, <http://www.mmv.org/research-development/project-portfolio/oz439> Last updated: 2013, Access date: **October 2013**.
- 20 Williams, D. H. & Fleming, I. *Spectroscopic methods in Organic chemistry*. Sixth edn, (McGraw-Hill Education, 2008).
- 21 Jackson, K. E., Klonis, N., Ferguson, D. J. P., Adisa, A., Dogovski, C. & Tilley, L. Food vacuole-associated lipid bodies and heterogeneous lipid environments

Chapter 4 – Examination of the role of ferrous iron and phosphatidylcholine in the bioactivation of novel tetraoxane antimalarials

- in the malaria parasite, *Plasmodium falciparum*. *Molecular Microbiology* **54**, 109-122, doi:10.1111/j.1365-2958.2004.04284.x (2004).
- 22 Spiteller, G. Linoleic acid peroxidation—the dominant lipid peroxidation process in low density lipoprotein—and its relationship to chronic diseases. *Chemistry and Physics of Lipids* **95**, 105-162, doi:10.1016/S0009-3084(98)00091-7 (1998).
- 23 Rang, H. P., Dale, M. M., Ritter, J. M., Flower, R. J. & Henderson, G. *Pharmacology*. Seventh edn, (Elsevier Churchill Livingstone, 2012).
- 24 Schlesinger, P. H., Krogstad, D. J. & Herwaldt, B. L. Antimalarial agents: mechanisms of action. *Antimicrobial Agents and Chemotherapy* **32**, 793-798, doi:10.1128/aac.32.6.793 (1988).
- 25 Sugioka, Y., Suzuki, M., Sugioka, K. & Nakano, M. A ferriprotoporphyrin IX-chloroquine complex promotes membrane phospholipid peroxidation A possible mechanism for antimalarial action. *FEBS Letters* **223**, 251-254, doi:10.1016/0014-5793(87)80299-5 (1987).
- 26 Oliveira, R., Newton, A. S., Guedes, R. C., Miranda, D., Amewu, R. K., Srivastava, A., Gut, J., Rosenthal, P. J., O'Neill, P. M., Ward, S. A., Lopes, F. & Moreira, R. An Endoperoxide-Based Hybrid Approach to Deliver Falcipain Inhibitors Inside Malaria Parasites. *ChemMedChem* **8**, 1528-1536, doi:10.1002/cmdc.201300202 (2013).
- 27 Antoine, T., Fisher, N., Amewu, R., O'Neill, P. M., Ward, S. A. & Biagini, G. A. Rapid kill of malaria parasites by artemisinin and semi-synthetic endoperoxides involves ROS-dependent depolarization of the membrane potential. *Journal of Antimicrobial Chemotherapy* **69**, 1005-1016, doi:10.1093/jac/dkt486 (2014).

CHAPTER 5

Design and synthesis of click functionalised derivatives of artemisinin and CDDO as probes for investigating chemical mechanism of action.

Chapter 5

5.1	Introduction	224
5.1.1	Biotin tag	225
5.1.2	Photoaffinity labelling	228
5.1.3	Synthesised tagged probes	230
5.1.4	Aims	236
5.2	Results and discussion	237
5.2.1	The chemical synthesis of artemisinin click probes	237
5.2.1.1	Preliminary parasite protein identification with artemisinin click probes	245
5.2.2	The chemical synthesis of CDDO and DDO click probes.	248
5.2.3	Click reaction proof of concept.	253
5.3	Conclusion	254
5.4	Chemistry Experimental	256
5.4.1	General	256
5.4.2	Purification of solvents and reagents	256
5.4.2.1	Stains	256
5.4.3	Purification of products	256
5.4.4	Analysis	256
5.4.5	Numbering	257
5.4.6	General procedure.	258
5.4.7	Synthesis artemisinin click probes	259
5.4.8	Synthesis of CDDO click probes	270
		222

Chapter 5 – Design and synthesis of click functionalised derivatives of artemisinin and CDDO as probes for investigating chemical mechanism of action

5.5 Biological experimental	277
5.5.1 Materials	277
5.5.2 Cell culture	277
5.5.3 Plating	277
5.5.4 Treatment of cells for luciferase activity assay.	277
5.5.5 Preparation of cells for luciferase reporter assay	277
5.6 Reference	278

5.1 Introduction

Drug target identification and validation can be complicated due to the vast number of potential targets within a complex biological system. As discussed in detail in Chapter 1, the physical binding of a drug to a relevant protein responsible for the pharmacological response is the perfect scenario during target identification and validation. However, obtaining such proof can be a challenge as detection of a drug target interaction generally requires high abundance of the target protein and a high affinity between the drug and the target.^{1,2} For compounds and targets that do not meet these criteria, alternative methods are required, such as manipulation of the biological systems (i.e. increasing/decreasing the expression of a gene resulting in a phenotypic change),² chemical modification of the drug to enhance selectivity (increasing affinity towards a specific protein)³ and labelling of potential proteins.⁴

The design and synthesis of chemical probes provides a unique tool for interrogating biological mechanisms. Such chemical probes are generally bespoke and consists of three elements.⁴

- i. The parent drug containing the pharmacophore or warhead
- ii. A tag which enables detection or purification
- iii. A linker connecting the parent drug with the tag

The purification of probe-protein complexes enables the use of proteomic strategies to identify potential drug targets (Figure 5.1).

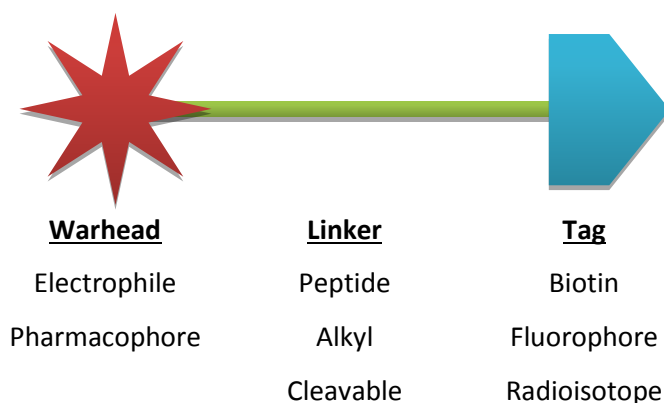


Figure 5.1: The three key elements of a chemical probe.⁴

5.1.1 Biotin tag

The biotin tag is commonly used in the synthesis of chemical probes. The interaction between avidin/streptavidin and biotin is the strongest biological non-covalent interaction known.⁵ The ability to form a fast and stable interaction between biotin and avidin/streptavidin over a range of temperatures and pH has enabled the identification of the biological targets of numerous compounds that was previously difficult with traditional techniques.⁵

An example of this kind of probe is the serine hydrolase probe FP-Biotin⁶ and the cysteine protease probe DCG-04.⁷ The mechanism of FP-Biotin involves the substitution of fluorine located on the phosphorous in FP-Biotin with the hydroxyl group located on serine. The DCG-04 probe contains an epoxide, which upon electrophilic attack by cysteine forms an irreversible interaction. Biotin avidin/streptavidin pull-down allows for the purification of the target protein. The mechanism of action is shown in Figure 5.2.

Chapter 5 – Design and synthesis of click functionalised derivatives of artemisinin and CDDO as probes for investigating chemical mechanism of action

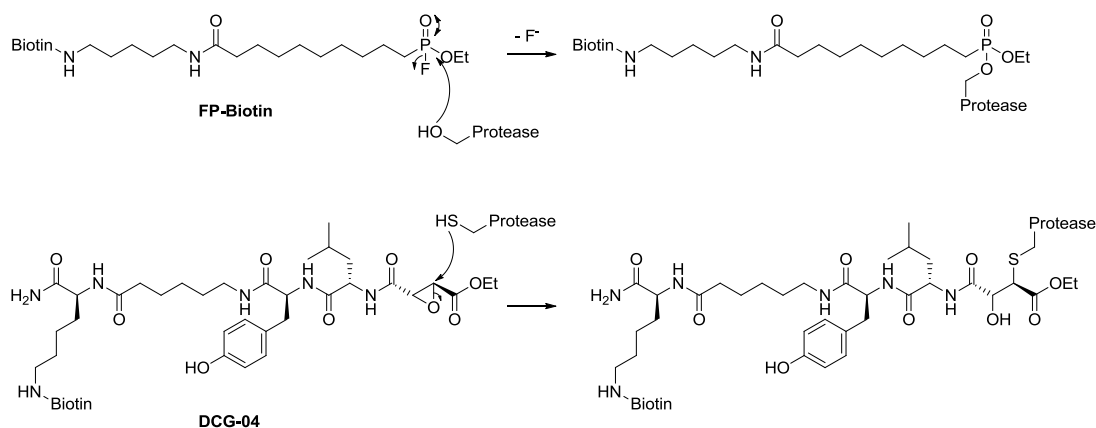


Figure 5.2: The chemical structures and mechanism of action of the serine protease probe FP-Biotin and cysteine protease probe DCG-04.^{6,7}

There are many other examples of biotinylated probes (BP) for investigating molecular targets including a wide range of probes dedicated to protease inhibitors.^{4,8} The majority of these probes require an irreversible mechanism which limits the approach somewhat, as most drugs operate through a reversible interaction as described in detail in Chapter 1.^{6,8} However, there are examples where BPs have been used to characterise protein interactions that are reversible. An example of a reversible BPs is the potent inhibitor of γ -secretase, L-685,485., which has been shown to mimic the transition state of the aspartate protease catalytic process. This discovery was facilitated through the use of a biotinylated derivative of L-685,485 (Figure 5.3).⁸ Another example is the biotinylated CBS9106 probe that is found to inhibit CRM1. CRM1 is responsible for the nuclear export of cargo proteins. The inhibition of CRM1 results in the arrest of cell cycle and induction of apoptosis (Figure 5.3).⁹

Chapter 5 – Design and synthesis of click functionalised derivatives of artemisinin and CDDO as probes for investigating chemical mechanism of action

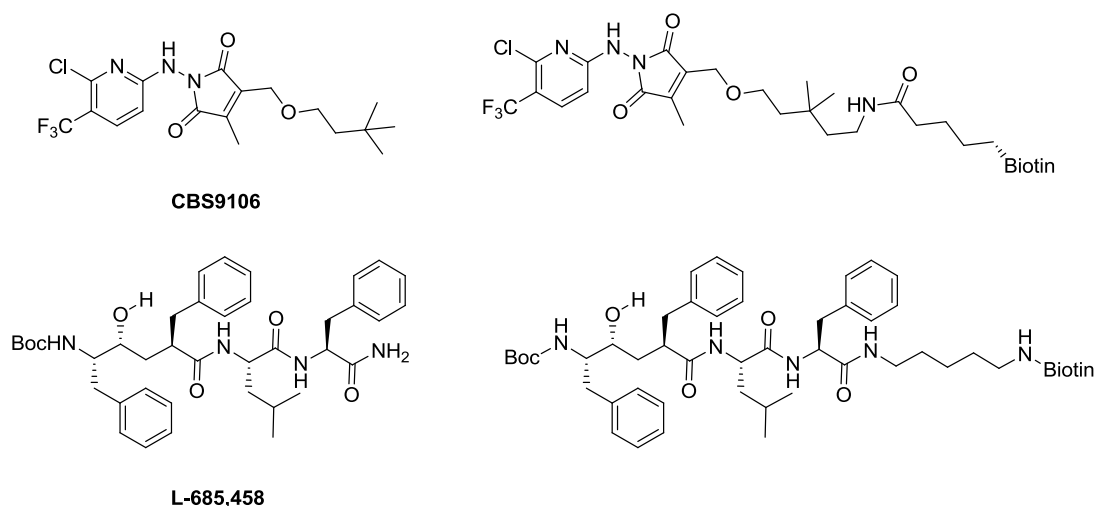


Figure 5.3: Chemical structures for reversible CBS9106 and L-685,458 and their biotin functionalised counterparts.^{8,9}

Reversible BPs provide an ideal tool for isolating and identifying drug targets as they mimic natural binding interactions with the molecular target. However, due to their reversible nature, the successful pull down of molecular target(s) is often difficult. This is due to stringent washing during purification which result in the disruption of the equilibrium between the molecular target and the BP.³ A solution to this problem is the use of photoaffinity labelling.

5.1.2 Photoaffinity labelling

Photoaffinity labelling (PAL) involves the use of a photoreactive group and upon irradiation, a highly reactive intermediate is formed which is capable of covalently binding with the nearest fragment of a biomolecule.¹⁰ PAL was first introduced in the 1960s and development of different photophores has resulted in three types of photoreactive classes that are regularly incorporated in PAL probes. These are benzophenones, arylazides and diazirines (Figure 5.4).^{10,11}

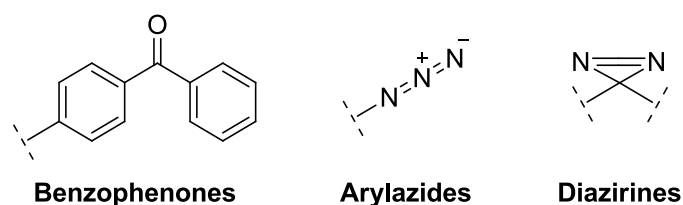


Figure 5.4: Chemical structure of common photoreactive groups; benzophenones, arylazides and diazirines.

Despite the use of a photoreactive tag, the probe still requires a purification tag such as biotin or reporter group (fluorescent, radioactive, chromophore or immune) to enable detection and measurement of the molecular target.¹⁰ An example of this is the use of the matrix metalloproteinase (MMP) inhibitor, ilomastat (Figure 5.5). The MMPs are zinc-dependent proteases and are known to play important roles in a number of pathological processes.^{8,11} Ilomastat is a broad reversible inhibitor of MMPs.¹² Due to the reversibility of ilomastat, analysis of the MMP family was inaccessible. The PAL derivative of ilomastat (Figure 5.5) enabled the covalent binding, purification and identification of the MMPs. This allowed the use of

standard genomic and proteomic methods to identify and analyse the MMP family.

The mechanism of the photoaffinity tag is shown in Figure 5.5B

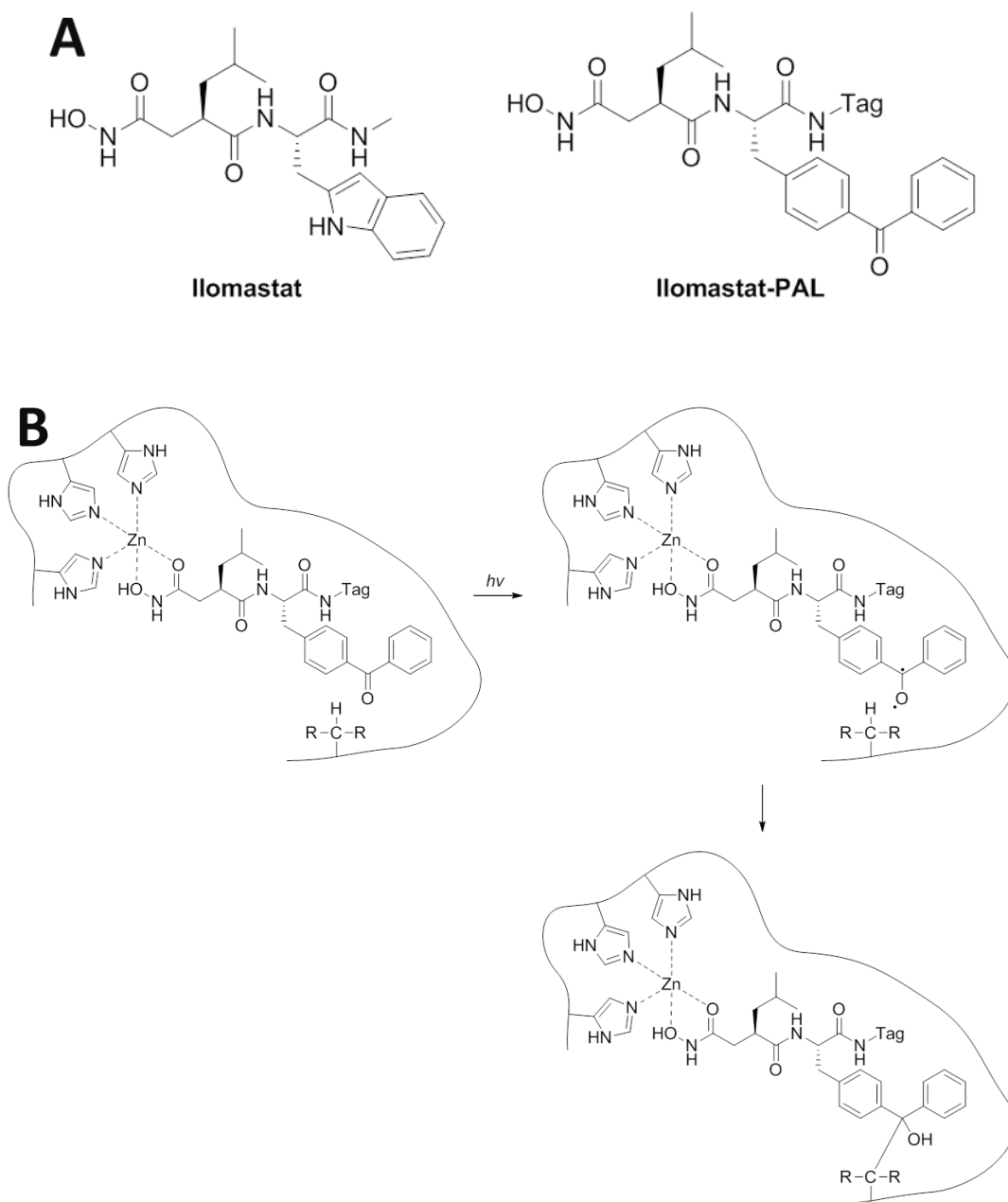


Figure 5.5: (A) Chemical structure of Ilomastat and the photoaffinity derivative of Ilomastat (Ilomastat-PAL). (B) The mechanism of metallohydrolase labelling with Ilomastat-PAL.

5.1.3 Synthesised tagged probes

The artemisinin semi synthetic derivatives (artemether **49** and artesunate **50**) are considered to be the forefront of malaria chemotherapy.¹³ CDDO derivatives (CDDO **8**, CDDO-Me **7** and CDDO-Im **51**) are some of the most potent inducers of Nrf2 and exhibit a wide range of properties including anti-inflammatory and anti-cancer activity.¹⁴

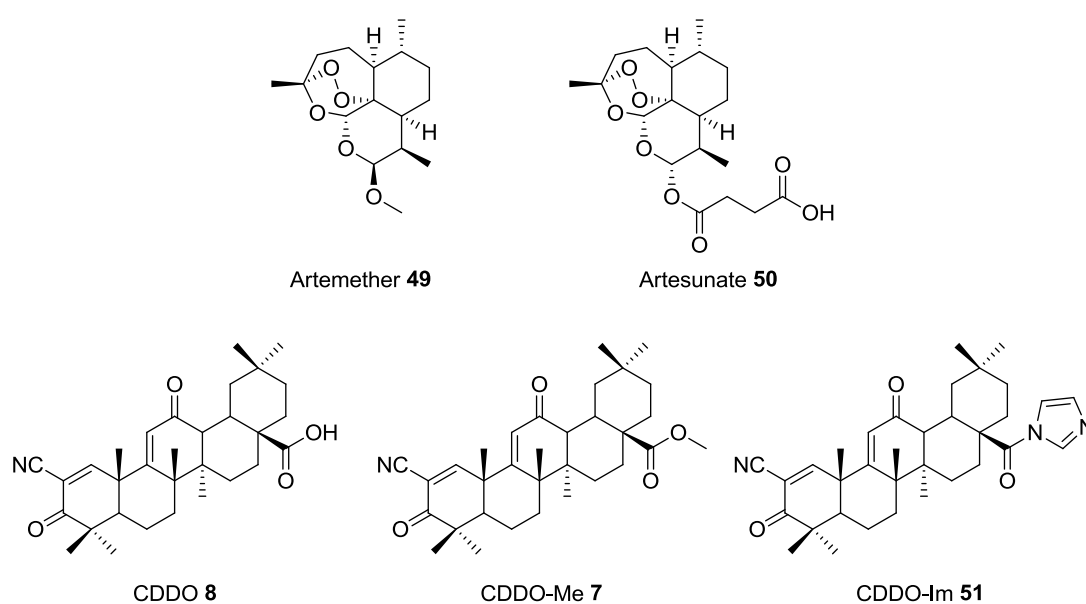


Figure 5.6: Chemical structures of artemether, artesunate, CDDO, CDDO-Me and CDDO-Im

Studies of the chemical mechanism of action of artemisinin endoperoxides and the CDDO class have highlighted the important pharmacophores such as the free radical chemistry of endoperoxides¹⁵ and the reversible 1,4 conjugate addition of the α,β unsaturated ketone in CDDO.¹⁶ However, little is known about the biological target(s) of these compounds and the mechanisms responsible for their therapeutic effects. Attempts to formally identify the target proteins through a proteomic

Chapter 5 – Design and synthesis of click functionalised derivatives of artemisinin and CDDO as probes for investigating chemical mechanism of action

approach have led to the synthesis of biotin tagged probes. Biotin tagged artemisinin **52**, fluorescently tagged artemisinin **53** and biotinylated CDDO derivatives **54** were synthesised by O'Neill *et al*^{13,17} and Honda *et al*¹⁸ respectively.

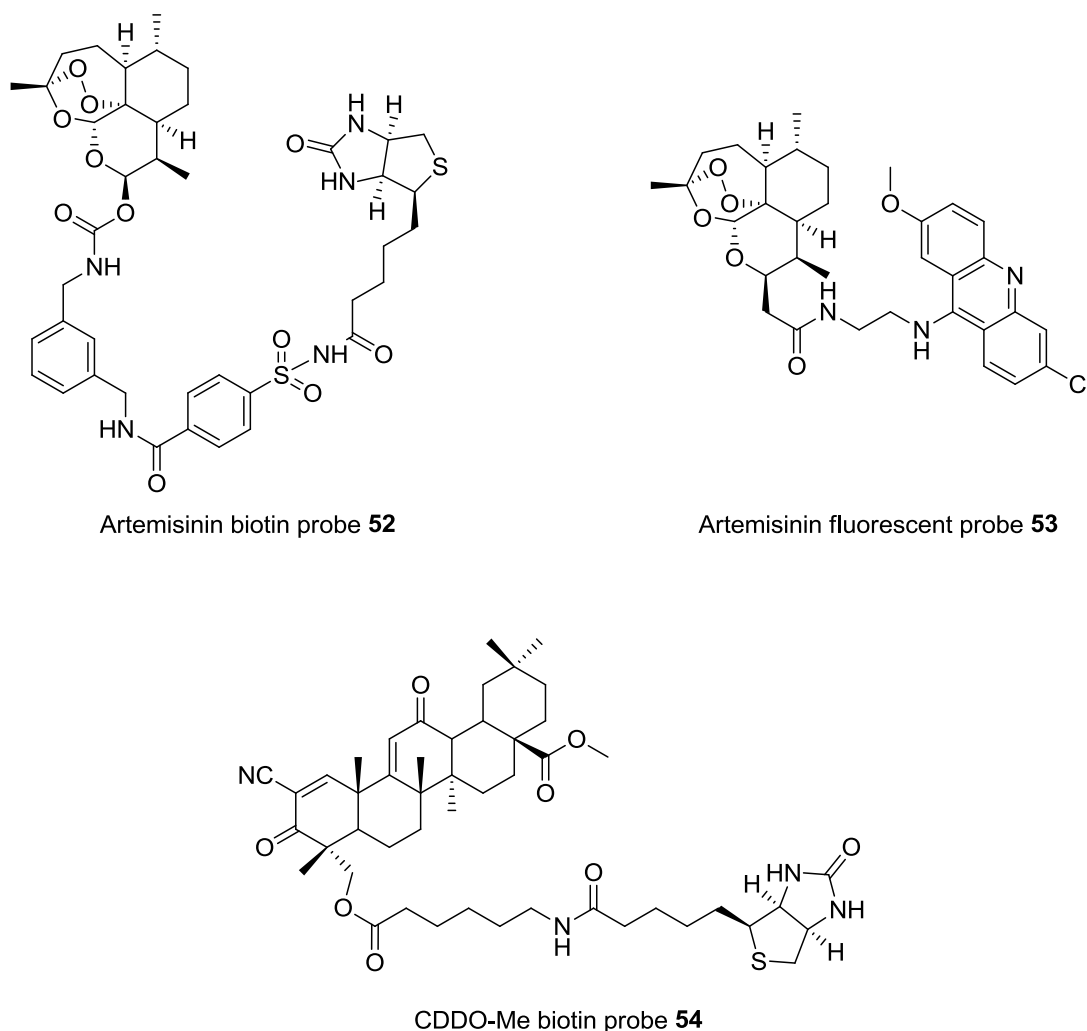


Figure 5.7: Chemical structures of the artemisinin biotin probe, artemisinin fluorescent probe and CDDO-Me biotin probe.

Biotylated CDDO derivatives have been shown to interact directly with Cys-179 of the inhibitor of nuclear factor kappa B kinase (IKK β), which is responsible for the activation of the pro-inflammatory transcription factor, nuclear factor kappa B (NF- κ B).¹⁹ CDDO-Me-Biotin was incubated with wild type (WT-IKK β) recombinant-IKK β

Chapter 5 – Design and synthesis of click functionalised derivatives of artemisinin and CDDO as probes for investigating chemical mechanism of action

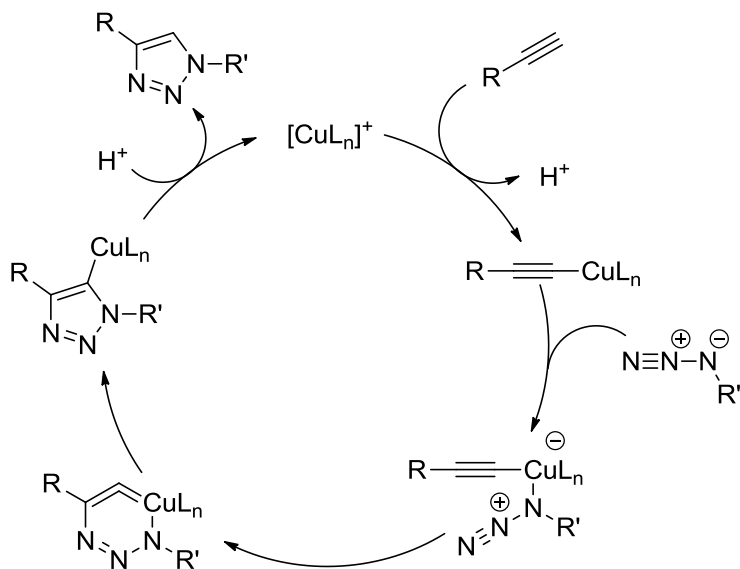
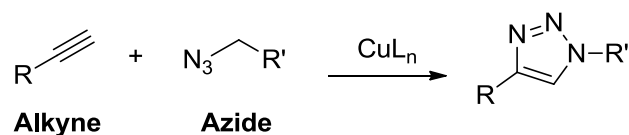
and IKK β with a Cys-179 mutation (C179A-IKK β). Analysis using SDS-PAGE and a streptavidin peroxidase reporter demonstrated labelling of WT-IKK β , but not C179A-IKK β by CDDO-Me-Biotin that was consistent with the ability of the probe to inhibit NF- κ B.¹⁹ CDDO-Me-Biotin were also used to determine the interaction with Cys-1077 of Janus-activated kinase-1 (JAK1) and Cys-259 of signal transducer and activator of transcription 3 (STAT3), which regulate apoptosis and cell cycle progression.²⁰ Determining the interaction with JAK1 and STAT3 required the use of pull down purification with streptavidin-beads followed by immunoblotting. The chemical interaction with these and other targets may explain the pharmacodynamics effects of CDDO and its analogues. However, such an approach has failed to identify compounds of the Keap1-Nrf2 pathway as direct targets of this compound class, despite their potency as inducers of Nrf2.

Fluorescently tagged artemisinin containing an acridine moiety conjugated to the artemisinin framework through a C-10 ether link has demonstrated that artemisinin can covalently bind within the malaria parasite.^{17,21} However, direct formal identification of the target site(s) has yet to be performed and therefore further investigation is required.

The successful identification of potential target proteins with biotinylated probes is important for interrogating biological mechanisms. However there are many disadvantages to using biotin tags within probes. For example, detection of potential targets may be hindered due to the steric bulk of the linker and biotin tag. Cell permeability of the probe could also be affected due to the increase in molecular size.

It is often assumed that direct interaction with a single target is responsible for the pharmacological effects of a molecule. Consideration of off-target protein interaction is also important in the safe development of drugs and due to the harsh conditions required to disrupt the biotin-streptavidin bond, these off-target proteins could be missed with conventional proteomic approaches.^{2,4}

Activity based protein profiling (ABPP) was developed and applied by the Cravatt group.²² This method involves the functionalization of small molecules with alkyne or azide instead of bulky acridine and biotin. (Scheme 5.1) The alkyne and counterpart azide probes rely on copper (I) catalysed cycloaddition that was initially developed by Sharpless *et al* and is well known as “click chemistry”.²³ This click chemistry was adapted from the Huisgen 1,3-dipolar cycloaddition which required elevated temperatures to overcome the activation energy required for the formation of triazoles.²⁴ Sharpless *et al*²⁵ and Meldal *et al*²⁶ developed the click chemistry by introduction of a copper(I) catalyst. This enabled the reaction to proceed selectively giving the 1,4 substituted [1,2,3]-triazole at ambient temperatures due to lowering of the activation barrier when copper(I) is used as a catalyst.²⁴ The utilisation of such groups overcomes the disadvantages of the bulky biotin/streptavidin and fluorescent tags. The chemical mechanism of the click reaction is shown in Scheme 5.1.



Scheme 5.1: Chemical structure of alkyne and azide with the chemical mechanism of action for copper (I) catalysed click reaction

In the absence of copper(I), no reaction is observed as demonstrated by Meldal *et al.*²⁶ Copper(I) has undesirable toxic side effects at low concentrations.²⁷ Therefore, for this click chemistry to be useful for *in vitro* and *in vivo* applications, the development of a copper-free reaction is therefore advantageous.²⁷ Bertozzi *et al* developed a substituted cyclooctyne that possess electron withdrawing fluorine substituents together with a strained alkyne group to promote cycloaddition.²⁸ Since then a range of copper-free reagents has been developed including 4-dibenzocyclooctynol (DIBO), dibenzocyclooctyne group (DBCO) and difluorinated cyclooctyne (DIFO) (Figure 5.8).^{27,28}

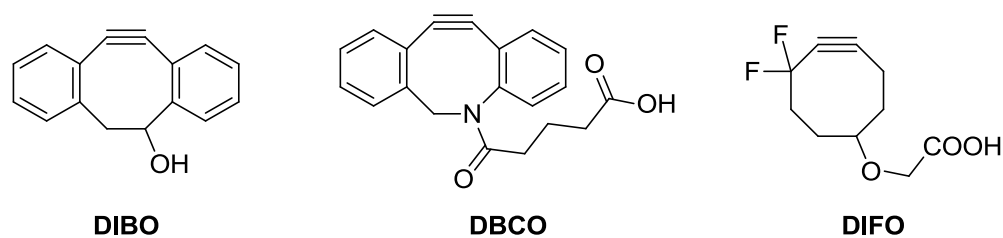


Figure 5.8: Chemical structures for copper-free click probes, 4-dibenzocyclooctynol (**DIBO**), dibenzocyclooctyne group (**DBCO**) and difluorinated cyclooctyne (**DIFO**).

Applying the click chemistry technique requires the bespoke synthesis of the drug containing the alkyne (or azide) functional group and treatment of cells to label the target protein(s). The complementary part to the click functionalised drug is also known as the reporter tag. The reporter tag can contain a fluorescent group that allows for analysis of tagged proteins or a biotin group which enables protein enrichment by streptavidin pull down and mass spectral analysis. This is shown in Figure 5.9.

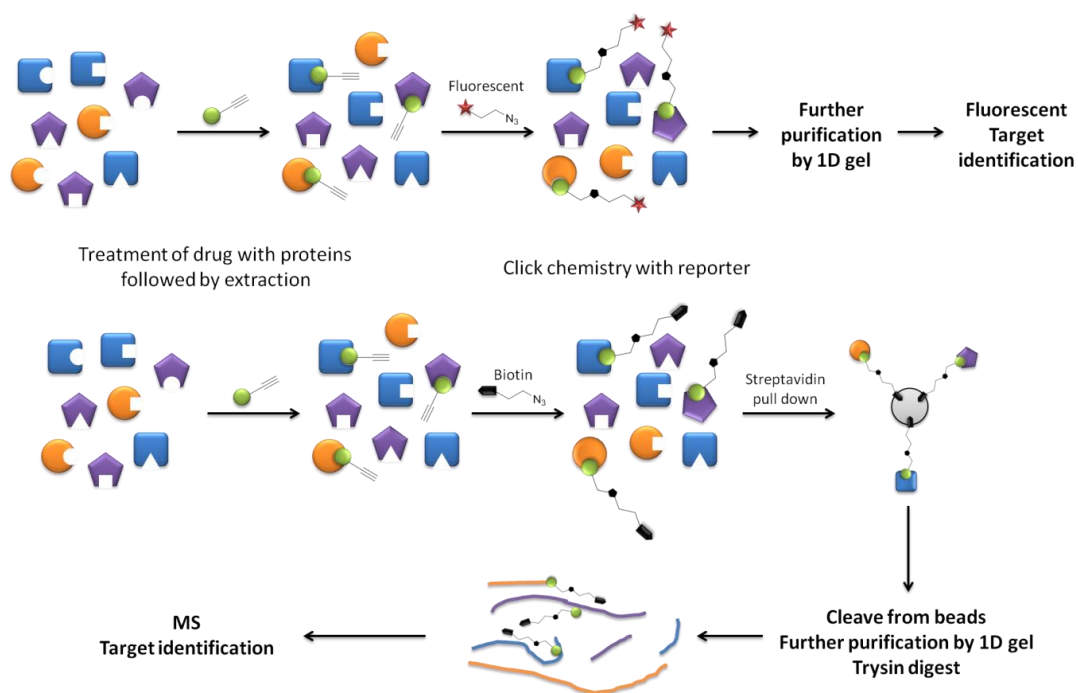


Figure 5.9: The ABPP method for analysis of drug target interactions *via* fluorescent detection or MS/MS detection.^{2-4,29}

5.1.4 Aims

The aims of this chapter are to design and synthesize novel reversible and irreversible functionalised probes for the artemisinin and CDDO class of compounds that are also pharmacologically active within their relevant contexts. These probes could be used to identify protein targets and perhaps resolve mechanisms of action.

5.2 Results and discussion

5.2.1 The chemical synthesis of artemisinin click probes

In order to link the click tag to the artemisinin moiety, an *N*-amide link was utilised. Chemical modification at the C-10 position within artemisinin to produce the amide link would provide metabolic stability compared with the C-10-ether link. Previous studies have demonstrated that cytochrome P450 converts the ether link back to dihydroartemisinin (**55**, DHA).³⁰

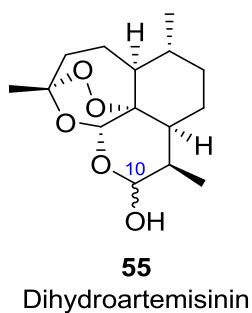
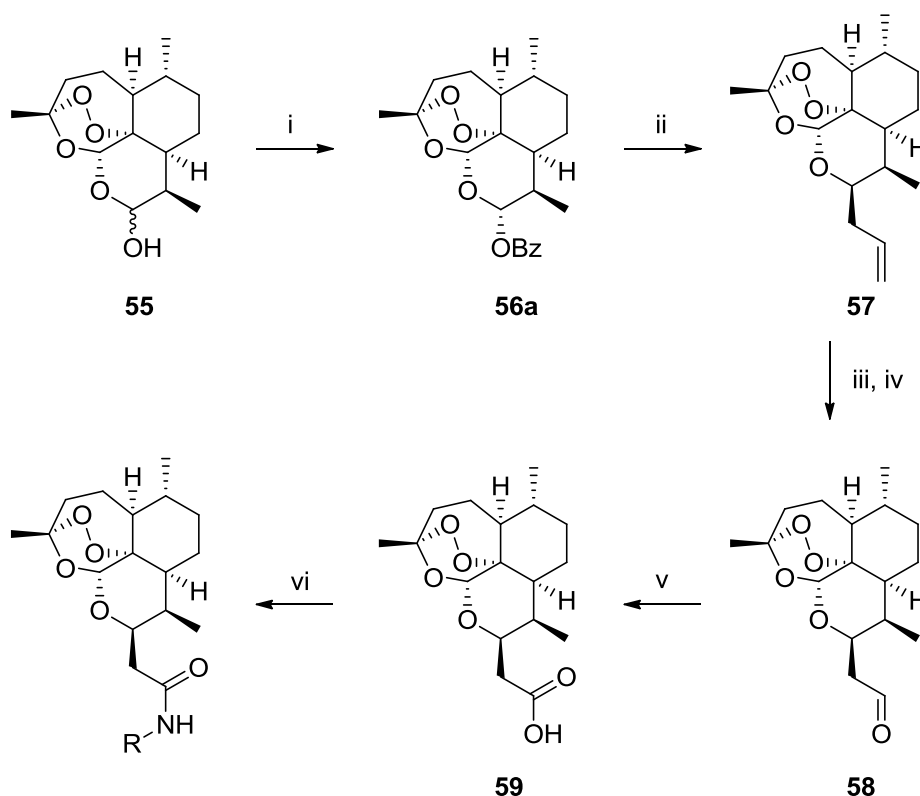


Figure 5.10: Chemical structure of dihydroartemisinin

The generation of artemisinin click probes involves a 5 step synthesis from commercially available semi-synthetic DHA (**55**). (Scheme 5.2).



Scheme 5.2: Reagents and conditions: (i) BzCl (1.6 equiv), pyridine (6.5 equiv), DCM, 0°C, 16 hours, 94%; (ii) allyltrimethylsilane (5 equiv), ZnCl₂ (1.5 equiv), 4 Å molecular sieves, 1,2-dichloroethane, 0°C, 3 hours, 38%; (iii) O₃, methanol, -78°C, 1 hour; (iv) PPh₃ (2 equiv), -78°C to r.t., overnight, 60%; (v) NaH₂PO₄ (0.26 equiv), NaClO₂ (1.95 equiv), 2-methyl-2-butene [2.0M in THF] (11.7 equiv), *t*-BuOH:H₂O [5:1 ratio], r.t. 2 hours, 100%; (vi) EDCI (3 equiv), DMAP (5 equiv), alkyne or azide amine (3 equiv), DCM, r.t. overnight, 81%;

The first step involves the acylation of dihydroartemisinin (**55**) with benzoyl chloride in DCM and pyridine to produce dihydroartemisinin 10 α -benzoate (**56a**) with a yield of 94%. **56a** is selectively formed under these conditions due the geometry of the 10 position. Studies by Haynes *et al* have revealed that the 10- α diastereoisomer (**56a**) is in the equatorial position while the 10- β diastereoisomer (**56b**) is in the axial position resulting in 1,3 diaxial interaction with the C-8, thus,

the steric effect raises the energy of the transition state for an acylation reaction to occur.³¹ This is shown in Figure 5.11

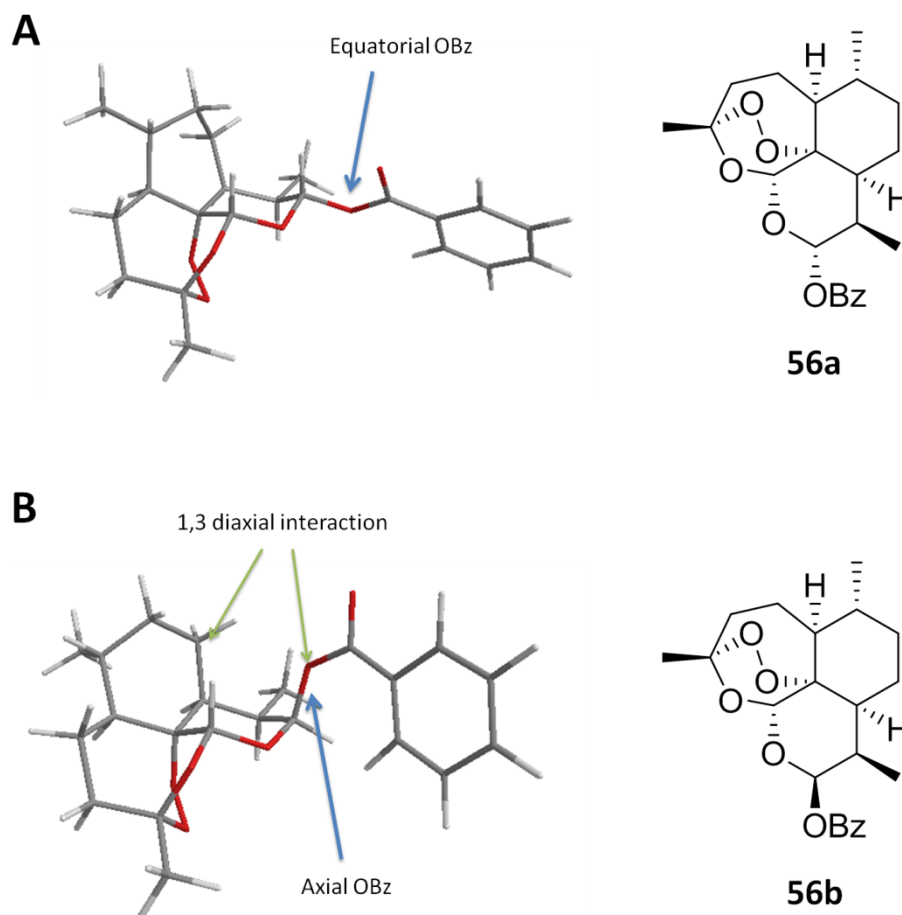
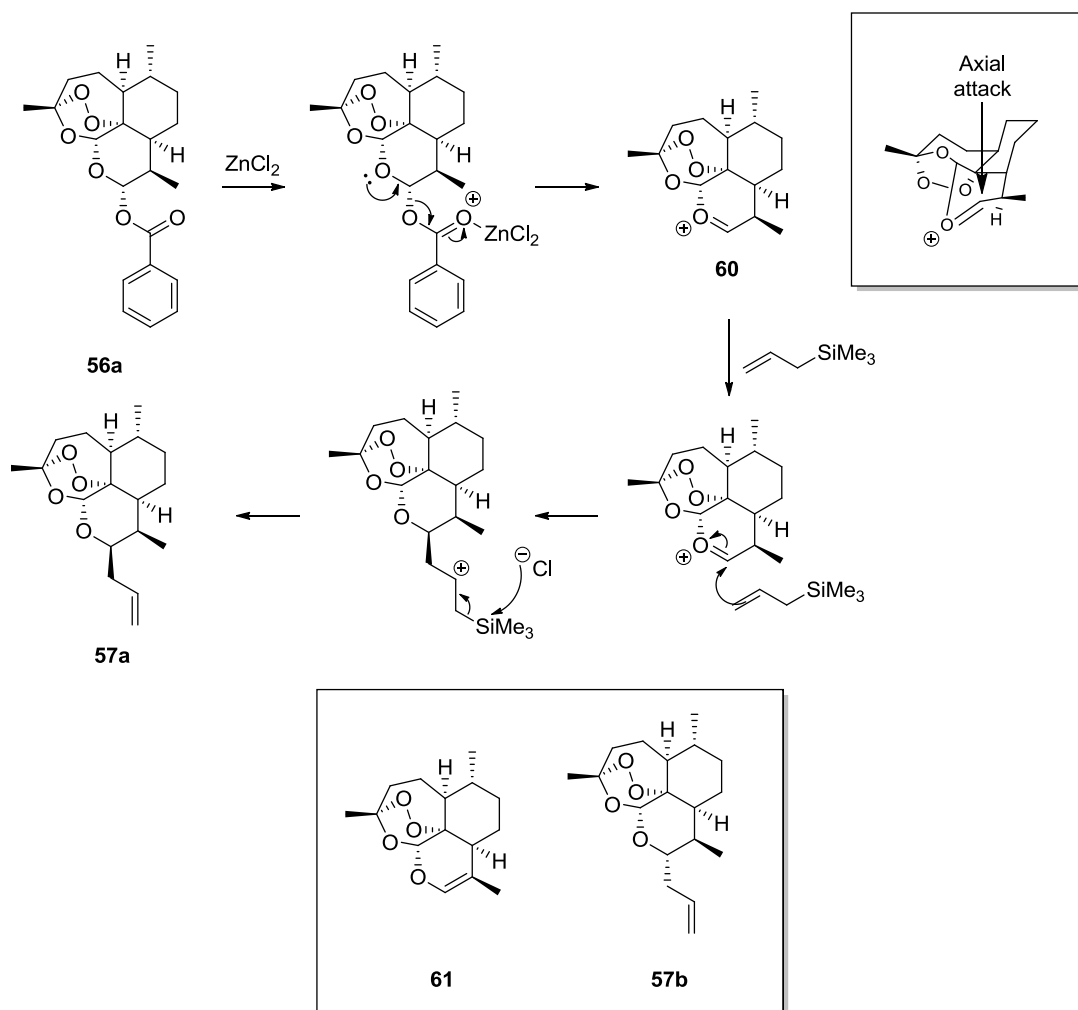


Figure 5.11: (A) The 10- α diastereoisomer in the equatorial position. (B) The 10- β diastereoisomer in the axial position and the highlighted 1,3 diaxial steric interaction between C-10 and C-8.

The synthesis of **57a** involves **56a** reacting with allyltrimethylsilane and zinc chloride as catalyst, selectively yielding 10 β -allyldeoxoartemisinin (**57a**) in 47%. 10 α -allyldeoxoartemisinin **57b** is not formed due to the orientation of the oxonium intermediate **60** resulting in the axial attack of the allyltrimethylsilane as depicted in Scheme 5.3. During the synthesis of **57a**, a small amount of anhydroartemisinin **61**

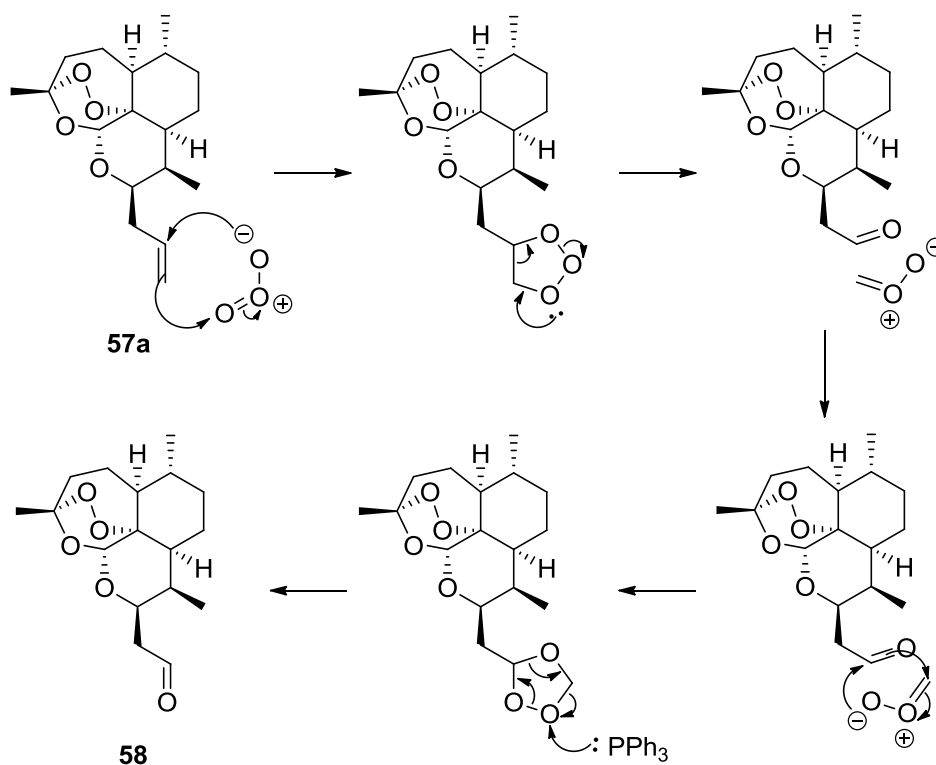
was formed making purification difficult due to similar R_f values. HPLC was required to obtain **57a**. This was also reported in O'Neill *et al.*³²



Scheme 5.3: Chemical mechanism for Lewis acid catalysed reaction with allyltrimethylsilane *via* the oxonium ion intermediate. Chemical structures for 10 α -allyldeoxyartemisinin **57b** and the anhydroartemisinin **61**.

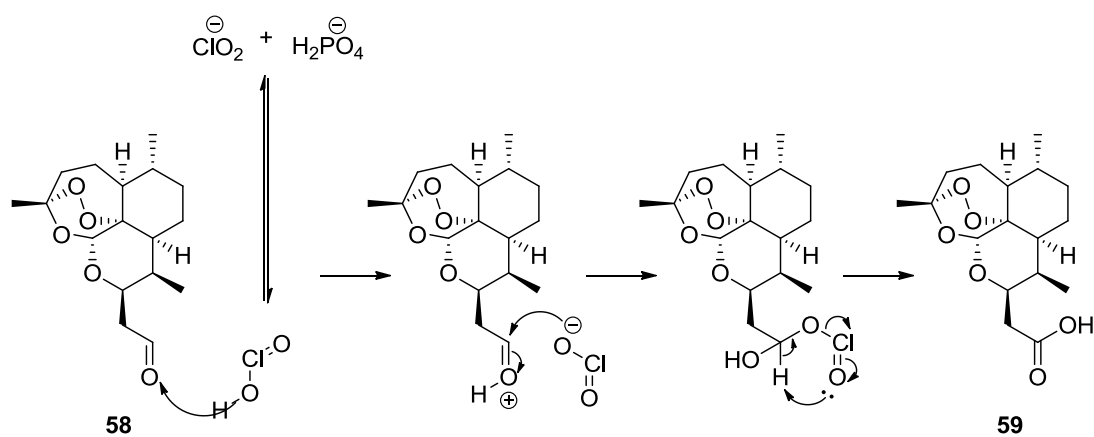
Ozonolysis of the **57a** followed by reduction with triphenylphosphine afforded **58** in 60% yield. The mechanism for the ozonolysis reaction is shown in Figure 5.7.

Chapter 5 – Design and synthesis of click functionalised derivatives of artemisinin and CDDO as probes for investigating chemical mechanism of action



Scheme 5.4: Chemical mechanism for ozonolysis of **57a** to give the aldehyde **58**

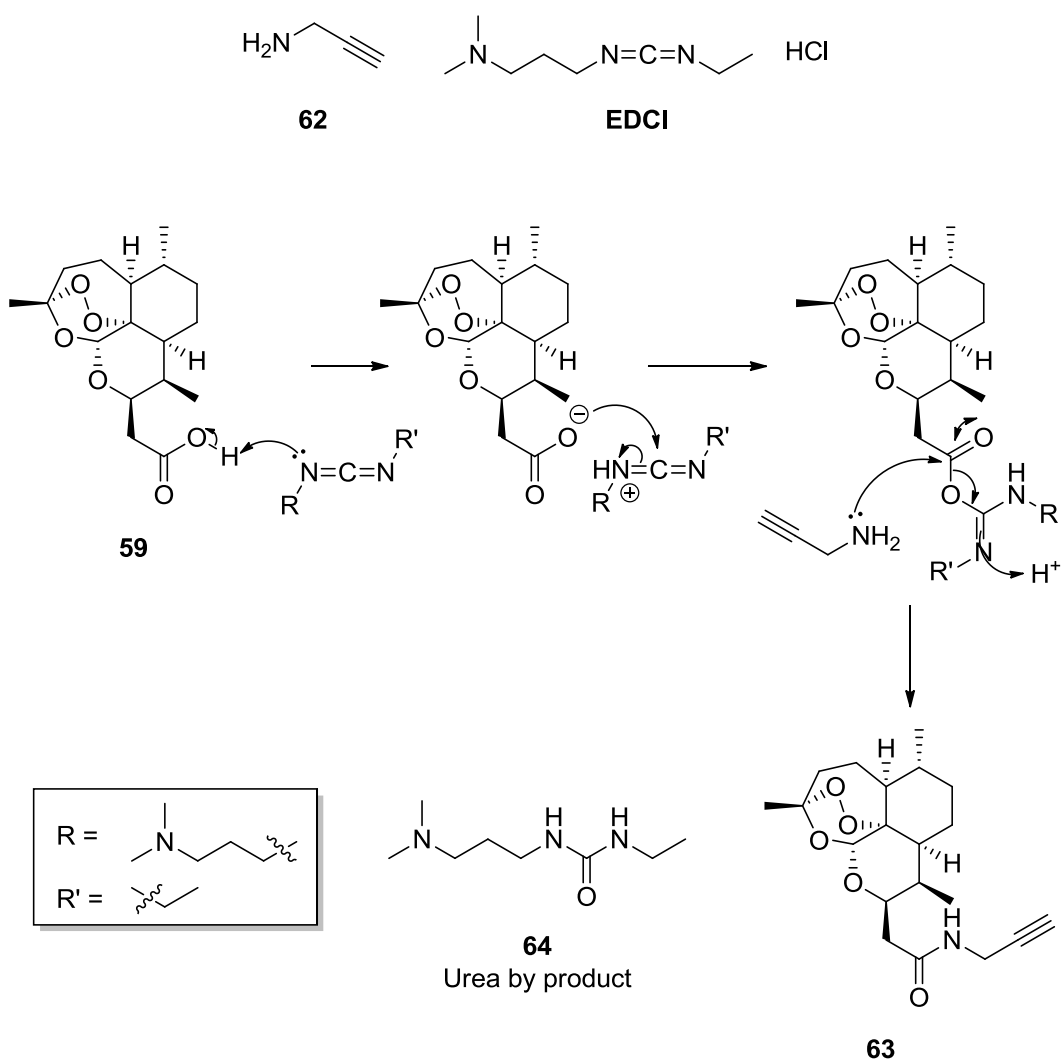
Pinnick oxidation of **58** yielded carboxylic acid **59**. The mechanism is shown in Scheme 5.5.



Scheme 5.5: Chemical mechanism for Pinnick oxidation of **58** to give **59**

Chapter 5 – Design and synthesis of click functionalised derivatives of artemisinin and CDDO as probes for investigating chemical mechanism of action

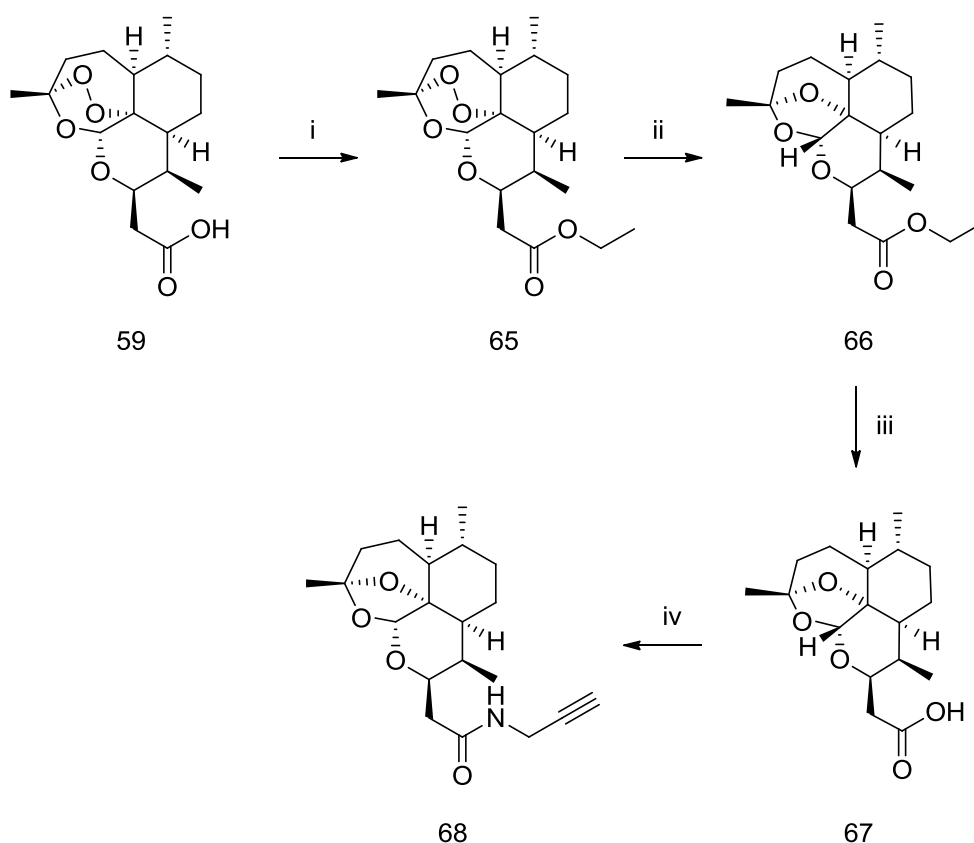
The coupling of the alkyne or azide click tag to the artemisinin moiety required the use of *N*-(3-dimethylaminopropyl)-*N'*-ethylcarbodiimide hydrochloride (EDCI) commonly used for the formation of amide bonds. EDCI is a water soluble carbodiimide and does not require activation prior to use. The alkyne amine **62** was selected for coupling with the artemisinin moiety forming **63**. The mechanism is depicted in Scheme 5.6 where the formation of the urea **64** is a by produce of EDCI.



Scheme 5.6: Chemical mechanism for amide coupling with EDCI between **62** and

59

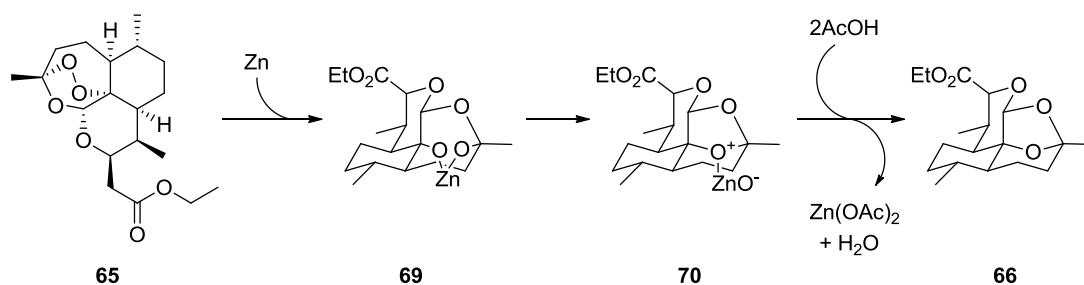
In addition to the alkyne artemisinin click probe **63**, a control is required to ensure activity and any substituent pull down experiments are not due to the presence of the alkyne side chain. In order to achieve this, the endoperoxide bridge is reduced to produce deoxyartemisinin. This is obtained in four steps from **59**.



Scheme 5.7: Reagents and conditions: (i) EDCI (3 equiv), DMAP (5 equiv), DCM, EtOH (3 equiv), r.t. overnight, 44%; (ii) Zn dust (3 x 1.5 equiv at 24 hour intervals), acetic acid, r.t., 72h, 38%; (iii) NaOH (15% w/v), EtOH, 3 hours, r.t., 80%; (iv) EDCI (3 equiv), DMAP (5 equiv), propargylamine (3 equiv), DCM, r.t. overnight, 34%.

Prior to reduction of the endoperoxide within **59**, protection of the carboxylic acid is required. This was achieved by using EDCI, 4-dimethylaminopyridine (DMAP) and ethanol to obtain the ethyl ester artemisinin **65** in 44% yield. **65** in acetic acid followed by addition of zinc dust over 72 hour yielding **66** in 38%. The endoperoxide

is reduced due to the oxophilic nature of zinc. A pair of electrons from zinc is donated to the endoperoxide which is cleaved and a bidentate species (**69**) is formed. Rearrangement of **69** to give the intermediate (**70**) enables the liberation of ZnO. The resulting ZnO dissolves in the acetic acid to give Zn(OAc)₂ and yielding deoxyartemisinin (**66**). This is shown in Scheme 5.8



Scheme 5.8: The chemical mechanism of action for the formation of deoxyartemisinin. Zinc donates a pair of electrons into the endoperoxide forming a bidentate species **69**. This rearranges to give **70** and elimination of ZnO gives the desired product **66**.

Deprotection of the carboxylic acid with sodium hydroxide yields **67** in 80%. Coupling of propargylamine with EDCI as described earlier yielded the alkyne deoxyartemisinin **68** in 34% yield.

The two artemisinin click probes obtained from the synthesis described above were submitted to the Liverpool School of Tropical Medicine to test their ability to inhibit the proliferation of *Plasmodium falciparum* 3D7 (chloroquine sensitive) strain *in vitro*. This data is shown in Figure 5.12

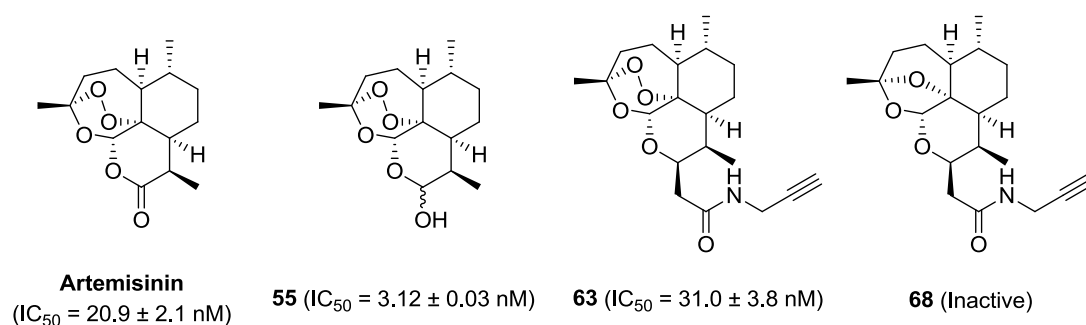


Figure 5.12: Artemisinin, DHA (**55**), artemisinin click probes **63** and **68** and the concentration that provoke a 50% inhibition (IC_{50}) of the proliferation of *Plasmodium falciparum* 3D7 strain *in vitro*

The artemisinin click probe **63** was active against 3D7 strain of *P. falciparum* giving an IC_{50} of 31.0 ± 3.8 nM. As expected, the deoxyartemisinin click probe **68** was inactive. Comparing **63** to artemisinin and DHA, the click probe is 1.5 times less active than artemisinin and 10 times less active than DHA. These data indicate that the novel click probes are suitable for proteomic studies and further emphasises the importance of the endoperoxide functional group to maintain the antimalarial activity of artemisinins.

5.2.1.1 Preliminary parasite protein identification with artemisinin click probes

The artemisinin click probes **68** and **63** were used by colleagues at the Liverpool School of Tropical Medicine to identify parasite target proteins. The technique used is based on a fully automated LC-MS/MS-based protocol known as the multidimensional protein Identification Technology (MudPIT).³³ Following LC-MS/MS analysis of samples prepared for *P. falciparum* exposed *in vitro* to **68** or **63** for 1-24 hours, Mascot search algorithms were used to match peptides to proteins based on sequence coverage. Semi quantification using exponentially modified

protein abundance index (emPAI) allowed approximate relative quantification of proteins in a mixture.³⁴ The preliminary data has so far identified a number of candidate target proteins including ornithine δ -aminotransferase (OAT), L-lactate dehydrogenase, enolase and V-type proton ATPase catalytic subunit, which are redox-active proteins that play a crucial role in the maintenance and control of redox reactions. An example of this is the thioredoxin-mediated control of OAT activity for coordinating ornithine homeostasis, polyamine synthesis, proline synthesis, and mitotic cell division in rapidly growing cells. This pathway also has links to the suggested non-heme mediated mechanism proposed by Haynes *et al.*³⁵ As described in more detail in Chapter 4, Haynes *et al* suggested that the FADH₂ and FAD pathway is involved in the non-heme mediated cleavage of the endoperoxide bridge and is also linked to the thioredoxin pathway. Despite this being preliminary data, the artemisinin click probes have identified several potential *Plasmodia* molecular targets. Of those identified the interacting patterns of the thioredoxin pathway represents potential targets for chemotherapeutic intervention, given that existing antimalarial drugs do not specifically target this pathway.

Further work is underway within the group to complete the characterisation of the plasmodia molecular targets of the artemisinins, tetraoxanes and trioxolanes. It will be important to determine if the classes of endoperoxide have common and/or unique molecular targets, which may become promising targets for next-generation antimalarial drugs. Further work will also involve artemisinin resistant parasites and mammalian cells to define the level of selectivity and potential to interact with the appropriate mammalian-falciparum counterparts, in order to better understand the

Chapter 5 – Design and synthesis of click functionalised derivatives of artemisinin and CDDO as probes for investigating chemical mechanism of action

risk:benefit of the use of these drugs in humans, and to determine the potential for enhancing pharmacological efficacy whilst minimising off-target toxicity to the host.

5.2.2 The chemical synthesis of CDDO and DDO click probes.

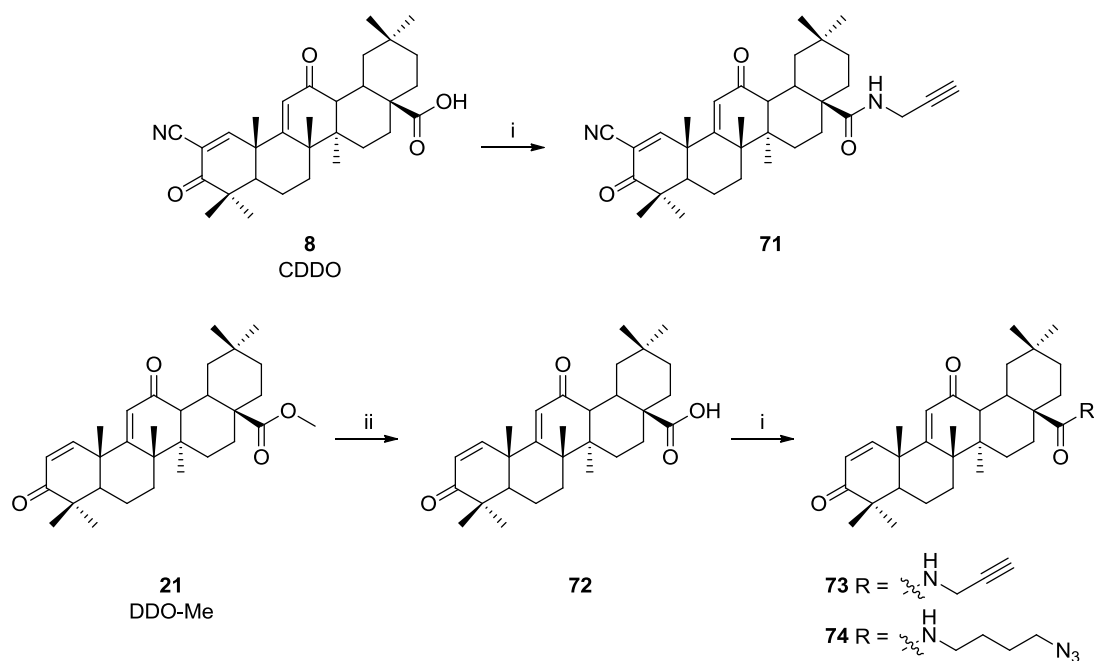
As described in Chapter 3, irreversible probes are important tools as they enable the use of traditional techniques for determining molecular targets where previous attempts with the original compound have failed. The concept of irreversible probes was adopted and this resulted in the design and synthesis of DDO-Me and CDDO-Epoxyde. Both of these probes were active as inducers of the Nrf2 sensitive luciferase reporter assay. As discussed earlier, biotinylated CDDO derivatives have been used to identify three molecular targets that contain cysteine residues, IKK β at Cys-179, JAK1 at Cys-1077 and STAT3 at Cys-259. Despite this discovery, direct evidence for interaction with components of the Keap1-Nrf2 pathway has yet to be produced. In order to investigate further the mechanism of action of CDDO derivatives as inducers of Nrf2, click tagged probes were targeted.

The synthesis of CDDO click probes required the formation of a carboxylic acid group followed by the amine coupling reaction used earlier for the formation of the artemisinin click probes. This involved a further two steps for the formation of DDO click derivative and one step from CDDO as shown in Scheme 5.9.

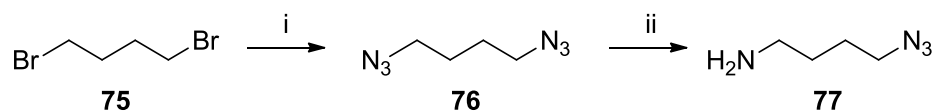
The synthesis of **71** required the use of **8** which was synthesised in Chapter 2 and the EDCI coupling reaction with propargyl amine giving **71** in 33% yield. Synthesis of **21** was described in Chapter 3 and is used to form the carboxylic acid **72** in 64% yield. Lithium iodide was used to form **72** as described in Chapter 2 for the formation of **8**. EDCI coupling reaction with propargyl amine and **72** gave **73** in 40% yield. Formation of **74** required the synthesis of the azide amine. This involved a two-step synthesis from 1,4-dibromobutane **75** where the first step involved the

Chapter 5 – Design and synthesis of click functionalised derivatives of artemisinin and CDDO as probes for investigating chemical mechanism of action

use of sodium azide in DMF to form 1,4-diazidobutane **76** in 100%. Reduction of **76** using triphenylphosphine gave 4-azidobutane-1-amine **77** in 95% yield. EDCI coupling reaction between **77** and **72** gave **74** in 38% yield.



Scheme 5.9: Reagents and conditions: (i) EDCI (3 equiv), DMAP (5 equiv), click amine (3 equiv), DCM, r.t. overnight; (ii) Lil (19 equiv), anhydrous DMF, N_2 (g), reflux, overnight, 22%.



Scheme 5.10: Reagents and conditions: (i) DMF, NaN_3 (2.1 equiv) H_2O , 80°C , 20 hours, 100%; (ii) EtOAc:Et₂O (1:1), PPh_3 (1 equiv), HCl (1 M), 0°C to r.t., overnight, 90%

Chapter 5 – Design and synthesis of click functionalised derivatives of artemisinin and CDDO as probes for investigating chemical mechanism of action

The ability of **71**, **73** and **74** to induce Nrf2 signalling was determined using the Nrf2 sensitive luciferase reporter assay used in previous chapters. The data is shown in Table 5.1 and Graph 5.1

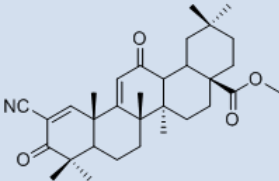
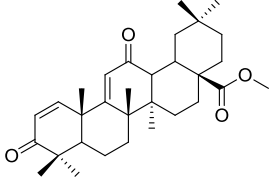
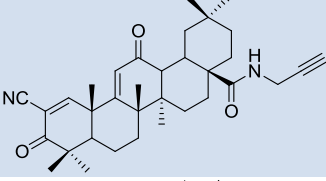
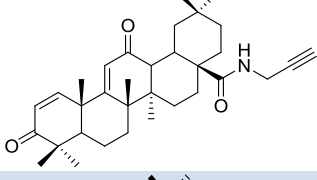
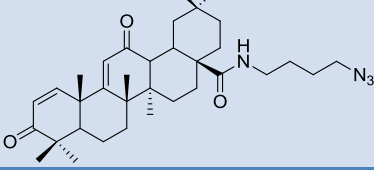
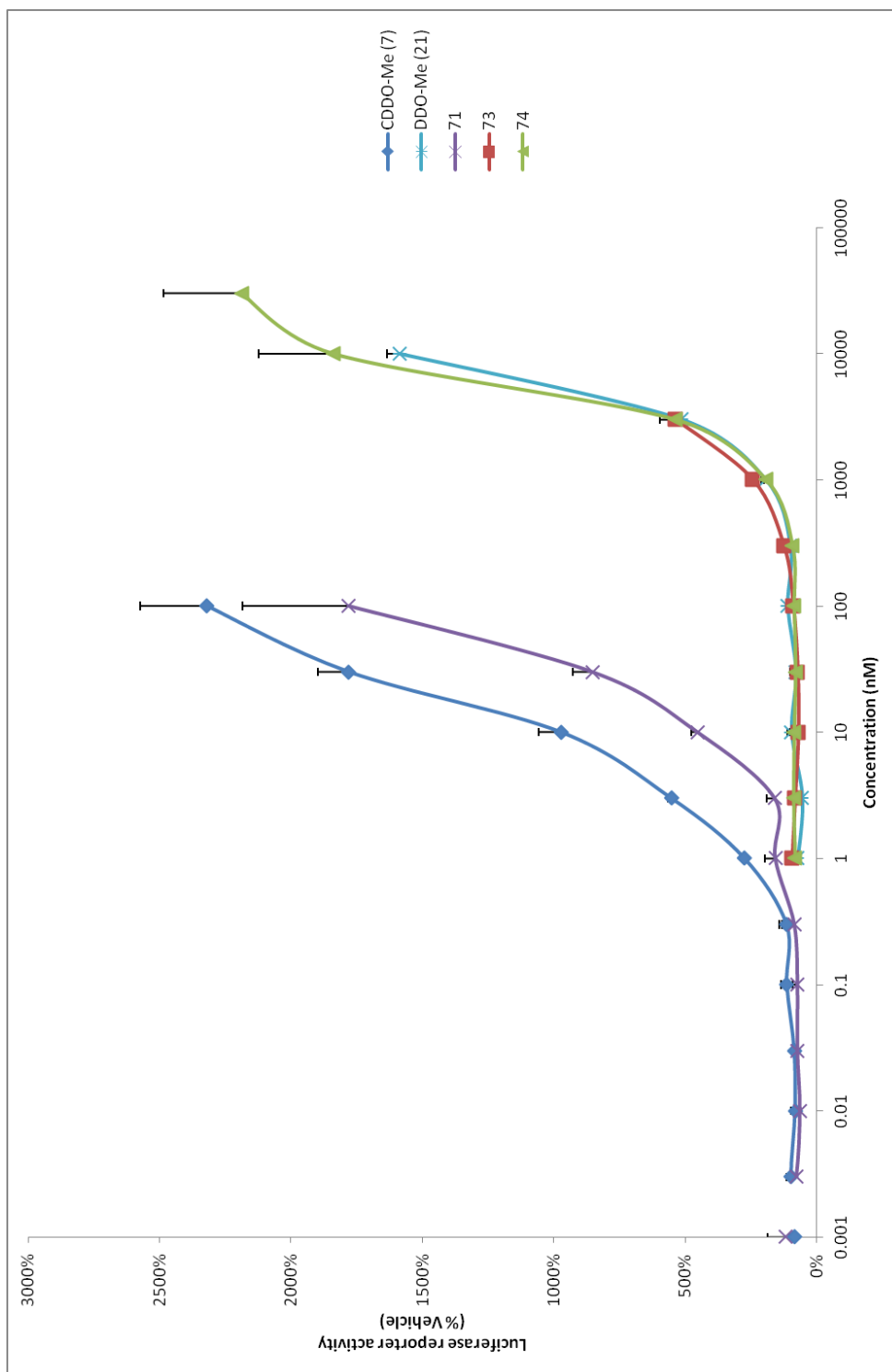
Compound	Structure	Concentration that induces Nrf2 reporter to 200% (EC ₂₀₀)
CDDO-Me (7)		0.62 nM ± 0.02
DDO-Me (21)		0.90 μM ± 0.08
71		2.76 nM ± 0.67
73		0.73 μM ± 0.05
74		1.01 μM ± 0.05

Table 5.1: Relative potencies of CDDO-Me, DDO-Me, **71**, **73** and **74** as inducers of an Nrf2 regulated luciferase reporter transgene in H4IIE-ARE cells.

Similar to the potent compound CDDO-Me, **71** is a potent inducer of Nrf2. Furthermore, compounds **73** and **74** are comparable to DDO-Me. This data shows that in comparison of alkyne and azide groups into the CDDO and DDO scaffolds does not impact on pharmacological potency; therefore, these novel probes are

Chapter 5 – Design and synthesis of click functionalised derivatives of artemisinin and CDDO as probes for investigating chemical mechanism of action

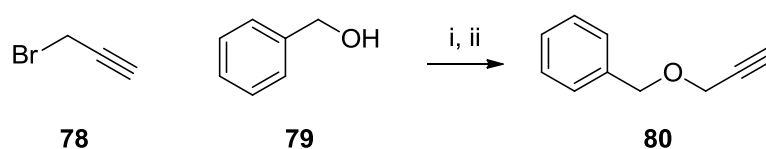
suitable for determining the molecular target(s) of the CDDO class and determining mechanisms of action.



Graph 5.1: Relative abilities of CDDO-Me, **71**, **73** and **74** to induce an Nrf2 regulated luciferase transgene in H4IIE-ARE cells over 24h. Data points were normalised to the vehicle control (DMSO). Data is mean + S.D., n=3.

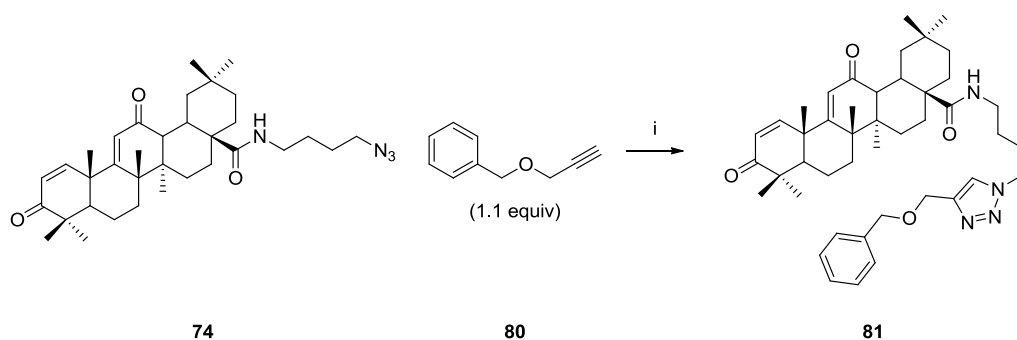
5.2.3 Click reaction proof of concept.

As described earlier in this chapter, biotin tagged probes are a useful tool for the investigation of biological processes. However, the use of such probes comes with disadvantages including steric bulk, altered cell permeability and harsh conditions required to disrupt the biotin-streptavidin interaction during purification. This has resulted in the synthesis of click tagged derivatives of irreversible CDDO probes. In order to determine if the click probes are viable tools for *in vitro* and eventually *in vivo* experiments, it is necessary to demonstrate their ability to undergo the click reaction with a relevant counterpart. Towards this goal, a counterpart was synthesised for **74**. This involved a one-step synthesis between propargyl bromide (**78**) and benzyl alcohol (**79**) with the addition of sodium hydride to form benzyl propargyl ether (**80**) in 74% yield. This is shown in Scheme 5.11.



Scheme 5.11: Reagents and conditions: (i) benzyl alcohol, THF, 0°C, NaH (1 equiv), 30 mins, (ii) propargyl bromide added dropwise, warm to r.t., stir 1 hour, 78%.

The click reaction between **74** and **80** was performed in a dichloromethane water solution in the presence of sodium ascorbate and copper (II) sulphate catalyst to obtain **81** in 40% yield. This demonstrates that the click reaction can occur between the synthesised CDDO click probes and a counterpart, providing proof-of-concept that such probes can be used in a biological context to enable purification and identification of drug targets.



Scheme 5.12: Reagents and conditions: (i) DCM:H₂O (1:1), CuSO₄·5H₂O (5%), sodium ascorbate (15%), r.t., 2 hours, 40%.

5.3 Conclusion

The work described here resulted in the synthesis of five novel click functionalised probes, two in the artemisinin series and three in the CDDO series. The artemisinin click probes have demonstrated acceptable antimalarial activity against *P. falciparum* 3D7 strain while the CDDO click probes demonstrated similar activity as inducers of the Nrf2-regulated luciferase reporter compared to their parent compounds. The reaction between synthesised click probe **74** and the simple click tag counterpart **80** has demonstrated that these novel compounds are capable of forming the resulting triazole, enabling their use for pull down purification and target identification and verification.

Future work will include synthesising the click tagged CDDO-Epoxy and the azide tagged artemisinin. Lengthening the linker between the drug and click tag will aid in developing an SAR profile between the linker length. This SAR profile will provide information on drug activity vs pull-down purification. This data will enable the selection of the most viable probe for ABPP testing and eventually enable the full characterisation of the target proteins in both *in vitro* and ultimately, *in vivo*

Chapter 5 – Design and synthesis of click functionalised derivatives of artemisinin and CDDO as probes for investigating chemical mechanism of action

context. Therefore, the click probes described here will inform the design and development of safe and efficacious new drugs. Specifically for CDDO-Me, the reversibility of a click-functionalised probe may be an issue. Photoaffinity functionalised probes can be produced to overcome the reversibility issue, as described in detail earlier in this chapter. Such a strategy will further ensure that all potential drug targets can be characterised and identified, thus informing the design and development of next-generation drug candidates.

5.4 Chemistry experimental

5.4.1 General

See sections 2.4.1

5.4.2 Purification of solvents and reagents

See sections 3.4.2

5.4.2.1 Stains

See sections 3.4.2.1

5.4.3 Purification of products

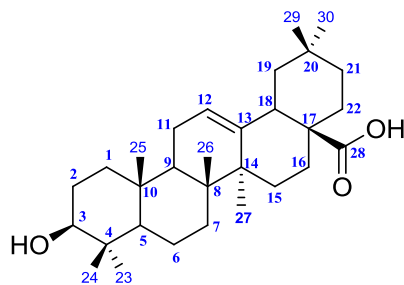
See sections 2.4.4

5.4.4 Analysis

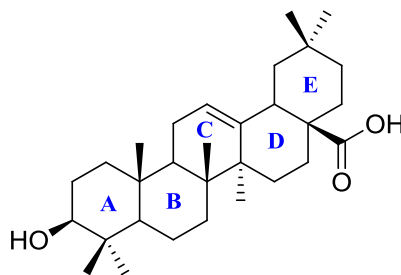
See sections 2.4.5

5.4.5 Numbering

Oleanolic acid

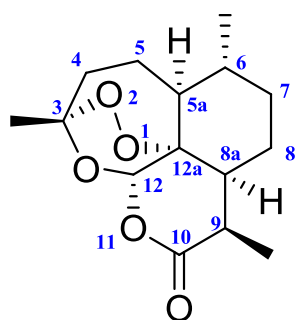


Carbon assignment

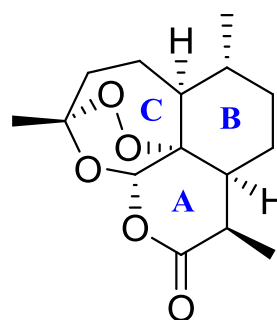


Ring assignment

Artemisinin



Carbon assignment



Ring assignment

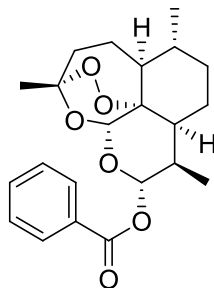
5.4.6 General procedure.

General procedure 1

Acid (**8**, **59**, **67** or **72**) was dissolved in DCM (50 mL) and *N*-(3-dimethylaminopropyl)-*N'*-ethylcarbodiimide hydrochloride (EDCI) (3 equivalents) was added to the reaction and left to stir at room temperature for 5 minutes. 4-(dimethylamino)pyridine (DMAP) (5 equivalents) and amine or alcohol was added to the reaction and left to stir at room temperature overnight. The reaction mixture was diluted with ethyl acetate (50 mL) and washed with ammonium chloride solution, water, brine, dried over magnesium sulfate and filtered. The solvent was removed to give crude product and purified by flash chromatography.

5.4.7 Synthesis artemisinin click probes

Preparation of dihydroartemisinin 10 α -benzoate (**56a**)^{36,37}

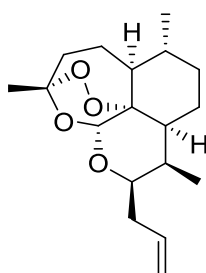


Dihydroartemisinin (2.05 g, 7.21 mmol) was dissolved in anhydrous DCM (50 mL) in a nitrogen atmosphere and cooled to 0°C. pyridine (3.77 mL, 46.86 mmol) and benzoyl chloride (1.34 mL, 11.54 mmol) were added to the reaction and left to stir for 16 hours. Citric acid (7% w/v) was added to the reaction and the reaction mixture was extracted with ethyl acetate (3 X 100 mL). Combined organic layers were washed with citric acid (7% w/v), saturated sodium hydrogen carbonate, water, brine, dried over magnesium sulfate and filtered. The solution was concentrated under reduced pressure to give crude product in which purification by flash chromatography using 30% ethyl acetate in hexane to give title compound **56a** (2.62 g, 94%) as a white solid; $R_f = 0.51$, 30% ethyl acetate in hexane; mp = lit³⁷ 115-118°C found 119-120°C; ¹H NMR (400 MHz, CDCl₃) δ 8.13 (dd, $J = 8.2, 1.1$ Hz, 2H), 7.64 – 7.54 (m, 1H), 7.50 – 7.41 (m, 2H), 6.02 (d, $J = 9.8$ Hz, 1H), 5.53 (s, 1H), 2.76 (dq, $J = 14.2, 7.1, 4.7$ Hz, 1H), 2.39 (ddd, $J = 14.4, 13.6, 4.0$ Hz, 1H), 2.10 – 1.99 (m, 1H), 1.96 – 1.87 (m, 1H), 1.83 (ddd, $J = 13.3, 7.5, 3.5$ Hz, 1H), 1.75 (ddd, $J = 14.2, 6.8, 3.6$ Hz, 1H), 1.69 (dt, $J = 13.7, 4.5$ Hz, 1H), 1.61 – 1.44 (m, 2H), 1.43 (s, 3H), 1.42 – 1.28 (m, 2H), 1.10 – 1.01 (m, 1H), 0.99 (d, $J = 6.1$ Hz, 3H) and 0.93 (d, $J = 7.1$ Hz, 3H); ¹³C NMR (100 MHz, CDCl₃) δ 165.5, 133.4, 130.3, 129.8, 128.4, 104.6, 92.7, 91.7,

Chapter 5 – Design and synthesis of click functionalised derivatives of artemisinin and CDDO as probes for investigating chemical mechanism of action

80.3, 51.8, 45.5, 37.4, 36.4, 34.3, 32.1, 26.1, 24.7, 22.2, 20.4 and 12.4; IR ν_{\max} (neat)/ cm^{-1} 2928 (Ar-H), 2876 (CH), 1736 (C=O) and 1018 (C-O-C); HRMS (ESI) calculated for $\text{C}_{22}\text{H}_{28}\text{O}_6$ $[\text{M}+\text{Na}]^+$ 411.1784 found 411.1794; Microanalysis Calculated for $\text{C}_{22}\text{H}_{28}\text{O}_6$ requires C 68.02%, H 7.27%, found C 67.93%, H 7.31%.

Preparation of 10 β -allyldeoxoartemisinin (**57a**)³²

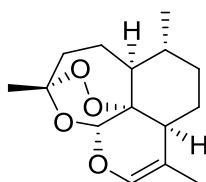


56a (3.21 g, 8.26 mmol) was dissolved in anhydrous DCM (50 mL) under a nitrogen atmosphere. Zinc chloride (1.69 g, 12.40 mmol) and 4 Å molecular sieves (2 mg) were added to a dry flask and introduced anhydrous DCM under a nitrogen atmosphere. The reaction mixture was cooled to 0°C and allyltrimethylsilane (6.57 mL, 41.32 mmol) was added to the zinc chloride solution. The solution of **56a** was added slowly to the solution of allyltrimethylsilane and left to stir for 3 hours at 0°C. The reaction was concentrated under reduced pressure to give the crude product in which purification by flash chromatography using 10% ethyl acetate in hexane to give the title compound **57a** (971.5 mg, 38%) as a white solid; R_f = 0.44; 10% ethyl acetate in hexane; mp = lit³⁶ 76-78°C found 76-78 °C; ^1H NMR (400 MHz, CDCl_3) δ 5.93 (ddt, J = 16.9, 10.2, 6.6 Hz, 1H), 5.33 (s, 1H), 5.09 (ddq, J = 19.9, 10.2, 1.5 Hz, 2H), 4.30 (ddd, J = 10.0, 6.1, 3.7 Hz, 1H), 2.69 (sex, J = 7.3 Hz, 1H), 2.45 – 2.37 (m, 1H), 2.33 (ddd, J = 14.5, 13.5, 4.0 Hz, 1H), 2.25 – 2.16 (m, 1H), 2.03 (ddd, J = 14.6, 4.7, 3.1 Hz, 1H), 1.96 – 1.87 (m, 1H), 1.81 (ddd, J = 13.4, 7.6, 3.5 Hz, 1H), 1.70 – 1.59

Chapter 5 – Design and synthesis of click functionalised derivatives of artemisinin and CDDO as probes for investigating chemical mechanism of action

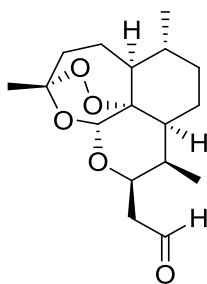
(m, 2H), 1.42 (s, 3H), 1.53 – 1.19 (m, 5H), 0.96 (d, $J = 6.0$ Hz, 3H) and 0.89 (d, $J = 7.6$ Hz, 3H); ^{13}C NMR (100 MHz, CDCl_3) δ 136.6, 116.2, 103.3, 89.3, 81.2, 74.8, 52.5, 44.5, 37.6, 36.8, 34.6, 34.4, 30.4, 26.2, 25.0, 24.9, 20.3 and 13.1; IR ν_{max} (neat)/ cm^{-1} 2957 (C-H), 2865, 1642 (C=C), 1056 (C-O-C), 1041 and 879 (C=CH); HRMS (ESI) calculated for $\text{C}_{18}\text{H}_{28}\text{O}_4$ $[\text{M}+\text{Na}]^+$ 331.1885 found 331.1882; Microanalysis Calculated for $\text{C}_{18}\text{H}_{28}\text{O}_4$ requires C 70.1%, H 9.15%, found C 69.86%, H 9.13%.

Side product anhydroartemisinin (61)³²



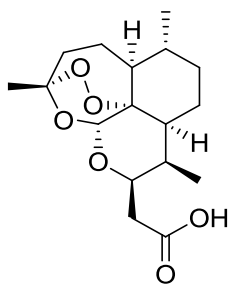
^1H NMR (400 MHz, CDCl_3) δ 6.09 (d, $J = 1.4$ Hz, 1H), 5.46 (s, 1H), 2.32 (ddd, $J = 14.5$, 13.2, 4.0 Hz, 1H), 2.03 – 1.93 (m, 2H), 1.89 – 1.81 (m, 1H), 1.52 (d, $J = 1.4$ Hz, 3H), 1.69 – 1.35 (m, 5H), 1.34 (s, 3H), 1.21 – 0.97 (m, 2H) and 0.92 (d, $J = 6.0$ Hz, 3H); ^{13}C NMR (100 MHz, CDCl_3) δ 134.8, 107.6, 104.1, 89.3, 78.6, 51.2, 44.2, 37.2, 36.00, 33.9, 29.7, 25.6, 24.2, 20.1 and 16.0; HRMS (CI) calculated for $\text{C}_{15}\text{H}_{22}\text{O}_4$ $[\text{M}+\text{H}]^+$ 267.1591 found 267.1599.

Preparation of 10 β -(2-oxoethyl)deoxyartemisinin (**58**)³²



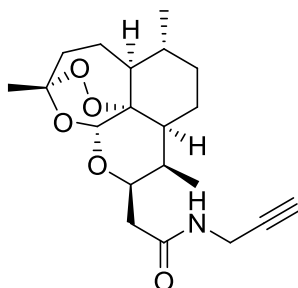
57a (2.27 g, 7.36 mmol) was dissolved in anhydrous methanol and cooled to -78°C in an acetone-dry ice bath. Ozone was bubbled through the solution for 1 hour until the solution became saturated with ozone and appeared blue. Nitrogen was bubbled through the reaction to purge excess ozone. Triphenylphosphine (3.86 g, 14.72 mmol) was added to the reaction mixture at -78°C where it was allowed to warm to room temperature and left to stir for 18 hours. The reaction mixture was concentrated to give the crude product in which purification by flash chromatography using 10% ethyl acetate in hexane to give the title compound **58** (1.37 g, 60%) as a white solid; $R_f = 0.05$; 10% ethyl acetate in hexane; $^1\text{H NMR}$ (400 MHz, CDCl_3) δ 9.80 (dd, $J = 3.2, 1.4$ Hz, 1H), 5.32 (s, 1H), 4.99 – 4.91 (m, 1H), 2.73 (tdd, $J = 13.9, 12.4, 5.3$ Hz, 2H), 2.46 (ddd, $J = 16.3, 3.5, 1.5$ Hz, 1H), 2.33 (ddd, $J = 14.5, 13.4, 4.0$ Hz, 1H), 2.04 (ddd, $J = 14.7, 4.6, 3.2$ Hz, 1H), 1.98 – 1.89 (m, 1H), 1.80 (ddd, $J = 13.3, 7.4, 3.5$ Hz, 1H), 1.73 – 1.64 (m, 2H), 1.41 (s, 3H), 1.49 – 1.22 (m, 5H), 0.97 (d, $J = 5.9$ Hz, 3H) and 0.87 (d, $J = 7.5$ Hz, 3H); $^{13}\text{C NMR}$ (100 MHz, CDCl_3) δ 202.0, 103.3, 89.4, 81.0, 69.6, 52.2, 44.5, 44.1, 37.6, 36.6, 34.4, 29.8, 26.1, 24.8, 24.8, 20.3 and 13.2; HRMS (ESI) calculated for $\text{C}_{17}\text{H}_{26}\text{O}_5$ $[\text{M}+\text{Na}]^+$ 333.1678 found 333.1664; Microanalysis Calculated for $\text{C}_{17}\text{H}_{26}\text{O}_5$ requires C 65.78%, H 8.44%, found C 65.68%, H 8.54%.

Preparation of 10 β -(2-carboxyethyl)deoxoartemisinin (**59**)²²



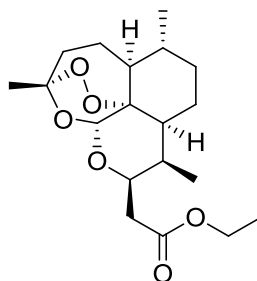
58 (1.37 g, 4.41 mmol) was dissolved in *tert*-butanol (90 mL) and water (18 mL). 2-methyl-2-butene (2.0 M in THF, 25.85 mL, 51.64 mmol), monosodium phosphate (137.69 mg, 1.15 mmol) and sodium chlorite (778.43 mg, 8.61 mmol) was added to the solution and left to stir at room temperature for 3 hours. The yellow solution will slowly turn to a pale yellow over time. *tert*-butanol was removed *in vacuo* and crude product was dissolved in DCM (50 mL). Sodium hydroxide (1 M, 50 mL) was added and washed with DCM (3 x 50 mL). Aqueous layer was acidified with hydrochloric acid (1 M) and extracted with DCM (3 x 50 mL). Combined organic layers were dried over magnesium sulfate, filtered and solvent was removed under vacuum to yield the title compound **59** (1.44 g, 100%) as a white solid; ¹H NMR (400 MHz, CDCl₃) δ 5.36 (s, 1H), 4.83 (ddd, *J* = 10.0, 6.2, 3.7 Hz, 1H), 2.81 – 2.62 (m, 2H), 2.50 (dd, *J* = 15.6, 3.7 Hz, 1H), 2.38 – 2.27 (m, 1H), 2.07 – 1.99 (m, 1H), 1.96 – 1.88 (m, 1H), 1.80 (ddd, *J* = 10.7, 7.0, 3.2 Hz, 1H), 1.72 – 1.61 (m, 2H), 1.41 (s, 3H), 1.58 – 1.20 (m, 6H), 0.97 (d, *J* = 6.0 Hz, 3H) and 0.88 (d, *J* = 7.5 Hz, 3H); ¹³C NMR (100 MHz, CDCl₃) δ 176.9, 103.4, 89.3, 80.9, 71.2, 52.2, 44.0, 37.5, 36.5, 35.9, 34.4, 29.8, 25.9, 24.8, 24.7, 20.2 and 12.9; HRMS (ESI) calculated for C₁₇H₂₆O₆ [M+Na]⁺ 349.1627 found 349.1623.

Preparation of *N*-(prop-2-yn-1-yl)-2-[(5*a*S,6*R*,8*a*S,9*R*,10*R*,12*R*,12*a*R)-3,6,9-trimethyldecahydro-3,12-epoxy[1,2]dioxepino[4,3-*i*]isochromen-10-yl]acetamide (**63**)



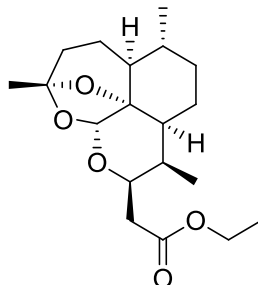
The preparation of **63** involved the use of acid **59** (237 mg, 726 μ mol), propargylamine (139.5 μ L, 2.18 mmol), EDCI (338.2 mg, 2.18 mmol) and DMAP (443.6 mg, 3.63 mmol) following general procedure 1. Purification of the crude product by flash chromatography using 60% ethyl acetate in hexane to give title compound **63** (213.1 mg, 81%) as a white solid; R_f = 0.65, 60% ethyl acetate in hexane; mp = 129-130°C; ^1H NMR (400 MHz, CDCl_3) δ 5.39 (s, 1H), 4.82 (ddd, J = 11.3, 6.2, 1.7 Hz, 1H), 4.06 (dd, J = 5.2, 2.6 Hz, 2H), 2.60 – 2.48 (m, 2H), 2.41 – 2.28 (m, 2H), 2.19 (t, J = 2.6 Hz, 1H), 2.07 (ddd, J = 14.6, 4.4, 3.2 Hz, 1H), 2.03 – 1.94 (m, 1H), 1.84 – 1.71 (m, 2H), 1.71 – 1.61 (m, 2H), 1.44 (s, 3H), 1.42 – 1.11 (m, 5H), 0.98 (d, J = 5.9 Hz, 3H) and 0.87 (d, J = 7.6 Hz, 3H); ^{13}C NMR (100 MHz, CDCl_3) δ 171.6, 103.1, 90.5, 81.0, 79.9, 71.4, 69.2, 51.8, 43.4, 37.7, 37.5, 36.7, 34.3, 30.6, 29.1, 26.0, 25.0, 25.0, 20.1 and 12.0; IR ν_{max} (neat)/ cm^{-1} 3359 ($\equiv\text{C}-\text{H}$), 3286 (CONH), 2976 (CH), 2948 (CH), 2921, 2858, 1675 (CONH), 1203 and 1044 (C-O-C); HRMS (ESI) calculated for $\text{C}_{20}\text{H}_{29}\text{NO}_5$ $[\text{M}+\text{Na}]^+$ 386.1943 found 386.1942; Microanalysis Calculated for $\text{C}_{20}\text{H}_{29}\text{NO}_5$ requires C 66.09%, H 8.04%, N 3.85%, found C 65.97%, H 8.01%, N 3.72%.

Preparation of ethyl [(5*a*S,6*R*,8*a*S,9*R*,10*R*,12*R*,12*a*R)-3,6,9-trimethyldecahydro-3,12-epoxy-[1,2]dioxepino[4,3-*i*]isochromen-10-yl]acetate (**65**)³⁸



The preparation of **65** involved the use of acid **59** (470 mg, 1.44 mmol), anhydrous ethanol (252.2 μ L, 4.32 mmol), EDCI (670.7 mg, 4.32 mmol) and DMAP (879.6 mg, 7.20 mmol) following general procedure 1. Purification of the crude product by flash chromatography using 10% ethyl acetate in hexane to give title compound **65** (226.6 mg, 44%) as a colourless oil; R_f = 0.18, 10% ethyl acetate in hexane; mp = 101-103 $^{\circ}$ C; ^1H NMR (400 MHz, CDCl_3) δ 5.33 (s, 1H), 4.81 (ddd, J = 10.1, 6.2, 4.0 Hz, 1H), 4.25 – 4.10 (m, 2H), 2.82 – 2.71 (m, 1H), 2.65 (dd, J = 15.2, 9.9 Hz, 1H), 2.45 (dd, J = 15.2, 4.0 Hz, 1H), 2.33 (ddd, J = 14.4, 13.5, 4.0 Hz, 1H), 2.03 (ddd, J = 14.6, 4.6, 3.2 Hz, 1H), 1.96 – 1.87 (m, 1H), 1.80 (ddd, J = 13.3, 7.4, 3.5 Hz, 1H), 1.71 – 1.57 (m, 2H), 1.42 (s, 3H), 1.51 – 1.20 (m, 4H), 1.27 (t, J = 7.1 Hz, 3H), 0.96 (d, J = 6.0 Hz, 3H), 1.01 – 0.92 (m, 1H) and 0.87 (d, J = 7.5 Hz, 3H); ^{13}C NMR (100 MHz, CDCl_3) δ 171.8, 103.4, 89.2, 81.0, 71.8, 60.8, 52.4, 44.3, 37.6, 36.6, 36.2, 34.6, 29.8, 26.1, 24.8, 24.8, 20.3, 14.3 and 13.2; IR ν_{max} (neat)/ cm^{-1} 3212, 2973 (CH), 2956, 2949, 2935, 2919, 2874, 2852, 1734 (C=O) and 1056 (C-O-C); HRMS (ESI) calculated for $\text{C}_{19}\text{H}_{30}\text{O}_6$ $[\text{M}+\text{Na}]^+$ 377.1940 found 377.1934.

Preparation of ethyl [(2*R*,3*R*,3*aS*,6*R*,6*aS*,10*aR*,10*bR*)-3,6,9-trimethyldecahydro-9,10*b*-epoxyoxepino[4,3,2-*ij*]isochromen-2(10*aH*)-yl]acetate (**66**)



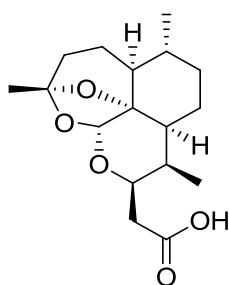
Preparation of activated zinc dust: Zinc dust (2.00 g) was activated by washing with hydrochloric acid (5%, v/v, 3 x 50 mL), water (3 x 50 mL) and diethyl ether (3 x 50 mL). Zinc dust was dried under reduced atmosphere.

65 (559.2 mg, 1.58 mmol) was dissolved in acetic acid (50 mL). Activated zinc dust (3 x 154.7 mg, 2.37 mmol) was added in triplicate over 72 hours at 24 hour periods to the reaction and left to stir at room temperature. The reaction was diluted with DCM and filtered through a pad of celite. NaHCO₃ was used to neutralise the solution and the organic layer and removed. Organic layer was washed with NaHCO₃, water, brine, dried over magnesium sulfate and filtered. The reaction was concentrated under reduced pressure to give the crude product in which purification by flash chromatography using 10% ethyl acetate in hexane to give the title compound **66** (203.7 mg, 38%) as a white solid; R_f = 0.29; 10% ethyl acetate in hexane; ¹H NMR (400 MHz, CDCl₃) δ 5.24 (s, 1H), 4.64 (dt, *J* = 8.4, 6.7 Hz, 1H), 4.34 – 4.03 (m, 2H), 2.52 – 2.39 (m, 2H), 2.38 – 2.26 (m, 1H), 2.00 – 1.91 (m, 1H), 1.90 – 1.82 (m, 1H), 1.81 – 1.66 (m, 3H), 1.64 – 1.53 (m, 1H), 1.56 (s, 3H), 1.27 (t, *J* = 7.1 Hz, 3H), 1.36 – 1.10 (m, 4H), 1.06 – 0.79 (m, 1H), 0.89 (d, *J* = 5.8 Hz, 3H) and 0.86 (d, *J* =

Chapter 5 – Design and synthesis of click functionalised derivatives of artemisinin and CDDO as probes for investigating chemical mechanism of action

7.6 Hz, 3H); ^{13}C NMR (100 MHz, CDCl_3) δ 171.6, 107.1, 97.0, 82.4, 65.8, 60.4, 45.3, 40.3, 37.5, 35.5, 34.5, 34.5, 29.0, 25.0, 23.6, 22.2, 18.8, 14.2 and 12.4; IR ν_{max} (neat)/ cm^{-1} 2952 (CH), 2873, 1737 (C=O), 1093 (C-O-C), 1008 (C-O-C); HRMS (ESI) calculated for $\text{C}_{19}\text{H}_{30}\text{O}_5$ $[\text{M}+\text{Na}]^+$ 361.1991 found 361.1997.

Preparation of [(2*R*,3*R*,3*aS*,6*R*,6*aS*,10*aR*,10*bR*)-3,6,9-trimethyldecahydro-9,10*b*-epoxy oxepino[4,3,2-*ij*]isochromen-2(10*aH*)-yl]acetic acid (**67**)

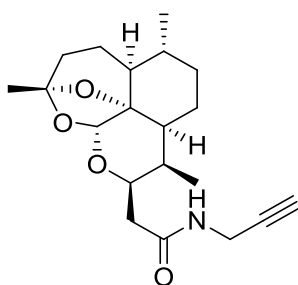


66 (194 mg, 573 μmol) was dissolved in ethanol (25 mL). Sodium hydroxide (25 mL, 15%, w/v) was added to the reaction and left to stir for 3 hours at room temperature. The reaction was acidified with hydrochloric acid (1 M) and the ethanol was removed. Aqueous layer was extracted with DCM (3 x 50 mL). The combined organic layers were dried over magnesium sulfate, filtered and concentrated under reduced pressure to give the crude product. The crude product was purified by flash chromatography using 50% ethyl acetate in hexane to give the title compound **67** (142 mg, 80%) as a white solid; R_f = 0.26; 50% ethyl acetate in hexane; ^1H NMR (400 MHz, CDCl_3) δ 5.27 (s, 1H), 4.62 (dd, J = 14.3, 7.3 Hz, 1H), 2.59 – 2.43 (m, 2H), 2.34 (dd, J = 15.4, 7.7 Hz, 1H), 2.03 – 1.91 (m, 1H), 1.86 (dd, J = 9.7, 5.2 Hz, 1H), 1.82 – 1.74 (m, 1H), 1.73 – 1.66 (m, 2H), 1.62 (t, J = 5.6 Hz, 1H), 1.54 (s, 3H), 1.33 – 1.12 (m, 5H), 0.97 (dd, J = 13.8, 10.8 Hz, 1H), 0.89 (d, J = 5.9 Hz, 3H) and

Chapter 5 – Design and synthesis of click functionalised derivatives of artemisinin and CDDO as probes for investigating chemical mechanism of action

0.88 (d, $J = 7.9$ Hz, 3H); ^{13}C NMR (100 MHz, CDCl_3) δ 176.6, 107.6, 97.0, 82.6, 65.7, 45.4, 40.3, 37.3, 35.7, 34.6, 34.5, 29.1, 25.2, 23.7, 22.3, 18.9 and 12.5; IR ν_{max} (neat)/ cm^{-1} 3210 (br, OH), 2951 (CH), 2933, 2873, 1735 (C=O), 1710, 1094 (C-O-C), 1009; HRMS (ESI) calculated for $\text{C}_{17}\text{H}_{26}\text{O}_5$ $[\text{M}+\text{Na}]^+$ 333.1678 found 333.1672.

Preparation of *N*-(prop-2-yn-1-yl)-2-[(2*R*,3*R*,3*aS*,6*R*,6*aS*,10*aR*,10*bR*)-3,6,9-trimethyldeca-hydro-9,10*b*-epoxyoxepino[4,3,2-*ij*]isochromen-2(10*aH*)-yl]acetamide (**68**)



The preparation of **68** involved the use of acid **67** (141.5 mg, 455.9 μmol), propargylamine (87.6 μL , 1.37 mmol), EDCI (212.3 mg, 1.37 mmol) and DMAP (278.5 mg, 2.28 mmol) following general procedure 1. Purification of the crude product by flash chromatography using 50% ethyl acetate in hexane to give title compound **68** (53.7 mg, 34%) as a white solid; $R_f = 0.34$, 50% ethyl acetate in hexane; mp = 119-120 $^\circ\text{C}$; ^1H NMR (400 MHz, CDCl_3) δ 6.98 (s, 1H), 5.32 (s, 1H), 4.54 (ddd, $J = 10.0, 6.9, 3.1$ Hz, 1H), 4.13 (ddd, $J = 17.5, 5.8, 2.5$ Hz, 1H), 3.98 (ddd, $J = 17.5, 4.9, 2.5$ Hz, 1H), 2.40 – 2.37 (m, 1H), 2.31 – 2.21 (m, 1H), 2.19 (t, $J = 2.5$ Hz, 1H), 1.99 (ddd, $J = 13.1, 8.7, 4.1$ Hz, 1H), 1.93 – 1.86 (m, 1H), 1.85 – 1.77 (m, 1H), 1.76 – 1.67 (m, 2H), 1.66 – 1.56 (m, 1H), 1.55 (s, 3H), 1.36 – 1.11 (m, 6H), 0.91 (d, $J = 5.9$ Hz, 3H) and 0.87 (d, $J = 7.6$ Hz, 3H); ^{13}C NMR (100 MHz, CDCl_3) δ 171.5, 107.9, 97.3, 82.7, 80.0, 71.1, 65.2, 45.3, 39.9, 38.1, 35.7, 34.5, 29.7, 28.9, 25.4, 23.8, 22.3,

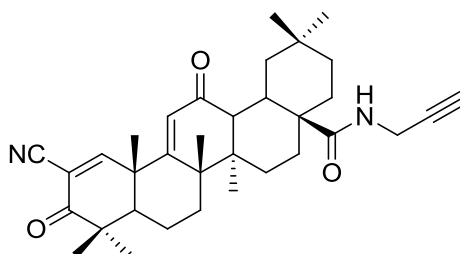
Chapter 5 – Design and synthesis of click functionalised derivatives of artemisinin and CDDO as probes for investigating chemical mechanism of action

18.9 and 11.9; IR ν_{max} (neat)/ cm^{-1} 3358 ($\equiv\text{C}-\text{H}$), 3318 (CONH), 2962 (CH), 2932, 2875, 1683 (CONH), 1076 (C-O-C) and 1007; HRMS (ESI) calculated for $\text{C}_{20}\text{H}_{29}\text{NO}_4$ $[\text{M}+\text{Na}]^+$ 348.2175 found 348.2177.

5.4.8 Synthesis of CDDO click probes

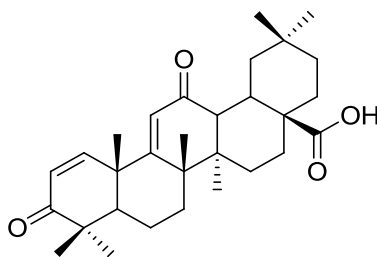
Preparation of 2-cyano-3,12-dioxo-*N*-(prop-2-yn-1-yl)oleana-1,9(11)-dien-28-amide

(71)



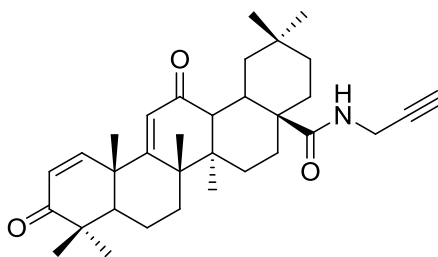
For the synthesis of **8** see section 2.4.7. The preparation of **71** involved the use of acid **8** (86 mg, 174.9 μmol), propargylamine (33.6 μL , 524.8 μmol), EDCI (81.5 mg, 524.8 μmol) and DMAP (106.9 mg, 874.6 μmol) following general procedure 1. Purification of the crude product by flash chromatography using 50% ethyl acetate in hexane to give title compound **71** (30.8 mg, 33%) as a white solid; $R_f = 0.32$, 50% ethyl acetate in hexane; mp = 256-258°C; ^1H NMR (400 MHz, CDCl_3) δ 8.09 (s, 1H), 6.10 (t, $J = 5.4$ Hz, 1H), 6.00 (s, 1H), 4.07 (dd, $J = 5.4, 2.5$ Hz, 2H), 3.08 (d, $J = 4.5$ Hz, 1H), 2.90 (dd, $J = 9.8, 3.0$ Hz, 1H), 2.18 (t, $J = 2.5$ Hz, 1H), 2.04 – 1.95 (m, 1H), 1.88 – 1.53 (m, 10H), 1.49 (s, 3H), 1.36 (s, 3H), 1.26 (s, 3H), 1.33 – 1.19 (m, 4H), 1.17 (s, 3H), 1.02 (s, 3H), 1.00 (s, 3H) and 0.91 (s, 3H); ^{13}C NMR (100 MHz, CDCl_3) δ 199.2, 196.7, 177.0, 169.0, 166.0, 124.1, 114.7, 114.5, 80.3, 71.3, 49.6, 47.8, 46.6, 46.1, 45.1, 42.7, 42.2, 36.1, 34.6, 33.9, 33.4, 32.0, 31.8, 30.7, 29.3, 27.8, 27.1, 26.7, 25.0, 23.2, 23.1, 21.9, 21.7 and 18.4; IR ν_{max} (neat)/ cm^{-1} 3306 ($\equiv\text{C}-\text{H}$), 2926 (CH), 2865, 2360 (CN), 2341, 1733 (C=O), 1687 (CONH) and 1659; HRMS (ESI) calculated for $\text{C}_{34}\text{H}_{44}\text{N}_2\text{O}_3$ $[\text{M}+\text{Na}]^+$ 551.3250 found 551.3249.

Preparation of 3,12-dioxooleana-1,9(11)-dien-28-oic acid (**72**)³⁹



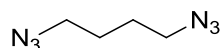
For the synthesis of **21** see section 3.4.6. **21** (116 mg, 241 μmol) was dissolved in anhydrous DMF. Lithium iodide (613.7 mg, 4.59 mmol) was added to the reaction and left to reflux overnight. The reaction was cooled and water (50 mL) was added. 5% HCl was added to the solution and washed with ethyl acetate (3 x 50 mL). Combined organic layers were washed with water (3 x 50 mL), brine (3 x 50 mL) and dried over magnesium sulfate. The solution was filtered and the solvent was removed under vacuum. The crude product was purified by flash chromatography using 50% ethyl acetate in hexane to give the title compound **72** (100.3 mg, 89%) as a hygroscopic white solid; $R_f = 0.35$, 50% ethyl acetate in hexane; $^1\text{H NMR}$ (400 MHz, CDCl_3) δ 7.33 (d, $J = 10.6$ Hz, 1H), 6.02 (s, 1H), 5.93 (d, $J = 10.4$ Hz, 1H), 3.97 (s, 1H), 3.17 – 2.88 (m, 2H), 2.05 (s, 2H), 1.93 (s, 2H), 1.75 (s, 7H), 1.55 (dd, $J = 25.5, 11.6$ Hz, 4H), 1.41 (s, 3H), 1.33 (s, 3H), 1.20 (s, 3H), 1.12 (s, 3H), 1.02 (s, 3H), 1.01 (s, 3H) and 0.90 (s, 3H); $^{13}\text{C NMR}$ (100 MHz, CDCl_3) δ 203.7, 199.6, 183.6, 171.7, 154.9, 126.0, 123.7, 49.8, 48.4, 47.2, 45.8, 44.8, 42.1, 41.9, 35.8, 34.5, 33.3, 33.0, 32.2, 31.6, 30.8, 28.1, 27.2, 27.0, 24.7, 23.2, 22.6, 21.8, 21.7 and 18.5; IR ν_{max} (neat)/ cm^{-1} 3206 (br, OH), 2939 (CH), 2871, 1722 (C=O), 1690 (C=O) and 1660; HRMS (ESI) calculated for $\text{C}_{30}\text{H}_{42}\text{O}_4$ $[\text{M}+\text{Na}]^+$ 489.2981 found 489.2979.

Preparation of 3,12-dioxo-*N*-(prop-2-yn-1-yl)oleana-1,9(11)-dien-28-amide (**73**)



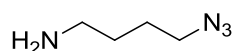
The preparation of **73** involved the use of acid **72** (89.6 mg, 192.0 μmol), propargylamine (36.9 μL , 576.0 μmol), EDCI (89.4 mg, 576.0 μmol) and DMAP (117.3 mg, 960.0 μmol) following general procedure 1. Purification of the crude product by flash chromatography using 50% ethyl acetate in hexane to give title compound **73** (38.4 mg, 40%) as a white solid; $R_f = 0.47$, 50% ethyl acetate in hexane; mp = 136-137°C; ^1H NMR (400 MHz, CDCl_3) δ 7.33 (d, $J = 10.6$ Hz, 1H), 6.10 (t, $J = 5.3$ Hz, 1H), 6.01 (s, 1H), 5.93 (d, $J = 10.4$ Hz, 1H), 4.07 (dd, $J = 5.4, 2.5$ Hz, 2H), 3.04 (d, $J = 4.4$ Hz, 1H), 2.89 (d, $J = 13.0$ Hz, 1H), 2.18 (t, $J = 2.5$ Hz, 1H), 2.00 (td, $J = 13.8, 3.7$ Hz, 1H), 1.87 – 1.56 (m, 11H), 1.54 – 1.45 (m, 3H), 1.42 (s, 3H), 1.34 (s, 3H), 1.19 (s, 3H), 1.12 (s, 3H), 1.02 (s, 3H), 1.00 (s, 3H) and 0.90 (s, 3H); ^{13}C NMR (100 MHz, CDCl_3) δ 203.6, 199.8, 177.1, 172.1, 154.9, 126.0, 123.6, 80.2, 71.3, 49.5, 48.4, 46.7, 46.0, 44.8, 42.2, 41.9, 36.2, 34.7, 34.0, 33.4, 32.2, 32.0, 30.7, 29.3, 27.9, 27.2, 27.0, 25.0, 23.3, 23.1, 21.9, 21.8 and 18.5; IR ν_{max} (neat)/ cm^{-1} 3343 ($\equiv\text{C}-\text{H}$), 3308 (CONH), 2937 (CH), 2868, 1731 (C=C) and 1657 (CONH); HRMS (ESI) calculated for $\text{C}_{33}\text{H}_{45}\text{NO}_3$ $[\text{M}+\text{Na}]^+$ 526.3297 found 526.3292.

Preparation of 1,4-diazidobutane (**76**)⁴⁰



Sodium azide (632.3 mg, 9.73 mmol) in water was added to a solution of **75** (553.1 μ L, 4.63 mmol) in DMF (5 mL). The reaction was heated to 80°C and left to stir for 20 hours. The reaction was cooled and brine was added to the reaction. The mixture was extracted with hexane (3 x 50 mL) and combined organic layers were dried over magnesium sulfate and filtered. The solvent was removed under reduced pressure to yield title compound **76** (649.1 mg, 100%) as a colourless oil; ¹H NMR (400 MHz, CDCl₃) δ 3.32 (t, J = 5.6 Hz, 4H) and 1.67 (dt, J = 5.4, 3.2 Hz, 4H); ¹³C NMR (100 MHz, CDCl₃) δ 50.9 and 26.1. Cannot obtain MS due to fragmentation: MS (CI) [C₄H₈N₂+H]⁺ m/z 85.1.

Preparation of 4-azidobutan-1-amine (**77**)^{40,41}

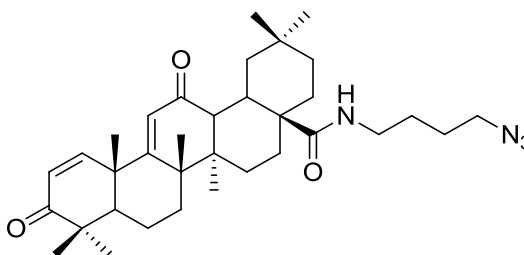


Hydrochloric acid (20 mL, 1 M) was added to a solution of **76** (649.1 mg, 4.63 mmol) in ethyl acetate:diethyl ether (1:1, 20 mL). The reaction was cooled to 0°C and triphenylphosphine (1.21 g, 4.63 mmol) was added to the reaction in portions. The reaction was left to stir at room temperature overnight. The organic layer was removed using separating funnel and aqueous layer is washed with ethyl acetate (2 x 50 mL). The aqueous layer was basified to pH 12 with aqueous sodium hydroxide solution and extracted with DCM (3 x 20 mL). The combined organic layers were dried over magnesium sulfate, filtered and solvent was removed under reduced pressure to give title compound **77** (488 mg, 92%) as a colourless oil; ¹H NMR (400

Chapter 5 – Design and synthesis of click functionalised derivatives of artemisinin and CDDO as probes for investigating chemical mechanism of action

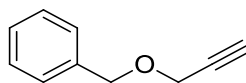
MHz, CDCl₃) δ 3.36 – 3.22 (m, 4H, diazido form), 2.73 (t, *J* = 6.9 Hz, 2H) and 1.72 – 1.47 (m, 6H, 4H, diazido form); ¹³C NMR (100 MHz, CDCl₃) δ 51.4, 41.8, 30.9 and 26.4; HRMS (CI+) calculated for C₄H₁₀N₄ [M+H]⁺ 115.0978 found 115.0983.

Preparation of *N*-(4-azidobutyl)-3,12-dioxooleana-1,9(11)-dien-28-amide (**74**)



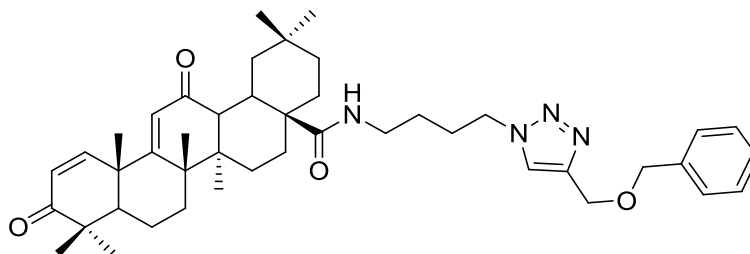
The preparation of **74** involved the use of acid **72** (89 mg, 190.7 μmol), **77** (65.31 mg, 572.2 μmol), EDCI (88.8 mg, 572.2 μmol) and DMAP (116.5 mg, 953.6 μmol) following general procedure 1. Purification of the crude product by flash chromatography using 50% ethyl acetate in hexane to give title compound **74** (41 mg, 38%) as a white solid; *R_f* = 0.35, 50% ethyl acetate in hexane; mp = 130-131°C; ¹H NMR (400 MHz, CDCl₃) δ 7.32 (d, *J* = 10.5 Hz, 1H), 6.01 (s, 1H), 5.92 (d, *J* = 10.4 Hz, 1H), 3.38 – 3.23 (m, 4H), 3.01 (d, *J* = 4.4 Hz, 1H), 2.86 (dt, *J* = 7.5, 4.0 Hz, 1H), 1.97 (td, *J* = 13.6, 3.5 Hz, 1H), 1.85 – 1.14 (m, 29H), 1.42 (s, 3H), 1.32 (s, 3H), 1.19 (s, 3H), 1.12 (s, 3H), 1.02 (s, 3H), 1.00 (s, 3H) and 0.90 (s, 3H); ¹³C NMR (100 MHz, CDCl₃) δ 203.6, 199.9, 177.4, 172.1, 154.8, 126.0, 123.6, 51.2, 49.6, 48.4, 46.7, 45.9, 44.8, 42.2, 41.9, 39.1, 36.3, 34.7, 34.3, 33.4, 32.2, 32.2, 30.7, 27.9, 27.3, 27.2, 27.0, 26.5, 24.9, 23.3, 23.1, 21.9, 21.8 and 18.5; IR *v*_{max} (neat)/cm⁻¹ 3355 (CONH), 2930 (CH), 2865, 2162 (N₃) and 1658 (C=O); HRMS (ESI) calculated for C₃₄H₅₀N₄O₃ [M+Na]⁺ 585.3781 found 585.3783; Microanalysis Calculated for C₃₄H₅₀N₄O₃ requires C 72.56%, H 8.95%, N 9.96%, found C 72.40%, H 9.26%, N 8.79%.

Preparation of benzyl propargyl ether (**80**)⁴²



Sodium hydride (148.0 mg, 3.70 mmol, 60%) was washed with hexane (5 mL) under an anhydrous nitrogen atmosphere. Anhydrous THF (30 mL) was added to the sodium hydride and the reaction was cooled to 0°C. Benzyl alcohol (382.8 μ L, 3.70 mmol) was added to the reaction and left to stir for 30 minutes. Propargyl bromide (432.6 μ L, 3.88 mmol, 80%) was added dropwise and left to stir for 5 minutes prior to warming to room temperature. The reaction was left to stir for a further 1 hour at room temperature. The reaction was quenched with sodium sulphate, filtered through a pad of celite and washed with ethyl acetate. The solvent was removed under vacuum to give the crude product which was purified by flash chromatography using 30% ethyl acetate in hexane to give the title compound **80** (400 mg, 74%) as a yellow oil; R_f = 0.76, 30% ethyl acetate in hexane; ^1H NMR (400 MHz, CDCl_3) δ 7.36 – 7.31 (m, 4H), 7.31 – 7.24 (m, 1H), 4.58 (s, 2H), 4.14 (d, J = 2.4 Hz, 2H) and 2.45 (t, J = 2.4 Hz, 1H); ^{13}C NMR (100 MHz, CDCl_3) δ 137.3, 128.4, 128.1, 127.9, 79.7, 74.7, 71.4 and 57.0; MS (CI) $\text{C}_{10}\text{H}_{10}\text{O}$ $[\text{M}+\text{NH}_4]^+$ m/z 164.1075.

Preparation of *N*-(4-(4-((benzyloxy)methyl)-1*H*-1,2,3-triazol-1-yl)butyl)-3,12-dioxooleana-1,9(11)-dien-28-amide (**81**)



74 (41 mg, 72.85 μmol) was dissolved in DCM:water (1:1, 4 mL). **80** (11.7 mg, 80.14 μmol), copper(II) sulphate pentahydrate (909.5 μg , 3.64 μmol) and sodium ascorbate (2.16 mg, 10.93 μmol) was added to the reaction and left to stir for 2 hours. The reaction was extracted with DCM (3 x 20 mL) and washed with water, brine and dried over magnesium sulfate. The solvent was removed under vacuum to give the crude product which was purified by flash chromatography using 40% ethyl acetate in hexane to give the title compound **81** (20.5 mg, 40%) as a white solid; $R_f = 0.03$, 50% ethyl acetate in hexane; ^1H NMR (400 MHz, CDCl_3) δ 7.56 (s, 1H), 7.41 – 7.28 (m, 6H), 5.99 (s, 1H), 5.93 (dd, $J = 12.4, 8.2$ Hz, 2H), 4.68 (s, 2H), 4.61 (s, 2H), 4.38 (t, $J = 7.0$ Hz, 2H), 3.31 (dd, $J = 13.2, 6.6$ Hz, 2H), 2.99 (d, $J = 4.3$ Hz, 1H), 2.87 (d, $J = 13.2$ Hz, 1H), 2.02 – 1.87 (m, 1H), 1.83 – 1.06 (m, 18H), 1.40 (s, 3H), 1.27 (s, 3H), 1.18 (s, 3H), 1.11 (s, 3H), 1.01 (s, 3H), 0.99 (s, 3H) and 0.89 (s, 3H); ^{13}C NMR (100 MHz, CDCl_3) δ 203.6, 199.8, 177.6, 172.0, 154.8, 145.5, 137.9, 128.6, 128.0, 127.9, 126.0, 123.6, 122.6, 72.8, 63.9, 49.8, 49.6, 48.4, 46.7, 45.9, 44.8, 42.1, 41.9, 38.8, 36.2, 34.7, 34.4, 33.4, 32.2, 32.1, 30.7, 27.9, 27.8, 27.2, 27.0, 27.0, 24.9, 23.3, 23.1, 21.8, 21.8 and 18.5; HRMS (ESI) calculated for $\text{C}_{44}\text{H}_{60}\text{N}_4\text{O}_4$ $[\text{M}+\text{Na}]^+$ 731.4512 found 731.4516.

5.5 Biological experimental

5.5.1 Materials

See section 3.5.1

5.5.2 Cell culture

See section 2.5.2

5.5.3 Plating

See section 2.5.3

5.5.4 Treatment of cells for luciferase activity assay.

See section 2.5.5

5.5.5 Preparation of cells for luciferase reporter assay

See section 2.5.6

5.6 Reference

- 1 Bantscheff, M., Scholten, A. & Heck, A. J. R. Revealing promiscuous drug–target interactions by chemical proteomics. *Drug Discovery Today* **14**, 1021-1029, doi:10.1016/j.drudis.2009.07.001 (2009).
- 2 Schenone, M., Dancik, V., Wagner, B. K. & Clemons, P. A. Target identification and mechanism of action in chemical biology and drug discovery. *Nature Chemical Biology* **9**, 232-240 (2013).
- 3 Ong, S.-E., Schenone, M., Margolin, A. A., Li, X., Do, K., Doud, M. K., Mani, D. R., Kuai, L., Wang, X., Wood, J. L., Tolliday, N. J., Koehler, A. N., Marcaurelle, L. A., Golub, T. R., Gould, R. J., Schreiber, S. L. & Carr, S. A. Identifying the proteins to which small-molecule probes and drugs bind in cells. *Proceedings of the National Academy of Sciences* **106**, 4617-4622, doi:10.1073/pnas.0900191106 (2009).
- 4 Serim, S., Haedke, U. & Verhelst, S. H. L. Activity-Based Probes for the Study of Proteases: Recent Advances and Developments. *ChemMedChem* **7**, 1146-1159, doi:10.1002/cmdc.201200057 (2012).
- 5 Holmberg, A., Blomstergren, A., Nord, O., Lukacs, M., Lundeberg, J. & Uhlén, M. The biotin-streptavidin interaction can be reversibly broken using water at elevated temperatures. *Electrophoresis* **26**, 501-510, doi:10.1002/elps.200410070 (2005).
- 6 Liu, Y., Patricelli, M. P. & Cravatt, B. F. Activity-based protein profiling: The serine hydrolases. *Proceedings of the National Academy of Sciences* **96**, 14694-14699, doi:10.1073/pnas.96.26.14694 (1999).
- 7 Greenbaum, D., Medzihradzky, K. F., Burlingame, A. & Bogyo, M. Epoxide electrophiles as activity-dependent cysteine protease profiling and discovery tools. *Chemistry & Biology* **7**, 569-581, doi:10.1016/S1074-5521(00)00014-4 (2000).
- 8 Geurink, P., Prely, L., van der Marel, G., Bischoff, R. & Overkleeft, H. in *Activity-Based Protein Profiling Vol. 324 Topics in Current Chemistry* (ed Stephan A. Sieber) Ch. 286, 85-113 (Springer Berlin Heidelberg, 2012).
- 9 Sakakibara, K., Saito, N., Sato, T., Suzuki, A., Hasegawa, Y., Friedman, J. M., Kufe, D. W., VonHoff, D. D., Iwami, T. & Kawabe, T. CBS9106 is a novel reversible oral CRM1 inhibitor with CRM1 degrading activity. *Blood* **118**, 3922-3931 (2011).
- 10 Vodovozova, E. L. Photoaffinity labeling and its application in structural biology. *Biochemistry (Moscow)* **72**, 1-20, doi:10.1134/S0006297907010014 (2007).
- 11 Dubinsky, L., Krom, B. P. & Meijler, M. M. Diazirine based photoaffinity labeling. *Bioorganic & Medicinal Chemistry* **20**, 554-570, doi:10.1016/j.bmc.2011.06.066 (2012).
- 12 Daniels, J. T., Cambrey, A. D., Occleston, N. L., Garrett, Q., Tarnuzzer, R. W., Schultz, G. S. & Khaw, P. T. Matrix Metalloproteinase Inhibition Modulates Fibroblast-Mediated Matrix Contraction and Collagen Production In Vitro. *Investigative Ophthalmology & Visual Science* **44**, 1104-1110, doi:10.1167/iovs.02-0412 (2003).

- 13 Barton, V., Ward, S. A., Chadwick, J., Hill, A. & O'Neill, P. M. Rationale Design of Biotinylated Antimalarial Endoperoxide Carbon Centered Radical Prodrugs for Applications in Proteomics. *Journal of Medicinal Chemistry* **53**, 4555-4559, doi:10.1021/jm100201j (2010).
- 14 Liby, K., Hock, T., Yore, M. M., Suh, N., Place, A. E., Risingsong, R., Williams, C. R., Royce, D. B., Honda, T., Honda, Y., Gribble, G. W., Hill-Kapturczak, N., Agarwal, A. & Sporn, M. B. The Synthetic Triterpenoids, CDDO and CDDO-Imidazolide, Are Potent Inducers of Heme Oxygenase-1 and Nrf2/ARE Signaling. *Cancer Research* **65**, 4789-4798, doi:10.1158/0008-5472.can-04-4539 (2005).
- 15 Meshnick, S. R. Artemisinin: mechanisms of action, resistance and toxicity. *International Journal for Parasitology* **32**, 1655-1660, doi:10.1016/S0020-7519(02)00194-7 (2002).
- 16 Couch, R. D., Browning, R. G., Honda, T., Gribble, G. W., Wright, D. L., Sporn, M. B. & Anderson, A. C. Studies on the reactivity of CDDO, a promising new chemopreventive and chemotherapeutic agent: implications for a molecular mechanism of action. *Bioorganic & Medicinal Chemistry Letters* **15**, 2215-2219, doi:10.1016/j.bmcl.2005.03.031 (2005).
- 17 O'Neill, P. M., Amewu, R. K., Nixon, G. L., Bousejra ElGarah, F., Mungthin, M., Chadwick, J., Shone, A. E., Vivas, L., Lander, H., Barton, V., Muangnoicharoen, S., Bray, P. G., Davies, J., Park, B. K., Wittlin, S., Brun, R., Preschel, M., Zhang, K. & Ward, S. A. Identification of a 1,2,4,5-Tetraoxane Antimalarial Drug-Development Candidate (RKA 182) with Superior Properties to the Semisynthetic Artemisinins. *Angewandte Chemie International Edition* **49**, 5693-5697, doi:10.1002/anie.201001026 (2010).
- 18 Honda, T., Janosik, T., Honda, Y., Han, J., Liby, K. T., Williams, C. R., Couch, R. D., Anderson, A. C., Sporn, M. B. & Gribble, G. W. Design, Synthesis, and Biological Evaluation of Biotin Conjugates of 2-Cyano-3,12-dioxooleana-1,9(11)-dien-28-oic Acid for the Isolation of the Protein Targets. *Journal of Medicinal Chemistry* **47**, 4923-4932, doi:10.1021/jm049727e (2004).
- 19 Ahmad, R., Raina, D., Meyer, C., Kharbanda, S. & Kufe, D. Triterpenoid CDDO-Me Blocks the NF- κ B Pathway by Direct Inhibition of IKK β on Cys-179. *Journal of Biological Chemistry* **281**, 35764-35769, doi:10.1074/jbc.M607160200 (2006).
- 20 Ahmad, R., Raina, D., Meyer, C. & Kufe, D. Triterpenoid CDDO-Methyl Ester Inhibits the Janus-Activated Kinase-1 (JAK1) \rightarrow Signal Transducer and Activator of Transcription-3 (STAT3) Pathway by Direct Inhibition of JAK1 and STAT3. *Cancer Research* **68**, 2920-2926, doi:10.1158/0008-5472.can-07-3036 (2008).
- 21 Eckstein-Ludwig, U., Webb, R. J., van Goethem, I. D. A., East, J. M., Lee, A. G., Kimura, M., O'Neill, P. M., Bray, P. G., Ward, S. A. & Krishna, S. Artemisinins target the SERCA of Plasmodium falciparum. *Nature* **424**, 957-961, doi:10.1038/nature01813 (2003).
- 22 Speers, A. E., Adam, G. C. & Cravatt, B. F. Activity-Based Protein Profiling in Vivo Using a Copper(I)-Catalyzed Azide-Alkyne [3 + 2] Cycloaddition. *Journal of the American Chemical Society* **125**, 4686-4687, doi:10.1021/ja034490h (2003).

- 23 Kolb, H. C., Finn, M. G. & Sharpless, K. B. Click Chemistry: Diverse Chemical Function from a Few Good Reactions. *Angewandte Chemie International Edition* **40**, 2004-2021, doi:10.1002/1521-3773(20010601)40:11<2004::AID-ANIE2004>3.0.CO;2-5 (2001).
- 24 Jones, G. O., Ess, D. H. & Houk, K. N. Activation Energies and Reaction Energetics for 1,3-Dipolar Cycloadditions of Hydrazoic Acid with C≡C and C≡N Multiple Bonds from High-Accuracy and Density Functional Quantum Mechanical Calculations. *Helvetica Chimica Acta* **88**, 1702-1710, doi:10.1002/hlca.200590134 (2005).
- 25 Rostovtsev, V. V., Green, L. G., Fokin, V. V. & Sharpless, K. B. A Stepwise Huisgen Cycloaddition Process: Copper(I)-Catalyzed Regioselective “Ligation” of Azides and Terminal Alkynes. *Angewandte Chemie International Edition* **41**, 2596-2599, doi:10.1002/1521-3773(20020715)41:14<2596::AID-ANIE2596>3.0.CO;2-4 (2002).
- 26 Tornøe, C. W., Christensen, C. & Meldal, M. Peptidotriazoles on Solid Phase: [1,2,3]-Triazoles by Regiospecific Copper(I)-Catalyzed 1,3-Dipolar Cycloadditions of Terminal Alkynes to Azides. *The Journal of Organic Chemistry* **67**, 3057-3064, doi:10.1021/jo011148j (2002).
- 27 Thirumurugan, P., Matosiuk, D. & Jozwiak, K. Click Chemistry for Drug Development and Diverse Chemical–Biology Applications. *Chemical Reviews* **113**, 4905-4979, doi:10.1021/cr200409f (2013).
- 28 Baskin, J. M., Prescher, J. A., Laughlin, S. T., Agard, N. J., Chang, P. V., Miller, I. A., Lo, A., Codelli, J. A. & Bertozzi, C. R. Copper-free click chemistry for dynamic in vivo imaging. *Proceedings of the National Academy of Sciences* **104**, 16793-16797, doi:10.1073/pnas.0707090104 (2007).
- 29 Mah, R., Thomas, J. R. & Shafer, C. M. Drug discovery considerations in the development of covalent inhibitors. *Bioorganic & Medicinal Chemistry Letters* **24**, 33-39, doi:10.1016/j.bmcl.2013.10.003 (2014).
- 30 Hindley, S., Ward, S. A., Storr, R. C., Searle, N. L., Bray, P. G., Park, B. K., Davies, J. & O'Neill, P. M. Mechanism-Based Design of Parasite-Targeted Artemisinin Derivatives: Synthesis and Antimalarial Activity of New Diamine Containing Analogues. *Journal of Medicinal Chemistry* **45**, 1052-1063, doi:10.1021/jm0109816 (2002).
- 31 Haynes, Richard K., Chan, H.-W., Cheung, M.-K., Lam, W.-L., Soo, M.-K., Tsang, H.-W., Voerste, A. & Williams, Ian D. C-10 Ester and Ether Derivatives of Dihydroartemisinin – 10- α Artesunate, Preparation of Authentic 10- β Artesunate, and of Other Ester and Ether Derivatives Bearing Potential Aromatic Intercalating Groups at C-10. *European Journal of Organic Chemistry* **2002**, 113-132, doi:10.1002/1099-0690(20021)2002:1<113::AID-EJOC113>3.0.CO;2-N (2002).
- 32 O'Neill, P. M., Pugh, M., Stachulski, A. V., Ward, S. A., Davies, J. & Park, B. K. Optimisation of the allylsilane approach to C-10 deoxo carba analogues of dihydroartemisinin: synthesis and in vitro antimalarial activity of new, metabolically stable C-10 analogues. *Journal of the Chemical Society, Perkin Transactions 1*, 2682-2689, doi:10.1039/B104340B (2001).

- 33 Washburn, M. P., Wolters, D. & Yates, J. R. Large-scale analysis of the yeast proteome by multidimensional protein identification technology. *Nat Biotech* **19**, 242-247, doi:10.1038/85686 (2001).
- 34 Ishihama, Y., Oda, Y., Tabata, T., Sato, T., Nagasu, T., Rappsilber, J. & Mann, M. Exponentially Modified Protein Abundance Index (emPAI) for Estimation of Absolute Protein Amount in Proteomics by the Number of Sequenced Peptides per Protein. *Molecular & Cellular Proteomics* **4**, 1265-1272, doi:10.1074/mcp.M500061-MCP200 (2005).
- 35 Haynes, R. K., Cheu, K.-W., Tang, M. M.-K., Chen, M.-J., Guo, Z.-F., Guo, Z.-H., Coghi, P. & Monti, D. Reactions of Antimalarial Peroxides with Each of Leucomethylene Blue and Dihydroflavins: Flavin Reductase and the Cofactor Model Exemplified. *ChemMedChem* **6**, 279-291, doi:10.1002/cmdc.201000508 (2011).
- 36 Chadwick, J., Jones, M., Mercer, A. E., Stocks, P. A., Ward, S. A., Park, B. K. & O'Neill, P. M. Design, synthesis and antimalarial/anticancer evaluation of spermidine linked artemisinin conjugates designed to exploit polyamine transporters in Plasmodium falciparum and HL-60 cancer cell lines. *Bioorganic & Medicinal Chemistry* **18**, 2586-2597, doi:10.1016/j.bmc.2010.02.035 (2010).
- 37 Cloete, T. T., Krebs, H. J., Clark, J. A., Connelly, M. C., Orcutt, A., Sigal, M. S., Kiplin Guy, R. & N'Da, D. D. Antimalarial activity of 10-alkyl/aryl esters and -aminoethylethers of artemisinin. *Bioorganic Chemistry* **46**, 10-16, doi:10.1016/j.bioorg.2012.10.002 (2013).
- 38 Liu, Y., Wong, V. K.-W., Ko, B. C.-B., Wong, M.-K. & Che, C.-M. Synthesis and Cytotoxicity Studies of Artemisinin Derivatives Containing Lipophilic Alkyl Carbon Chains. *Organic Letters* **7**, 1561-1564, doi:10.1021/ol050230o (2005).
- 39 Honda, T., Rounds, B. V., Bore, L., Finlay, H. J., Favaloro, F. G., Suh, N., Wang, Y., Sporn, M. B. & Gribble, G. W. Synthetic Oleanane and Ursane Triterpenoids with Modified Rings A and C: A Series of Highly Active Inhibitors of Nitric Oxide Production in Mouse Macrophages†. *Journal of Medicinal Chemistry* **43**, 4233-4246, doi:10.1021/jm0002230 (2000).
- 40 Jung, M. E., Ouk, S., Yoo, D., Sawyers, C. L., Chen, C., Tran, C. & Wongvipat, J. Structure–Activity Relationship for Thiohydantoin Androgen Receptor Antagonists for Castration-Resistant Prostate Cancer (CRPC). *Journal of Medicinal Chemistry* **53**, 2779-2796, doi:10.1021/jm901488g (2010).
- 41 Su, Y.-H., Chiang, L.-W., Jeng, K.-C., Huang, H.-L., Chen, J.-T., Lin, W.-J., Huang, C.-W. & Yu, C.-S. Solution-phase parallel synthesis and screening of anti-tumor activities from fenbufen and ethacrynic acid libraries. *Bioorganic & Medicinal Chemistry Letters* **21**, 1320-1324, doi:10.1016/j.bmcl.2011.01.068 (2011).
- 42 Sammelson, R. E., Miller, R. B. & Kurth, M. J. Linear Tetraheterocycles Composed of Both Bidentate Diisoxazole and Bidentate Isoxazole–Furyl/Thienyl/Pyridyl Motifs¹. *The Journal of Organic Chemistry* **65**, 2225-2228, doi:10.1021/jo991551e (2000).

CHAPTER 6

Final conclusion and future work

Chapter 6

6.1. Final conclusions	284
6.2. Future work	288
6.2.1. Future work for the CDDO class	288
6.2.2. Future work for the endoperoxide class	290
6.3. References	292

6.1. Final conclusions

The major aim of this thesis was to produce novel chemical probes for the investigation and identification of molecular targets in biologically-relevant contexts. These probes were rationally designed based on knowledge of the pharmacophore and appropriate sites for chemical modification (Figure 6.1).

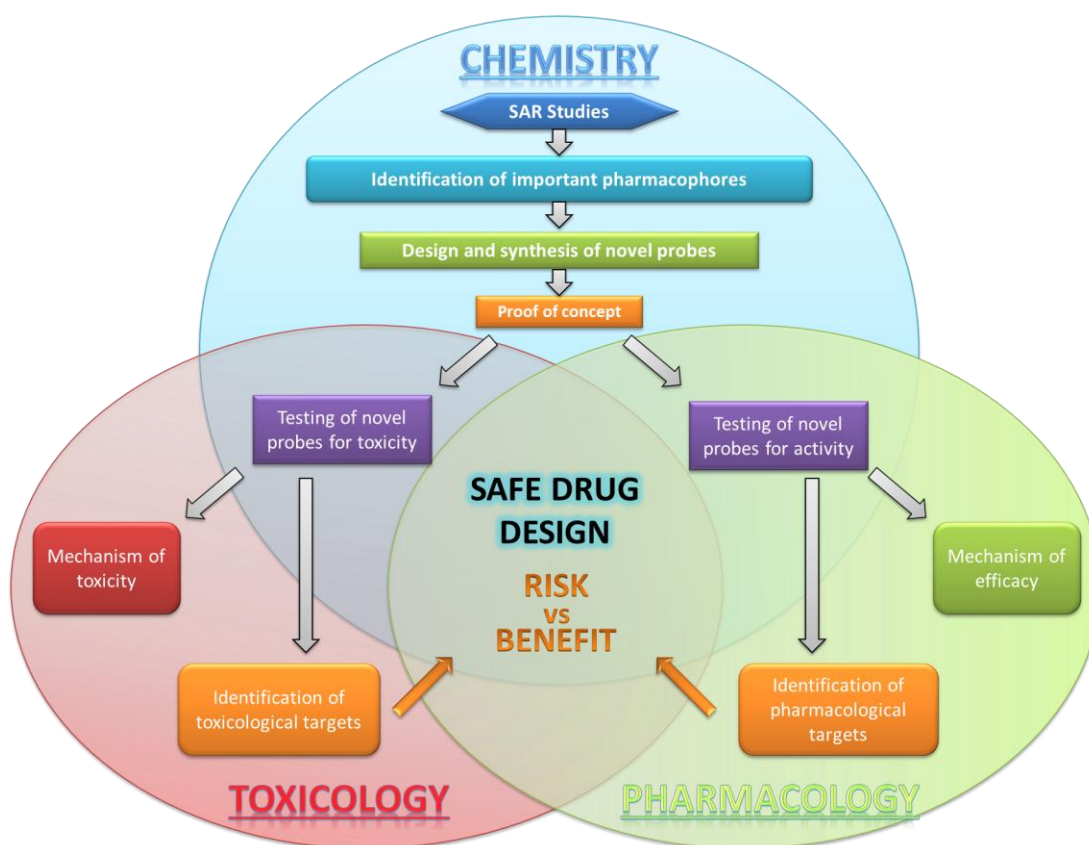


Figure 6.1: Flow diagram depicting the strategy adopted throughout this thesis for the successful development of chemical probes for biological target identification.

Specifically for the CDDO series, a SAR profile was generated *via* the synthetic modification of oleanolic acid. NMR and MS analyses enabled the identification of the active pharmacophore and candidate sites for chemical modification. This information, together with literature data on the endoperoxide (tetraoxanes and

artemisinins) antimalarials enabled the design and synthesis of a total of fifteen novel probes. These include DDO-Me and CDDO-Epoxyde (Figure 6.2), for which irreversible protein binding was demonstrated following reaction with the model protein GSTP1, further supporting the use of these probes to define the molecular targets of CDDO-Me and its derivatives in cells.

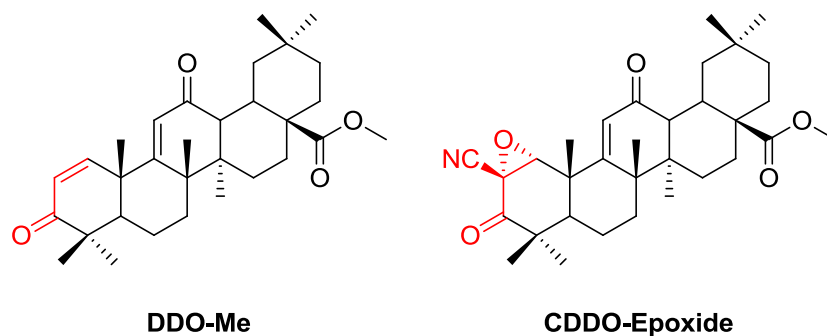


Figure 6.2: Chemical structures for DDO-Me and CDDO-Epoxyde included the highlighted pharmacophore responsible for irreversible binding.

Eight novel phenyl amide tetraoxane probes were also successfully synthesised and tested for their activity to inhibit the proliferation of *P. falciparum in vitro*. The tetraoxane probe **35** (Figure 6.3) was utilised for the examination of the role of ferrous iron and phosphatidylcholine in the bioactivation of this compound class.

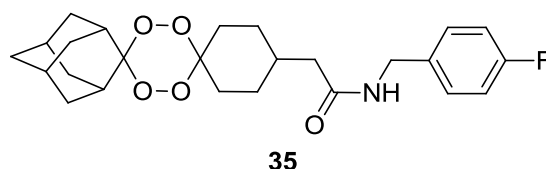


Figure 6.3: Chemical structure for tetraoxane probe **35**.

This has provided a deeper understanding of the radical formation induced by ferrous iron, and identified a potential novel molecular mechanism *via* the lipid-

peroxidation of phosphatidylcholine. Click functionalised probes (Figure 6.4) were also designed and synthesised.

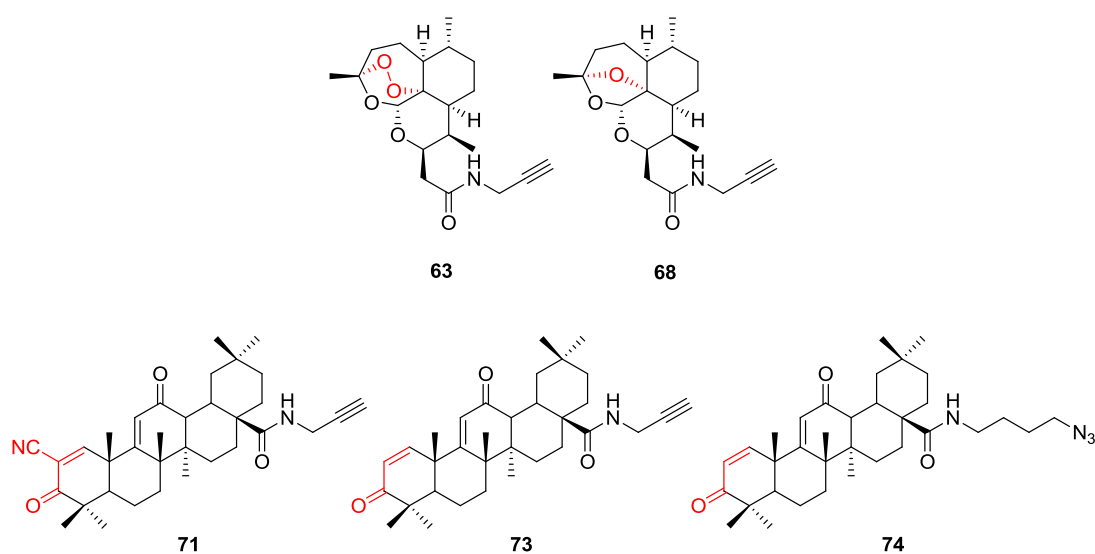


Figure 6.4: Chemical structures of click functionalised probes and their highlighted pharmacophores. Three in the CDDO class and two in the artemisinin class.

These probes could be used to identify protein targets and resolve mechanisms of action through traditional proteomic techniques that would have previously been difficult to use due to the harsh conditions required to elute drug-protein complexes for affinity matrices. Proof-of-concept of the ability of these probes to undergo the click reaction with a relevant counterpart has provided evidence of their utility as investigational tools. A summary of the strategy used is depicted in Figure 6.5.

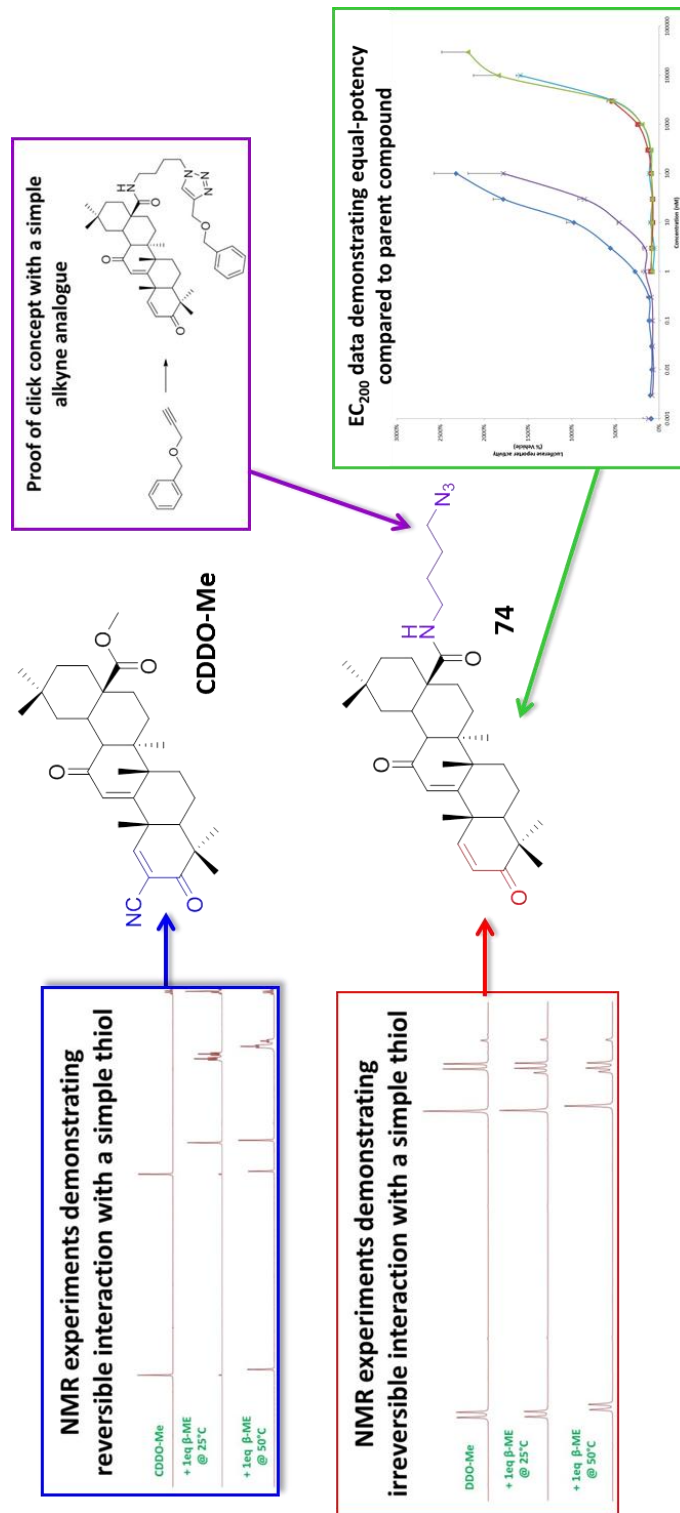


Figure 6.5: A summary of the strategy adopted to produce a viable click probe that will enable the investigation of molecular targets and mechanism of action.

6.2. Future work

The successful synthesis of irreversible probes will allow a range of previously unsuitable biological techniques to be used for the identification of molecular targets.

6.2.1. Future work for the CDDO class

Despite reports of a direct interaction of biotinylated CDDO derivatives with Cys-179 of IKK β ,¹ Cys-1077 of JAK1 and Cys-259 of STAT3,² the failure to identify direct targets responsible for the potency of these compounds as inducer of Nrf2 has raised questions about the chemical and molecular mechanism for this class and other small molecule Nrf2 inducers. As discussed in chapter 1, CDDO-Me failed phase III clinical trials (BEACON trial) for the treatment of advanced chronic kidney disease (CKD) due to serious adverse events and mortality in patients.^{3,4} It is now thought that CDDO-Me modulates the endothelin signalling pathway,⁵ resulting in fluid retention, raised blood pressure and cardiovascular failure in CKD patients. The effects are similar to those observed in CKD patients with endothelin receptor antagonists.⁵ Therefore, the adverse events associated with CDDO-Me do not appear to be related to Nrf2 *per se*, and are specific to advanced CKD patients. As a result, Nrf2 inducers continue to hold promise as novel drug candidates. Indeed, a new phase I clinical trial (LARIAT) of CDDO-Me for the treatment of pulmonary arterial hypertension (PAH) has been launched with the aim of targeting inflammation in PAH patients *via* the induction of Nrf2.^{6,7}

With a lack of clinical data, it is currently unclear whether the beneficial effects of CDDO-Me in CKD patients are linked to its ability to induce Nrf2. Understanding whether CDDO-Me specifically targets the endothelin pathway and whether other Nrf2 inducers have similar effects is important, as there is an urgent need for new therapies in CKD. Such knowledge would allow the design and development of more potent, specific and safe alternative inducers of Nrf2, which have potential applications in numerous diseases. Preliminary data indicates that CDDO-Epoxyde modifies six cysteine residues in Keap1. However, it is unclear whether the modification of one or more of these targets is directly responsible for the induction of Nrf2 by CDDO-Epoxyde and related compounds. With further work, it may be possible to refine the chemistry of a small molecule inducer to retain pharmacological efficacy and avoid undesirable interactions with off-target proteins, therefore minimising the risk of toxicity. For the induction of the Keap1-Nrf2 pathway the next question is 'is the induction of Nrf2 due to specific interaction with critical cysteines in Keap1?'. As there is an urgent need for new therapies in CKD, the CDDO-Epoxyde and click probes will be useful tools to investigate the exact targets within the endothelin pathway, further revealing the toxicological target(s) and mechanism(s) responsible for the ADRs. Depending on the data obtained a decision can be made based on the benefits vs risk of the use of triterpenoids in CKD, and indeed other relevant diseases. This information is also useful for the chemist, who can manipulate the chemical structure to selectively target the beneficial pharmacological pathway and potentially eliminate the toxicological effects.

6.2.2. Future work for the endoperoxide class

The endoperoxide class of antimalarial drugs are currently the front line treatment against multi-resistant strains of *P. falciparum* due to their broad stage specificity against the *Plasmodium* life cycle. The precise mechanism of action of these compounds is still highly controversial despite the identification of the endoperoxide as the active pharmacophore. There is strong evidence to suggest that the mechanism of action requires endoperoxide activation *via* an iron source.⁸ However, an alternative non-iron mediated mechanism of bioactivation cannot be excluded and further additional biological support is required for both mechanisms.^{9,10} Although protein alkylation in *Plasmodia* is well established, the identity of molecular targets responsible for parasite cell death has so far evaded researchers. Novel probes, such as those synthesised as part of this thesis will aid ongoing research to resolve the chemical and molecular targets responsible for parasite cell death. In recent years, the emergence of artemisinin resistance in *P. falciparum* in Southeast Asia has posed a threat to efforts to control and eliminate malaria.¹¹ Therefore the identification of molecular target(s) will aid the design and synthesis of next-generation antimalarial drugs that can delay or reverse parasite resistance to existing drugs. A molecular marker of artemisinin resistance within *P. falciparum* has also been recently identified.¹² This marker is known as PF3D7_1343700 kelch propeller domain ('K13-propeller'). It is currently unknown whether artemisinin directly targets the K13-propeller, however, this protein exhibits homology with human Keap1 (which contains a kelch propeller at its C-terminal). Studies by Olnagier *et al* have demonstrated that CD36 is the major receptor mediating *Plasmodium* phagocytosis by macrophages, a process that is

mainly controlled by PPAR γ . Therefore, promotion of CD36 expression on inflammatory macrophages aids the clearance of *Plasmodia* parasite. Nrf2 controls CD36 expression, independently of PPAR γ . As a result, the Nrf2 pathway could be an alternative mechanism for clearance of *Plasmodia* parasites.¹³ The discovery of the K13-propeller further questions whether a similar Keap1-Nrf2 system exists within the *P. falciparum* parasite. Therefore, whilst more work is required to define the function of K13-propeller within the malaria parasite, this protein may become a novel molecular target *via* which new drugs could selectively target resistant strains of *P. falciparum*.

Artemisinin are also known for their anticancer properties. Indeed, they are cytotoxic towards drug and radiation resistant cancer cells. This suggests that artemisinins have a different mode of action compared with traditional anticancer therapies.¹⁴ Similar to malaria, the exact chemical mechanism and molecular target(s) responsible for the anticancer effects of artemisinins is unknown, but identifying such targets could provide opportunities to design and develop novel cancer therapies.

The discovery of the K13-propeller as a marker of artemisinin resistance in *P. falciparum* along with its similarity to Keap1 raises interesting questions. It is known that CDDO and related compounds possess anticancer properties. Could Keap1 also be a molecular target for artemisinin within cancer therapy? Such a concept warrants further investigation. The probes described here will facilitate the testing of this and other hypothesis, potentially revealing novel drug targets in important diseases, this informing the design and synthesis of much needed new medicines.

6.3. References

- 1 Ahmad, R., Raina, D., Meyer, C., Kharbanda, S. & Kufe, D. Triterpenoid CDDO-Me Blocks the NF- κ B Pathway by Direct Inhibition of IKK β on Cys-179. *Journal of Biological Chemistry* **281**, 35764-35769, doi:10.1074/jbc.M607160200 (2006).
- 2 Ahmad, R., Raina, D., Meyer, C. & Kufe, D. Triterpenoid CDDO-Methyl Ester Inhibits the Janus-Activated Kinase-1 (JAK1) \rightarrow Signal Transducer and Activator of Transcription-3 (STAT3) Pathway by Direct Inhibition of JAK1 and STAT3. *Cancer Research* **68**, 2920-2926, doi:10.1158/0008-5472.can-07-3036 (2008).
- 3 Pharmaceuticals, R. *Reata Pharmaceuticals Completes \$78 Million Equity Financing for Second Pivotal Trial of Bardoxolone Methyl*, [http://www.reatapharma.com/investors-media/news/news-timeline/archive/reata-pharmaceuticals-completes-\\$78-million-equity-financing-for-second-pivotal-trial-of-bardoxolone-methyl.aspx](http://www.reatapharma.com/investors-media/news/news-timeline/archive/reata-pharmaceuticals-completes-$78-million-equity-financing-for-second-pivotal-trial-of-bardoxolone-methyl.aspx) Last updated: 2012, Access date: **July 2013**.
- 4 Pharmaceuticals, R. *Company Statement: Termination of the BEACON Trial*, <http://www.reatapharma.com/investors-media/news/news-timeline/2012/company-statement-termination-of-beacon-trial.aspx> Last updated: 2012, Access date: **July 2013**.
- 5 Chin, M. P., Reisman, S. A., Bakris, G. L., O'Grady, M., Linde, P. G., McCullough, P. A., Packham, D., Vaziri, N. D., Ward, K. W., Warnock, D. G. & Meyer, C. J. Mechanisms Contributing to Adverse Cardiovascular Events in Patients with Type 2 Diabetes Mellitus and Stage 4 Chronic Kidney Disease Treated with Bardoxolone Methyl. *American Journal of Nephrology* **39**, 499-508, doi:10.1159/000362906 (2014).
- 6 Reata Pharmaceuticals, I. *Bardoxolone Methyl Evaluation in Patients With Pulmonary Arterial Hypertension (PAH) (LARIAT)*, <http://www.clinicaltrials.gov/ct2/show/NCT02036970?term=Bardoxolone+Methyl&rank=4> Last updated: August 2014, Access date: **August 2014**.
- 7 News, P. H. *Experimental Therapy Targets Inflammation in Pulmonary Arterial Hypertension*, <http://pulmonaryhypertensionnews.com/2014/07/16/experimental-therapy-targets-inflammation-pulmonary-arterial-hypertension/> Last updated: August 2014, Access date: **August 2014**.
- 8 O'Neill, P. M., Barton, V. E. & Ward, S. A. The Molecular Mechanism of Action of Artemisinin—The Debate Continues. *Molecules* **15**, 1705-1721, doi:10.3390/molecules15031705 (2010).
- 9 Haynes, R. K., Chan, W.-C., Wong, H.-N., Li, K.-Y., Wu, W.-K., Fan, K.-M., Sung, H. H. Y., Williams, I. D., Prosperi, D., Melato, S., Coghi, P. & Monti, D. Facile Oxidation of Leucomethylene Blue and Dihydroflavins by Artemisinins: Relationship with Flavoenzyme Function and Antimalarial Mechanism of Action. *ChemMedChem* **5**, 1282-1299, doi:10.1002/cmdc.201000225 (2010).
- 10 Haynes, R. K., Cheu, K.-W., Tang, M. M.-K., Chen, M.-J., Guo, Z.-F., Guo, Z.-H., Coghi, P. & Monti, D. Reactions of Antimalarial Peroxides with Each of Leucomethylene Blue and Dihydroflavins: Flavin Reductase and the Cofactor

- Model Exemplified. *ChemMedChem* **6**, 279-291, doi:10.1002/cmdc.201000508 (2011).
- 11 Ashley, E. A., Dhorda, M., Fairhurst, R. M., Amaratunga, C., Lim, P., Suon, S., Sreng, S., Anderson, J. M., Mao, S., Sam, B., Sopha, C., Chuor, C. M., Nguon, C., Sovannaroeth, S., Pukrittayakamee, S., Jittamala, P., Chotivanich, K., Chutasmit, K., Suchatsoonthorn, C., Runchaoren, R., Hien, T. T., Thuy-Nhien, N. T., Thanh, N. V., Phu, N. H., Htut, Y., Han, K.-T., Aye, K. H., Mokuolu, O. A., Olaosebikan, R. R., Folaranmi, O. O., Mayxay, M., Khanthavong, M., Hongvanthong, B., Newton, P. N., Onyamboko, M. A., Fanello, C. I., Tshefu, A. K., Mishra, N., Valecha, N., Phyo, A. P., Nosten, F., Yi, P., Tripura, R., Borrmann, S., Bashraheil, M., Peshu, J., Faiz, M. A., Ghose, A., Hossain, M. A., Samad, R., Rahman, M. R., Hasan, M. M., Islam, A., Miotto, O., Amato, R., MacInnis, B., Stalker, J., Kwiatkowski, D. P., Bozdech, Z., Jeeyapant, A., Cheah, P. Y., Sakulthaew, T., Chalk, J., Intharabut, B., Silamut, K., Lee, S. J., Vihokhern, B., Kunasol, C., Imwong, M., Tarning, J., Taylor, W. J., Yeung, S., Woodrow, C. J., Flegg, J. A., Das, D., Smith, J., Venkatesan, M., Plowe, C. V., Stepniewska, K., Guerin, P. J., Dondorp, A. M., Day, N. P. & White, N. J. Spread of Artemisinin Resistance in *Plasmodium falciparum* Malaria. *New England Journal of Medicine* **371**, 411-423, doi:10.1056/NEJMoa1314981 (2014).
 - 12 Ariey, F., Witkowski, B., Amaratunga, C., Beghain, J., Langlois, A.-C., Khim, N., Kim, S., Duru, V., Bouchier, C., Ma, L., Lim, P., Leang, R., Duong, S., Sreng, S., Suon, S., Chuor, C. M., Bout, D. M., Menard, S., Rogers, W. O., Genton, B., Fandeur, T., Miotto, O., Ringwald, P., Le Bras, J., Berry, A., Barale, J.-C., Fairhurst, R. M., Benoit-Vical, F., Mercereau-Puijalon, O. & Menard, D. A molecular marker of artemisinin-resistant *Plasmodium falciparum* malaria. *Nature* **505**, 50-55, doi:10.1038/nature12876 (2014).
 - 13 Olganier, D., Lavergne, R.-A., Meunier, E., Lefèvre, L., Dardenne, C., Aubouy, A., Benoit-Vical, F., Ryffel, B., Coste, A., Berry, A. & Pipy, B. Nrf2, a PPAR γ Alternative Pathway to Promote CD36 Expression on Inflammatory Macrophages: Implication for Malaria. *PLoS Pathog* **7**, e1002254, doi:10.1371/journal.ppat.1002254 (2011).
 - 14 Efferth, T., Sauerbrey, A., Olbrich, A., Gebhart, E., Rauch, P., Weber, H. O., Hengstler, J. G., Halatsch, M.-E., Volm, M., Tew, K. D., Ross, D. D. & Funk, J. O. Molecular Modes of Action of Artesunate in Tumor Cell Lines. *Molecular Pharmacology* **64**, 382-394, doi:10.1124/mol.64.2.382 (2003).